

Stratigraphy, Petrology, and Geochemistry of
Nevado de Longaví Volcano,
Chilean Andes (36.2°S).

THÈSE

présentée à la Faculté des Sciences de l'Université de Genève
pour obtenir le grade de Docteur ès sciences, mention Sciences de la Terre

par

Daniel Fernando SELLÉS MATHIEU

de

Santiago (CHILI)

Thèse n° 3752

GENÈVE

Atelier de reproduction Uni Mail

2006

La Faculté des sciences, sur le préavis de Messieurs M. DUNGAN, professeur ordinaire et directeur de thèse (Département de minéralogie), O. BACHMANN, docteur (Département de minéralogie), P. ULMER, professeur (Eidgenössische Technische Hochschule Zürich – Institut für Mineralogie und Petrographie – Zürich, Schweiz), W. P. LEEMAN, docteur (National Science Foundation – Earth Science Division – Arlington, U.S.A.), et F. BUSSY, docteur (Université de Lausanne – Institut de minéralogie et géochimie – Lausanne, Suisse), autorise l'impression de la présente thèse, sans exprimer d'opinion sur les propositions qui y sont énoncées.

Genève, le 16 juin 2006



Thèse - 3752 -

Le Doyen, Pierre SPIERER

Sellés Mathieu, D. F.: Stratigraphy, petrology, and geochemistry of Nevado de Longaví Volcano, Chilean Andes (36.2°S).
Terre & Environnement, vol. 61, iii + 103 pp. (2006)

ISBN 2-940153-60-4

Section des Sciences de la Terre, Université de Genève, 13 rue des Maraîchers, CH-1205 Genève, Suisse

Téléphone ++41-22-702.61.11 - Fax ++41-22-320.57.32

<http://www.unige.ch/sciences/terre/>

TABLE OF CONTENTS

Abstract	1
Resumen	3
Résumé étendu	5
<u>Chapter 1: Geochemistry of Nevado de Longaví Volcano (36.2°S): a compositionally atypical arc volcano in the Southern Volcanic Zone of the Andes.</u>	13
Abstract	13
Resumen	14
Introduction	14
General SVZ framework	15
Nevado de Longaví volcano	17
Early units	19
Cone-forming units	19
Holocene units	19
Plutonic-textured and quenched mafic enclaves	20
Whole rock chemistry and comparison with the SVZ	22
Two magma series at Nevado de Longaví	22
Mineral chemistry: amphibole composition and oxygen fugacity	25
Discussion	27
Are oceanic fractures playing a role?	32
Summary and conclusions	32

Aknowledgements	33
References	34
Chapter 2: Long-term geochemical and petrologic evolution of the magmatism at Nevado de Longaví: evidence for increasing influence of a subducted fracture zone.	37
Introduction	37
Geological context	39
Volcanic Stratigraphy	39
Pre-Longaví volcanics (Late Pliocene?-Early Pleistocene)	39
Internal stratigraphy of Nevado de Longaví volcano	41
Basal Longaví sequences (Units 1 and 2)	41
Main Cone Andesites (Units 3a and 3b)	42
Holocene products	43
Whole-rock Chemistry	44
Major elements	50
Trace elements	50
Isotopes	53
Mineral Chemistry	53
Fe-Ti oxides	53
Plagioclase	54
Amphibole	55
Pyroxenes and Olivine	58
Discussion	62
Closed-system evolution	63
Open-system processes	65
Origin of mafic magmas	67

Conclusions	71
References	72
Chapter 3: Plutonic-textured xenoliths in NLV: characterization and petrogenetic significance.	77
Introduction	77
Xenolith types	77
Group I	78
Group II	80
Granoblastic metamorphic rocks	81
Tertiary biotite-bearing granitoids	82
Mineral Chemistry	83
Plagioclase	83
Amphibole	85
Pyroxenes	86
Olivine	88
Biotite (phlogopite)	88
Whole-rock chemistry	88
Discussion	94
Summary	97
Conclusions	99
References	99
Remerciements	103

ABSTRACT

Nevado de Longaví volcano (NLV) is a Quaternary stratovolcano of the Southern Volcanic Zone of the Andes (SVZ). It is located on the western slope of the Andes at 36.2°S, close to the Central Depression of Chile. With its 3.242 masl summit, it is the highest peak of the area despite its modest volume (~20 km³). NLV is a single volcanic cone, mainly composed of andesitic lava flows, with the remnants of a dacitic dome on its summit. A great part of this dome collapsed during the Holocene towards the East, covering an andesitic flow and a dacitic pumice-fall deposit, both also Holocene in age.

The NLV edifice covers the distal northern flank of an older, mafic stratovolcano (Villalobos volcano; ~1Ma), which is part of a volcanic formation of regional extent (Cola de Zorro Fm.). Mildly folded Paleogene volcanoclastic beds intruded by Neogene plutons form the basement of both volcanoes.

Holocene NLV dacites have chemical compositions that are, in many respects, distinct from other evolved rocks of the region. They have La/Yb and Sr/Y values among the highest of the SVZ, comparable to those of magmas from the northern end of the SVZ. But unlike northern SVZ magmas, NLV dacites contain no mineralogical, isotopic or trace-element evidence of participation of a crustal component. Indeed, Holocene NLV dacites have the lowest incompatible-element contents (K₂O, Rb, Zr, Th, REE, etc.) of the whole SVZ. The mineralogy of these dacites is simple: plagioclase + amphibole + late orthopyroxene + Fe-Ti oxides. Fine-grained mafic enclaves quenched into the dacite have the same mineralogy, in addition to some olivine phenocrysts.

Andesitic lava flows that make up the outermost shell of the edifice show the same

chemical tendency towards high La/Yb ratios and low incompatible element contents. These andesites, in addition to the Holocene dacites and their mafic enclaves, constitute a compositional pattern (the low-Rb series) that can be reproduced by a model of fractionation of the observed mineral phases. Amphibole plays a fundamental role in the model to keep low levels on incompatible element enrichment in the derivative liquids.

Older andesitic flows of the edifice define a trend of higher incompatible element enrichments (high-Rb series), and some do present evidence of partial assimilation of plutonic rocks. These assimilated rocks are distinct from the Miocene plutons of the area, but could be fragments of more or less contemporaneous plutonic roots.

In the first chapter of this thesis I present the whole-rock geochemistry of NLV and I define the two Rb series. I show some of the chemical parameters that distinguish NLV rocks from its regional context, and I advance an hypothesis to explain our observations. The recent lavas from NLV are unusually water-rich magmas, in which amphibole appears early in the paragenetic sequence (right after olivine and clinopyroxene), whereas plagioclase is retarded and restricted to very calcic compositions. Such mineralogy is found in gabbroic xenoliths, some of which have clear cumulate textures, that we interpret as cogenetic. The model requires also deep fractionation of garnet, the only phase for which we do not have independent evidence.

Trace element ratios indicative of subduction-zone fluids (Ba/Th, Pb/Th, B/Zr, etc.) are systematically higher in low-Rb magmas than in other SVZ, suggesting that the fluid component in the magmas comes from the

subducted slab. A fracture zone in the oceanic floor offshore (the Mocha Fracture Zone; MFZ) projects underneath NLV, and could be the vehicle and conduit through which large amounts of fluids reach the mantle source region. This chapter was published in 2004 in the *Revista Geológica de Chile*.

The effect of the fracture zone in the genesis and evolution of older NLV magmas seems to be relatively less important. As the MFZ trends oblique to the plate convergence vector, its projection under the volcanic arc migrates southwards at a rate of 20-30 km/Ma. In the second chapter I present a refined stratigraphy of the volcano, and I document the chemical and mineralogical characteristics of the defined units, including samples from the underlying Villalobos volcano. Amphibole is absent from the lavas of Villalobos and from the basal NLV units, but increases in abundance through the two units that form the cone, and is predominant among Holocene products. The oxidation state of magmas also varies systematically from reduced (NNO-1) in early units to highly oxidized (NNO+2) in recent units, positively correlated with Ba/Zr and B/Th. One of the early NLV units has trace-element and isotopic evidence that suggest participation of a crustal component, probably sediments subducted along with the fracture zone.

In the third and last chapter of the thesis I present the whole-rock and mineral chemistry of diverse plutonic-textured xenoliths recovered from all NLV units. Two main groups of xenoliths are distinguished. Amphibole-rich xenoliths (amphibole gabbros and hornblendites), which are only found within the youngest units of NLV, have compositions consistent with amphibole accumulation. The compositions of the amphibole in these xenoliths correspond completely with the range of amphibole composition from recent lavas. On the other hand, plagioclase- and pyroxene-rich xenoliths (norites and gabbro-norites), which are also found in older NLV units, have nearly basaltic compositions, with some post-cumulus biotite and amphibole (of a distinct composition). These xenoliths could represent plutonic equivalents of water-poor magmas, such as Villalobos lavas, and have been partially assimilated by high-Rb andesites. A third group is represented by only three samples of high-grade metamorphic rocks (garnulites), with refractory mineral assemblages. Its provenance and meaning is unclear.

Nevado de Longaví volcano is an extraordinary example of long-term tendency in the nature of magmas produced in response to the increasing influence of a major geodynamic feature.

RESUMEN

El volcán Nevado de Longaví (VNL) es un estratovolcán Cuaternario perteneciente a la Zona Volcánica Sur de los Andes (ZVS). Está ubicado en la vertiente occidental de los Andes, a los 36.2°S, cercano a la Depresión Central de Chile. Con su cima de 3.242 msnm, es la máxima altura de la zona pese a su modesto volumen de ~20 km³. El VNL es un cono único compuesto principalmente por coladas andesíticas, y con los restos de un domo dacítico en la cumbre. Gran parte de este domo colapsó durante el Holoceno hacia el Este, cubriendo una colada andesítica y un depósito de pómez de caída dacítica, también Holocenos.

El cono del VNL se sobrepone al borde norte de un estratovolcán máfico más antiguo (volcán Villalobos; ~1 Ma), representante local de una secuencia de extensión regional (Fm. Cola de Zorro). Rocas volcanoclásticas del Paleógeno, levemente plegadas e intruidas por plutones Neógenos forman el basamento de ambos volcanes.

Las dacitas Holocenas del VNL tienen composiciones químicas en muchos aspectos distintas de otras rocas evolucionadas de la región. Sus razones La/Yb y Sr/Y están dentro de las más altas de la ZVS, comparables a las documentadas para volcanes del extremo norte de la SVZ. Pero al contrario de éstas, las dacitas del NLV no presentan evidencias isotópicas, de elementos traza o mineralógicas que indiquen la participación de un componente cortical. De hecho, las dacitas Holocenas tienen los contenidos de elementos altamente incompatibles (K₂O Rb, Zr, Th, REE, etc.) más bajos de la zona. La mineralogía de estas dacitas es simple: plagioclasa + anfíbola + ortopiroxeno tardío + óxidos de Fe-Ti. Enclaves andesítico basálticos de grano fino congelados ("quenched") en la dacita presentan la misma

mineralogía además de algunos fenocristales de olivino.

Las coladas andesíticas que forman el envoltorio externo del volcán presentan la misma tendencia química de las dacitas hacia altos valores La/Yb y bajos contenidos de elementos incompatibles. Estas andesitas, además de las dacitas y los enclaves máficos de éstas, conforman un patrón composicional (la serie de bajo Rb) que se puede reproducir mediante un modelo de fraccionamiento de las fases minerales observadas. La anfíbola juega un rol fundamental en el modelo, ya que permite mantener un bajo enriquecimiento en elementos incompatibles en los líquidos derivados.

Las coladas más antiguas del cono definen un patrón de evolución de mayor enriquecimiento en elementos trazas incompatibles (serie de alto Rb), en las que sí se encuentran evidencias de asimilación de rocas plutónicas. Estas rocas plutónicas son claramente distintas de los plutones Miocenos del área, y podrían ser fragmentos de raíces plutónicas más o menos coetáneas.

En el primer capítulo de la tesis presento la geoquímica de roca total del VNL, y distingo entre las dos series mencionadas. Muestro algunos de los parámetros químicos que distinguen a las rocas del VNL de su contexto regional, y avanzo una hipótesis para explicar nuestras observaciones. Las rocas recientes del VNL son magmas inusualmente ricos en agua, en los cuales la anfíbola comienza a participar temprano en la paragénesis (inmediatamente después del olivino y clinopiroxeno), mientras que la plagioclasa es retardada y restringida a composiciones muy cálcicas. Tal mineralogía se encuentra de manera remarcable en ciertos xenolitos gabbróicos, algunos con clara

textura de cumulado, que interpretamos como cogenéticos. El modelo requiere también el fraccionamiento profundo de pequeñas proporciones de granate, la única fase de la que no tenemos evidencia directa independiente.

Las razones de elementos traza indicadoras de fluidos de subducción (Ba/Th, Pb/Th, B/Zr, etc.) de la serie de bajo Rb son sistemáticamente altas relativas a otros magmas de la ZVS, sugiriendo que el componente fluido en los magmas es un fluido de la zona de subducción. Una zona de fractura en la placa oceánica, la Zona de Fractura Mocha (ZFM), que proyecta directamente bajo el VNL, puede ser el conducto y vehículo por el cual ingresan al manto grandes cantidades de fluidos. Este capítulo fue publicado en el año 2004 en la Revista Geológica de Chile.

El efecto de la zona de fractura en las lavas más antiguas del VNL parece ser menor, tanto en términos de mineralogía como de composición química. Dado que la ZFM es oblicua al vector de convergencia entre placas, su proyección bajo el arco migra hacia el sur a razón de 20-30 km/Ma. En el segundo capítulo presento una estratigrafía refinada del volcán, documento sus características químicas y mineralógicas, e incluyo muestras del precedente volcán Villalobos. La anfíbola está ausente de la mineralogía del volcán Villalobos, así como de las unidades basales del VNL, pero aumenta progresivamente en las dos unidades que forman el cono, y es claramente predominante en las unidades Holocenas. El estado de oxidación de los magmas también varía sistemáticamente de reducido (NNO-1) en las unidades tempranas a altamente oxidadas (NNO+2) en las unidades recientes, en cierta correlación positiva con las razones

Ba/Zr, B/Th, etc. Una de las unidades tempranas del VNL presenta evidencias isotópicas y de elementos traza que sugieren la participación de un componente cortical, probablemente de sedimentos subductados en la zona de fractura misma.

En el tercer y último capítulo presento la química de roca total y de minerales de una colección de xenolitos plutónicos recuperados de las diversas unidades. Dos grupos fundamentales se distinguen. Los xenolitos ricos en anfíbola (gabbros de anfíbola y hornblenditas), que se encuentran exclusivamente en las unidades más jóvenes del volcán, tienen composiciones consistentes con acumulación de anfíbola. La composición de las anfíbolas en estos xenolitos se corresponde completamente con el rango de anfíbolas en las lavas recientes. Por otra parte, xenolitos ricos en plagioclasa y piroxeno (noritas, gabbro-noritas), que se encuentran también en unidades más antiguas del volcán, tienen composiciones basálticas, con algo de acumulación de plagioclasa, en los que biotita y anfíbola (de distinta composición) aparecen sólo como fases *post-cumulus*. Tales xenolitos podrían representar raíces plutónicas de magmas pobres en agua, tal como los del volcán Villalobos, y han sido asimilados parcialmente por andesitas de alto Rb. Un tercer grupo está representado por sólo tres muestras de metamorfitas de alto grado (granulitas), con asociaciones minerales refractarias, son de procedencia y significado inciertos.

El volcán Nevado de Longaví es un ejemplo excepcional de tendencia de largo plazo en la naturaleza de los magmas producidos por un volcán en respuesta a la influencia creciente de un rasgo geodinámico.

RÉSUMÉ ÉTENDU

STRATIGRAPHIE, PÉTROLOGIE ET GÉOCHIMIE DU VOLCAN NEVADO DE LONGAVÍ, ANDES DU CHILI (36.2°S)

Le volcan Nevado de Longaví (VNL) est un stratovolcan appartenant à la chaîne de volcans Quaternaires des Andes du sud. Cette chaîne de volcans, connue comme la Zone Volcanique Sud (ZVS), résulte de la subduction de la plaque océanique de Nazca sous la marge occidentale de l'Amérique du sud, et s'étend entre les parallèles 33 et 46 de latitude sud.

D'importants paramètres géologiques, tels que l'épaisseur, l'âge et la composition de la croûte continentale, varient le long des ~1500 km de la ZVS. A l'extrémité nord de la SVZ (33-34.5°S), les volcans sont situés sur une croûte qui peut atteindre 60 km d'épaisseur (le mont Aconcagua, le plus haut sommet des Amériques, est situé quelques kilomètres plus au nord). Vers le sud, la légère obliquité de la chaîne de volcans par rapport à l'axe de l'orogène andin fait que les volcans Quaternaires soient placés sur une croûte de moins en moins épaisse. A la latitude de Longaví, la croûte a une épaisseur d'environ 40 km et celle-ci s'amincit encore légèrement vers le sud.

La composition chimique des laves émises par les divers volcans de la ZVS change également avec la latitude. La géochimie des magmas du segment nord de la ZVS suggère une importante contamination crustale, tandis que vers le sud de Longaví, le fractionnement à basse pression est le mécanisme dominant la genèse des magmas évolués. Ceci est illustré par les variations des rapports isotopiques de Sr en fonction de la latitude, de moins en moins radiogéniques vers le sud (Figure 1). D'autres paramètres géochimiques varient de façon plus ou moins systématique du nord au sud

montrent néanmoins des anomalies marquées au niveau du VNL (Figure 2).

L'une des caractéristiques géochimiques les plus notables des magmas andésitiques et dacitiques du VNL est leur faible teneur en éléments incompatibles. Ces concentrations sont non seulement nettement plus basses que dans les laves des volcans du nord, dans lesquelles la contribution de la croûte continentale est importante, mais aussi que dans la plupart des laves émises au sud du 36°S pour lesquelles la contamination crustale est moindre. Ceci signifie que les mécanismes d'évolution magmatique au VNL doivent être différents de ceux du reste de la SVZ. Les variations du rapport K_2O/SiO_2 en fonction de la latitude (Figure 2A), mais aussi celles des autres éléments incompatibles (Rb, La, Zr, Nb, Th, etc.), illustrent parfaitement la spécificité géochimique des laves du VNL au sein de la ZVS.

L'ampleur de cet appauvrissement en éléments incompatibles dans les laves du VNL n'est pas la même pour tous les éléments. Les éléments considérés comme étant solubles dans les fluides provenant de la plaque subductée (Ba, Pb, Cs, etc.) sont moins appauvris que ceux non solubles et provenant essentiellement de la source mantélique (Th, Nb, Zr). Les rapports des éléments solubles sur les éléments insolubles sont donc très élevés au VNL, comme l'indique la Figure 2B. D'un autre côté, certains éléments solubles, notamment le B, sont enrichis dans les laves du VNL par rapport aux autres volcans de la ZVS. L'ensemble de ces observations suggère que l'apport de fluides est plus élevé lors de la

formation des magmas du VNL que pour celle des autres magmas de la ZVS.

Une troisième caractéristique importante des laves du VNL est leur ressemblance aux roches dites « adakitiques ». Celles-ci ont été définies comme des magmas issus de la fusion de la croûte océanique subductée, et présentent des rapports La/Yb et Sr/Y élevés par rapport aux roches d'arc « normales ». L'origine des adakites est actuellement très controversée car les magmas à caractère adakitique sont beaucoup plus répandus que

ce que les modèles thermiques de fusion de croûte océanique subductée prévoient. Au niveau de la ZVS, des rapports La/Yb et Sr/Y élevés sont caractéristiques des laves du VNL mais aussi des laves de volcans plus au nord situés sur une croûte épaisse (Figure 2C). Pour ces dernières, une assimilation de croûte inférieure dont le grenat est une phase résiduelle a été proposée comme explication. Dans le cas du VNL cette interprétation n'est pas applicable car les faibles teneurs en éléments incompatibles ne permettent pas de supposer

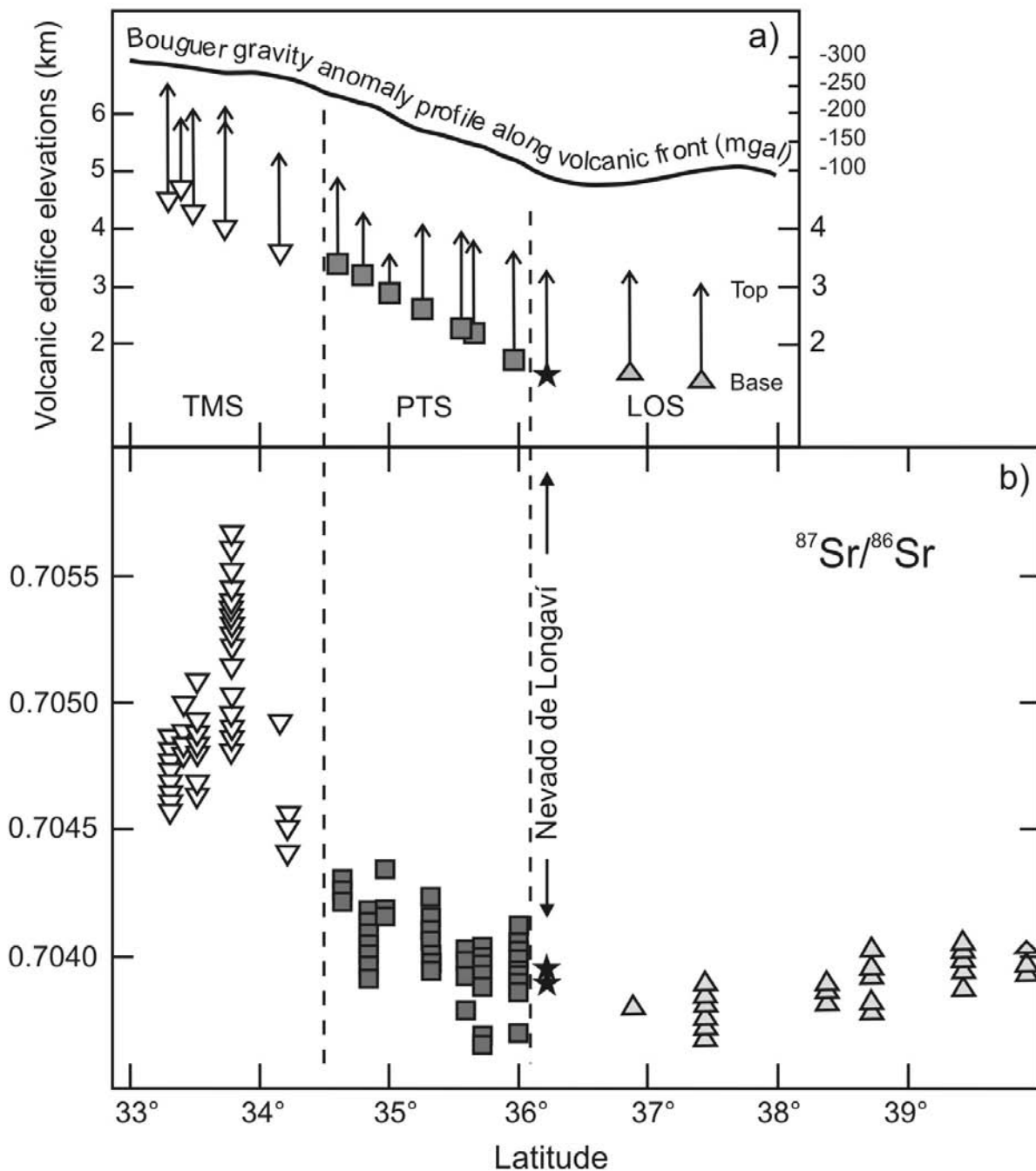


Figure 1: a) Variation de l'altitude des volcans de la ZVS en fonction de la latitude. Ceci constitue un bon indice de l'épaisseur crustale comme le montre la corrélation avec l'anomalie gravimétrique de Bouguer. b) Variation du rapport isotopique de Sr en fonction de la latitude. Noter l'étroite corrélation avec l'épaisseur crustale.

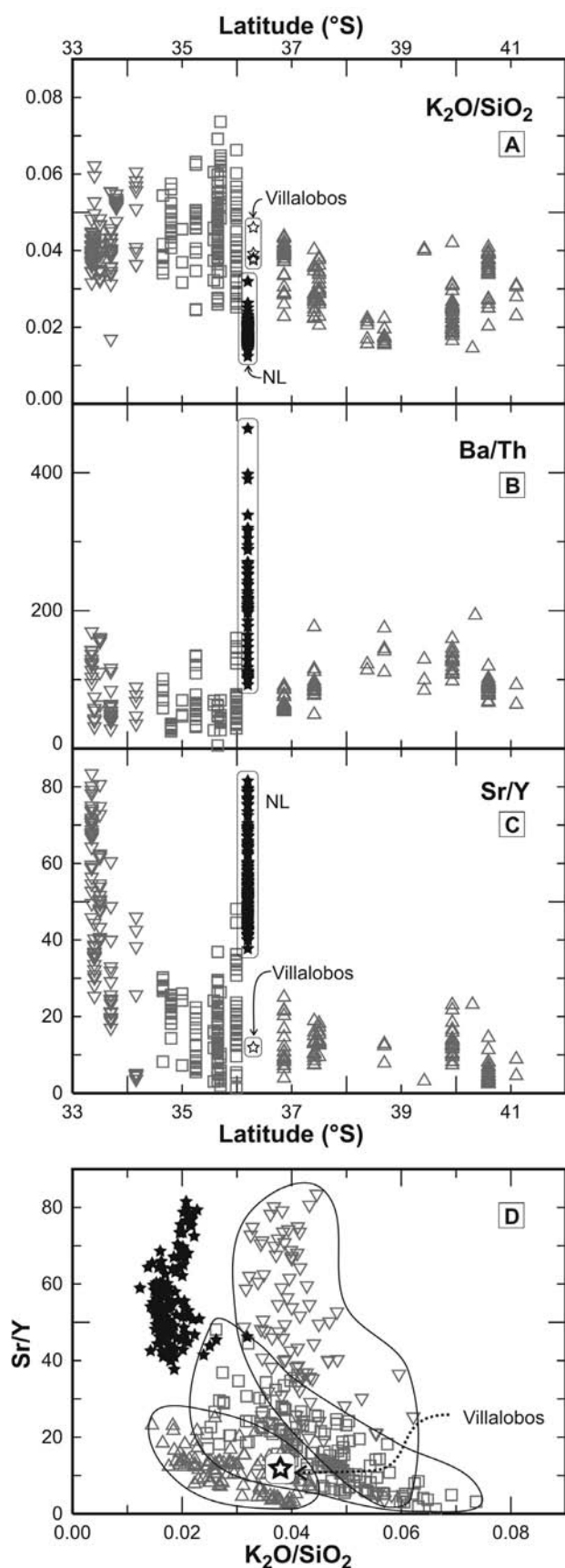


Figure 2 : (A, B, C) Variations géochimiques en fonction de la latitude des laves de la ZVS. Etoiles noires : Nevado de Longaví (VNL). Etoiles blanches : volcan Villalobos, à la même latitude mais plus ancien que le VNL. (D) Variations de Sr/Y en fonction de K_2O/SiO_2 montrant aussi la spécificité du VNL par rapport aux autres volcans de la ZVS.

une assimilation crustale importante. La Figure 2D (variation de Sr/Y en fonction de K_2O/SiO_2) montre que les laves du VNL sont les seules de la ZVS à présenter à la fois des caractéristiques adakitiques et un appauvrissement général en éléments incompatibles.

Le Chapitre 1 de cette thèse constitue le premier travail montrant le caractère unique des laves du VNL dans le contexte de la ZVS. Ce chapitre a été publié en 2004 dans un volume spécial de la Revista Geológica de Chile paru lors de l'assemblée générale de l'Association Internationale de Volcanologie et Chimie de l'Intérieur de la Terre (IAVCEI) tenue au Chili. Dans cette contribution nous montrons que plusieurs des spécificités des laves du VNL sont compatibles avec des teneurs en eau élevées dans les magmas. Outre les rapports des éléments solubles et insolubles mentionnés précédemment, la minéralogie du VNL est marquée par la prédominance d'amphibole comme minéral ferromagnésien dès les compositions andésitiques, ce qui requiert des teneurs en eau magmatique d'au moins 4% poids. L'abondance d'amphibole est aussi un caractère distinctif des laves du VNL. Dans les volcans au sud du VNL, l'amphibole est extrêmement rare même dans des laves rhyolitiques, tandis qu'au nord, elle est plus fréquente mais toujours subordonnée aux pyroxènes. Un scénario d'évolution magmatique dominée par le fractionnement d'amphibole permet d'atteindre des compositions dacitiques après ~50% de fractionnement. Ceci contraste avec les 65-75% de fractionnement nécessaire pour arriver aux mêmes teneurs en silice par fractionnement d'assemblages riches en pyroxènes tels que ceux proposés pour l'évolution d'autres volcans de la ZVS. Cette différence est fondamentale car elle permet d'expliquer l'une des plus importantes spécificités du VNL, c'est-à-dire, la faible teneur en éléments incompatibles de ses laves évoluées. L'amphibole contient moins de silice dans sa structure cristalline que les pyroxènes, ce qui permet un enrichissement plus rapide en silice des liquides résiduels issus d'un fractionnement d'amphibole que ceux dérivés d'un fractionnement

de pyroxène. L'hypothèse du fractionnement d'amphibole comme mécanisme prédominant dans l'évolution des magmas du VNL semble être confirmé par la présence de cumulats d'amphibole retrouvés sous forme de xénolites dans certaines laves.

Nous avançons une hypothèse pour expliquer la présence très localisée de ces magmas hautement hydratés. Le VNL se situe dans le prolongement d'une fracture de la plaque océanique adjacente connue comme la Zone de Fracture Mocha (ZFM). Les fractures

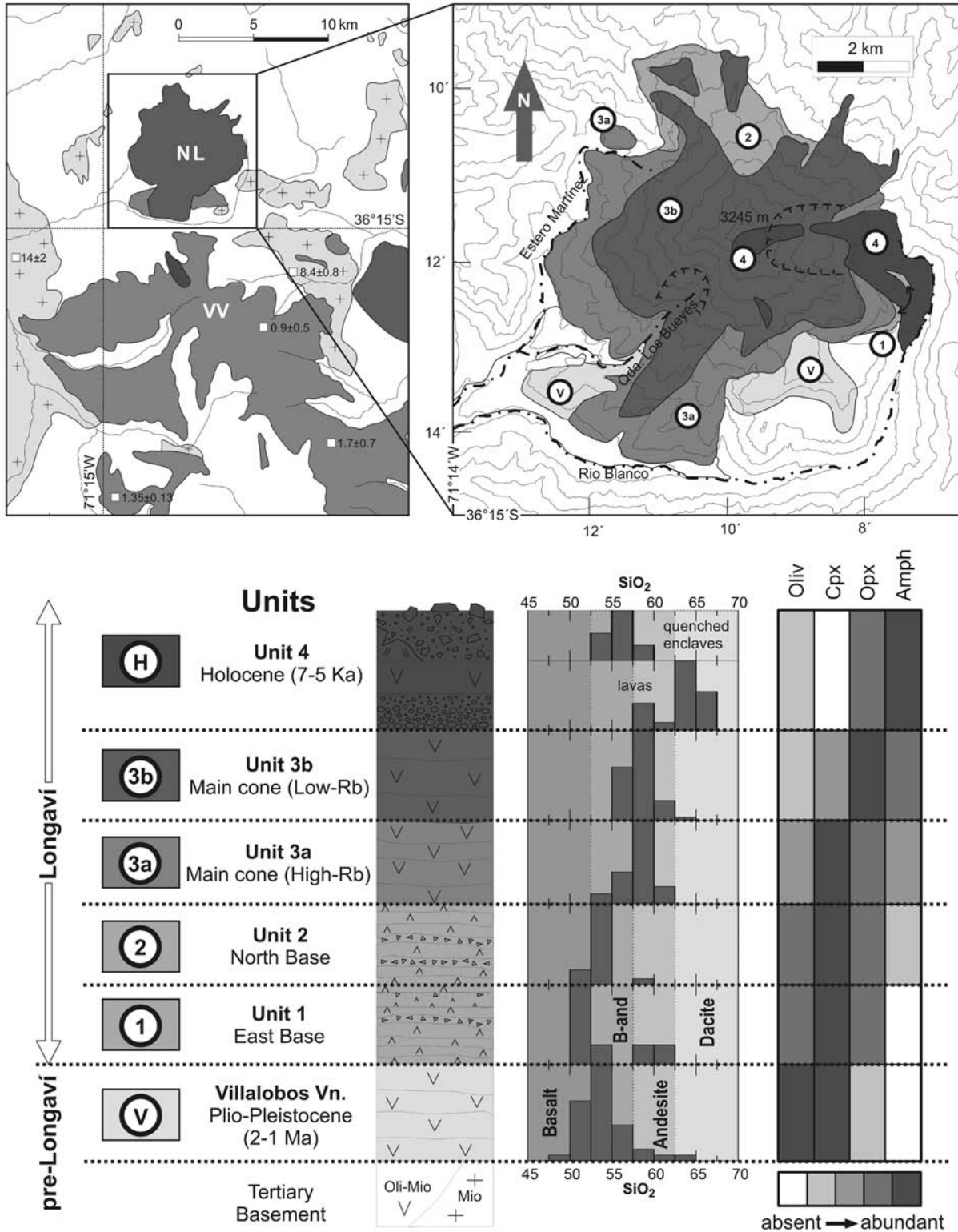


Figure 3 : Carte géologique simplifiée de la région du VNL (en haut à gauche) avec la distribution des unités volcaniques et intrusives (VV= volcan Villalobos). A droite, carte visualisant la distribution des unités définies pour le VNL. En bas, colonne stratigraphique schématique avec des histogrammes de composition des laves pour chaque unité. A droite, abondance relative des phases ferromagnésiennes.

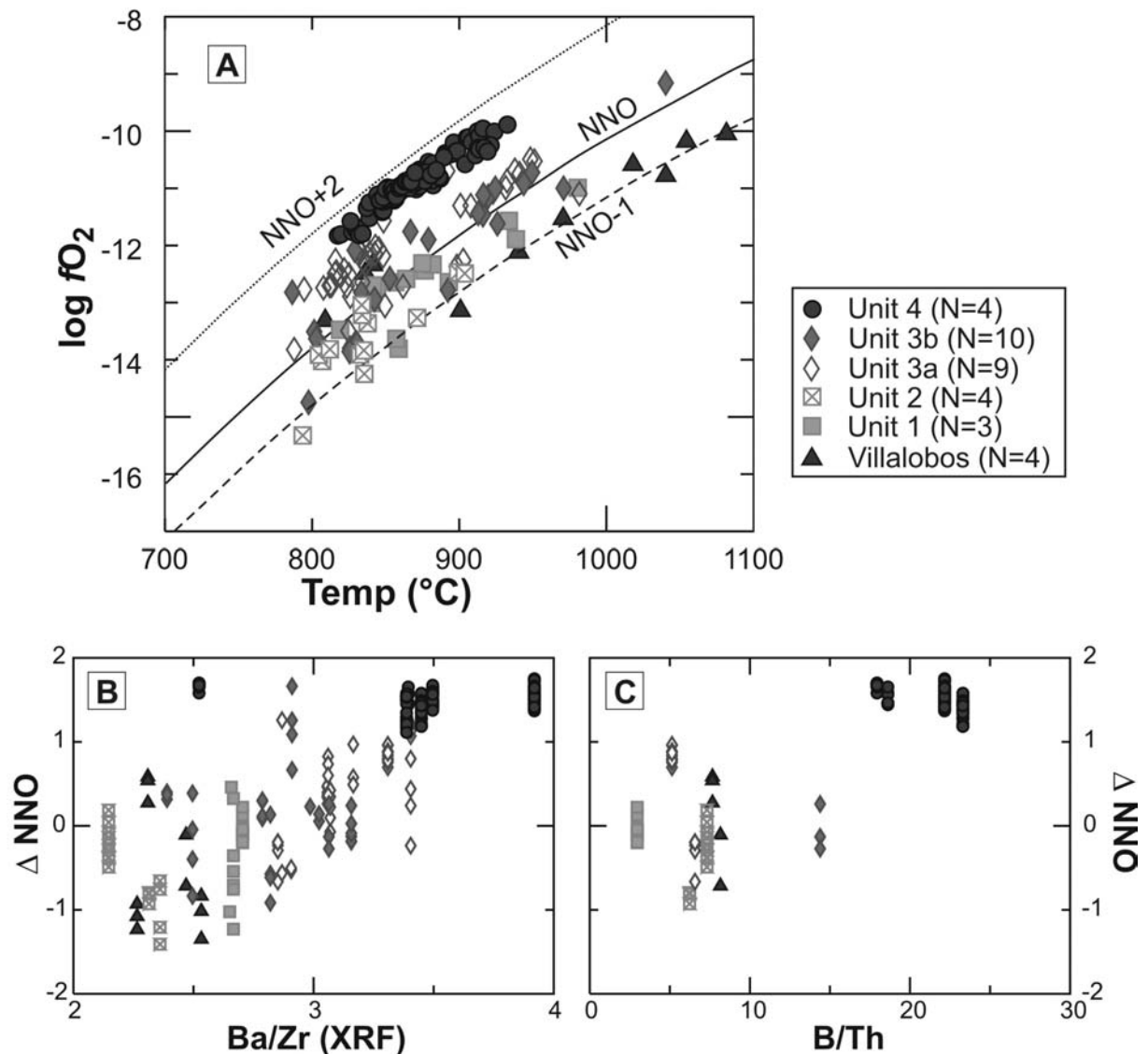


Figure 4 : Variation des conditions de température et de fugacité d'oxygène des magmas dans la zone d'étude (A). L'augmentation progressive de l'état d'oxydation des magmas est accompagnée par une augmentation des rapports d'éléments en trace caractéristiques de la participation de fluides.

océaniques sont des discontinuités de la croûte basaltique à travers lesquelles l'eau de mer peut circuler et interagir avec les peridotites du manteau lithosphérique formant des corps de serpentinite. Les peridotites serpentinisées peuvent contenir jusqu'à 13 % de leur poids en eau, c'est-à-dire un ordre de grandeur de plus que la croûte océanique altérée. La subduction de tels corps de serpentinites est donc un vecteur très efficace de transport de fluides vers le manteau asthénosphérique situé sous le continent. Nous proposons donc que la subduction de la ZFM sous le volcan VNL est responsable des caractéristiques chimiques particulières de son magmatisme. Une comparaison avec les compositions chimiques de laves évoluées des volcans au sud du VNL montre que ceux placés dans le prolongement

d'autres zones de fracture océanique partagent certaines des caractéristiques chimiques du VNL, quoique de façon moins prononcées.

L'orientation de la ZFM est légèrement oblique au vecteur de convergence des plaques océanique et continentale, et donc sa position relative à l'arc volcanique n'est pas stationnaire et migre vers le sud à une vitesse de 20-30 km/Ma. Si la ZFM contrôle la nature du magmatisme au VNL, alors l'importance de ses effets doit changer au cours du temps. Dans le Chapitre 2 j'explore les variations temporelles de la chimie des laves et des minéraux à travers une section stratigraphique générale du volcan. Le VNL a été divisé en cinq unités stratigraphiques (Figure 3), auxquelles s'ajoute le volcanisme Pléistocène qui précède le VNL (volcan Villalobos ; ~1 Ma). Les magmas du

volcan Villalobos ainsi que ceux à la base du VNL sont des basaltes et andésites basaltiques à olivine et clinopyroxène (amphibole absente) et leur chimie est comparable à celle des magmas émis ailleurs dans la ZVS (Figure 2). L'amphibole devient progressivement plus abondante dans les unités plus jeunes, et constitue le minéral ferromagnésien prédominant dans les produits Holocènes du volcan VNL (Figure 3). L'évolution géochimique des différentes unités peut être modélisée par des calculs de bilan de masse introduisant une augmentation de la proportion d'amphibole fractionnée avec le temps.

La composition chimique des minéraux montre aussi d'importantes variations au cours du temps, dont l'une des plus notables est l'état d'oxydation des magmas. Dans la séquence

étudiée la fugacité d'oxygène varie presque de 3 unités logarithmiques entre la base et le sommet de la colonne stratigraphique (Figure 4). Cette variation est accompagnée par des incréments dans les paramètres géochimiques indicateurs de fluides. Les variations en éléments mineurs dans le plagioclase sont cohérentes avec cette évolution. Par exemple, le rapport Fe/Mg dans le plagioclase augmente systématiquement au cours du temps en réponse à l'augmentation de la fugacité d'oxygène des magmas car le fer oxydé (Fe^{3+}) peut substituer le Al^{3+} dans la structure cristalline beaucoup plus facilement que le Fe^{2+} .

Les basses teneurs en éléments incompatibles des magmas du VNL sont en grande partie expliquées par le fractionnement

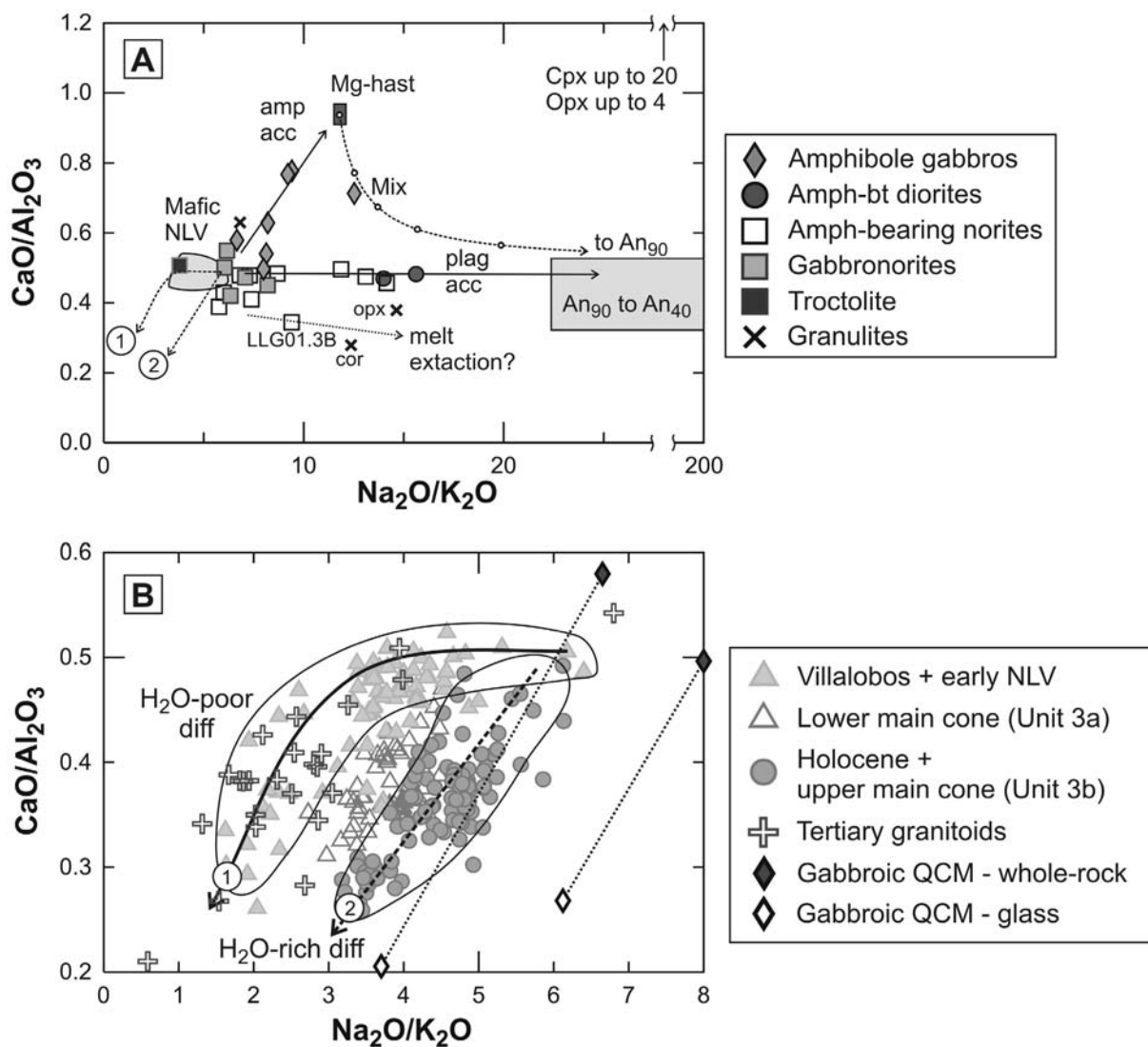


Figure 5 : En haut, compositions des xénolites du VNL. On peut y distinguer les tendances d'accumulation d'amphibole et de plagioclase. La différenciation de magmas basaltiques (zone grise) par l'extraction de plagioclase produit le trend 1, tandis que la stabilisation d'amphibole produit le trend 2. En bas, le trend de différenciation des magmas dans des conditions de faible teneur en eau est représenté par les unités anciennes du VNL. Les unités récentes suivent un trend dominé par le fractionnement d'amphibole produisant des magmas évolués avec Na_2O/K_2O élevés. L'unité 3a suit un trend intermédiaire.

d'une association minéralogique dont la proportion d'amphibole augmente au cours du temps. Les variations chimiques des magmas mafiques, donc peu différenciés, ne peuvent pas être expliquées de la même façon. Les magmas mafiques des unités récentes sont plus riches en silice et plus pauvres en éléments incompatibles que les magmas mafiques à la base du volcan, ce qui peut être expliqué par une augmentation du taux de fusion de la source mantellique. Ceci est aussi compatible avec l'hypothèse d'une augmentation de la quantité d'eau incorporée dans le manteau asthénosphérique, car le taux de fusion des péridotites fertiles augmente de façon linéaire avec la quantité de fluides ajoutés

Non seulement la quantité de fluides intervenant dans la genèse des magmas du VNL semble avoir changé au cours de temps, mais aussi leur nature et composition. La première unité du VNL témoignant de l'influence d'un apport de fluides élevés est marquée par des rapports Th/La et $^{87}\text{Sr}/^{86}\text{Sr}$ élevés, ce qui a été interprété comme la signature d'une composante crustale dans ces magmas. La source la plus probable de cette composante crustale correspond aux sédiments subductés. Le volcanisme le plus récent du VNL est, au contraire, très appauvri en Th. Ces basses teneurs en Th sont également caractéristiques des magmas mafiques, ce qui exclut une explication par le fractionnement d'une phase accessoire et témoigne probablement d'une signature héritée des magmas primaires. L'explication la plus convaincante réside dans l'appauvrissement des fluides en Th, ce qui a

été observé dans les fluides provenant de la déshydratation de serpentinites.

Le Chapitre 3 est dédié à l'étude des xénolites qui ont été retrouvés dans les différentes unités du volcan. Quatre types de xénolites ont été définis en accord avec leur minéralogie et leur texture. Les fragments de roches plutoniques du soubassement, ainsi que de rares exemples de roches métamorphiques de haut degré (probablement en faciès granulite) semblent ne pas avoir eu une influence significative sur la chimie des magmas. Au contraire, des fragments de norites, gabbro-norites et gabbros, à la chimie proche des basaltes des unités anciennes, sont une source probable des xénocristaux présents dans certaines laves du volcan, peu hydratées et relativement réduites. Des xénolites riches en amphibole ont été retrouvés dans les unités récentes du volcan. Les amphiboles dans ces xénolites ont la même composition que celles des laves qui les contiennent. Ces xénolites représentent très probablement des cumulats extraits des magmas hydratés du VNL. Les diagrammes de la Figure 5 présentent la relation entre la composition des xénolites et les trends d'évolution magmatique au Nevado de Longaví.

Le volcan Nevado de Longaví représente un cas unique de magmatisme hautement hydraté dans le contexte du volcanisme andin. Les magmas à caractère adakitique des éruptions récentes représentent la culmination d'une tendance générale d'augmentation dans la teneur en eau des magmas émis par le volcan au cours du temps en réponse à la subduction d'une zone de fracture océanique.

CHAPTER 1*

GEOCHEMISTRY OF NEVADO DE LONGAVÍ VOLCANO (36.2°S): A COMPOSITIONALLY ATYPICAL ARC VOLCANO IN THE SOUTHERN VOLCANIC ZONE OF THE ANDES

**Daniel Sellés M.
Ana Carolina Rodríguez S.
Michael A. Dungan**

Section de Sciences de la Terre
University of Geneva
Switzerland

José Antonio Naranjo S.

Sernageomin, Chile

Moyra Gardeweg P.

Aurum Consultores, Stgo., Chile

ABSTRACT

The Quaternary Nevado de Longaví volcano of the Andean Southern Volcanic Zone (SVZ) has erupted magmas that range in composition from basalt to low-silica dacite, although andesites are the dominant erupted magma type. Amphibole is a common phenocryst phase in andesites throughout the volcano, and it is the dominant mafic phase in Holocene dacites and their included mafic enclaves. Compositions of magmas erupted at Longaví volcano define arrays that diverge from trends delineated by neighboring frontal-arc volcanoes. Although mafic compositions at Longaví are broadly similar to basalts at other SVZ centers, Longaví intermediate and evolved magmas have systematically lower abundances of incompatible major (K_2O , P_2O_5) and trace elements (Rb, Zr, Nb, REE, Th, etc), as well as high Ba/Th, Sr/Y, and La/Yb ratios. Longaví volcano magmas define two differentiation series with regard to enrichments of Rb (and other incompatible elements) with increasing silica. A high-Rb series that includes the oldest units of the volcano comprises basalts to andesites dominated by anhydrous mineral assemblages with chemical compositions similar to other SVZ magmatic series. The series with low Rb, on the other hand, includes the Holocene units that evolved from basaltic andesites to dacites by means of fractional crystallization wherein amphibole and calcic plagioclase dominate the mineral assemblage. Magmas parental to low-Rb series are interpreted to be high-degree mantle melts, highly hydrous and oxidized, formed as a response to high fluid inputs into the subarc mantle. Enhanced water transport to the subarc mantle is a plausible effect of the subduction of the oceanic Mocha Fracture Zone that projects beneath Nevado de Longaví. Volcanoes located over oceanic fracture zones further south along the SVZ have erupted hornblende-bearing magmas that share some chemical similarities with Longaví volcano magmas.

Key words: *Southern Volcanic Zone, Nevado de Longaví volcano, SVZ segmentation, amphibole fractionation.*

* This chapter was published as an article in 2004 in the *Revista Geológica de Chile* (vol. 31, No. 2, p. 293-315).

GEOQUÍMICA DEL VOLCÁN NEVADO DE LONGAVÍ (36.2°S): UN VOLCÁN DE ARCO COMPOSICIONALMENTE ATÍPICO EN LA ZONA VOLCÁNICA SUR DE LOS ANDES

RESUMEN

El estratovolcán cuaternario Nevado de Longaví de la Zona Volcánica Sur de los Andes (ZVS) ha emitido magmas de composición basáltica a dacítica, si bien los productos predominantes son andesíticos. La anfíbola es fenocristal común en andesitas de todo el volcán, y es la fase máfica predominante en dacitas de edad Holocena y en enclaves máficos coetáneos. La composición química de los magmas del Nevado de Longaví define patrones que difieren de las tendencias mostradas por otros centros del frente volcánico. Si bien las lavas máficas del Nevado de Longaví son, en términos generales, similares a otros basaltos de la ZVS, las lavas intermedias y evolucionadas exhiben valores sistemáticamente bajos de elementos incompatibles, tanto mayores (K_2O , P_2O_5) como trazas (Rb, Zr, Nb, REE, Th, etc), así como altos valores de Ba/Th, Sr/Y y La/Yb. Dos series magmáticas se definen en base al grado de enriquecimiento en Rb (y otros elementos incompatibles) con el aumento de sílice. La serie de alto Rb, que incluye a las unidades más antiguas del volcán, pero que podría ser en parte coetánea a la serie de bajo Rb, está conformada por basaltos a andesitas de composición química próxima a otras series magmáticas de la ZVS dominadas por asociaciones minerales anhidras. La serie de bajo Rb, que incluye a las unidades holocenas del volcán, evoluciona desde andesitas basálticas a dacitas por vía de cristalización fraccionada involucrando importantes proporciones de anfíbola y plagioclasa cálcica. Los magmas parentales de esta serie serían fundidos parciales de alto grado, altamente hidratados y oxidados, consecuencia de un elevado aporte de agua a la fuente astenosférica. Un elevado transporte de agua hacia el manto astenosférico probablemente resulta de la subducción de la Zona de Fractura oceánica Mocha que se proyecta bajo el Nevado de Longaví. Otros volcanes de la ZVS situados sobre fracturas oceánicas han emitido magmas con anfíbola que comparten algunas similitudes químicas con los magmas del Nevado de Longaví.

Palabras clave: *Zona Volcánica Sur, volcán Nevado de Longaví, segmentación de la ZVS, fraccionamiento de anfíbola.*

INTRODUCTION

First-order geodynamic factors that may control arc magma chemistry include: 1) subducting plate parameters such as thermal state and buoyancy of the slab, depth and extent of dehydration, ability to drag trench sediments and/or to erode the forearc lithosphere; 2) the chemistry and mineralogy of the sub-arc asthenospheric mantle, as well as melting and melt migration mechanisms involved in basalt generation, and 3) the potential of the overriding plate to contaminate mantle-derived magmas, which can be a function of crustal thickness, lithologic composition, and stress regime. The mutual interdependence of some of

these factors (e.g. length and depth of melting of the mantle column will vary with thickness of the overriding plate; stress regime of the continental plate can be related to buoyancy of the subducted plate) further complicates the quantification of the conditions that control magma evolution paths in the course of the construction of large volcanic edifices.

The Southern Volcanic Zone of the Andes (SVZ) is an example of a volcanic arc that exhibits systematic along-strike chemical and mineralogical variations which have been related to regional-scale variations in some of these factors. We present whole-rock and mineral chemistry data from lavas of the Nevado

de Longaví volcano that do not conform to previously documented along-arc chemical variations, and which challenge existing composition-based schemes for division of the arc into magmatic provinces. Although most of the broad-scale variations within the SVZ lend themselves to explanations linked to upper-plate controls, namely crustal thickness and age, the unusual chemistry and mineralogy of Nevado de Longaví magmas may be best explained by the local character of the oceanic plate.

Holocene hornblende-bearing dacites erupted at Longaví volcano show geochemical and mineralogical characteristics that render them different from other dacites of the SVZ. Low abundances of incompatible elements coupled with high Sr/Y and LREE/HREE ratios, and relatively high Mg and Cr contents are among the characteristics that distinguish Longaví dacites from evolved magmas elsewhere in the SVZ. Longaví dacites have an 'adakitic' chemical signature (without implying any particular genesis). The presence of presumably cogenetic mafic magmas allows the evolution of Longaví dacites to be tested.

We present the first overview of the magmatic evolution of Nevado de Longaví based on the volcanic stratigraphy, whole-rock major and trace element chemistry, petrography, and mineral chemistry, and present a working hypothesis for the formation of these magmas.

GENERAL SVZ FRAMEWORK

The SVZ is the Quaternary volcanic arc developed on the western margin of the South American plate that extends between latitudes 33 and 46°S (Figure 1). The SVZ is separated from the Central and Austral Volcanic Zones by volcanic gaps that coincide with the subduction of the aseismic Juan Fernandez Ridge and the active Chile Rise respectively. Between these latitudes, the estimated thickness of the continental crust varies from ~55-65 km in the north to ~30-35 km in the south (Hildreth & Moorbath, 1988), and frontal-arc volcanoes are located at progressively lower altitudes, ranging from 4500 m in the north to sea-level in the south. The chemistry and mineralogy of the arc's eruptive products vary with latitude. Volcanic centers close to the northern termination of

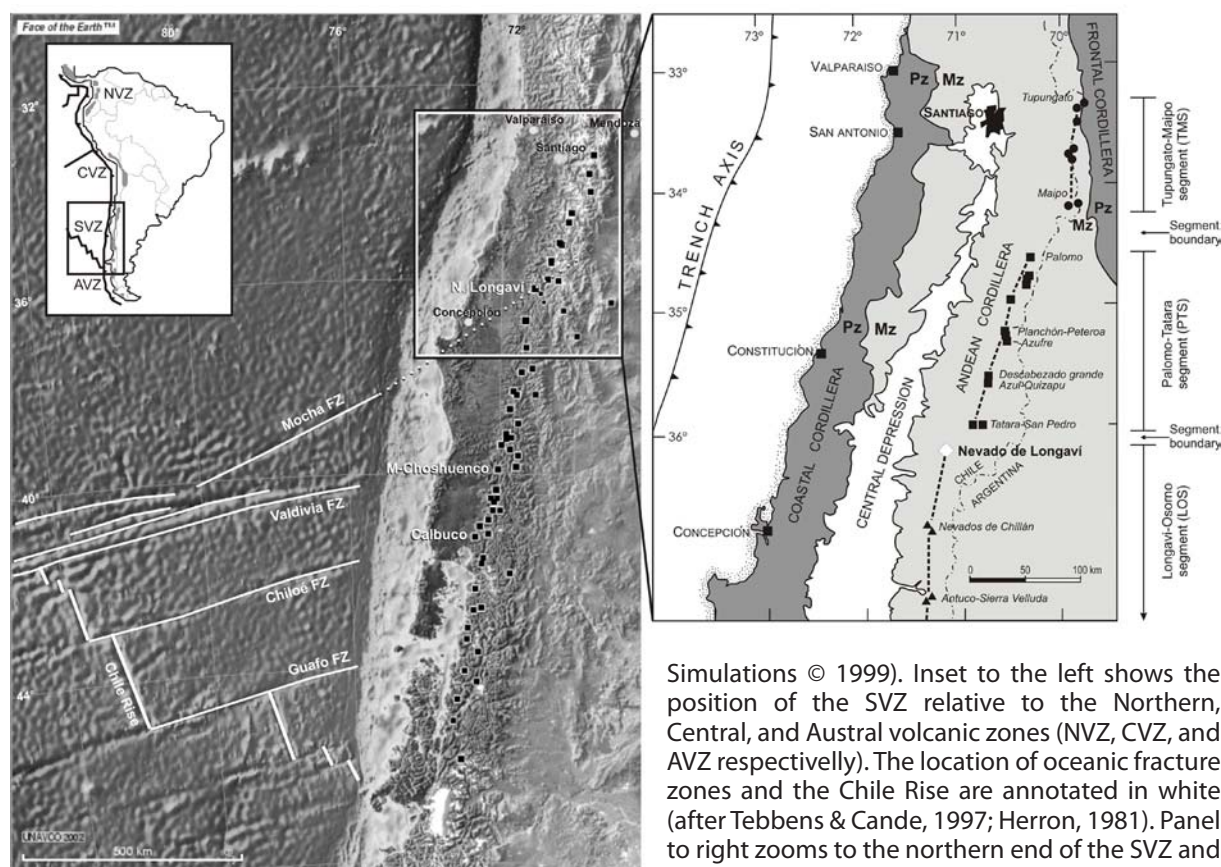


Figure 1: Location of Nevado de Longaví volcano and some other volcanic centers of the SVZ. Digital elevation model is reproduced from <http://jules.unavco.ucar.edu> (Face of the Earth is a registered trademark, ARC Science

Simulations © 1999). Inset to the left shows the position of the SVZ relative to the Northern, Central, and Austral volcanic zones (NVZ, CVZ, and AVZ respectively). The location of oceanic fracture zones and the Chile Rise are annotated in white (after Tebbens & Cande, 1997; Herron, 1981). Panel to right zooms to the northern end of the SVZ and shows the segmentation scheme used in text; figure modified from Hildreth & Moorbath (1988) after Wood & Nelson (1988) and Dungan *et al.* (2001). The oldest age of exposed basement units is indicated as Paleozoic (Pz) or Mesozoic (Mz).

the SVZ (33-34.5°S) are composed primarily of andesites and more evolved lavas wherein hydrous mineral phases are common and olivine is usually absent. These variably evolved lavas are characterized by the highest contents of incompatible elements (for a given SiO₂ content) within the SVZ. In contrast, volcanoes from 37 to 41.2°S are largely composed of mafic lavas and they occur west of the continental divide, located progressively closer to the Central Depression and at lower base elevations to the south. Evolved magmas rarely contain hydrous minerals and are less enriched in incompatible elements than are lavas to the north. A much greater extent of crustal contamination is also inferred in northern volcanoes on the basis of isotopic signatures. Volcanoes located between these two extremes occur at progressively higher base elevations to the north, and they are intermediate in terms of some geochemical parameters such as Sr isotopic ratios (Figure 2).

Although arc-scale systematic variations in magma composition have been recognized

previously in the SVZ, there is little consensus on the origin of these geographic trends. The relative roles of depth of magma differentiation, the proportion and chemical signature of continental crust assimilated during magma storage and ascent, source contributions related to sediment subduction and tectonic erosion, and the length of the asthenospheric melting column are currently a matter of debate (Hildreth & Moorbath, 1988; Futa & Stern, 1988; Sigmarsson *et al.*, 1990; Stern, 1991; Hildreth & Moorbath, 1991; Tormey *et al.*, 1991).

A number of different schemes have been proposed for grouping SVZ volcanoes into provinces or segments. The location of boundaries, nomenclature, and the criteria for defining these subdivisions vary from one scheme to the next (Figure 3). We have adopted the segmentation nomenclature proposed by Dungan *et al.* (2001), based on arguments by Wood & Nelson (1988), wherein the arc has been divided according to changes in orientation and lateral shifts in the position of

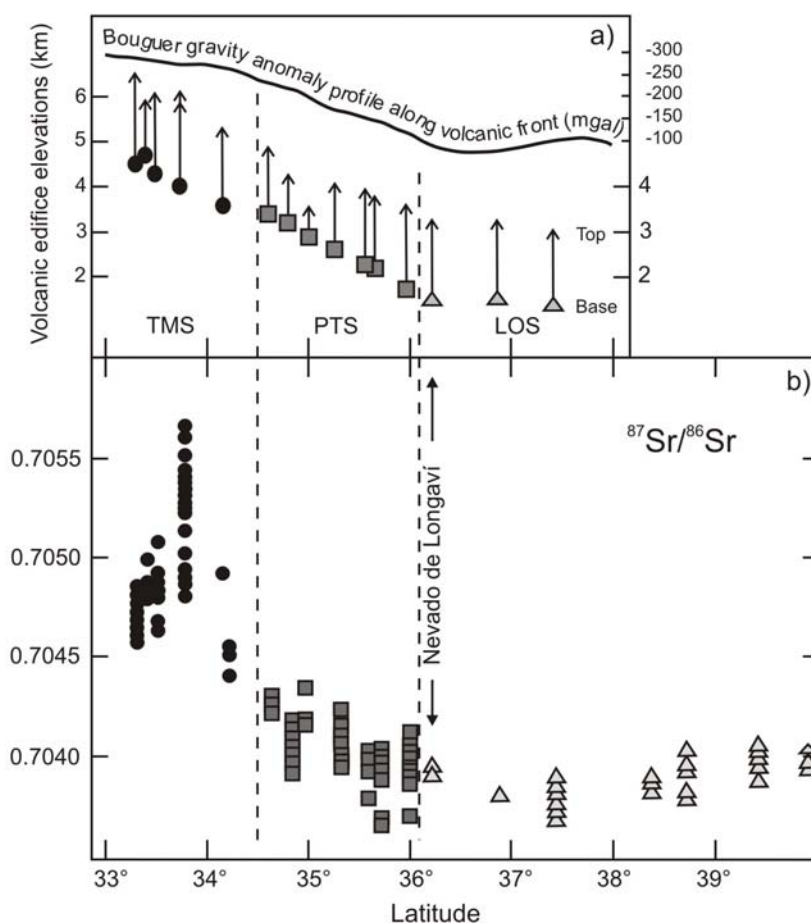


Figure 2: a) Basal and summit elevations of centers along the volcanic front between 33 and 37.5°S relative to sea level. These topographic data and the Bouguer gravity-anomaly profile along the arc suggest increasing crustal thickness to the north of Longaví. b) Sr isotopic ratios vs. latitude for volcanic front centers. Both figures are taken from Hildreth & Moorbath (1988) where original data sources are cited. TMS, PTS, and LOS refer to segments shown in Figure 1.

"Lat S	Dungan <i>et al.</i> , 2001	López-Escobar, 1984	Futa and Stern, 1988	Tormey <i>et al.</i> , 1991	López-Escobar <i>et al.</i> , 1993	López-Escobar <i>et al.</i> , 1995a	"Lat S
33	TMS			NSVZ	NSVZ	NSVZ	33
34.5	PTS	Province I	NSVZ	TSVZ	TSVZ	TSVZ	34.5
36							37
41.2	LOS	Province II	SSVZ	SSVZ	SSVZ	CSVZ	42
						SSVZ	46

Figure 3: Comparison of the SVZ segmentation scheme used in this article (first column, after Dungan *et al.*, 2001) to other schemes. Note that the main difference is related to the placement of a segment boundary at 36 vs. 37°S. NSVZ, TSVZ, CSVZ, and SSVZ stand for northern, transitional, central, and southern SVZ respectively. TMS, PTS and LOS are acronyms for Tupungato-Maipo, Palomo-Tatara, and Longaví-Osorno Segments respectively.

the volcanic front, and segments are named after the northernmost and southernmost volcanic center in each segment.

The northernmost SVZ or Tupungato-Maipo Segment (TMS; Figure 1) of Dungan *et al.* (2001) comprises the north-south trending Quaternary volcanic centers located at the crest of the Andean range between 33 and 34.5°S. Magmas erupted in this segment are dominantly andesitic or more evolved, and mafic magmas (<54% SiO₂) have not been observed. High abundances of incompatible elements, coupled with high Sr isotopic ratios in volcanic rocks from this segment are considered to be a consequence of substantial amounts of lower crustal assimilation by mantle derived magmas (Hildreth and Moorbath, 1988; Ruiz *et al.*, 2001). Alternatively, they may also be the result of source contamination by subduction of trench sediments and/or erosion and drag of forearc lower crust (Futa & Stern, 1988; Stern, 1991). South of this segment, the Palomo-Tatara Segment (PTS; 34.5-36°S) trends slightly oblique to the Andean crest and the volcanoes are located at progressively lower altitudes to the south. Andesites are the most abundant products, although the proportions of basaltic andesites and basalts increase southward, and are dominant at Planchón volcano (35.2°S; Naranjo & Haller, 2002) and in the Tatara-San Pedro complex (36°S). Crustal contributions to evolved magmas are well documented within the Planchón-Peteroa (Tormey *et al.*, 1995) and Tatara-San Pedro (Davidson *et al.*, 1987) complexes. South of 36°S extends the central SVZ or Longaví-Osorno Segment (LOS, 36-41.2°S), wherein the trend of frontal-arc

volcanoes is nearly parallel to the cordilleran axis, and the basal elevation of centers varies less steeply. Volcanic edifices within this segment are mostly dominated by mafic lavas.

Previous composition-based subdivisions considered Nevado de Longaví and Nevados de Chillán volcanoes, both dominantly andesitic, to be part of the "transitional" SVZ. Tormey *et al.* (1991) suggest that 37°S (*i.e.* south of Nevados de Chillán) is the point where: 1) the thickness of the crust below the volcanic front starts to sharply increase northwards, and 2) the axis of the arc intersects the subsurface projection of the oceanic Mocha Fracture Zone. Both of these inferences, however, seem to be incorrect. Figure 2 shows that along the volcanic front, basal elevations of volcanoes and Bouguer gravity anomalies have inflection points around 36°S. Likewise, when the projection of the Mocha Fracture Zone is corrected for the dip of the slab (30°; Bohm *et al.*, 2002), it intersects the arc close to Nevado de Longaví rather than south of Nevados de Chillán. A segment boundary at 36°S leaves the andesitic Longaví and Chillán edifices grouped together with more mafic volcanoes to the south, but unlike andesitic volcanoes north of 36°S, evolved lavas from Longaví and Chillán do not seem to have experienced significant crustal contamination (not more than volcanoes to the south, in any case), or at least the chemical signature of contamination is much less 'enriched' than it is to the north. Calbuco volcano (42°S) is in many ways different from volcanoes to the north (much like Longaví volcano, López-Escobar *et al.*, 1995b).

NEVADO DE LONGAVÍ VOLCANO

Nevado de Longaví is a late Quaternary SVZ stratovolcano located at 36°12'S-71°10'W (Figure 1). Reconnaissance mapping by Gardeweg (1980 and 1981) was included within the regional framework presented by Muñoz & Niemeyer (1984), and analyses of various samples from Longaví volcano were discussed by Hildreth & Moorbath (1988) and Hickey *et al.* (1984). The volcanic edifice was constructed on folded volcanoclastic strata of the Cura-Mallín Formation (Eocene to Early Miocene; Muñoz & Niemeyer, 1984), which is intruded by Miocene plutons, and unconformably covered by basaltic to basaltic andesitic lavas and breccias of the Late Pliocene-Pleistocene Cola de Zorro Formation. South of Longaví volcano, in the

Cordón de Villalobos, outcrops of this formation define a large, low-profile, deeply eroded volcanic edifice. Nevado de Longaví volcano is a relatively small, single cone (basal altitude ~1500 m; summit altitude 3242 m; ~20 km³ estimated volume), mainly composed of thick andesitic flows that radiate from the current summit area. There is no evidence of caldera-forming eruptions but sector collapse scars are present on the east and southwestern slopes of the cone (Figure 4). No historical eruptions are recorded, although Holocene volcanism was frequently explosive and the pyroclastic deposits from this phase of activity partly fill the sector-collapse depression on the east flank (headwaters of Río Blanco).

Lavas from Longaví volcano range in composition from basalts to dacites (51-65 wt% SiO₂). Andesites with 56-60 wt% SiO₂ are the most abundant products and represent more than 80% of the total output. Basaltic (51.5 wt% SiO₂) and dacitic (64-65 wt% SiO₂) products are subordinate. Dacitic compositions have been only identified among Holocene units, and scarce basalts are found within the mainly basaltic andesitic early stages of growth of the edifice. Fine-grained magmatic enclaves of basaltic andesitic composition are common, and locally very abundant in andesitic and dacitic lavas.

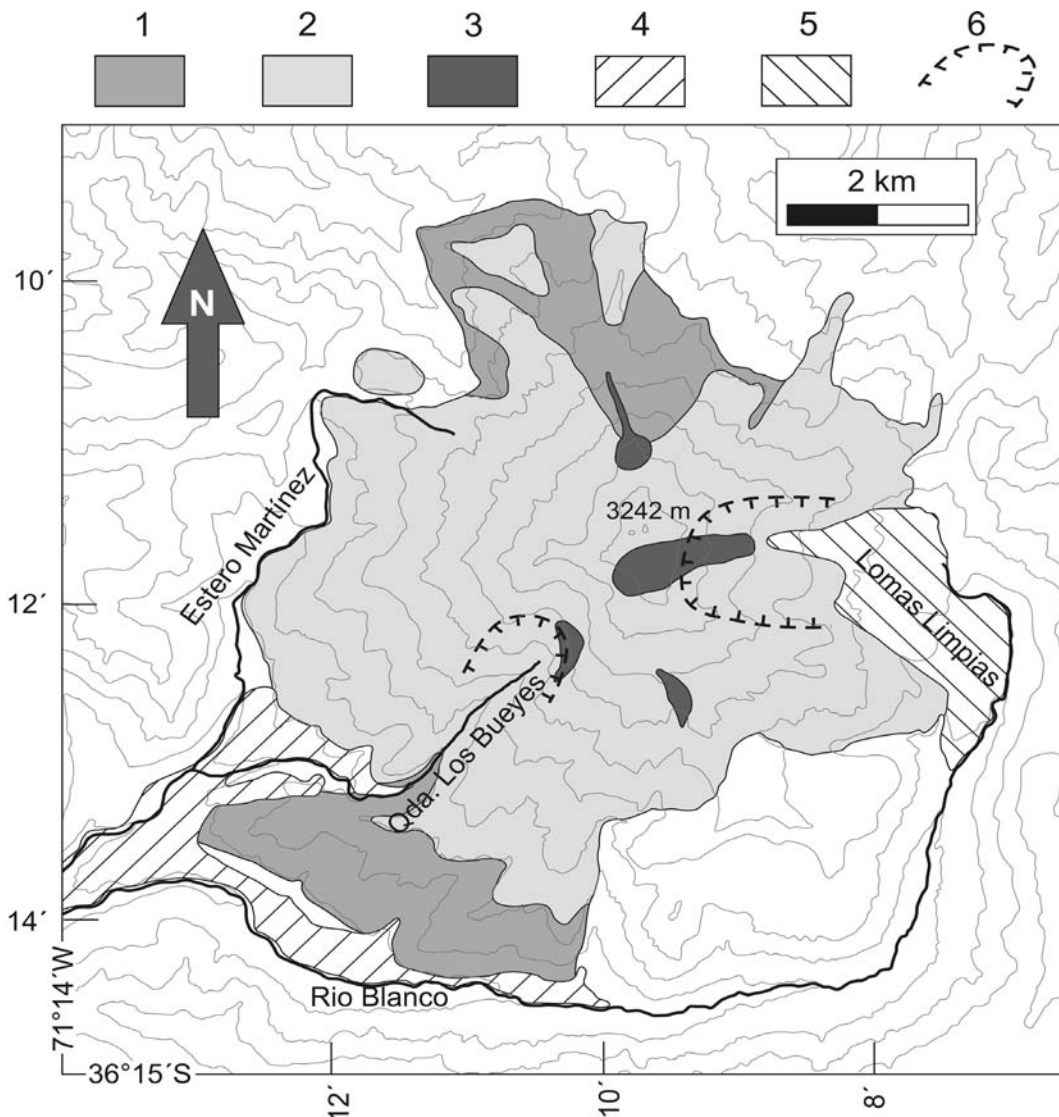


Figure 4: Schematic map of Nevado de Longaví volcano showing the units discussed in the text. 1) Early units, mainly basaltic andesitic lava flows. 2) Main cone andesites. 3) Summit area andesitic to dacitic domes, central dome of presumably Holocene age. 4) Pre-Holocene terrace deposits associated to Los Bueyes sector collapse and Martínez and Río Blanco streams. 5) Holocene pyroclastic deposits of Lomas Limpias collapse bowl. 6) Collapse scars. Contour curves every 200 m.

Early units

The oldest units of Longaví volcano are sequences of basaltic andesitic flows that are exposed on the north and southwest flank of the edifice (Figure 4). The northern flank of the volcano exposes a 100-150 m thick sequence of basaltic and basaltic andesitic flows (51.9 to 54.3 wt% SiO₂) that radiate from a point ~400 m lower than the present-day summit. This inferred fossil vent is now occupied by a partly intrusive andesitic dome. Individual lava flows are 1-3 m thick, but massive flows pinch out towards the vent where mafic scoriaceous deposits form up to 80% of the exposures, probably reflecting dominantly strombolian eruption style. Abundant plagioclase (plag, An₆₀₋₇₅) +olivine (oliv, Fo₇₀₋₇₅) +clinopyroxene (cpx, En₄₃₋₄₅Wo₃₉₋₄₃Fs₁₃₋₁₄) phenocrysts in an intergranular groundmass are characteristic of this unit. A sequence of basaltic andesites with similar composition and mineralogy is exposed on the south wall of Quebrada Los Bueyes (Figure 4). The total exposed thickness is about 150 m, the base of which corresponds to ~50 m of mafic epiclastic and pyroclastic beds that directly overlie basement-derived colluvium and *in situ* Cura-Mallín basement. The upper part of the sequence is composed of olivine-phyric basaltic andesitic flows, 1-5 m thick each, which are in turn covered by thicker, amphibole-bearing andesites.

Cone-forming units

The main cone of Nevado de Longaví volcano is composed of thick (4-15 m) lava flows and flow breccias that radiate from the summit area. Lavas forming the main cone are andesites with 55.1-62.2 wt% SiO₂ (most of them between 57 and 61%, though), wherein the typical mineral association is plag +opx (En₆₅₋₇₆) +cpx (En₃₅₋₅₀Wo₃₇₋₄₈Fs₈₋₁₅) ±oliv (Fo₇₀₋₈₁) ±amph. Both olivine and amphibole commonly show disequilibrium reaction textures, especially when they coexist in the same host. Lava flows also commonly contain abundant amphibole-bearing gabbroic fragments and quenched mafic enclaves (see below). Internal stratigraphy is difficult to extend from one locality to another due to the homogeneous compositions involved and because the source area seems to have remained static throughout the construction of the edifice. Important erosion periods, however, are recorded within

the units on the northern flank of the volcano, where late lavas, themselves glaciated, have flowed into deep U-shaped valleys excavated into older andesites.

Holocene units

Holocene activity was concentrated in the summit area and on the eastern flank of the edifice, which has been substantially modified by pre-Holocene flank failure and collapse. The Lomas Limpias sector collapse depression (~2 km²; Figure 5) was subsequently partially filled with effusive and pyroclastic materials of Holocene age that range in composition from basaltic andesitic to dacitic, and therefore span a broader compositional range than the main edifice.

The oldest deposits (unknown age) exposed in the collapse depression comprise a thin (~30m) volcanoclastic sequence formed by an alternation of decimeter thick, coarsely reverse-graded breccias with sandy matrices and centimeter-thick beds of fine sand and silt. The breccias host fragments of glassy basaltic andesites and andesites up to 20 cm in diameter, which are variably vesiculated and contain plag +oliv +cpx phenocrysts. These clastic beds interfinger with thin basaltic flows and hyaloclastic breccias that have the same composition as the associated clasts, which range from 52 to 62% SiO₂, and which have the highest K₂O contents found at Longaví volcano. These deposits, which may have been erupted sub-glacially, are overlain by a more silicic sequence of pyroclastic and effusive units in which three distinct evolved magma compositions are present.

The first of these is a thick, white pumice fall deposit that proximally overlies the volcanoclastic deposits and that extends for more than 20 km to the southeast of Longaví volcano. Proximal pumice accumulations have a maximum thickness of 30 m, although the deposits thin rapidly away from the summit and in the collapse bowl pumice accumulation is <15 m thick. The pumices have a dacitic composition (65.1-65.8 wt% SiO₂) and host amph +plag ±opx phenocrysts. Charcoal collected from below the pumice deposit has yielded a ¹⁴C age of 6'835±65 ybp*.

* Necessary preparation and pre-treatment of the sample material for radiocarbon dating was carried out by the ¹⁴C laboratory of the Department of Geography

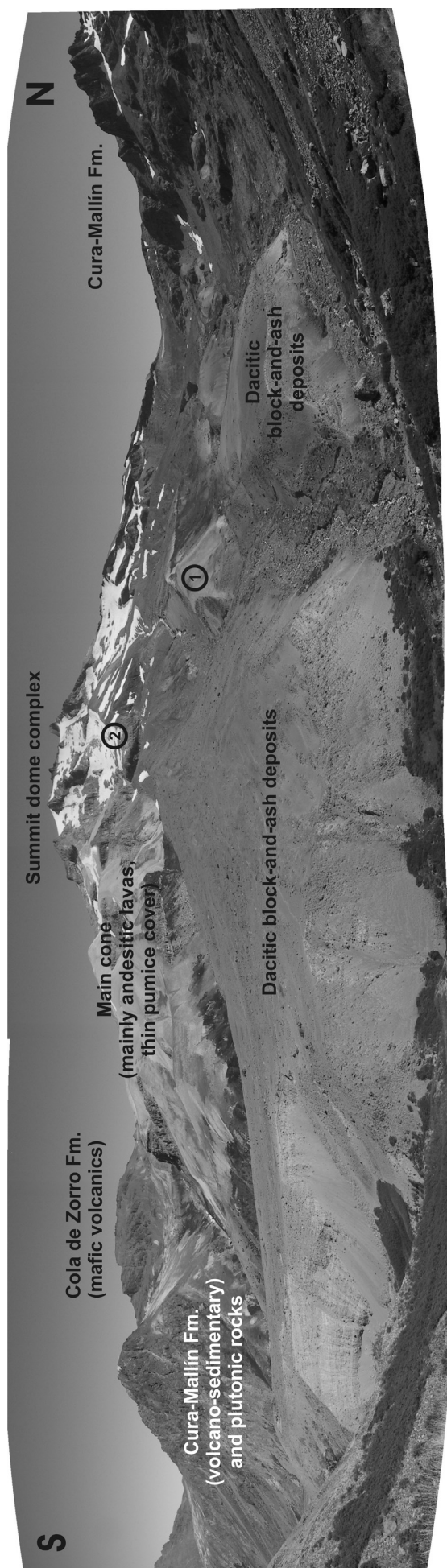


Figure 5: Panoramic view of the eastern flank of Nevado de Longaví volcano, showing the Lomas Limpías collapse bowl and deposits filling the depression. In the foreground, dacitic block and ash deposits from collapse of summit dome overlying hyaloclastic breccias (1) and Holocene andesitic lava (2). Main cone andesites are partly covered by ~7'000 ybp pumice fall deposit. Left (south) of the volcano crop out Cura-Mallín Formation volcanoclastic strata intruded by Miocene granitoids and covered by Plio-Pleistocene mafic lavas from the Villalobos volcano (Cola de Zorro Formation).

The second is a thick andesitic lava flow (59.8 wt% SiO₂) that postdates the pumice bed. It is confined to the proximal collapse bowl and partially fills an erosional depression cut into the white pumice. The phenocryst assemblage of this less evolved magma includes olivine (Fo₇₉₋₈₀) and orthopyroxene (En₇₀₋₇₄) phenocrysts in addition to plagioclase and oxidized amphibole. Abundant fine-grained and plutonic- and cumulate-textured enclaves are present.

The last volcanic event recorded at the volcano is the extrusion of a dacitic (63.1-64.3 wt% SiO₂) dome in the upper part of the collapse bowl and part of the summit area. The dome partly collapsed towards the east, forming block and ash deposits (estimated volume ~0.12 km³) that cover most of the previously described deposits. These dacitic magmas contain abundant calcic amphibole phenocrysts, as well as zoned plagioclase (An₆₀₋₃₀) and lesser amounts of orthopyroxene (En_{~70}). The dacite also contains a high proportion (~3%) of quenched mafic enclaves. The major and trace element composition of this dacite is similar to that of the underlying pumices and they constitute the most evolved products found at Longaví volcano. Other amphibole-bearing andesitic domes have been found intercalated in lava flows around the summit area, but their age is unknown.

Plutonic-textured and quenched mafic enclaves

Lavas from Nevado de Longaví volcano commonly contain abundant fine-grained inclusions and coarse- to medium-grained plutonic-textured fragments. We refer to them as 'fine-grained' or 'quenched' enclaves

at the University of Zurich (GIUZ). The dating itself was done by AMS (accelerator mass spectrometry) with the tandem accelerator of the Institute of Particle Physics at the Swiss Federal Institute of Technology Zurich (ETZ). This age is part of Carolina Rodríguez' Ph.D. research project.

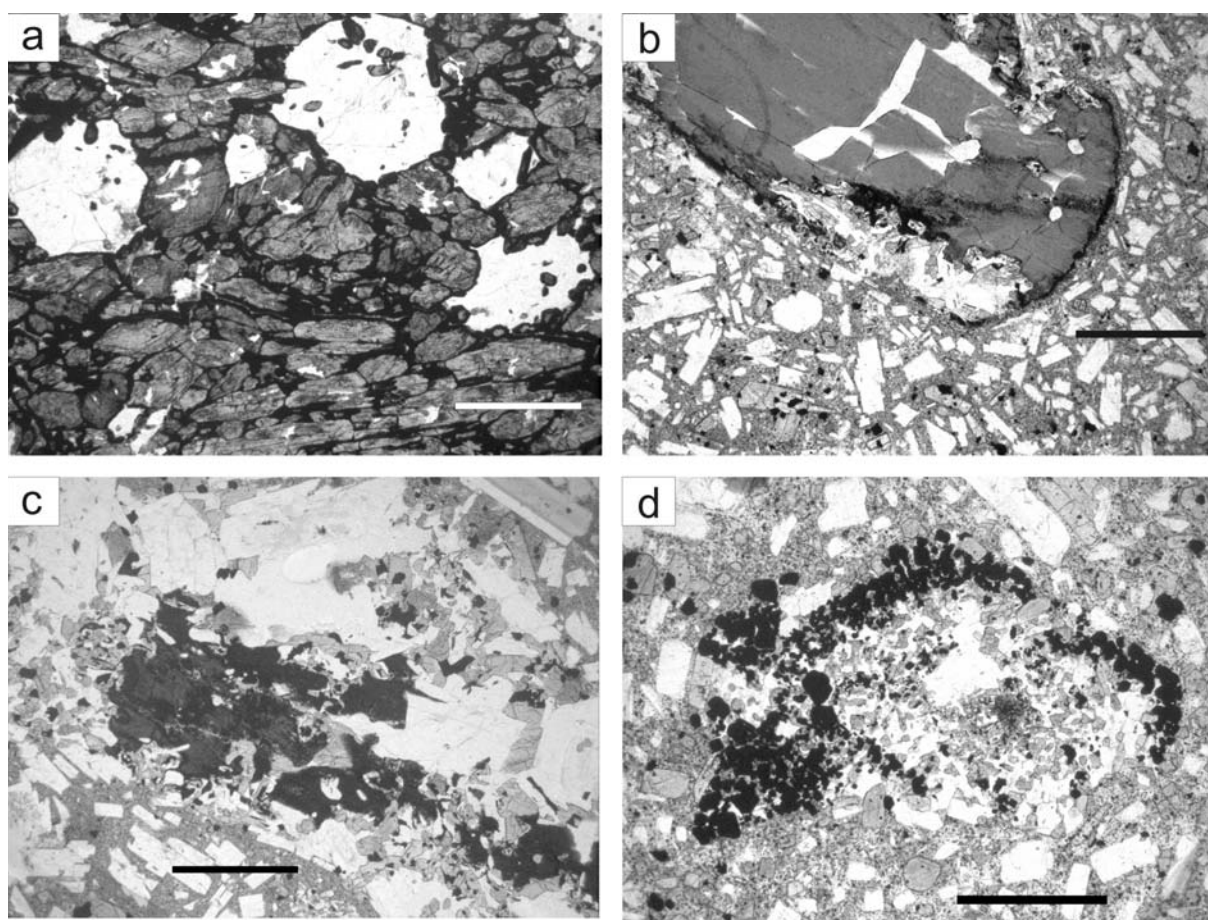


Figure 6: a) Cumulate texture in a gabbroic enclave (NL 120E). Note alignment of dark amphibole crystals and small amphibole inclusions within plagioclase (clear). Amphibole phenocrysts in Longaví magmas are replaced to varying extents by reaction products. b) Fine-grained dusty magnetite amphibole breakdown zone localized along the grain margin. c) More advanced reaction involving extensive replacement of the grain interior. d) Complete replacement of an amphibole grain wherein the original outline of the amphibole is marked by concentrations of oxides. Scale bars = 1 mm.

if they display textures indicative of injection in a molten state and for which whole-rock chemistry can be considered to represent the composition of a magma. 'Plutonic-textured' or 'coarse-grained' enclaves are fragments that were mostly crystalline when incorporated into the host magma, and that do not necessarily correspond to a magma composition (e.g. cumulates).

Quenched mafic enclaves are gray to dark green, fine-grained, crystal-rich (<15% interstitial glass), rounded, and up to 40 cm in diameter. Acicular microphenocrysts of amphibole and plagioclase are set in a vesiculated glassy groundmass that contains smaller orthopyroxene and iron-oxide granules. Plagioclase, pyroxene, and olivine phenocrysts (variably reacted or overgrown) are rare. Whole-rock compositions of quenched enclaves range from 52 to 59 wt% SiO₂, although quenched enclaves in the Holocene dacites are slightly richer in silica (53.8-58.8%) than fine-grained enclaves from the rest of the volcano (52.3-

56.5%). Partially resorbed plagioclase xenocrysts incorporated into quenched enclaves from the host dacite record mixing (Feeley and Dungan, 1996), which causes them to depart to varying degrees from the original liquid composition.

Plutonic textured enclaves are of two main types: 1) biotite and quartz-bearing granitoids, and 2) hornblende-rich gabbroids. Granitoid xenoliths have only been found in the Holocene pumice-fall deposit as accidental ballistic fragments. They are petrologically and chemically similar to Miocene plutons that crop out in this area, and lack evidence of partial melting or other reactions with the juvenile magma despite their fertile mineralogy. Thus, as they probably were ripped from the basement at shallow levels during the explosive eruption and have not participated as contaminants of the magmatic system, they are not considered further.

Gabbroic plutonic-textured enclaves (44-56% SiO₂) are common in the cone-forming and Holocene units, and are very abundant

in certain flows (~5% volume). Plutonic-textured enclaves are rounded or occasionally angular, ranging from less than a centimeter to >30 cm in diameter. They are primarily medium- to coarse-grained hornblende gabbros and pyroxene-hornblende norites and gabbro-norites (nomenclature after Le Maitre, 1989). Gabbroic enclaves are composed of calcic amphibole (pargasite, magnesiohastingsite), calcic plagioclase (An₈₀₋₉₀), less abundant orthopyroxene (En₇₁₋₈₀Wo₁₋₂Fs₂₀₋₂₈), and scarce clinopyroxene (En₄₃₋₄₅Wo₄₅₋₄₇Fs₁₀₋₁₁); olivine (Fo₇₆₋₈₉) is present as rounded cores in some amphiboles. Amphibole is mantled by dehydration coronas that range from opaque margins with irregular interior limits to fine-grained aggregates of clino- and orthopyroxene plus less calcic plagioclase (An_{~40-65}) and iron oxides. These textures are probably due to dehydration reactions and are often associated with grain-boundary partial melting that can represent up to 30% volume in some samples. The grain boundary melts crystallized to plagioclase and pyroxene microlites (±apatite) upon eruption. The most mafic of the coarse-grained enclaves, which display cumulate textures (Figure 6a), are composed of up to 70% amphibole, less than 20% plagioclase and 10% of a probably residual interstitial liquid. Large crystals of interstitial plagioclase commonly contain small amphibole inclusions indicating that amphibole and plagioclase could have co-crystallized. We will show below that the compositions of these amphiboles are indistinguishable within error from those found in Longaví lavas, which suggests that gabbroic enclaves represent cumulates related to the active magmatic system, not fragments of unrelated crust.

WHOLE ROCK CHEMISTRY AND COMPARISON WITH THE SVZ

Nevado de Longaví mafic magmas overlap extensively for major and trace elements with basaltic rocks from both the LOS (Longaví-Osorno Segment) and PTS (Palomo-Tatara Segment; Figure 3). However, for rocks with SiO₂ >56 wt% they display chemical variation trends that are in many ways dissimilar to SVZ volcanoes located to the north and to the south (Figure 7). We stress that Longaví volcano, which lies at the segment boundary in an intermediate geographic position, does not define trends that are intermediate

between typical LOS and PTS lavas, and that this distinction becomes increasingly well defined with increasing SiO₂. Longaví magmas are characterized by: 1) high Al₂O₃, CaO, and Sr contents (Figure 7a-b-c) that lie at the upper limits of both the PTS and LOS data for magmas with >56 wt% SiO₂, 2) correspondingly low TiO₂ and Fe₂O₃ contents (Figure 7d) in mafic and intermediate compositions, 3) moderately high MgO and Cr contents (Figure 7e-f) in intermediate and evolved compositions, and 4) low concentrations of a variety of incompatible element, including P₂O₅, K₂O, LILE, HFSE and REE (Figure 7g-h-i-j) which are most pronounced in intermediate and evolved compositions. In summary, elements that are most compatible with plagioclase and olivine plus Cr-spinel have the highest relative concentrations, whereas elements such as K, which would increase most rapidly in the case of crustal assimilation, are low in Longaví andesites relative to all other SVZ centers.

The generally low abundances of most incompatible elements in Longaví dacites are further illustrated by normalization of comparable silicic magmas from throughout the SVZ to average SVZ basalt (Figure 8, Table 1). Longaví dacites are up to an order of magnitude less enriched in highly incompatible elements like Rb and Th, and exhibit HREE depletions comparable to those in volcanoes underlain by putatively thicker crust (TMS). The closest compositional analog to Longaví dacites comes from Mount Burney volcano (52.6°S), which is located in the Austral Volcanic Zone in a considerably different geological and geodynamic context. Adakitic arc magmas from this part of the Andes have been interpreted as oceanic slab melts (Stern & Kilian, 1996). Although we propose a different interpretation for Longaví volcano, it is worth noting that Longaví dacites have the chemical features that characterize 'adakitic' rocks, including (but not limited to) high La/Yb and Sr/Y ratios.

Two magma series at Nevado de Longaví

The aggregate Longaví data set displays broad, poorly correlated variations in a number of chemical parameters that can be resolved into two series, here referred to as the low- and high-Rb series (Figure 9). The chemical signature that renders Longaví volcano unusual is most clearly manifested in the low-Rb series, whereas high-Rb magmas are closer to typical magmas

Table 1: Major and trace element analyses for selected Nevado de Longaví samples. Major elements were determined by X-ray fluorescence at the University of Lausanne, Switzerland. Values are normalized to 100% anhydrous basis but analytical total (1) is shown. Trace element data were obtained by ICP-MS at Harvard University, USA, except samples from the early units (2), determined by X-ray fluorescence at Lausanne (n.d.= not determined). Reproducibility result for duplicate analysis is better than 5% for all elements.

Series	Low-Rb series							
	Main cone		Holocene					
Unit	Lava		Pumice		Enclave		Dacitic clast (block and ash deposit)	
Sample type	NL009	NL028A	Pomez01	Pomez02	LLLINC.3A	MDCP01.1	LLLB01.3	MADHST-2
Sample code	NL009	NL028A	Pomez01	Pomez02	LLLINC.3A	MDCP01.1	LLLB01.3	MADHST-2
SiO ₂	58.11	59.84	65.78	65.13	53.83	54.32	63.59	64.21
TiO ₂	0.82	0.73	0.52	0.53	0.97	1.02	0.60	0.57
Al ₂ O ₃	18.53	18.39	16.95	17.28	18.27	18.21	17.38	17.33
Fe ₂ O ₃ (t)	6.57	6.18	4.09	4.22	8.33	8.74	4.91	4.67
MnO	0.11	0.11	0.08	0.08	0.13	0.13	0.09	0.09
MgO	3.53	2.86	2.00	2.03	5.27	4.97	2.37	2.23
CaO	6.80	6.17	4.39	4.58	8.99	7.79	5.13	4.92
Na ₂ O	4.43	4.49	4.61	4.62	3.49	3.84	4.46	4.52
K ₂ O	0.86	1.00	1.43	1.36	0.57	0.73	1.28	1.28
P ₂ O ₅	0.23	0.23	0.16	0.17	0.16	0.24	0.18	0.18
Total (1)	99.97	100.36	100.20	100.03	99.47	99.12	99.96	99.57
Nb	3.2	3.6	3.8	3.8	2.6	3.1	3.9	4.4
Zr	98	107	84	83	53	90	88	100
Y	12	12	8	8	17	13	9	9
Rb	14.4	18.2	26.9	25.5	9.2	11.0	23.6	26.5
Sr	671	644	509	523	611	646	592	581
Ba	294	338	454	449	201	235	433	442
Sc	13	12	8	8	30	17	10	9
Cr	34	17	18	24	80	67	30	26
Ni	28	16	18	18	29	31	19	19
La	10.4	11.4	12.4	12.2	9.3	9.8	12.1	13.9
Ce	22.6	26.3	25.4	25.4	23.8	23.0	27.8	32.0
Nd	14.0	15.2	12.2	12.3	14.9	14.6	13.4	15.5
Sm	2.91	3.26	2.22	2.25	3.52	3.32	2.57	2.92
Eu	0.99	1.03	0.75	0.77	1.32	1.14	0.85	0.93
Gd	2.81	2.85	1.96	1.95	3.23	3.22	2.24	2.49
Tb	0.40	0.42	0.30	0.29	0.51	0.45	0.32	0.35
Yb	1.03	1.10	0.61	0.62	1.65	1.11	0.78	0.86
Lu	0.15	0.17	0.09	0.09	0.25	0.17	0.12	0.13
Hf	2.41	2.85	2.23	2.17	1.74	2.41	2.44	2.79
Pb	9.3	13.0	16.1	13.8	7.4	8.3	10.3	11.6
Th	1.09	1.60	2.31	2.21	1.08	0.80	1.38	1.64
U	n.d.	0.4	0.6	0.5	0.3	0.2	0.5	0.6

Table 1: (continued)

Series	High-Rb series									
	Early units (2)			Main cone						Holocene(?)
Unit	Lava			Enclave		Lava			Lava	
Sample type	NL110	NL073	NL078	NL050B	NL050D	NL049	LLG01.4	LMG01.8	NL013	NL014
SiO ₂	51.94	52.75	53.85	53.83	53.99	57.13	58.96	62.22	51.65	52.40
TiO ₂	1.03	1.05	1.02	1.05	1.07	0.82	0.79	0.62	1.07	1.09
Al ₂ O ₃	18.65	18.43	18.33	18.55	18.61	17.82	18.10	17.81	19.43	18.90
Fe ₂ O ₃ (t)	9.24	8.81	8.53	8.43	8.53	7.07	6.53	5.38	8.91	8.81
MnO	0.14	0.13	0.14	0.13	0.14	0.12	0.11	0.10	0.14	0.14
MgO	5.82	5.41	5.03	5.25	5.01	4.63	3.40	2.42	5.13	4.93
CaO	9.05	9.13	8.58	8.12	7.96	7.32	6.63	5.54	9.27	9.22
Na ₂ O	3.16	3.20	3.44	3.59	3.53	3.85	4.10	4.28	3.45	3.47
K ₂ O	0.79	0.89	0.88	0.85	0.93	1.03	1.19	1.44	0.76	0.84
P ₂ O ₅	0.19	0.20	0.21	0.19	0.22	0.21	0.20	0.19	0.20	0.21
Total (1)	99.19	99.27	98.89	100.16	99.98	100.64	99.56	99.83	99.82	100.27
Nb	2.5	2.7	3.1	2.6	3.3	3.7	3.4	4.1	2.6	2.9
Zr	112	118	126	77	93	109	106	126	79	87
Y	16	15	15	14	15	15	12	12	16	17
Rb	10.6	13.8	13.7	18.0	23.2	26.5	33.1	44.0	12.9	15.1
Sr	761	744	714	588	582	586	602	564	797	730
Ba	238	249	264	259	271	318	344	428	184	206
Sc	n.d.	n.d.	n.d.	20	20	17	15	12	21	23
Cr	88	82	70	86	71	97	28	13	134	24
Ni	52	56	39	47	43	50	23	14	35	23
La	9.0	11.0	11.0	8.9	10.0	11.9	12.4	13.8	8.7	9.7
Ce	18.0	20.0	21.0	20.9	23.2	25.9	26.5	30.3	20.9	22.6
Nd	n.d.	n.d.	n.d.	13.3	15.1	15.4	13.4	13.7	14.3	14.9
Sm	n.d.	n.d.	n.d.	2.95	3.50	3.32	2.96	2.73	3.29	3.50
Eu	n.d.	n.d.	n.d.	1.08	1.15	1.10	0.99	0.89	1.10	1.15
Gd	n.d.	n.d.	n.d.	3.14	3.55	3.30	2.97	2.66	3.43	3.47
Tb	n.d.	n.d.	n.d.	0.48	0.49	0.47	0.42	0.39	0.51	0.54
Yb	n.d.	n.d.	n.d.	1.20	1.26	1.39	1.02	1.06	1.48	1.51
Lu	n.d.	n.d.	n.d.	0.18	0.18	0.20	0.15	0.16	0.22	0.23
Hf	n.d.	n.d.	n.d.	1.96	2.20	2.66	2.69	3.07	2.06	2.38
Pb	10.0	11.0	11.0	14.0	6.4	10.6	11.2	14.3	7.2	6.5
Th	5.00	6.00	5.00	1.69	1.69	2.94	3.14	4.28	1.43	1.73
U	n.d.	n.d.	n.d.	n.d.	n.d.	n.d.	n.d.	n.d.	n.d.	0.5

Table 1: (continued)

Series	—		
Unit	Xenoliths		
Sample type	hbl gabbro	hbl-opx norite	px-hbl gabbro norite
Sample code	NL033B	NL015B	NL027B
SiO ₂	50.26	51.00	52.63
TiO ₂	0.99	1.10	0.94
Al ₂ O ₃	19.94	20.57	19.32
Fe ₂ O ₃ (t)	9.46	7.51	8.77
MnO	0.15	0.12	0.14
MgO	5.39	5.59	5.17
CaO	9.60	10.20	8.81
Na ₂ O	3.75	3.49	3.82
K ₂ O	0.24	0.33	0.27
P ₂ O ₅	0.20	0.08	0.14
Total (1)	99.65	99.68	100.07
Nb	2.7	2.7	2.5
Zr	21	25	46
Y	13	17	9
Rb	2.7	4.2	3.7
Sr	745	747	788
Ba	168	183	162
Sc	19	29	20
Cr	37	44	42
Ni	30	48	34
La	8.4	7.8	6.8
Ce	22.1	19.7	16.7
Nd	15.3	15.3	11.3
Sm	3.41	3.77	2.23
Eu	1.22	1.29	0.93
Gd	3.23	3.86	2.14
Tb	0.45	0.58	0.32
Yb	1.23	1.43	0.80
Lu	0.17	0.20	0.12
Hf	0.87	1.03	1.34
Pb	5.9	6.1	6.0
Th	0.64	0.50	0.64
U	n.d.	n.d.	n.d.

at other nearby centers. The low-Rb series is represented by Holocene dacites and andesites, as well as their quenched mafic enclaves, but it also appears in some of the andesitic flows of the main cone. The high-Rb series is more prevalent in basaltic to andesitic lavas from the early units, some cone-forming andesites, and most of their quenched enclaves. The dominant long-term trend at Nevado de Longaví, thus, is a shift from high- to low-Rb magmas. The timing of this transition, however, is unknown, and the degree to which both series coexisted or alternated remains uncertain, but there is some evidence of mixing between the two series in cone-forming andesitic lavas.

The low-Rb series is characterized by systematically lower concentrations of Th, K₂O, Zr and HREE, and less markedly low Nb, Pb, P₂O₅ and LREE contents (Figure 10). Moreover, low-Rb magmas of basaltic andesitic composition (53-56 wt% SiO₂) have Rb, Th and Zr concentrations below the average content of SVZ basalts (<52 wt% SiO₂). As the most mafic low-Rb magmas do not represent primitive magmas (low MgO, Cr), this observation is consistent with parental magmas that also had low concentrations of these elements. Similarly, greater enrichments of fluid-mobile elements relative to less fluid-mobile elements in the low-Rb series (*e.g.* high Ba/Th, Pb/Th, Pb/Zr, and Ba/La; Figure 11a-b) could be inherited from more primitive magmas. Conversely, ratios of elements of similar fluid mobility (Zr/Nb, Zr/La, La/Nb, and Ba/Pb; Figure 11c-d) show similar values in both series and are comparable to values reported for other volcanic centers. Both series also share a sharp increase in Sr/Y and La/Yb ratios with increasing silica, and at evolved compositions show values that are significantly higher than other SVZ volcanoes despite the fact that mafic magmas are comparable (Figure 11e-f). The above suggests that the differences between the two series (and between Nevado de Longaví and the rest of the SVZ) are a consequence of both inheritance from distinct parental magmas and of magmatic evolution.

MINERAL CHEMISTRY: AMPHIBOLE COMPOSITION AND OXYGEN FUGACITY

High modal amphibole proportions in Longaví magmas are the most obvious mineralogical difference with respect to other SVZ volcanic centers. Amphibole is the dominant mafic phase in quenched mafic enclaves (up to

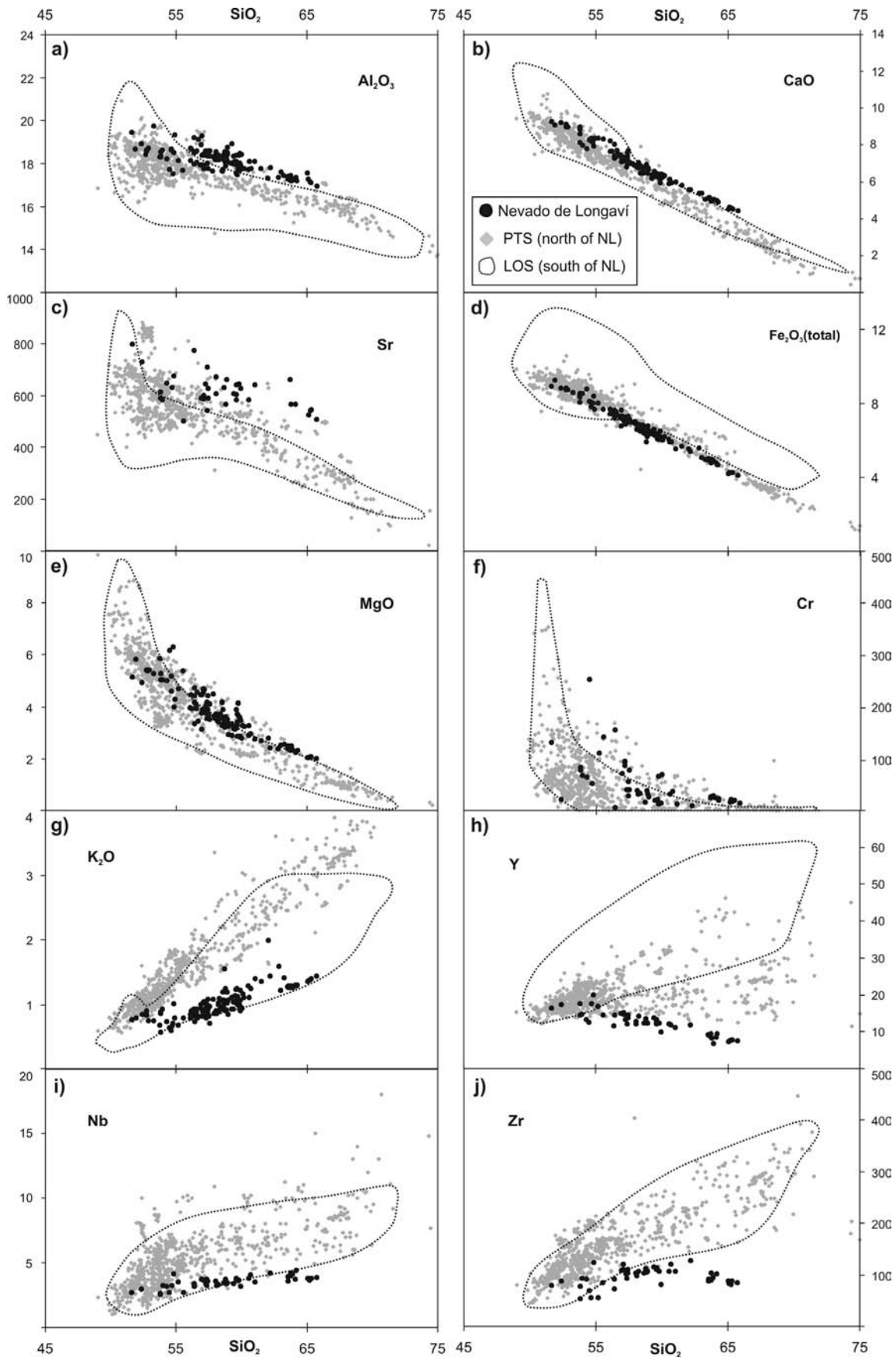


Figure 7: Major and trace element variations as a function of wt% SiO₂. The data base used as reference includes 383 analyses from the LOS and 910 from the PTS (Fig. 3), 638 of which are from the Tatara-San Pedro complex. Data include literature analyses (various references in text) as well as unpublished data from ongoing projects at the University of Geneva.

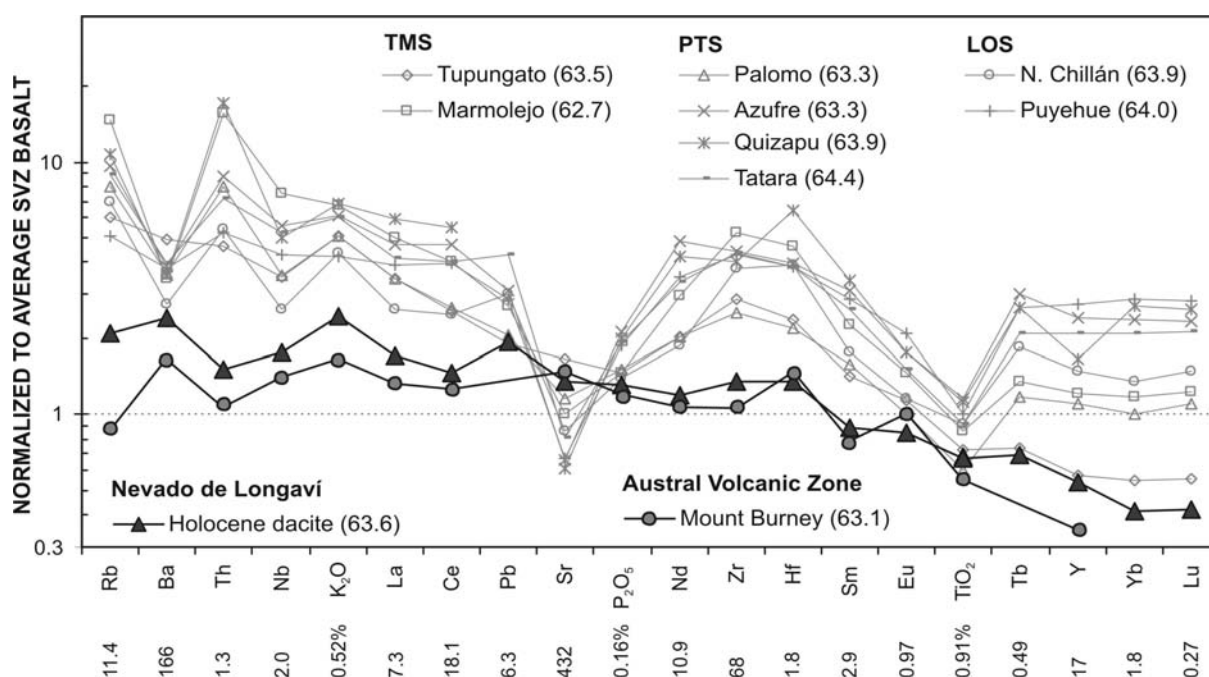


Figure 8: Nevado de Longaví dacites compared to rocks with similar SiO_2 contents in the SVZ (numbers in parenthesis are SiO_2 content in an anhydrous basis). All analyses normalized to an average composition of 32 SVZ basalts (<52% SiO_2 ; normalizing values shown at the base of the diagram). Note that Longaví dacites have lower concentrations of all these elements, except Sr. Note also that a dacite from Mt. Burney (Austral Volcanic Zone; Stern & Kilian, 1996) exhibits a similar pattern.

30 vol%) and in dacites (7-10 vol%), and it is commonly present in andesites of both magma series. In neighboring centers amphibole first appears in rocks with >60 wt% SiO_2 and it is never as abundant as it is at Nevado de Longaví. Amphibole phenocrysts in high-Rb andesites commonly show disequilibrium textures in which amphibole is reacted to fine-grained aggregates of plag +px +opaques (Figure 6b-c-d). Microprobe analyses of amphiboles from a wide range of whole-rock compositions at Nevado de Longaví are presented in Figure 12, including core analyses from reacted phenocrysts. Important things to notice from these diagrams are: 1) the general distribution into high-Al/Si and low-Al/Si population, plus a less well defined group of transitional character, 2) the nearly identical compositions of amphiboles from low- and high-Rb series andesites, as well as the gabbroic enclaves, and 3) the bimodal distribution of amphiboles from Holocene dacites, in which low-Al/Si amphibole compositions correspond to rims of phenocrysts and cores are high-Al/Si. Amphibole crystals from gabbroic enclaves have compositions that completely overlap those from the lavas, which suggests that gabbroic enclaves are cumulates fractionated from evolving batches of magmas.

Temperature and $f\text{O}_2$ conditions for the magmas have been estimated from microprobe

analyses of magnetite-ilmenite pairs. Coexisting grains were analyzed in two dacitic samples and a low-Rb quenched mafic enclave, in addition to two andesites from the high-Rb series. Temperature and $f\text{O}_2$ (Figure 13) were obtained by the algorithms of Andersen *et al.* (1993) using QUILF95 software for oxide pairs that satisfy the empirical Mg/Mn partitioning test of Bacon and Hirschmann (1988). The dacitic samples record the highest $f\text{O}_2$ (NNO+2) and extend to high temperatures around 880°C. These temperatures, however, might need a temperature correction of -30°C whenever high oxygen fugacities are involved (Rutherford & Devine, 1996). Oxide grains in the quenched enclaves record slightly lower temperatures and less oxidizing conditions than the dacite, and probably represent post-mingling conditions because of the late appearance of these phases. The two high-Rb andesite samples record less oxidizing conditions (<NNO+1) than the low-Rb magmas. Although data are still limited, oxidation state may well be another important difference between the two series.

DISCUSSION

Amphibole is commonly present in andesites throughout the volcano, but is especially abundant in the low-Rb series (54-

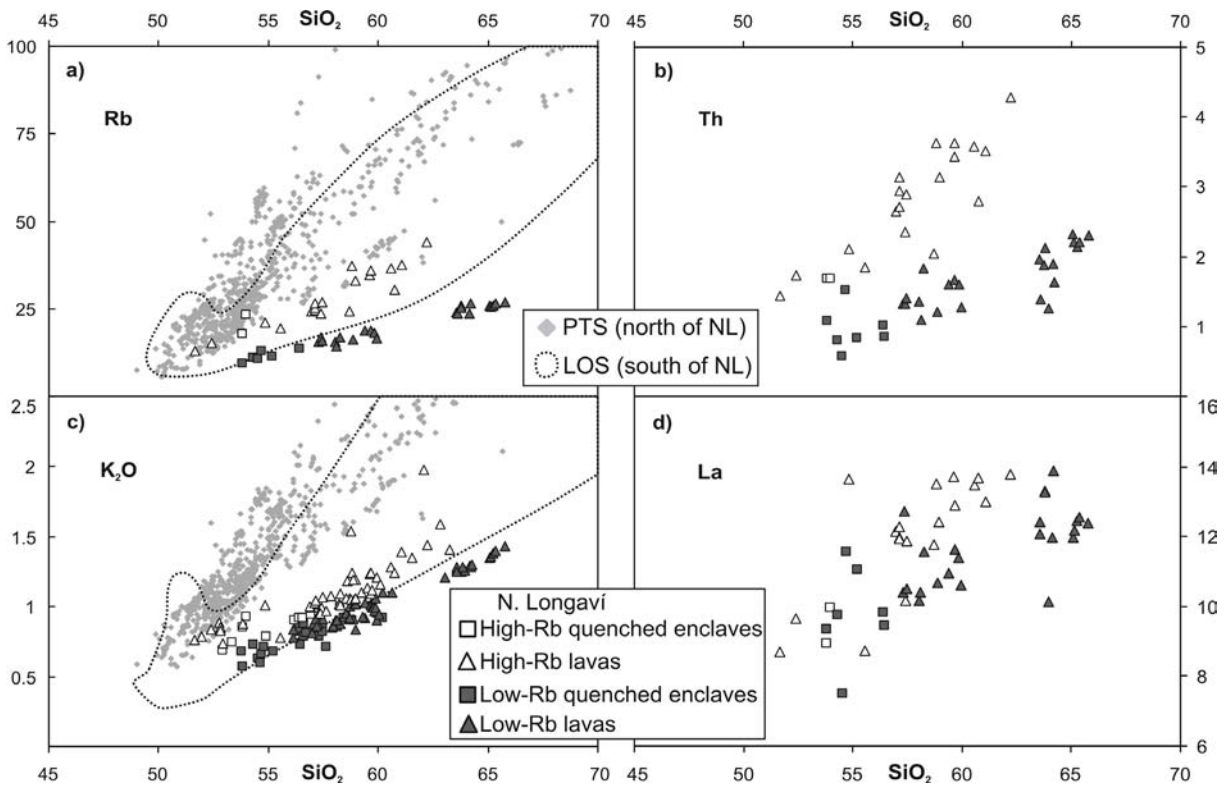


Figure 9: Distinction between the low-Rb and high-Rb series at Nevado de Longaví volcano. This distinction is particularly clear for Rb vs. silica (a), but the two groups are also clearly distinguished on the basis of Th (b) and K₂O (c), and less clearly for La (d). Note that the low-Rb series diverges from the SVZ data field (a-c).

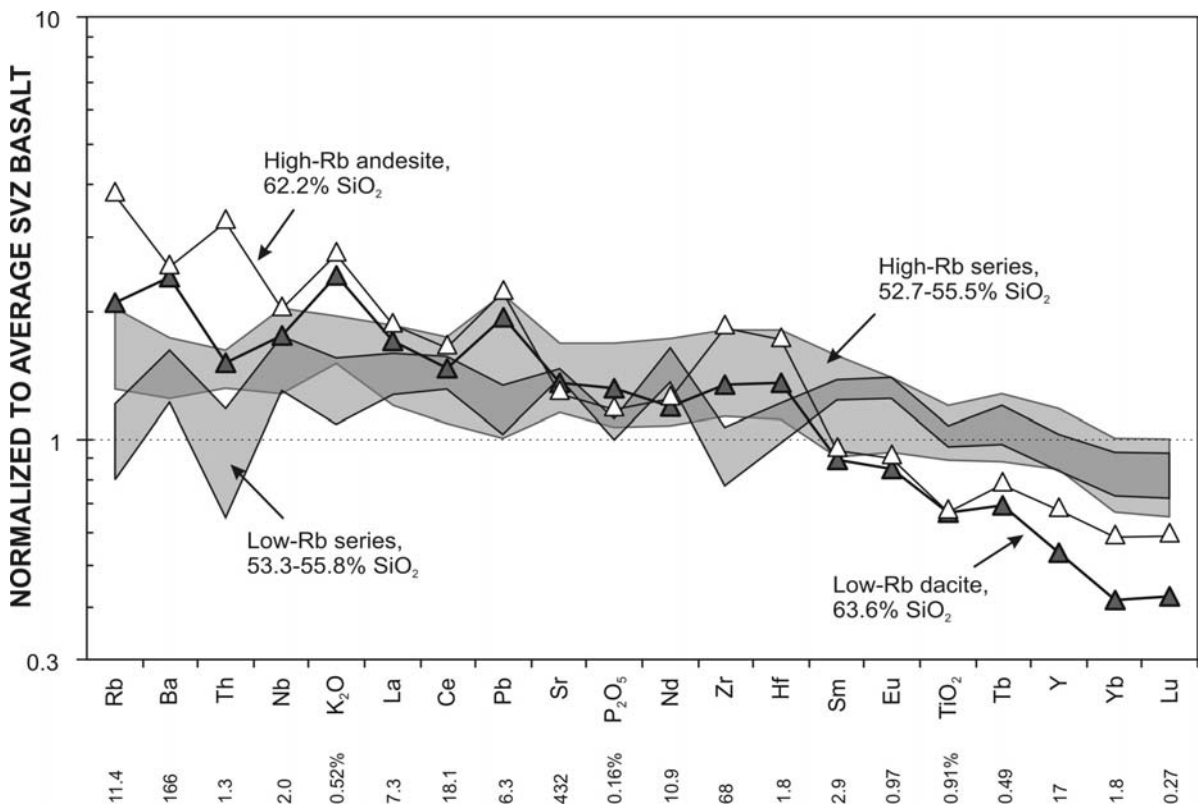


Figure 10: Comparisons of high-Rb and low-Rb magmas (normalization as in Fig. 8). Individual analyses of evolved magmas are shown by triangles and lines, whereas shaded areas enclose bulk composition of basaltic andesitic magmas. Note that both evolved and mafic low-Rb magmas have noticeably lower abundances of Rb, Th, K₂O, Zr, and HREE despite their slightly higher silica content.

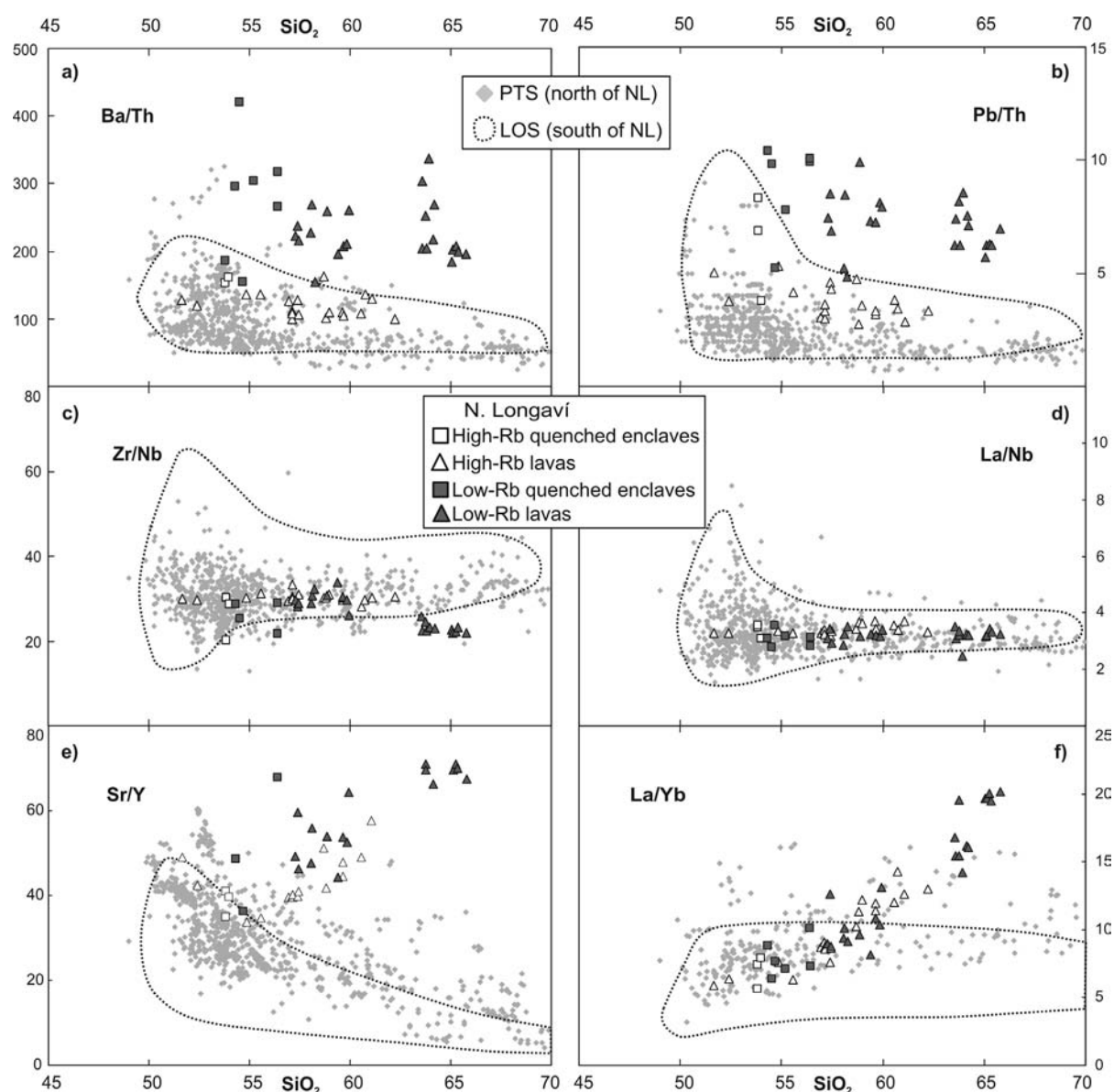


Figure 11: Trace element ratios versus silica content for Nevado de Longaví magmatic series compared to PTS and LOS segments. Note that in (a) and (b) only low-Rb magmas fall outside the range of values of LOS+PTS; in (c) and (d) both series are within the range, and in (e) and (f) both series diverge from reference values.

65 wt% SiO_2). Amphibole is, moreover, the dominant mafic phase in the Holocene dacites and mafic enclaves, wherein clinopyroxene is absent. Amphibole crystallization requires high H_2O contents in host magmas (e.g. Rutherford & Devine, 1988), and amphibole proportions can correlate with water contents (e.g. Müntener *et al.*, 2001). Calcic plagioclase (An_{80-90}) crystallized in part simultaneously with amphibole as is recorded in gabbroic cumulates; low-pressure, less calcic plagioclase, however, was probably not largely removed from the magma as is indicated by the positive Al_2O_3 and Sr anomalies in Longaví dacites. Suppression of early plagioclase crystallization and a shift towards more calcic compositions is indicative of high water contents (Sisson & Grove, 1993; Grove *et al.*, 1997), and high mobile-to-immobile

element ratios (Ba/Th, Pb/Th) in the low-Rb series is consistent with the water being derived from the subducting slab.

Accumulation of amphibole in enclaves thought to be residual cumulates suggests that, unlike elsewhere in the SVZ, amphibole may be playing a major role in the evolution of Longaví magmas. Amphibole phenocryst cores have SiO_2 contents of 41 to 44 wt%, much lower than the silica contents of clinopyroxene (47-53 wt%) or orthopyroxene (50-55 wt%), thus amphibole fractionation has a higher potential to raise the silica content of the remaining liquid than pyroxene-dominated assemblages. This further implies that liquids derived by fractionation of amphibole-rich assemblages would have a less pronounced increase in the abundance of

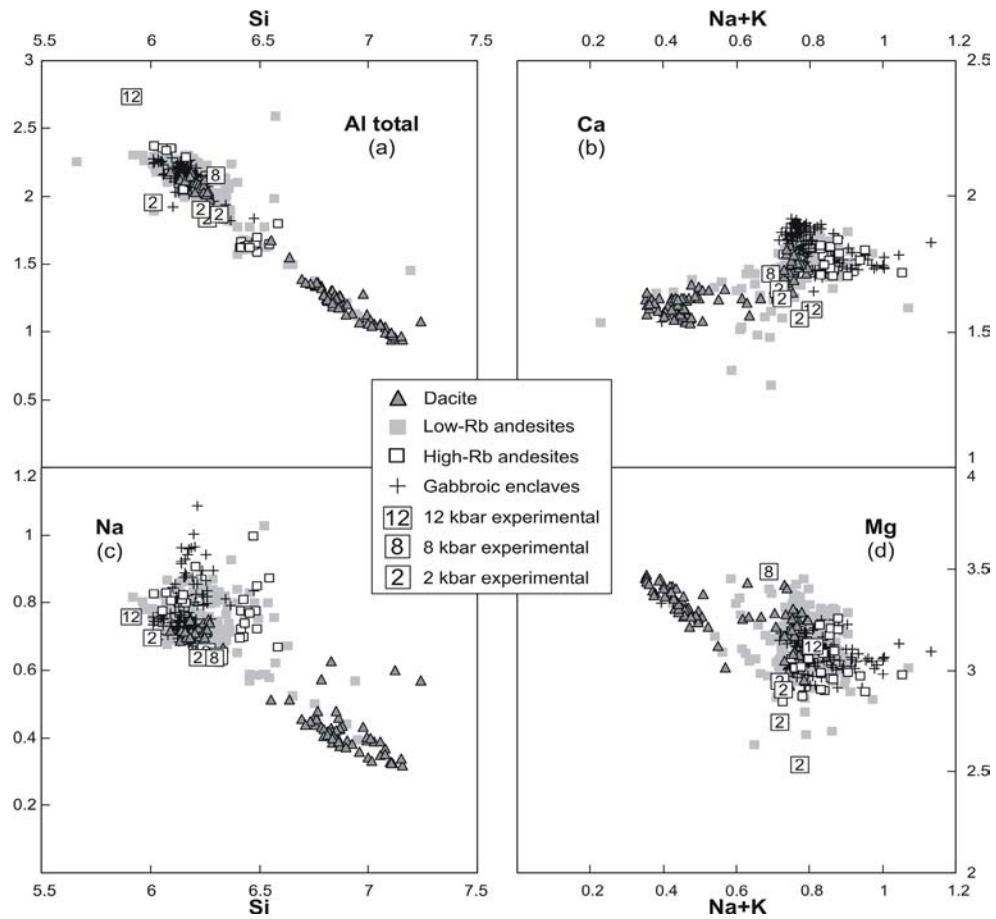
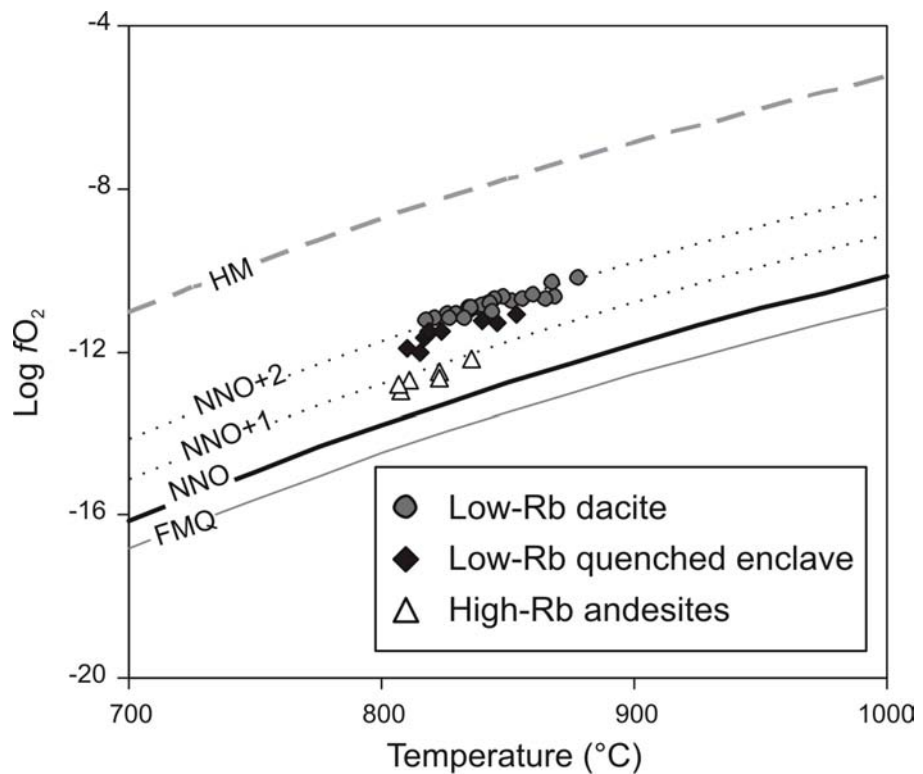


Figure 12: Chemical compositions of amphiboles in lavas, pyroclastic units and gabbroic enclaves from Nevado de Longaví. Values are in cations per formula unit calculated on a 13-cation basis. Also included for comparison are the chemical compositions of amphiboles crystallized in experiments (12 kbar experiment from Müntener *et al.*, 2001; 8 kbar experiment from Grove *et al.*, 2003; 2 kbar experiments from Grove *et al.*, 1997 and Grove *et al.*, 2003).

Figure 13: Temperature versus oxygen fugacity data from magnetite-ilmenite pairs calculated on the basis of the Andersen *et al.* (1993) algorithm. Oxygen fugacity buffers are FMQ= fayalite-magnetite-quartz; NNO= nickel-nickel oxide; HM= hematite-magnetite.



incompatible elements than liquids derived by fractionation of an anhydrous assemblage.

Large compositional changes in residual liquids due to amphibole crystallization have been documented at Medicine Lake volcano, where the compositional gap between andesites and rhyolites (62-72 wt% SiO₂) was modeled by fractionation of amphibole-rich (17 wt%) assemblages (Grove & Donnelly-Nolan, 1986). What distinguishes Nevado de Longaví is that the proportion of fractionating amphibole might be substantially higher and that this phase starts crystallizing at much less evolved compositions. We have performed a simple mass balance test to calculate the major oxide compositions of residual magmas derived by fractionation of amphibole and An₈₅ plagioclase, using the average compositions of the minerals from gabbroic enclaves. Taking a quenched mafic enclave (53.8 wt% SiO₂) as the parental composition, 50% fractionation of 50% amph, 37% plag, 3% cpx, 7% opx, and 3% magnetite is able to produce a residual liquid with 63 wt% SiO₂ and a major element composition similar to Longaví dacites. If incompatible elements are enriched in the residual melt following the Rayleigh fractional crystallization equation $C_r/C_0 = F^{D-1}$ (where F is the fraction of remaining liquid and D is the bulk partition coefficient), then a perfectly incompatible element (D=0) will be concentrated in the liquid by a factor of 1/F relative to the original concentration. Removal of 50% of an amphibole-rich assemblage implies that elements with bulk D~0 will be enriched by a maximum factor of 2 (F=0.5), which is in good agreement with the observed enrichments for highly incompatible elements such as Rb, Th, U, Zr, and Nb (e.g. Figure 10). As a comparison, low-pressure fractionating assemblages such as those proposed for Villarrica volcano and the Planchón-Peteroa complex (Hickey-Vargas *et al.*, 1989; Tormey *et al.*, 1995), involving greater amounts of plagioclase, and pyroxenes and no amphibole, requires 65 to 75% fractionation to achieve the same silica increase, and incompatible elements would be enriched by factors of 3 to 4.

Crystallization of amphibole from relatively mafic magmas has been documented experimentally wherein starting materials are water-rich (up to water saturated) basalts and basaltic andesites (e.g. Grove *et al.*, 1997; Moore & Carmichael, 1998; Müntener *et al.*, 2001; Grove *et al.*, 2003), with a wide range of pressures from 2 to 20 kbar and fO_2 between NNO and NNO+4.

Amphibole has crystallized in high proportions in experiments wherein starting materials are hydrated arc basalts. For example, at 8 kbar and with a water-saturated high-Mg basalt as starting material, modal amphibole is 60 vol% only 25°C below the liquidus temperature, in equilibrium with basaltic andesitic glass (run 373; Grove *et al.*, 2003). At the same pressure, plagioclase is also inferred to join at lower temperatures. In higher pressure experiments (12 kbar), Müntener *et al.* (2001) obtained trace amounts of garnet (0.1%) in addition to amphibole and pyroxene from a basaltic starting material with ~5 wt% H₂O added.

Fractionation of a hornblende-rich assemblage from very hydrous magmas may thus account for some of the chemical characteristics of intermediate to evolved compositions, but it does not explain the low incompatible element abundances observed in the most mafic quenched magmatic enclaves and in their inferred parental magmas. Fluid-mobile elements such as Ba and Pb are interpreted in arc settings to be mostly supplied by fluids derived from dehydration of the subducted slab and/or sediments, whereas the concentration of less soluble elements like Th, Nb, and Zr will be largely controlled by their concentrations in the mantle source and the degree of melting (e.g. Davidson, 1996). Relative enrichments of fluid-mobile elements in the low-Rb series (higher Ba/Th, Ba/La, Pb/Th, and Rb/Zr ratios than in the high-Rb series), may reflect that the proportion of slab-derived fluids involved in the genesis of low-Rb parental magmas is higher than in those parental to high-Rb magmas. In contrast, similar Zr/Nb, Zr/La, and La/Nb ratios in both series argue in favor of a similar mantle source for both magma types. An expected consequence of enhanced water supply to the mantle source region is higher degrees of melting (Hickey-Vargas *et al.*, 1989; Asimow & Langmuir, 2003; Katz *et al.*, 2003), and hence, the resulting primitive liquids will be less enriched in non-fluid mobile incompatible elements than lower degree melts from the same source. If high-degree wet melts are parental to low-Rb quenched mafic enclaves, important olivine + pyroxene fractionation must be invoked in order to explain the relatively low concentrations of Mg, Ca and Sc observed in these enclaves. High-pressure olivine and pyroxene fractionation is the main mechanism inferred for the generation of SVZ basalts from primitive mantle-derived melts.

La/Yb and Sr/Y increases with increasing silica in both series are due to a decrease in concentrations of HREE and Y by a factor of ~0.5 within the range of 53 to 63 wt% SiO₂. If crystal fractionation is responsible for these depletions, bulk partition coefficients for HREE and Y must be in the neighborhood of 2 to 2.3. Assuming that amphibole constitutes 50% of the fractionating assemblage and F=0.5, in concert with the major element model, amphibole/liquid partition coefficients for Y and Yb should be around 4 and 4.3 respectively to account for the observed variations. Measured amphibole/melt partition coefficients for Y and Yb in calcalkaline magmas are within the range of 1.0-2.1 (e.g. Bacon & Druitt, 1988; Sisson 1994; Brenan *et al.*, 1995; Klein *et al.*, 1997), although at high pressures (12 kbar) and relatively low temperatures (~980°C) coefficients up to 3.4 for Y have been measured (Blundy, *pers. comm.*). It seems likely, therefore, that high La/Yb related to decreasing HREE in Longaví volcano magmas is in part due to garnet fractionation. Increasing La/Yb and Sr/Y are also observed in the high-Rb series, where amphibole appears to be a less abundant fractionating phase. An important corollary to this observation is that most of the evolution of Longaví magmas may have occurred at depths where garnet is stable in hydrous calcalkaline magmas (>~8 kbar; Ulmer *et al.*, 2003), and that little differentiation is taking place at the upper crustal levels.

Are oceanic fractures playing a role?

There are good reasons to suspect that the asthenospheric mantle below Longaví volcano may be supplied with unusual amounts of water. The horizontal projection of the Mocha Fracture Zone beneath the continent intersects the volcanic front in the vicinity of Longaví volcano. Oceanic fractures are a potentially very efficient means for transporting water into the asthenospheric mantle because they commonly host serpentinitic bodies deep into the oceanic lithosphere. Fully serpentinitized oceanic lithosphere can contain up to 11-13 wt% H₂O, *i.e.*, it is an order of magnitude more efficient in liberating H₂O at depth than hydrous minerals from altered oceanic crust (Ulmer & Trommsdorff, 1995). Singer *et al.* (1996) proposed that in the Aleutian arc the Amlia fracture zone acts as a transport of fluids and trench sediments into the subarc mantle, and that as a consequence, overlying volcanoes

erupt lavas derived from high melting degrees and with high fluid-mobile element concentrations.

Oceanic fracture zones are currently being subducted at other points along the arc, and are likely to be exerting a similar role to what is inferred to be happening at Longaví volcano (Figure 1). It is possible that the evolved products from the Mocho-Choshuenco complex and Calbuco volcano, located over the projections of the Valdivia and Chiloé fracture zones respectively, constitute somewhat similar cases to Longaví volcano. Both of these centers have erupted evolved rocks that contain amphibole and in which the behavior of incompatible element abundances and ratios is also similar to what is observed at Longaví volcano (Figure 14), although crustal contamination has been identified for magmas from both of these centers (McMillan *et al.*, 1989; López-Escobar *et al.*, 1992; Hickey-Vargas *et al.*, 1995). The incompatible element-poor nature of the andesites from Calbuco volcano has been suggested by López-Escobar *et al.* (1995b) to be a consequence of fractionation of hornblende-rich assemblages. They propose that the water needed to stabilize amphibole in the system is derived from the assimilation of hydrous, metasedimentary crust, which is in agreement with the relatively high Sr isotope ratios observed, but is contradicted by the low abundances of incompatible elements that characterize the volcanic suite. The fact that these volcanoes do not show significant Y depletions (and hence, low Sr/Y ratios) might be related to differences in crustal thickness, where garnet stability is not attained further south.

SUMMARY AND CONCLUSIONS

Nevado de Longaví magmas show a number of mineralogical and chemical features that make them distinctive from other SVZ magmas. Elevated water supply to the mantle source region is consistent with most first-order features that characterize Longaví magmas. The recognition of two magmatic series present at Longaví volcano suggests that magma generation conditions have not been stable through time, although the timing of transition from one series to the next is unconstrained. The low incompatible element abundances that characterize Longaví evolved magmas, and especially the low-Rb series, is probably the

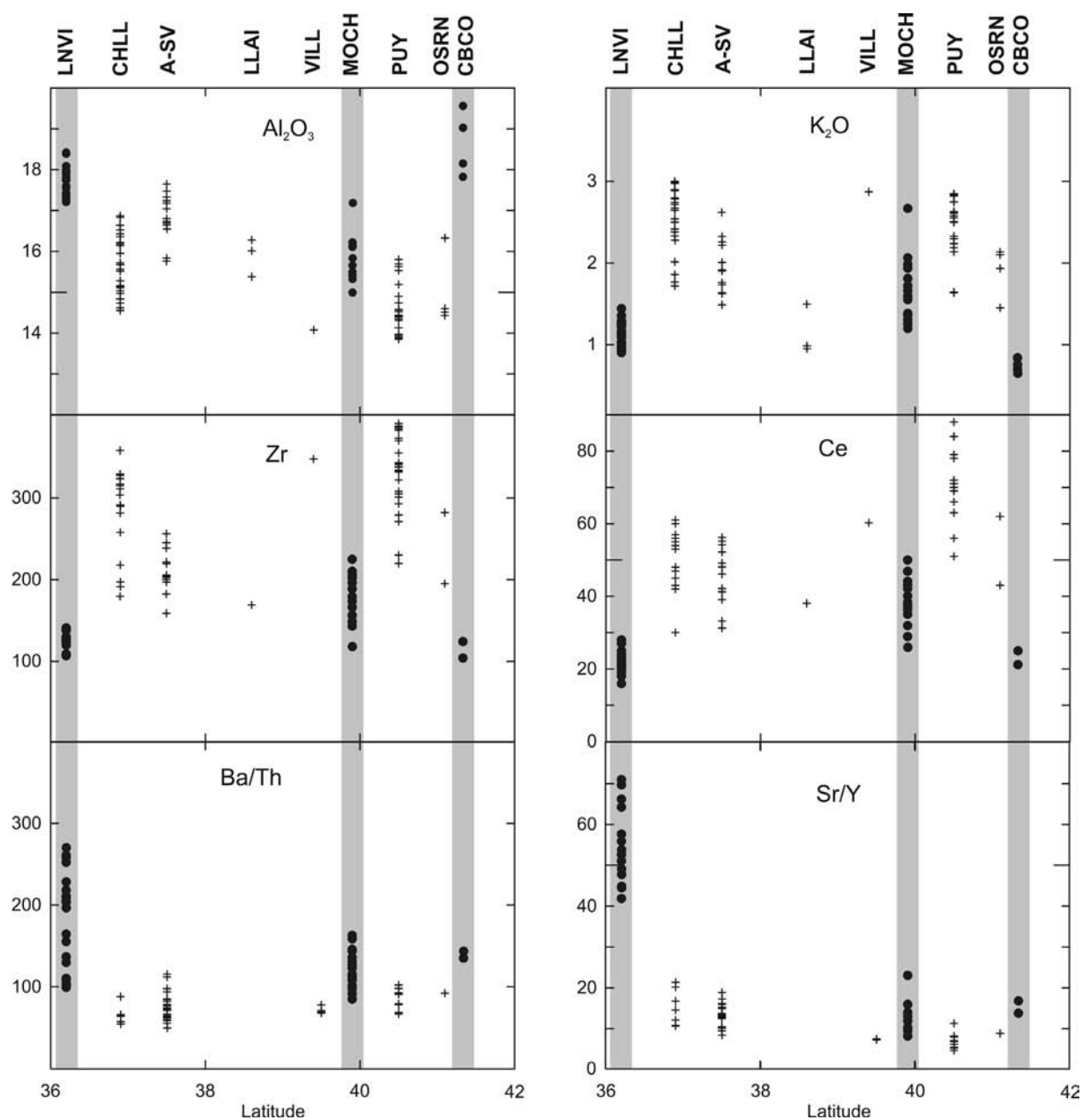


Figure 14: Compositions of rocks with $58\% < SiO_2 < 65\%$ versus latitude for centers south of Longaví volcano. LNV: Nevado de Longaví, CHLL: Nevados de Chillán, A-SV: Antuco-Sierra Velluda, LLAI: Llaima, VILL: Villarica, MOCH: Mocho-Choshuenco, PUY: Puyehue, OSRN: Osorno, CBO: Calbuco. Highlighted volcanoes correspond to those located over oceanic fracture zones (see Fig. 1).

result of fractionation of low- SiO_2 amphibole in much higher proportions than in other SVZ centers. Genesis of low-Rb mafic magmas is explained in terms of high degrees of melting of a mantle source in response to high fluid inputs coming from the slab. High-Rb andesitic magmas are less markedly distinct from other SVZ magmas, and may have evolved from less hydrous primitive melts. We propose that the oceanic Mocha Fracture Zones is responsible for the high water supply to the subarc mantle beneath Nevado de Longaví, and that oceanic fractures subducted further south could be influencing in a similar way the composition of magmas from other volcanoes in the SVZ.

ACKNOWLEDGEMENTS

Work for this project is financed by the Swiss Fonds National grant #2000-063950.00. D.S. benefited in 2001-2003 from a fellowship from the Swiss Confederation. Sue Kay, Wes Hildreth, and Leopoldo López-Escobar are sincerely acknowledged for constructive reviews that greatly helped improve the paper. We thank SERNAGEOMIN for logistical support provided during field work. F. Costa, G. Morris, A. Marzoli and R. Spikings made helpful revisions of early versions of the manuscript.

REFERENCES

- Andersen, D., Lindsley, D. and Davidson, P. (1993). *QUILF: a Pascal program to assess equilibria among the Fe-Mg-Mn-Ti oxides, pyroxenes, olivine, and quartz*. Computers and Geosciences **19**: 1333-1350.
- Asimow, P.D. and Langmuir, C.H. (2003). *The importance of water to oceanic mantle melting regimes*. Nature **421**: 815-820.
- Bacon, C.R. and Druitt, T.H. (1988). *Compositional evolution of the zoned calc-alkaline magma chamber of Mt. Mazama, Crater Lake, Oregon*. Contributions to Mineralogy and Petrology **98**: 224-256.
- Bacon, C. and Hirschmann, M. (1988). *Mg/Mn partitioning as a test for equilibrium between coexisting Fe-Ti oxides*. American Mineralogist **73**: 57-61.
- Bohm, M., Lüth, S., Echtler, H., Asch, G., Bataille, K., Bruhn, C., Rietbrock, A. and Wigger, P. (2002). *The Southern Andes between 36° and 40°S latitude: seismicity and average seismic velocities*. Tectonophysics **356**: 275-289.
- Brenan, J.M., Shaw, H.F., Ryerson, F.J. and Phinney, D.L. (1995). *Experimental determination of trace element partitioning between pargasite and a synthetic hydrous andesitic melt*. Earth and Planetary Science Letters **135**: 1-11.
- Davidson, J.P. (1996). *Deciphering mantle and crustal signatures in subduction zone magmatism*. In G. Bebout, S. Kirby, D. Scholl, and J. Platt (eds.). *Subduction from Top to Bottom*. American Geophysical Union, Washington D.C. Monograph **96**: 251-262.
- Davidson, J.P., Dungan, M.A., Ferguson, K.M. and Colucci, M.T. (1987). *Crust-magma interactions and the evolution of arc magmas; the San Pedro-Pellado volcanic complex, southern Chilean Andes*. Geology **15**: 443-446.
- Dungan, M.A., Wulff, A. and Thompson, R. (2001). *Eruptive stratigraphy of the Tatara-San Pedro complex, 36°S, Southern Volcanic Zone, Chilean Andes: Reconstruction method and implications for magma evolution at long-lived arc volcanic centers*. Journal of Petrology **42**(3): 555-626.
- Feeley, T.C. and Dungan, M.A. (1996). *Compositional and dynamic controls on mafic-silicic magma interactions at continental arc volcanoes: evidence from Cordón El Guadal, Tatara-San Pedro Complex, Chile*. Journal of Petrology **37**(6): 1547-1577.
- Futa, K. and Stern, C. (1988). *Sr and Nd isotopic and trace element compositions of Quaternary volcanic centers of the southern Andes*. Earth and Planetary Science Letters **88**: 253-262.
- Gardeweg, M. (1980). *Geología del área del Nevado de Longaví. Cordillera de Los Andes - VII Región del Maule*. Unpublished Thesis, 247 pp. Universidad de Chile, Santiago.
- Gardeweg, M. (1981). *El volcanismo Cenozoico Superior del área del Nevado de Longaví: una zona de transición en los Andes de Chile central*. VIII Congreso Geológico Argentino, San Luis, Argentina. Actas III: 221-240.
- Grove, T.L. and Donnelly-Nolan, J.M. (1986). *The evolution of young silicic lavas at Medicine Lake volcano, California: implications for the origin of compositional gaps in calc-alkaline series lavas*. Contributions to Mineralogy and Petrology **92**: 281-302.
- Grove, T.L., Donnelly-Nolan, J.M. and Housh, T. (1997). *Magmatic processes that generated the rhyolite of Glass Mountain, Medicine Lake volcano, N. California*. Contributions to Mineralogy and Petrology **127**: 205-223.
- Grove, T.L., Elkins-Tanton, L.T., Parman, S.W., Chatterjee, N., Müntener, O. and Gaetani, G.A. (2003). *Fractional crystallization and mantle-melting controls on calc-alkaline differentiation trends*. Contributions to Mineralogy and Petrology **145**: 515-533.
- Herron, E.M. (1981). *Chile margin near lat. 38°S: Evidence for a genetic relationship between continental and marine features or a cause of curious coincidences?* in L. D. Kulm, J. Dymond, E. J. Dasch and D. M. Hussong (eds.). *Nazca Plate: crustal formation and andean convergence*. GSA Memoir. **154**: 755-760.
- Hickey, R.L., Gerlach, D.C. and Frey, F.A. (1984). *Geochemical variations in volcanic rocks from central-south Chile (33-42°S)*. In Harmon, R.S. and Barreiro, B.A. (eds.). *Andean magmatism, chemical and isotopic constraints*. Shiva Publishing Ltd., Cheshire. 72-95.
- Hickey-Vargas, R., Moreno, H., López, L. and Frey, F.A. (1989). *Geochemical variations in Andean basaltic and silicic lavas from the Villarica-Lanin volcanic chain (39.5°S): an evaluation of source heterogeneity, fractional crystallization and crustal assimilation*.

- Contributions to Mineralogy and Petrology **103**: 361-386.
- Hickey-Vargas, R., Abdollahi, M.J., Parada, M.A., López-Escobar, L. and Frey, F.A.** (1995). *Crustal xenoliths from Calbuco volcano, Andean Southern Volcanic Zone: implications for crustal composition and magma-crust interaction*. Contributions to Mineralogy and Petrology **119**: 331-344.
- Hildreth, W. and Moobath, S.** (1988). *Crustal contributions to arc magmatism in the Andes of Central Chile*. Contributions to Mineralogy and Petrology **98**: 455-489.
- Hildreth, W. and Moobath, S.** (1991). *Reply to Comment on "Crustal contributions to arc magmatism in the Andes of Central Chile" by W. Hildreth and S. Moorbath*. Contributions to Mineralogy and Petrology **108**: 247-252.
- Katz, R., Spiegelman, M. and Langmuir, C.H.** (2003). *A New parameterization of hydrous mantle melting*. Geochemistry Geophysics Geosystems (G-cubed) **4**(9): 1073 doi:10.1029/2002GC000433.
- Klein, M., Stosch, H.G. and Seck, H.A.** (1997). *Partitioning of high-strength and rare-earth elements between amphibole and quartz-dioritic to tonalitic melts: an experimental study*. Chemical Geology **138**: 257-271.
- Le Maitre, R.W.** (editor). (1989). *A classification of igneous rocks and glossary of terms. Recommendations of the International Union of Geological Sciences, Subcommittee on the Systematics of Igneous Rocks*. Blackwell Scientific Publications, Oxford, 193 p.
- López-Escobar, L.** (1984). *Petrology and chemistry of volcanic rocks of the southern Andes*. In Harmon, R.S. and Barreiro, B.A. (eds.). *Andean magmatism, chemical and isotopic constraints*. Shiva Publishing Ltd., Cheshire. 47-71.
- López-Escobar, L., Parada, M.A., Moreno, H., Frey, F.A. and Hickey-Vargas, R.L.** (1992). *A contribution to the petrogenesis of Osorno and Calbuco volcanoes, Southern Andes (41°00'-41°30'S): comparative study*. Revista Geológica de Chile **19**(2): 211-226.
- López-Escobar, L., Kilian, R., Kempton, P.D. and Tagiri, M.** (1993). *Petrography and geochemistry of Quaternary rocks from the Southern Volcanic Zone of the Andes between 41°30' and 46°00'S, Chile*. Revista Geológica de Chile **20**(1): 33-55.
- López-Escobar, L., Cembrano, J. and Moreno, H.** (1995a). *Geochemistry and tectonics of the Chilean Southern Andes basaltic Quaternary volcanism (37-46°S)*. Revista Geológica de Chile **22**(2): 219-234.
- López-Escobar, L., Parada, M.A., Hickey-Vargas, R., Frey, F.A., Kempton, P.D. and Moreno, H.** (1995b). *Calbuco volcano and minor eruptive centers distributed along the Liquiñe-Ofqui Fault Zone, Chile (41°-42°S): contrasting origins of andesitic and basaltic magma in the Southern Volcanic Zone of the Andes*. Contributions to Mineralogy and Petrology **119**: 345-361.
- McMillan, N.J., Harmon, R.S., Moorbath, S., López-Escobar, L. and Strong, D.F.** (1989). *Crustal sources involved in continental arc magmatism: a case study of volcán Mocho-Choshuencho, southern Chile*. Geology **17**: 1152-1156.
- Moore, G. and Carmichael, I.S.E.** (1998). *The hydrous phase equilibria (to 3 kbar) of an andesite and basaltic andesite from western Mexico: constraints on water content and conditions of phenocryst growth*. Contributions to Mineralogy and Petrology **130**: 304-319.
- Muñoz, J. and Niemeyer, C.** (1984). *Hoja Laguna del Maule, Regiones del Maule y del Bío Bío*. Carta Geológica de Chile **64**, SERNAGEOMIN, Santiago. Map scale 1:250.000 and accompanying booklet, 97 p.
- Müntener, O., Kelemen, P.B. and Grove, T.L.** (2001). *The role of H₂O during crystallization of primitive arc magmas under uppermost mantle conditions and genesis of igneous pyroxenites: an experimental study*. Contributions to Mineralogy and Petrology **141**: 643-658.
- Naranjo, J.A. and Haller, M.J.** (2002). *Erupciones holocenas principalmente explosivas del volcán Planchón, Andes del sur (35°15'S)*. Revista Geológica de Chile **29**(1): 93-113.
- Ruiz, J., Hildreth, W. and Chesley, J.** (2001). *Crust-mantle contributions to Andean magmas*. III Simposio Sudamericano de Geología Isotópica, Pucón. 340-341.
- Rutherford, M.J. and Devine, J.D.** (1988). *The may 18, 1988 eruption of Mt. St. Helens 3. Stability and chemistry of amphibole in the magma chamber*. Journal of Geophysical Research (93): 11949-11959.
- Rutherford, M.J. and Devine, J.D.** (1996). *Preeruption pressure-Temperature conditions and volatiles in the 1991 dacitic magma of Mount Pinatubo*. In Newhall, C.G. and Punongbayan, R.S. (eds.). *Fire and Mud, eruptions and lahars of Mount Pinatubo*,

- Philippines. Philippine Institute of Volcanology and Seismology & University of Washington Press, Hong Kong. 751-766.
- Sigmarsson, O., Condomines, M., Morris, J.D. and Harmon, R.S.** (1990). *Uranium and ¹⁰Be enrichments by fluids in Andean arc lavas.* *Nature* **346**: 163-165.
- Singer, B.S., Leeman, W.P., Thirlwall, M.F. and Rogers, N.W.** (1996). *Does fracture zone subduction increase sediment flux and mantle melting in subduction zones? Trace element evidence from Aleutian arc basalts.* In G. E. Bebout, D. W. Scholl, S. H. Kirby and J. P. Platt (eds.). *Subduction top to bottom.* American Geophysical Union, Geophysical Monograph Series. **96**: 285-291.
- Sisson, T.W.** (1994). *Hornblende-melt trace-element partitioning measured by ion microprobe.* *Journal Chemical Geology* **117**: 331-344.
- Sisson, T.W. and Grove, T.L.** (1993). *Experimental investigations of the role of water in calc-alkaline differentiation and subduction zone magmatism.* *Contributions to Mineralogy and Petrology* **113**: 143-166.
- Stern, C.R.** (1991). *Comment on "Crustal contributions to arc magmatism in the Andes of Central Chile" by W. Hildreth and S. Moorbath.* *Contributions to Mineralogy and Petrology* **108**: 241-246.
- Stern, C.R. and Kilian, R.** (1996). *Role of the subducted slab, mantle wedge and continental crust in the generation of adakites from the Andean Austral Volcanic Zone.* *Contributions to Mineralogy and Petrology* **123**: 263-281.
- Tebbens, S.F. and Cande, S.C.** (1997). *Southeast Pacific tectonic evolution from early Oligocene to Present.* *Journal of Geophysical Research* **102**: 12061-12084.
- Tormey, D.R., Hickey-Vargas, R., Frey, F.A. and López-Escobar, L.** (1991). *Recent lavas from the Andean volcanic front (33 to 42°S); interpretations of along-arc compositional variations.* In Harmon, R.S. and Rapela, C.W. (eds.). *Andean magmatism and its tectonic setting.* Geological Society of America, Special Paper **265**: 57-77.
- Tormey, D.R., Frey, F.A. and López-Escobar, L.** (1995). *Geochemistry of the active Azufre-Planchón-Peteroa volcanic complex, Chile (35°15'S): evidence for multiple sources and processes in a cordilleran arc magmatic system.* *Journal of Petrology* **36**(2): 265-298.
- Ulmer, P. and Trommsdorff, V.** (1995). *Serpentinite stability to mantle depths and subduction related magmatism.* *Science* **268**: 858-861.
- Ulmer, P., Müntener, O. and Alonso-Pérez, R.** (2003). *Potential role of garnet fractionation in H₂O-undersaturated andesite liquids at high pressure: an experimental study and a comparison with the Kohistan arc.* EGS-AGU-EUG Meeting, Nice, France. *Geophysical Research Abstracts* **5**: 08308,
- Wood, C.A. and Nelson, K.L.** (1988). *Inter-segment variation of magmatic composition in the Andes of Central Chile.* American Geophysical Union, EOS Transactions **69**: 1494.

CHAPTER 2

LONG-TERM GEOCHEMICAL AND PETROLOGIC EVOLUTION OF THE MAGMATISM AT NEVADO DE LONGAVÍ: EVIDENCE FOR INCREASING INFLUENCE OF A SUBDUCTED FRACTURE ZONE.

INTRODUCTION

The Southern Volcanic Zone of the Andes (SVZ) is the volcanic arc developed on the active western margin of the South American plate between the latitudes of the aseismic Juan Fernandez Ridge (33°S) and the actively spreading Chile Rise at 46.5°S (Figure 1). The chemical and mineralogical characteristics of SVZ magmas vary widely along the arc, as do the geological context and thickness of the underlying crust. Magmas erupted at volcanic centers to the north of 36°S, located over 45-60 km thick crust, are generally more evolved and have a more significant crustal component than those to south where the crust is <40 km thick (Hildreth and Moorbath, 1988). The consequent along-arc variation in the thickness of the asthenospheric column below the arc, and thus the average extent of melting, might account for some of the trace element differences in mantle-derived arc magmas (Tormey *et al.*, 1991), but most chemical variations have been explained in terms of increasing crustal contribution to the north, either as crustal assimilation (Hildreth and Moorbath, 1988) or as mantle source contamination by forearc tectonic erosion (Stern, 1991; Kay *et al.*, 2005).

Nevado de Longaví volcano (NLV) is located at 36.2°S, at an important juncture of tectonic elements. The northernmost SVZ (TMS in Figure 1) is built on continental crust that is estimated to be ~60 km thick. The thickness of the crust underlying the arc decreases southwards, and because the volcanic front is oblique to the Andean axis, there is a strong gradient in crustal thickness along the arc. The Moho at 36° S is estimated to be at a depth of ~40 km. The thickness of the subarc crust decreases at a lower rate from 36°S southwards, and by 40°S it might be as thin as ~30 km. In addition to the

southward decrease in total crustal thickness, modeled gravimetric data suggest that low density upper crust is also thinner south of 36°S than north of this latitude (Tassara and Yañez, 2003; Tassara *et al.*, 2006). Between 36 and 37°S there is a local minimum in crustal thickness (Tassara *et al.*, 2006), which seems to roughly coincide with the projection of the NW-SE-trending Cortaderas lineament

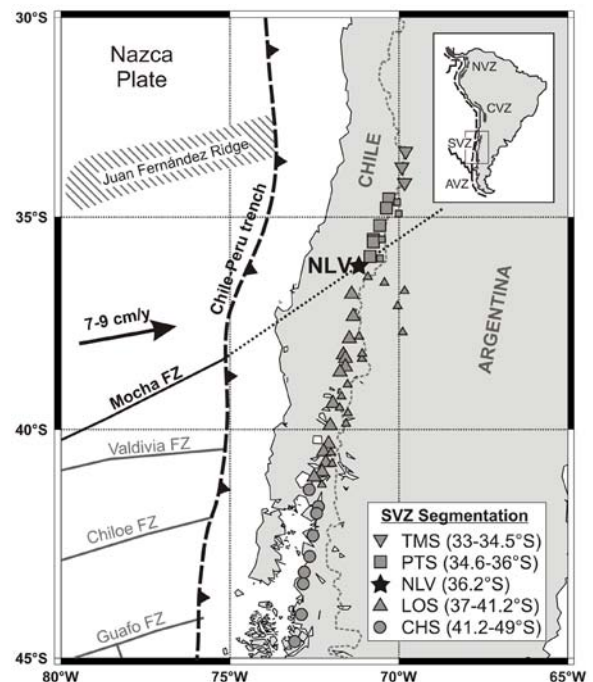


Figure 1. Location of Nevado de Longaví volcano (NLV) in the Andean Southern Volcanic Zone. Individual volcanic centers have different symbols according to the segmentation scheme of Dungan *et al.* (2001) and Sellés *et al.* (2004). TMS, PTS, LOS, and CHS are acronyms for Tupungato-Maipo, Palomo-Tatara, Longaví-Osorno, and Calbuco-Hudson Segments, respectively. Small symbols are centers behind the volcanic front. NVZ, CVZ, SVZ, and AVZ in inset stand for the Northern, Central, Southern, and Austral Volcanic Zones. Fracture zones annotated after Tebbens and Cande (1997)

in the Argentinean foreland. The Cortaderas lineament is the southern limit of intense Miocene to Holocene backarc effusive activity and thick-skinned Neogene deformation (Kay *et al.*, in press). The ~1000 km long strike-slip Liquiñe-Ofqui fault zone, which runs parallel to the arc and controls the emplacement of some volcanoes to the south (López-Escobar *et al.*, 1995a), dies out at this latitude in the retroarc region (Folguera *et al.*, 2004). Active extension in the inner retroarc is localized in a NNW-trending halfgraben structure, whose northern projection intersects the arc around 36°S (Ramos and Folguera, 2005).

A major fracture zone in the subducting oceanic Nazca plate projects beneath the Quaternary arc at the latitude of NLV, after correction for a subduction dip angle of 30° (Bohm *et al.*, 2002). The Mocha Fracture Zone (MFZ) separates 35 Ma old oceanic crust to the north from 25 Ma crust to the south where it enters the trench. This N60°E-trending fracture zone originated at the Pacific-Farallon spreading center, contrary to fracture zones to the south that trend ~N80E and affect oceanic crust generated at the Antarctic-Nazca spreading center or Chile Rise (Herron, 1981; Tebbens and Cande, 1997). The MFZ is a transient tectonic element that migrates southwards along the arc at a rate of 20-30 km/My.

Nevado de Longaví magmas have unique chemical and mineralogical characteristics within the SVZ (Figure 2). Andesitic and more evolved lavas ($\text{SiO}_2 > 57$ wt%) are characterized by incompatible element concentrations that are much lower than those in lavas to the north where contributions from crustal components are greatest. More importantly, they also have lower abundances than comparably evolved magmas at most volcanic centers south of 36°S, where the participation of the crust is minimal (e.g. Gerlach *et al.*, 1988; Hickey-Vargas *et al.*, 1989; López-Escobar *et al.*, 1995b). Thus, magma differentiation mechanisms at NLV appear to be distinct from those at other SVZ centers. This is illustrated by the low $\text{K}_2\text{O}/\text{SiO}_2$ ratios exhibited by intermediate and evolved NLV lavas in comparison with other SVZ magmas (Figure 2A); analogous patterns are reproduced by incompatible elements such as Rb, La, Zr, Nb, Th, etc. The extent to which incompatible elements are lower in NLV lavas relative to other SVZ volcanoes is greater for fluid-immobile elements. Elements such as Ba, Pb, and especially B, whose concentrations in arc magmas are

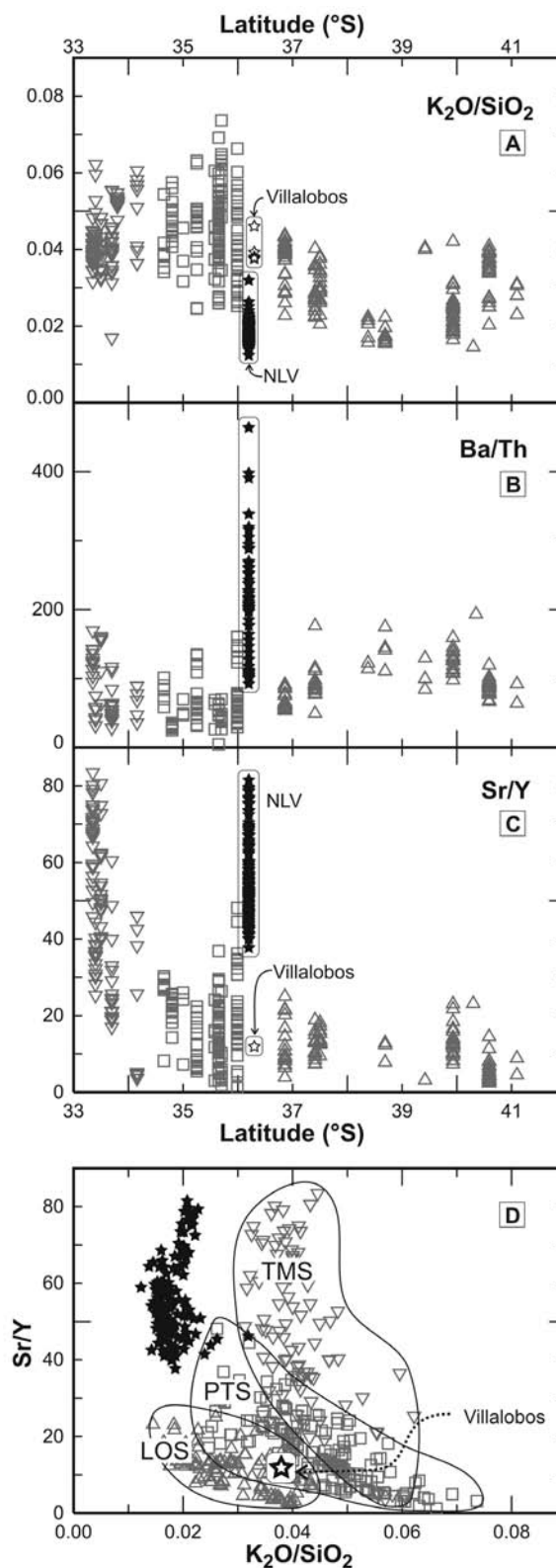


Figure 2. Along-arc chemical variation of SVZ intermediate to evolved magmas ($\text{SiO}_2 > 57$ wt%) showing some of the distinctive chemical characteristics of NLV lavas (black stars). Note that Villalobos intermediate lavas (empty stars) are indistinguishable from those of nearby centers. Different symbols stand for different arc segments, as in Figure 1; segment from Calbuco volcano to the south (CHS) not shown.

thought to be mostly provided by slab-derived fluids, are comparatively less anomalous (or actually enriched, as is the case for boron). Thus, mobile-to-immobile element ratios, such as Ba/Th (Figure 2B), are anomalously high at NLV. Elevated Sr/Y ratios in NLV lavas (Figure 2C) are the result of both elevated Sr contents and decreasing Y and HREE contents with increasing differentiation, indicating limited plagioclase removal during evolution and fractionation of a phase or phases with an affinity for HREE (amphibole and/or garnet). Comparably high Sr/Y ratios in the northern SVZ are inferred to be the result of deep assimilation of garnet-bearing crust coupled with high-pressure fractionation. However, NLV is the only volcanic center in the SVZ that embodies *all* of these characteristics (Figure 2D). An additional point is that Pliocene to lower Pleistocene arc magmas erupted at this latitude *prior* to NLV (empty stars labeled “Villalobos” in Figure 2) fall within the ranges of the segments immediately to the north and south. This implies that the factors that are controlling the anomalous character of NLV magmas have only recently been operating.

Most of the chemical peculiarities of NLV lavas are consistent with elevated magmatic water contents (Sellés *et al.*, 2004), which implies that the water budget in the melting region below NLV is substantially higher than in other parts of the arc. Dehydration of serpentinitic bodies hosted in the subducted part of the Mocha Fracture Zone could provide the asthenospheric mantle with unusually high amounts of fluids. As the Mocha Fracture Zone is not stationary with respect to the continental margin, its impact on the magmatism is also expected to change through time. In this contribution we document the changing chemical and mineralogical characteristics through a sequence of lavas extending from pre-Longaví magmatism to Holocene NLV eruptive events.

Geological context

The Pliocene-Quaternary volcanism in the area between 36°S and 37°S is constructed on volcanoclastic strata of late Oligocene-early Miocene age and middle to late Miocene granitoids. The volcanoclastic sequence, known in this area as the Cura-Mallín Formation, is a 2800 m thick sequence mainly composed of andesitic tuffs and breccias, with subordinate lava flows and continental sedimentary strata of fluvial and lacustrine facies with low-degree

burial metamorphism (Muñoz and Niemeyer, 1984; Jordan *et al.*, 2001). This formation was deposited in intra-arc extensional basins, and the associated volcanic rocks are isotopically primitive tholeiites with insignificant crustal contamination (Vergara *et al.*, 1999). The Cura-Mallín Formation was mildly folded during basin inversion and crustal shortening beginning in the Miocene. Batholith-scale granitoid plutons of middle Miocene age intruded to the west of the Quaternary arc, but small late Miocene stocks and plutons crop out in the vicinity of active volcanoes (Muñoz and Niemeyer, 1984). These are biotite and amphibole-bearing granitoids that range from quartz-diorites to tonalites and granodiorites.

VOLCANIC STRATIGRAPHY

Pre-Longaví volcanics (Late Pliocene?-Early Pleistocene)

Villalobos Volcano: Plio-Pleistocene volcanism between 36°S and 37°S has been regionally mapped as the Cola de Zorro formation (Muñoz and Niemeyer, 1984), and has been dated as Late Pliocene to Early Pleistocene (whole-rock K-Ar ages of 1.7 ± 0.7 , 1.35 ± 0.13 , 0.9 ± 0.5 Ma). This formation is represented in the proximity of NLV by a deeply dissected, mainly mafic stratocone complex that we have informally named Villalobos volcano. The inferred vent is located ~10-15 km south of the NLV summit, but the northernmost flank remnants are unconformably overlain by younger lavas from the Quaternary NLV edifice (Figure 3).

Sampled Villalobos lavas are mainly olivine- and clinopyroxene-phyric basalts and basaltic andesites (50-55 wt% SiO₂), although andesites and more evolved compositions are also present in lower proportions. Villalobos lavas are characterized by relatively high FeO*/MgO ratios and a wide range of incompatible element contents over a narrow range of SiO₂ (Figure 4). The compositional variation trends defined by Villalobos magmas are similar to those at other volcanic centers to the south of 36.2°S, and in this sense Villalobos is an appropriate reference point for monitoring the temporal evolution of magmatism at Nevado de Longaví.

Olivine and clinopyroxene are the modally dominant ferromagnesian phenocryst phases in Villalobos lavas, spanning a wide range of

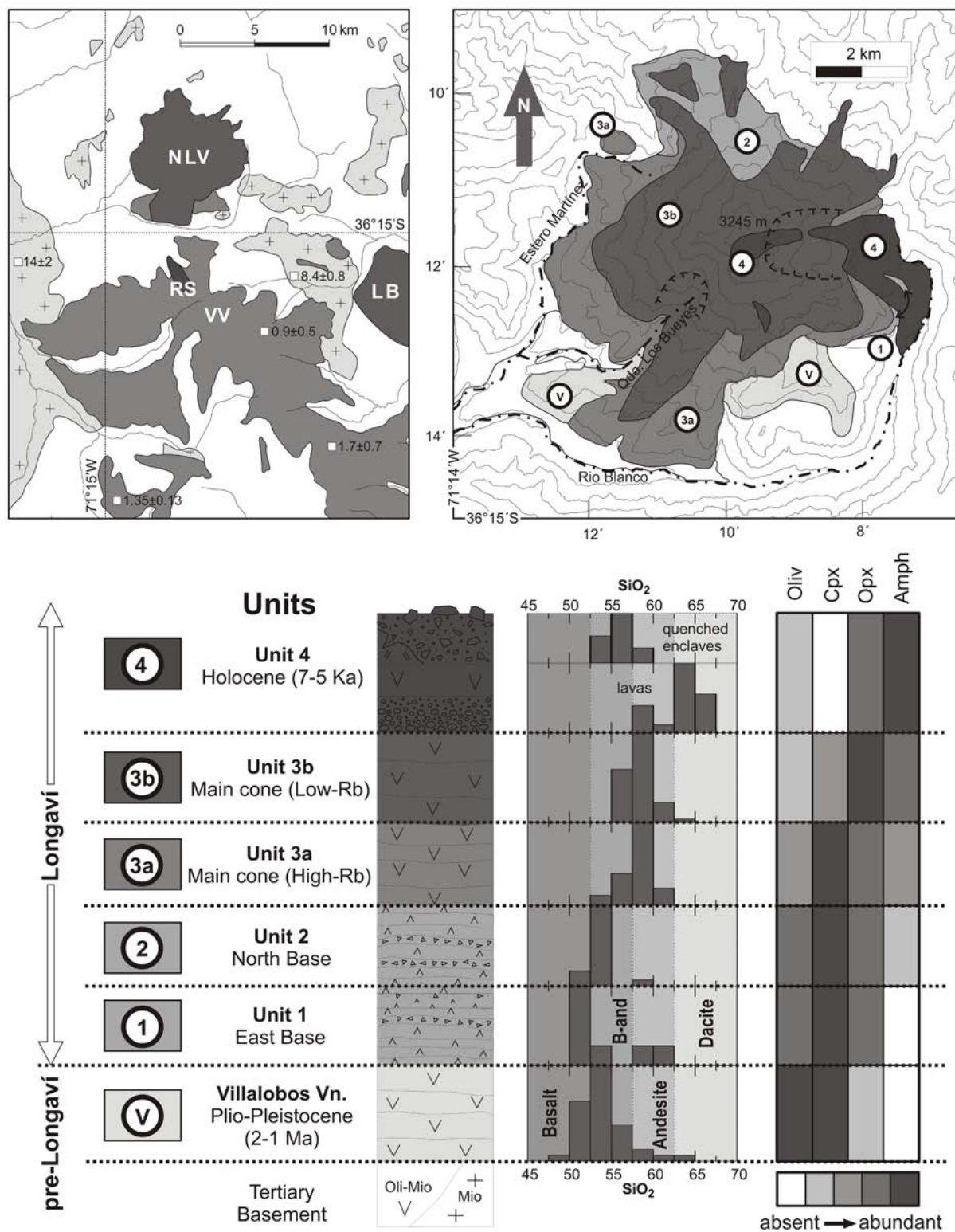


Figure 3. Upper left: Geological sketch map of the area of study (after Muñoz and Niemeyer, 1984). Basement rocks in white are Oligocene-Miocene volcanoclastic strata of the Cura-Mallín Formation, which are intruded by Middle to Late Miocene granitoids (light gray, with cross pattern). The deeply dissected Pleistocene Villalobos Volcano (VV) belongs to the regionally distributed Cola de Zorro Formation (mid-gray). Late Tertiary volcanic centers, in dark gray, include the Nevado de Longaví volcano (NLV), the Lomas Blancas volcano (LB) and the single-flow Rincón de Soto center (RS). Ages presented are K-Ar determinations. **Upper right:** Geological map of Nevado de Longaví volcano showing the distribution of units discussed in the text (topographic contours every 200 m). **Lower panel:** Schematic stratigraphic column and silica-frequency histograms for analyzed samples from each unit, showing a tendency towards increasingly evolved magmas being erupted with time. Relative ferromagnesian phase abundances (right) also show a tendency of increasing amphibole involvement at the expense of pyroxenes.

compositions from Fo₈₂ to Fo₅₈, and Mg#(cpx)=87-75 respectively (Mg#=100*Mg/[Mg+Fe*] in mol%). Most clinopyroxene crystals have Wo contents in the range of 50-40, relatively high Cr₂O₃ up to 0.4 wt%, and Al₂O₃ up to 4 wt%. Cr-spinel inclusions in olivines also vary widely from Cr#=60 to 20 (Cr#=100*Cr/[Cr+Al]). Plagioclase also shows a wide compositional variation, from very calcic cores up to An₉₀ and rims plus microlites down to An₄₅, with a mode in the range of An₆₀₋₅₀. Plagioclase is characterized by relatively high FeO* and MgO contents (up to ~1 and 0.1 wt% respectively). Magnetite-rich microphenocrysts and microlites and ilmenite grains in the groundmass complete the mineralogy.

Internal stratigraphy of Nevado de Longaví volcano:

Basal Longaví sequences (Units 1 and 2)

The oldest exposed portions of the edifice occur on the E and NW flanks of the volcano. The relative and absolute ages of the two basal units are not established as no dates have been determined.

Unit 1: Basal unit of the eastern flank:

The eastern flank of the volcano appears to have undergone a pre-Holocene structural collapse that created a large topographic bowl which is currently filled by Holocene pyroclastic deposits. A ~50 m thick sequence consisting mainly of mafic lavas, breccias, and intercalated coarse- and fine-grained volcanosedimentary deposits is exposed around the southern margin of the collapse scar and in some of the canyons excavated through younger deposits. This sequence is widely covered by Holocene deposits, and probably also by main cone lavas at one locality. We infer a low stratigraphic position based on these observations, but this inference may be revised as geochronological data become available.

All lava samples from this unit are basaltic (51.5-52.4 wt% SiO₂) with abundant plagioclase, olivine and clinopyroxene, and lesser orthopyroxene phenocrysts and microphenocrysts. Vitrophyric, prismatic jointed blocks (~20 cm) of more evolved compositions (54.8-62.0 wt% SiO₂) were also collected from volcanoclastic breccias. These andesitic fragments contain the same mineral

phases as the basalts, but orthopyroxene is more abundant than olivine and clinopyroxene.

Clinopyroxenes in Unit 1 basalts have Mg# between 88 and 77, and consistently low Al₂O₃ and Cr₂O₃ (<4 and 0.1 wt% respectively). Olivine phenocrysts have relatively evolved compositions from Fo₇₇ to Fo₆₁ and low NiO contents (<0.1 wt%), and the spinel inclusions in olivine are very low in Cr and Al (~1% and <8% respectively). Orthopyroxene in Unit 1 basalts is rare and limited to compositions of En₇₃₋₆₉. Plagioclase exhibits the widest variation in composition among the rocks studied (An₉₀Or_{0.1} to An₃Or₄₀; the mode is around An₇₀₋₈₀).

The most evolved sample from this unit, which is a breccia block, contains plagioclase with a tighter spread of compositions (An₇₆₋₄₃ and a mode of An₅₅₋₆₀), orthopyroxene En₇₉₋₇₂ with high Cr₂O₃ (up to 0.22 wt%), and sparse olivine mantled by orthopyroxene with compositions that overlap those of the basalts (Fo₇₀₋₆₈). The groundmass is a rhyolitic glass with 70 wt% SiO₂ and 0.6 wt% MgO.

Unit 2: Basal unit of the northern flank:

This sequence of ~40 thin lava flows (1-3 m) is exposed in deep glacial valleys on the north flank of the volcano. A ~600-700 m high cone that was later engulfed and almost completely covered by thick lava emissions of the main cone appears to have erupted from a vent located ~1500 m to the north of the current summit. The deepest exposed part of this unit consists of a few thick (>6 m) two-pyroxene andesitic to basaltic andesitic flows (53.8-58.4 wt% SiO₂) that are overlain by more numerous but thin basaltic andesitic flows (51.9-54.5 wt% SiO₂).

Olivine and two pyroxenes are the most common ferromagnesian phenocrysts in this unit. Olivine compositions vary from Fo₈₃ to Fo₆₁, with NiO contents up to 0.3 wt%, and olivines contain spinel inclusions that extend up to 30 wt% Cr₂O₃ and Al₂O₃. Clinopyroxene compositions vary from Mg#=91 to 72; the most Mg-rich are Cr-rich (up to 0.8 wt% Cr₂O₃) although most analyses have Cr₂O₃<0.1 wt%. Orthopyroxene is less abundant, with En contents between 78 and 68 and these are uniformly low in Cr. Plagioclase compositions are An₈₅ to An₃₆, with a strong peak near An₅₅ to An₇₀. Amphibole relics and pseudomorphs are present in some of the most evolved andesites. Relict amphibole cores are Mg-hastingsite with high Al₂O₃ contents of ~13 wt% and Mg# around 74.

Main Cone Andesites (Units 3a and 3b)

The bulk of the edifice consists of thick andesitic flows (55-63% SiO₂) that radiate from a vent area coincident with the current topographic summit. Main cone lavas exhibit greater chemical and mineralogical diversity than other units of the volcano, and they are texturally more complex. A useful distinction among main cone lavas is the degree of enrichment in incompatible elements as silica increases. Main-cone lavas define two divergent differentiation trends in terms of Rb and other incompatible element enrichments (*i.e.* the High-Rb and a Low-Rb series of Sellés *et al.*, 2004). All lavas from Units 1 and 2 fall within the High-Rb series and all Holocene products have exceptionally low Rb and other incompatible elements. This distinction among main-cone lavas is based on chemical criteria rather than a clear stratigraphic superposition. There is, however, a marked tendency for old lavas in several sections around the volcano to be of the High-Rb type. Low-Rb lavas, which are stratigraphically higher, tend to have higher modal proportions of amphibole. There are, however, no macroscopic criteria that enabled us to distinguish the lavas from these two series in the field. Similarly, there is no unambiguous chemical classification for some andesitic samples that are chemically intermediate between the most extreme samples of both series. Despite these uncertainties, main cone lavas record a transition from the older magmatism with dominantly anhydrous minerals to the Holocene amphibole-rich magmas.

Unit 3a: This unit includes andesites with relatively high incompatible element contents (High-Rb series), which range from 55.6 to 62.2 wt% SiO₂ (down to 53.3 wt% SiO₂ when quenched mafic enclaves are considered). These lava flows form the lower portions of several sections around the volcano, but overlie Unit 2 on the northern flank. Unit 3a andesites are commonly highly porphyritic, with abundant plagioclase and two pyroxenes as the main phenocrysts. Olivine is commonly present, often with orthopyroxene-overgrowths, whereas amphibole is only present in low abundances (a few crystals per thin section), and often shows disequilibrium textures.

Olivine phenocrysts in Unit 3a andesites generally are more magnesian than Fo₈₀, although a range of compositions from Fo₆₇

to Fo₈₅ is present. Most olivines have NiO >0.1 wt% (up to 0.33 wt%), and spinel inclusions normally have high Al₂O₃ (10-35 wt%) and Cr₂O₃ (>20 and up to 48 wt%). Clinopyroxene in Unit 3a lavas varies in composition from Mg# 72 to 93, although most analyses concentrate at about Mg#=80. The majority of augite phenocrysts have Al₂O₃ near 2 wt%, but some crystals extend up to 7.5 wt%, and the high-Al portions of these crystals have Cr₂O₃ up to 0.9 wt%. Orthopyroxenes have compositions ranging from En₇₆ to En₆₁, but they generally are between En₇₀ and En₇₅, and they have low Al and Cr. Plagioclase is the range An₈₃-An₁₅.

Two distinct populations of amphibole are present in lavas from this unit, and in some cases both occur in the same sample. The most common amphibole type is Mg-hastingsite, which is similar in composition to amphiboles found in other units. They are usually euhedral to slightly subhedral, commonly with dusty magnetite rims but otherwise little reacted. The second type corresponds to Ti-edenite, with TiO₂ and K₂O contents higher than those of typical Mg-hastingsite. Ti-edenites commonly have thick reaction rims of pyroxenes + plagioclase + oxides, and many have primary plagioclase (An₆₀₋₅₀) and orthopyroxene (En₇₀) inclusions. Ti-edenite amphiboles have not been recognized in other units of the volcano, but are present in potentially cogenetic noritic xenoliths that are present in many NLV lavas (Chapter 3).

Unit 3b: Younger andesitic lava flows that form the upper part of the main cone span a compositional range similar to that of Unit 3a lavas (55.3-62.4 wt% SiO₂), but these tend to have lower incompatible element contents (Low-Rb series). Andesites from Unit 3b commonly contain two pyroxenes, but olivine is rare and amphibole is more abundant and commonly less reacted than in the High-Rb lavas of the main cone.

Six olivine analyses from two different samples yielded compositions of Fo₇₄₋₇₁ and these contain spinels with relatively low Cr₂O₃ (<20 wt%). Clinopyroxene has a more restricted range of compositions than those in the older units, with Mg# contents between 85 and 76 and low Al₂O₃ (~2 wt%); Cr₂O₃ is usually below the detection limit. Orthopyroxene compositions are concentrated between En₇₀ and En₇₅, although a range from En₆₄ to En₇₉ is represented. Dominant plagioclase compositions are almost entirely in the range An₆₅ to An₃₅. High-Al Mg-

hastingsite is more abundant than in Unit 3a and it is usually less reacted.

Holocene products

Most of the Holocene activity of Nevado de Longaví volcano was concentrated in the summit area and within a preexisting collapse bowl on the eastern flank of the edifice. The Holocene sequence is composed of a dacitic pumice fall deposit (Río Blanco deposits of Rodríguez, in prep), followed by a thick andesitic lava (Castillo Andesite). The last eruptive event recorded at NLV consists of near-summit dome extrusion that in large part collapsed to the east forming block-and-ash flow deposits (Lomas Limpias deposits). The pumice fall and block-and-ash deposits are dated at ~7000 yrs B.P. and ~5000 yrs B.P. respectively (Rodríguez, in prep).

Unit 4: Both Holocene dacitic eruptions are similar in mineralogy and chemistry. The products of the early explosive eruption are slightly more evolved and glassy than the later dome-forming dacite (65.4 compared to 61.6–63.3 wt% SiO₂). The phenocryst mineralogy of

the Río Blanco and Lomas Limpias dacites is plagioclase, amphibole and orthopyroxene, with lesser Fe-Ti oxides, apatite, and sulfides; clinopyroxene is completely absent.

The Lomas Limpias dacite contains abundant quenched mafic enclaves with a broad range of compositions (53.8 to 58.8 wt% SiO₂). These have dictytaxitic textures (Bacon, 1986) with abundant acicular plagioclase and amphibole crystals. Some quenched mafic enclaves have scarce olivine phenocrysts, and rare plagioclase xenocrysts from the host dacite are present. Olivine phenocrysts are always mantled and partly replaced by Mg-hastingsitic amphibole with low TiO₂ (Rodríguez, in prep). Otherwise, quench-phases in the mafic enclaves are the same as those in the dacites and their mineral chemistry is similar. Residual glass pockets in the enclaves are rhyolitic in composition (~75 wt% SiO₂), as is the microcrystalline groundmass in the dacite.

A small andesitic lava-dome (59.7 wt% SiO₂) erupted between the dacitic events. Textural and chemical characteristics of this magma are consistent with mixing of a dacitic resident

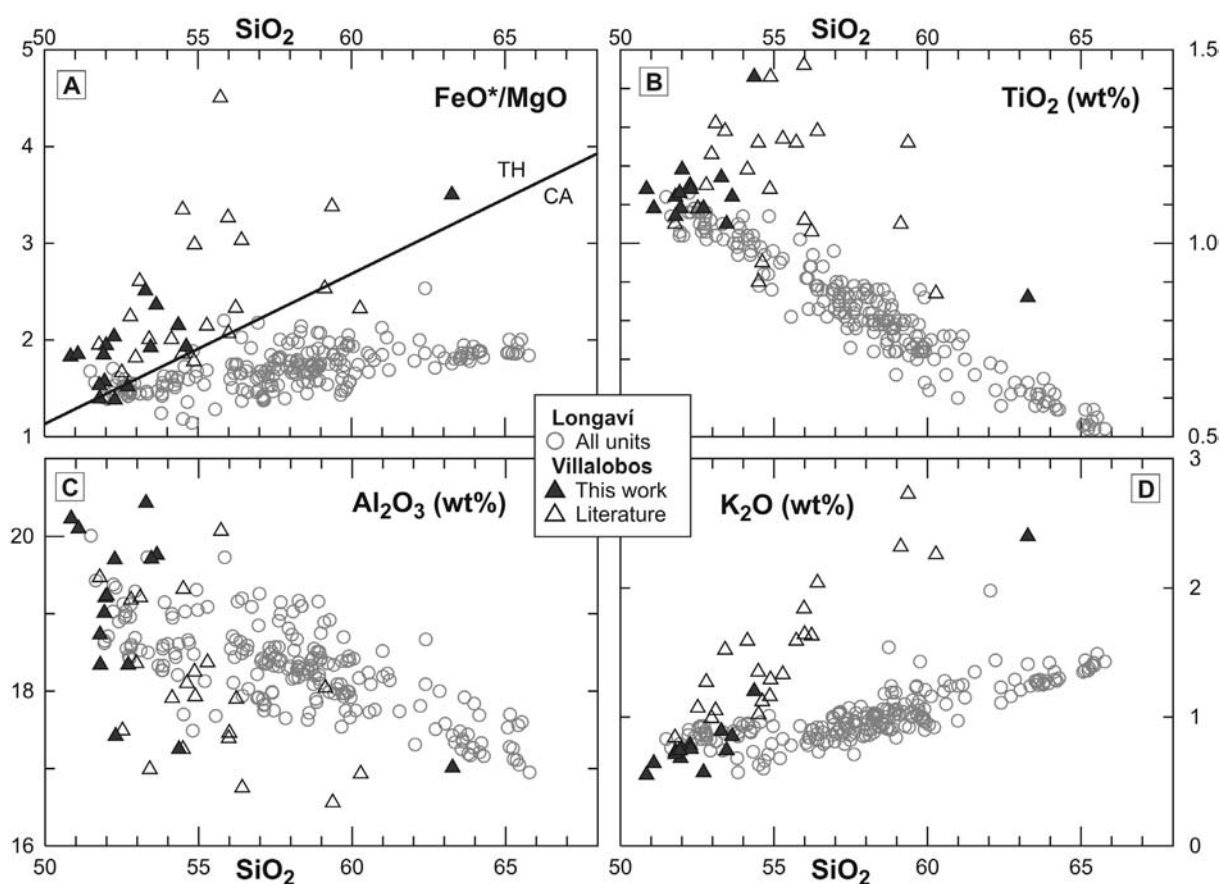


Figure 4. Major element variations of pre-Longaví volcanics (Villalobos volcano) compared to NLV magmas. Note early FeO* and TiO₂ enrichment of Villalobos lavas, typical of tholeiitic liquid lines of descent (dividing line in **A** is from Miyashiro, 1974). Compared to Longaví, Al₂O₃ in Villalobos lavas (as well as MgO and CaO) decreases more abruptly and K₂O (and Na₂O) increase more steeply with increasing differentiation. Literature analyses are from Gardeweg (1980) and Muñoz and Niemeyer (1984).

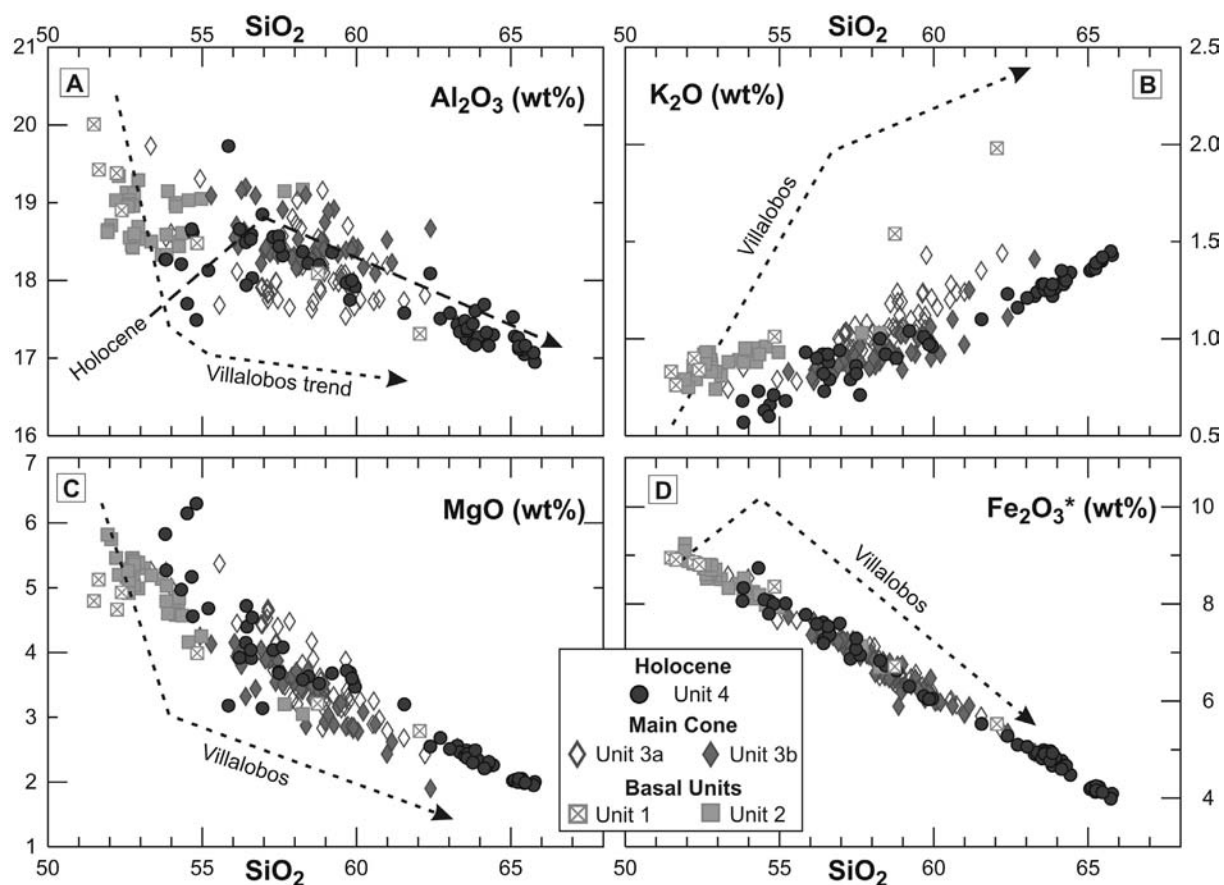


Figure 5. Whole-rock major element compositions of NLV lavas, and trends of variations of Villalobos lavas. Note for Unit 4 the kink in the Al₂O₃ and MgO trends around 57% SiO₂. Note also the systematic decrease in K₂O enrichments from Villalobos to Holocene NLV.

magma with a recharged mafic component. This hybrid andesite contains minor quenched mafic enclaves that are similar to those in the dacitic lavas.

Olivine phenocrysts in mafic enclaves and in the hybrid andesite are among the most Mg-rich at NLV (up to Fo₈₉), although most of them are Fo₈₅₋₇₈. Spinel inclusions in olivines have high Cr# values between 30 and 73. Orthopyroxene in dacites and enclaves is relatively Mg- and Ca-poor, with En contents of 67-75 and Wo contents mostly <1.5 mol%. They also have MnO contents between 0.7-1.1 wt%, which are distinctively higher than those in other units, in accord with lower temperatures in more evolved host magmas. A few data points richer in Mg and Ca and poorer in Mn are from the hybrid andesite. Plagioclase compositions tend to be concentrated at lower An contents than in other units, extending from An₇₁ to An₆, but prominent modes are present between An₃₀ and An₅₅ in dacites, and from An₃₀ to An₄₅ in the hybrid andesite. There are two modes around An₆₀ and An₄₀ in the mafic enclaves.

The most distinctive mineralogical characteristic of Unit 4 is the abundance of

amphibole in dacites (7-11 vesicle-free vol%) and enclaves (25-35%), where it is present as euhedral to slightly subhedral crystals. Amphibole in the hybrid Castillo Andesite is largely pseudomorphed by pyroxenes + plagioclase + oxides. Two populations of amphibole compositions are present. Mg-hastingsite with 11-14 wt% Al₂O₃, which is similar in composition to those in the underlying units, is the most abundant amphibole type in mafic enclaves. In dacites these are subordinate to Mg-hornblende with lower Al₂O₃ (9-6 wt%). Only a few points with compositions within the 11-9% Al₂O₃ gap were found.

WHOLE-ROCK CHEMISTRY

225 samples encompassing Villalobos and all units of Longaví were analyzed for major and trace elements by XRF on a Phillips PW 1400 spectrometer at the University of Lausanne's Centre for Mineral Analyses, using the standard techniques of Rhodes (1988). Analyses by XRF are precise to within 1-2 % percent. A subset of samples was also analyzed for trace elements by Inductively Coupled Plasma-Mass

Table 1: Selected Villalobos and NLV whole-rock analyses. Major elements by XRF, trace elements by ICP-MS, except where specified. 2-sigma errors for isotopic ratios are in parenthesis in terms of the last digit cited.

Unit Type Sample	Villalobos						1		
	Dike		Lava				Lava		
	VRN01-14	VRN01-13	NL153	NL173	VL04.03	VCS01.2	NL143	NL013	NL141
SiO ₂	51.41	50.56	51.53	53.13	54.43	62.60	51.39	51.77	51.94
TiO ₂	1.11	1.13	1.06	1.16	1.43	0.85	1.11	1.07	1.12
Al ₂ O ₃	18.59	20.11	18.24	20.37	17.28	16.83	19.98	19.47	19.27
Fe ₂ O ₃	8.89	8.83	9.37	8.29	9.48	5.32	8.93	8.93	8.81
MnO	0.14	0.14	0.15	0.13	0.22	0.14	0.13	0.14	0.13
MgO	5.22	4.34	6.04	2.97	3.96	1.37	4.80	5.14	4.66
CaO	9.74	10.16	9.12	8.93	7.67	4.40	9.34	9.29	9.24
Na ₂ O	3.22	3.38	3.07	3.63	4.14	4.86	3.26	3.45	3.22
K ₂ O	0.71	0.55	0.73	0.89	1.20	2.38	0.83	0.76	0.89
P ₂ O ₅	0.24	0.22	0.16	0.21	0.31	0.20	0.04	0.20	0.15
LOI	0.25	0.00	-0.08	-0.22	-0.03	0.98	-0.33	-0.43	-0.35
Total	99.51	99.42	99.40	99.48	100.09	99.92	99.48	99.81	99.08
Nb (XRF)	3.3	2.9	-	-	5.7	8	3	-	-
Zr (XRF)	98	98	-	-	163	259	95	-	-
Y (XRF)	16.3	17.7	-	-	23.7	31.8	15.3	-	-
Sr (XRF)	637	640	-	-	533	377	783	-	-
Rb (XRF)	9.2	2.8	-	-	27.1	63.3	9.6	-	-
Th (XRF)	3	4	-	-	4	6	3	-	-
Pb (XRF)	9	6	-	-	7	12	4	-	-
Ni (XRF)	46	30	-	-	14	4	33	-	-
Cr (XRF)	81	53	-	-	27	8	37	-	-
Ba (XRF)	217	222	-	-	317	513	199	-	-
B (ICP-AES)	-	-	11.1	15.1	-	-	-	8.9	8.1
B	-	-	-	-	-	-	-	13	-
Sc	25	24	26	21	-	-	17	21	35
V	225	237	206	211	-	-	228	229	235
Cr	76	51	149	25	-	-	37	134	25
Co	45	37	34	20	-	-	29	29	27
Ni	42	28	84	22	-	-	33	35	26
Rb	11.1	4.5	11.6	15.0	-	-	7.1	12.9	10.9
Sr	626	635	571	627	-	-	784	797	711
Y	17.2	18.4	17.0	20.3	-	-	14.0	16.3	12.9
Zr	89	89	88	106	-	-	79	79	90
Nb	3.2	3.0	3.0	3.4	-	-	2.7	2.6	2.9
Cs	0.91	0.32	0.53	0.88	-	-	0.22	0.59	0.22
Ba	206	212	218	245	-	-	181	184	194
La	10.9	9.8	10.1	11.5	-	-	7.5	8.7	7.3
Ce	23.3	23.1	22.8	26.8	-	-	18.9	20.9	22.3
Pr	3.43	3.33	3.15	3.66	-	-	2.74	3.03	2.66
Nd	16.6	14.4	14.3	16.6	-	-	12.8	14.3	12.9
Sm	3.52	3.54	3.43	4.02	-	-	3.17	3.29	3.27
Eu	1.16	1.22	1.12	1.28	-	-	1.05	1.10	1.03
Gd	3.51	3.61	3.38	3.94	-	-	2.96	3.43	3.09
Tb	0.54	0.57	0.50	0.59	-	-	0.46	0.51	0.43
Dy	2.91	3.19	2.90	3.44	-	-	2.69	2.79	2.55
Ho	0.60	0.64	0.57	0.69	-	-	0.53	0.59	0.51
Er	1.58	1.78	1.60	1.92	-	-	1.53	1.57	1.39
Yb	1.43	1.61	1.48	1.78	-	-	1.41	1.48	1.26
Lu	0.21	0.24	0.22	0.27	-	-	0.21	0.22	0.19
Hf	2.24	2.25	2.24	2.67	-	-	2.16	2.06	2.38
Ta	-	-	0.17	0.19	-	-	0.15	0.16	0.20
Pb	8.0	7.3	5.5	6.4	-	-	5.1	7.2	6.0
Th	1.39	1.54	1.36	1.97	-	-	1.07	1.43	1.11
U	-	-	0.34	0.52	-	-	0.42	-	0.51
¹⁴³ Nd/ ¹⁴⁴ Nd	-	0.512794 (4)	0.512749 (3)	-	-	-	-	0.512760 (2)	0.512747 (4)
⁸⁷ Sr/ ⁸⁶ Sr	-	0.70403 (1)	0.70408 (1)	-	-	-	-	0.70396 (1)	0.70388 (1)

Table 1: (continued)

Unit Type Sample	1		2								
	Fragment		Lava								
	NL012B	NL012C	NL110	NL109	NL073	NL066	NL077	NL083	NL081	NL113	NL124
SiO ₂	58.00	61.13	51.59	52.01	52.09	52.73	53.73	53.92	54.21	57.17	57.87
TiO ₂	0.85	0.68	1.02	1.02	1.03	1.06	1.00	1.01	0.98	0.78	0.77
Al ₂ O ₃	17.86	17.05	18.53	18.70	18.20	19.21	18.35	18.93	18.43	18.99	19.05
Fe ₂ O ₃	6.63	5.45	9.17	8.87	8.70	8.55	8.42	8.22	8.12	7.07	6.65
MnO	0.11	0.09	0.14	0.14	0.13	0.13	0.13	0.13	0.13	0.13	0.12
MgO	3.17	2.75	5.78	5.75	5.34	4.97	5.15	4.58	4.83	3.17	3.03
CaO	6.62	5.49	8.98	9.07	9.01	8.86	8.48	8.47	8.42	6.89	6.79
Na ₂ O	3.76	3.72	3.13	3.42	3.16	3.20	3.72	3.36	3.72	3.81	3.80
K ₂ O	1.52	1.95	0.78	0.75	0.88	0.82	0.89	0.93	0.88	1.02	1.03
P ₂ O ₅	0.23	0.20	0.19	0.20	0.20	0.07	0.21	0.08	0.21	0.12	0.23
LOI	0.45	0.96	-0.15	0.02	0.50	0.01	-0.15	-0.18	-0.09	0.33	0.28
Total	99.19	99.48	99.17	99.94	99.24	99.63	99.93	99.43	99.84	99.46	99.61
Nb (XRF)	5.2	5.5	2.5	2.7	2.7	3.1	3.1	3	-	3.9	3.8
Zr (XRF)	161	183	88	96	95	104	104	104	-	121	123
Y (XRF)	13.2	11.7	15.6	15.2	14.5	14.9	15	15	-	15.6	14.2
Sr (XRF)	599	540	761	786	744	750	725	733	-	622	625
Rb (XRF)	36.8	54.6	11.7	12.1	14.3	11.1	14.5	15	-	19.7	22.4
Th (XRF)	4	5	5	5	6	5	5	5	-	3	2
Pb (XRF)	10	12	10	12	11	13	11	15	-	8	9
Ni (XRF)	19	25	52	50	56	44	40	35	-	14	13
Cr (XRF)	38	64	88	79	82	69	66	63	-	14	15
Ba (XRF)	449	550	238	252	249	256	276	275	-	322	339
B (ICP-AES)	26.0	29.8	9.3	-	-	-	14.3	-	12.6	-	-
B	-	-	-	-	-	-	-	-	-	-	-
Sc	15	12	27	-	26	-	-	-	32	-	-
V	148	110	232	-	230	-	-	-	201	-	-
Cr	35	50	88	-	95	-	-	-	78	-	-
Co	18	15	31	-	29	-	-	-	25	-	-
Ni	20	22	53	-	51	-	-	-	39	-	-
Rb	38.9	57.3	13.4	-	15.7	-	-	-	14.1	-	-
Sr	607	552	768	-	754	-	-	-	714	-	-
Y	14.5	12.5	16.1	-	15.1	-	-	-	12.8	-	-
Zr	153	177	75	-	81	-	-	-	94	-	-
Nb	5.3	5.8	2.3	-	2.5	-	-	-	2.9	-	-
Cs	1.53	2.01	2.08	-	1.12	-	-	-	0.42	-	-
Ba	430	538	210	-	222	-	-	-	239	-	-
La	19.6	23.4	10.0	-	11.0	-	-	-	8.6	-	-
Ce	41.3	47.9	22.4	-	24.1	-	-	-	25.4	-	-
Pr	4.94	5.53	3.12	-	3.32	-	-	-	2.90	-	-
Nd	19.8	21.2	14.2	-	14.6	-	-	-	13.5	-	-
Sm	3.95	4.00	3.40	-	3.45	-	-	-	3.19	-	-
Eu	1.15	1.09	1.11	-	1.10	-	-	-	1.01	-	-
Gd	3.53	3.48	3.21	-	3.15	-	-	-	3.00	-	-
Tb	0.47	0.43	0.49	-	0.47	-	-	-	0.40	-	-
Dy	2.50	2.16	2.84	-	2.71	-	-	-	2.37	-	-
Ho	0.48	0.41	0.56	-	0.53	-	-	-	0.48	-	-
Er	1.34	1.11	1.58	-	1.49	-	-	-	1.30	-	-
Yb	1.22	1.02	1.43	-	1.34	-	-	-	1.23	-	-
Lu	0.18	0.15	0.22	-	0.20	-	-	-	0.19	-	-
Hf	3.57	4.08	2.05	-	2.19	-	-	-	2.36	-	-
Ta	0.33	0.40	0.13	-	0.14	-	-	-	0.18	-	-
Pb	11.3	13.4	11.0	-	11.4	-	-	-	12.8	-	-
Th	3.67	4.81	3.14	-	4.42	-	-	-	2.38	-	-
U	0.87	1.16	0.97	-	1.25	-	-	-	1.19	-	-
¹⁴³ Nd/ ¹⁴⁴ Nd	-	0.512792 (5)	0.512758 (5)	-	0.512731 (4)	-	-	-	-	-	-
⁸⁷ Sr/ ⁸⁶ Sr	-	0.70396 (1)	0.70407 (1)	-	0.70421 (1)	-	-	-	0.70415 (1)	-	-

Table 1: (continued)

Unit Type Sample	3a									3b	
	Enclave				Lava					Enclave	Lava
	NL050B	NL050D	LMG01.5	NL043A	LLRB01.1	NL046A	NL053	LMRB01.1	LMG01.8	NL022B	NL097
SiO ₂	53.93	53.95	55.85	57.15	57.30	59.35	60.52	60.81	62.07	56.57	55.84
TiO ₂	1.07	1.05	0.82	0.88	0.79	0.70	0.72	0.76	0.62	0.88	0.90
Al ₂ O ₃	18.59	18.59	18.02	17.98	18.47	17.45	17.72	17.78	17.77	19.26	18.62
Fe ₂ O ₃	8.52	8.45	7.41	7.30	7.06	6.15	6.03	5.93	5.37	7.50	7.61
MnO	0.14	0.13	0.13	0.12	0.12	0.11	0.11	0.10	0.10	0.11	0.12
MgO	5.01	5.26	4.43	4.44	3.50	3.86	3.25	2.97	2.42	3.33	3.92
CaO	7.95	8.14	8.15	7.35	6.92	6.32	5.90	5.93	5.53	7.29	7.59
Na ₂ O	3.53	3.60	3.68	3.93	4.11	4.11	4.21	4.38	4.27	4.24	3.91
K ₂ O	0.93	0.85	0.83	0.99	0.97	1.24	1.28	1.24	1.44	0.87	0.77
P ₂ O ₅	0.22	0.19	0.18	0.21	0.22	0.20	0.20	0.22	0.19	0.24	0.22
LOI	0.07	-0.08	-0.12	-0.24	0.16	0.17	0.01	-0.15	0.06	0.23	-0.28
Total	99.96	100.14	99.38	100.11	99.62	99.66	99.95	99.97	99.83	100.52	99.23
Nb (XRF)	3.1	3	2.8	3.8	3.3	3.7	3.9	3.8	3.6	-	3.2
Zr (XRF)	91	85	93	121	114	128	131	136	139	-	103
Y (XRF)	14.3	13.3	14.5	14.2	12.7	11.7	11.2	11.1	11.1	-	12.7
Sr (XRF)	596	585	544	598	645	602	593	616	564	-	650
Rb (XRF)	21.5	16.4	17.5	22.4	21.3	34.9	37.3	29.4	43.7	-	11.2
Th (XRF)	3	3	3	4	3	4	4	3	5	-	3
Pb (XRF)	6	10	6	7	9	10	9	8	11	-	7
Ni (XRF)	45	49	25	42	15	47	26	25	12	-	20
Cr (XRF)	66	87	59	68	15	79	37	38	14	-	27
Ba (XRF)	283	278	284	345	327	383	446	415	460	-	292
B (ICP-AES)	12.0	-	-	17.4	29.8	-	-	18.6	22.0	-	21.2
B	-	-	-	-	-	-	16	13	15	33	-
Sc	20	20	-	18	-	13	12	14	12	12	-
V	185	197	-	151	-	116	101	113	90	134	-
Cr	71	86	-	73	-	69	35	40	13	9	-
Co	28	28	-	24	-	19	17	36	39	20	-
Ni	43	47	-	43	-	42	29	27	14	15	-
Rb	23.2	18.0	-	24.3	-	35.8	36.6	30.3	44.0	13.5	-
Sr	582	588	-	591	-	602	583	-	-	773	-
Y	14.6	14.3	-	14.9	-	12.6	11.9	11.9	11.7	11.4	-
Zr	93	77	-	108	-	113	107	120	126	91	-
Nb	3.3	2.6	-	3.7	-	3.7	3.8	4.0	4.1	3.1	-
Cs	0.61	0.45	-	0.84	-	1.95	0.75	0.82	1.20	1.06	-
Ba	271	259	-	337	-	377	388	382	428	272	-
La	10.0	8.9	-	12.1	-	12.9	13.5	13.7	13.8	9.8	-
Ce	23.2	20.9	-	25.4	-	28.4	29.8	29.0	30.3	23.0	-
Pr	3.25	2.87	-	3.55	-	3.63	3.68	3.70	3.49	3.18	-
Nd	15.1	13.3	-	15.7	-	14.4	14.9	15.4	13.7	14.5	-
Sm	3.50	2.95	-	3.47	-	2.87	3.11	3.05	2.73	3.15	-
Eu	1.15	1.08	-	1.18	-	0.98	0.98	0.95	0.89	1.11	-
Gd	3.55	3.14	-	3.52	-	2.73	2.64	3.08	2.66	3.00	-
Tb	0.49	0.48	-	0.46	-	0.43	0.40	0.41	0.39	0.43	-
Dy	2.73	2.54	-	2.70	-	2.02	2.09	2.06	2.00	2.09	-
Ho	0.53	0.50	-	0.52	-	0.43	0.42	0.42	0.42	0.40	-
Er	1.36	1.37	-	1.35	-	1.18	1.16	1.06	1.09	1.01	-
Yb	1.26	1.20	-	1.40	-	1.13	1.12	0.96	1.06	0.97	-
Lu	0.18	0.18	-	0.20	-	0.16	0.17	0.16	0.16	0.14	-
Hf	2.20	1.96	-	2.62	-	2.65	2.80	2.93	3.07	2.36	-
Ta	0.19	0.16	-	0.22	-	0.26	0.27	-	-	0.17	-
Pb	6.4	14.0	-	8.0	-	12.2	13.6	9.6	14.3	10.1	-
Th	1.69	1.69	-	2.65	-	3.63	3.58	2.79	4.28	1.02	-
U	-	-	-	-	-	-	0.82	-	-	-	-
¹⁴³ Nd/ ¹⁴⁴ Nd	-	-	-	0.512784 (4)	-	-	-	-	0.512795 (6)	-	-
⁸⁷ Sr/ ⁸⁶ Sr	-	-	-	0.70394 (1)	-	-	-	-	0.70405 (1)	-	-

Table 1: (continued)

Unit Type Sample	3b					4				
	Lava					Enclave				
	NL006	NL024	NL040	NL028A	LURB01.1	LLINC01.3A	LL-040	MDCP01.1	LLINC01.3B	MDINCL3-13.1
SiO ₂	57.32	57.47	58.21	60.12	60.46	53.34	53.64	53.80	54.86	55.83
TiO ₂	0.87	0.86	0.88	0.73	0.66	0.96	0.99	1.01	0.95	0.94
Al ₂ O ₃	18.49	18.45	18.21	18.48	18.05	18.11	18.22	18.04	18.02	18.54
Fe ₂ O ₃	7.25	7.03	6.87	6.21	5.88	8.25	8.04	8.65	7.96	7.54
MnO	0.11	0.12	0.11	0.11	0.11	0.13	0.12	0.13	0.12	0.11
MgO	3.54	3.93	3.72	2.87	2.89	5.22	5.81	4.93	4.65	3.89
CaO	6.80	7.15	6.84	6.20	6.11	8.91	8.83	7.71	8.30	7.60
Na ₂ O	4.35	4.22	4.30	4.51	4.30	3.46	3.26	3.81	3.68	3.75
K ₂ O	0.92	0.88	0.90	1.00	1.09	0.57	0.68	0.72	0.68	0.90
P ₂ O ₅	0.25	0.22	0.24	0.23	0.20	0.16	0.12	0.24	0.18	0.23
LOI	-0.16	0.12	-0.16	-0.10	-0.21	0.35	0.28	0.08	0.27	0.29
Total	99.74	100.45	100.12	100.36	99.54	99.45	99.98	99.11	99.66	99.60
Nb (XRF)	3.6	-	3.6	-	3.4	2.7	2.4	3.1	3.2	3.1
Zr (XRF)	122	-	118	-	125	86	69	103	79	103
Y (XRF)	11.4	-	11.7	-	11.4	17.1	14.9	13	16.3	12.1
Sr (XRF)	686	-	607	-	630	627	524	677	629	692
Rb (XRF)	14.2	-	14.1	-	20.1	7.1	10.1	9.2	9.7	14.3
Th (XRF)	3	-	2	-	3	3	3	2	2	2
Pb (XRF)	8	-	6	-	12	5	7	7	7	7
Ni (XRF)	20	-	25	-	17	31	46	34	32	35
Cr (XRF)	30	-	40	-	20	85	87	71	81	46
Ba (XRF)	340	-	321	-	383	217	236	248	254	316
B (ICP-AES)	-	32.5	-	-	23.2	19.3	23.5	17.4	-	-
B	13	-	-	15	-	17	-	-	18	-
Sc	13	15	16	12	11	30	30	17	23	14
V	149	148	148	108	107	221	242	179	208	168
Cr	31	43	41	17	22	80	89	67	113	42
Co	22	21	20	17	39	38	29	38	33	51
Ni	24	32	27	16	21	29	42	31	29	31
Rb	16.8	15.4	15.5	18.2	21.7	9.2	12.1	11.0	11.2	16.1
Sr	708	644	607	644	619	611	518	646	-	688
Y	11.9	13.1	12.7	12.2	12.3	17.5	16.2	13.3	16.9	12.5
Zr	105	101	103	107	115	53	68	90	55	89
Nb	3.7	3.4	3.6	3.6	3.6	2.6	2.4	3.1	3.5	3.4
Cs	0.31	1.21	0.28	0.38	0.67	0.76	0.97	0.81	0.93	1.14
Ba	314	294	309	338	359	201	216	235	-	306
La	12.7	10.4	10.2	11.4	13.0	9.3	7.9	9.8	11.1	10.0
Ce	27.6	23.9	24.3	26.3	27.8	23.8	18.8	23.0	28.5	22.5
Pr	3.67	3.27	3.44	3.55	3.47	3.38	2.57	3.12	3.99	3.17
Nd	16.1	14.1	15.1	15.2	14.5	14.9	11.8	14.6	17.8	13.9
Sm	3.38	3.10	3.34	3.26	3.05	3.52	2.95	3.32	3.96	3.09
Eu	1.13	1.02	1.09	1.03	0.95	1.32	1.04	1.14	1.33	1.04
Gd	3.10	2.96	3.12	2.85	2.79	3.23	3.04	3.22	3.66	3.04
Tb	0.43	0.46	0.45	0.42	0.38	0.51	0.46	0.45	0.54	0.43
Dy	2.13	2.35	2.25	2.20	2.04	2.96	2.72	2.49	2.90	2.38
Ho	0.41	0.46	0.44	0.43	0.41	0.63	0.56	0.47	0.61	0.43
Er	1.04	1.27	1.14	1.17	1.09	1.72	1.50	1.25	1.64	1.14
Yb	1.01	1.16	1.08	1.10	1.06	1.65	1.40	1.11	1.55	0.97
Lu	0.15	0.17	0.16	0.17	0.17	0.25	0.21	0.17	0.23	0.15
Hf	2.64	2.53	2.50	2.85	2.70	1.74	1.89	2.41	1.85	2.26
Ta	0.20	0.19	0.20	0.22	-	-	0.14	-	-	-
Pb	11.2	9.9	7.1	13.0	11.6	7.4	6.3	8.3	6.5	7.3
Th	1.32	1.32	1.36	1.60	1.61	1.08	0.92	0.80	0.84	0.77
U	-	-	-	0.43	0.42	0.31	0.26	0.23	0.28	0.24
¹⁴³ Nd/ ¹⁴⁴ Nd	-	-	-	-	-	0.512777 (5)	0.512812 (3)	0.512805 (5)	-	-
⁸⁷ Sr/ ⁸⁶ Sr	-	-	-	-	-	0.70403 (1)	0.70407 (1)	0.70392 (1)	-	-

Table 1: (continued)

Unit Type Sample	4								
	Enclave	Lava						Pumice	
	LLLINC01.3E	NL015A	LCBS01.1	LL-015	MADHST-2	LLLBO1.1	LL-037	LRBPomez 01.1	Pomez- 04
SiO ₂	58.08	59.03	59.44	63.45	63.72	64.05	64.22	64.64	64.68
TiO ₂	0.81	0.73	0.71	0.61	0.57	0.58	0.65	0.53	0.52
Al ₂ O ₃	18.11	17.64	17.65	17.23	17.20	17.18	17.31	17.15	16.97
Fe ₂ O ₃	6.69	5.96	6.02	4.98	4.64	4.77	5.00	4.19	4.21
MnO	0.11	0.10	0.10	0.09	0.09	0.09	0.09	0.08	0.08
MgO	3.61	3.42	3.67	2.48	2.21	2.27	2.48	2.01	2.04
CaO	6.81	6.31	6.33	5.09	4.88	4.97	4.95	4.54	4.50
Na ₂ O	4.04	4.14	4.33	4.44	4.49	4.48	4.51	4.58	4.58
K ₂ O	0.92	0.95	0.98	1.27	1.27	1.29	1.27	1.35	1.36
P ₂ O ₅	0.20	0.20	0.19	0.21	0.18	0.18	0.19	0.17	0.17
LOI	0.27	0.31	-0.15	0.26	0.32	0.10	-0.10	0.79	1.17
Total	99.65	98.79	99.26	100.10	99.57	99.94	100.59	100.03	100.27
Nb (XRF)	3	3.1	2.8	3.4	3.5	3.4	3.4	3.3	3.2
Zr (XRF)	113	106	104	126	125	127	122	124	125
Y (XRF)	11	9.4	9.8	8.7	8.4	8	7.9	7.2	7.2
Sr (XRF)	657	644	629	584	581	587	596	573	566
Rb (XRF)	16	15.3	15.4	23	23.5	23.6	23.9	25.9	26.4
Th (XRF)	3	3	2	2	3	3	3	2	2
Pb (XRF)	8	7	7	13	9	10	14	9	10
Ni (XRF)	32	43	45	18	18	19	17	16	16
Cr (XRF)	37	62	77	27	23	24	47	24	31
Ba (XRF)	352	320	353	429	442	438	431	486	509
B (ICP-AES)	33.2	36.2	21.4	46.1	41.6	44.0	36.9	49.0	49.0
B	-	33	-	41	42	35	38	38	-
Sc	13	12	13	12	9	-	10	8	7
V	145	114	127	94	96	85	89	69	72
Cr	32	72	77	27	26	21	30	24	20
Co	40	19	27	13	40	-	13	11	10
Ni	29	43	45	22	19	19	20	18	19
Rb	17.4	16.6	17.3	23.9	26.5	23.7	25.4	25.5	26.0
Sr	653	626	626	-	-	563	563	523	540
Y	11.5	9.7	10.2	9.2	9.3	8.5	8.1	7.5	7.6
Zr	88	81	67	91	100	-	89	83	80
Nb	3.5	3.1	3.2	3.5	4.4	3.7	4.0	3.8	3.6
Cs	1.35	1.41	0.73	1.98	2.17	1.92	1.73	2.16	2.14
Ba	350	334	332	399	-	412	434	449	446
La	11.2	10.6	10.9	12.4	13.9	12.0	13.3	12.2	12.5
Ce	24.2	23.1	23.7	26.4	32.0	25.5	28.0	25.4	26.1
Pr	3.26	3.05	2.97	3.20	3.90	3.13	3.08	3.04	3.09
Nd	13.7	12.7	12.6	12.9	15.5	12.5	13.0	12.3	13.0
Sm	2.85	2.57	2.74	2.53	2.92	2.52	2.35	2.25	2.19
Eu	0.96	0.87	0.89	0.82	0.93	0.84	0.85	0.77	0.77
Gd	2.79	2.34	2.57	2.50	2.49	2.02	2.12	1.95	2.02
Tb	0.38	0.35	0.34	0.34	0.35	0.30	0.32	0.29	0.30
Dy	2.13	1.83	1.81	1.62	1.68	1.52	1.46	1.31	1.28
Ho	0.40	0.35	0.35	0.34	0.34	0.30	0.29	0.27	0.25
Er	1.07	0.90	0.91	0.83	0.89	0.81	0.75	0.65	0.67
Yb	0.95	0.81	0.83	0.74	0.86	0.74	0.68	0.62	0.62
Lu	0.15	0.13	0.12	0.11	0.13	0.11	0.10	0.09	0.10
Hf	2.27	2.24	1.85	2.39	2.79	2.47	2.28	2.17	2.18
Ta	-	0.21	-	0.27	-	-	0.25	0.24	0.25
Pb	8.0	10.1	7.6	12.2	11.6	14.2	13.3	13.8	13.5
Th	1.19	1.28	1.15	1.96	1.64	1.89	2.13	2.21	2.14
U	0.34	0.32	0.30	-	0.59	0.52	0.52	0.55	-
¹⁴³ Nd/ ¹⁴⁴ Nd	0.512793 (10)	0.512797 (3)	0.512766 (4)	0.512780 (5)	0.512799 (4)	0.512784 (3)	-	0.512801 (5)	-
⁸⁷ Sr/ ⁸⁶ Sr	0.70404 (1)	0.70402 (1)	0.70401 (1)	0.70404 (1)	0.70401 (1)	0.70402 (1)	-	0.70402 (1)	-

Spectrometry (ICP-MS) at the Department of Earth and Planetary Sciences, Harvard University for REE, V, Sc, Ni, Cu, Cr, Co, Nb, Ta, Pb, Th, Rb, Sr, Y, Cs and Ba. Standards used were MAR, BHVO-2, JB-2, BCR-2 and LUM37-3. Trace element data obtained by ICP-MS are accurate to within 5% standard deviation on the basis of duplicate analyses. Sr and Nd isotopic analyses were determined in the University of Geneva. Sample dissolution and Sr and Nd separations were done in the clean-laboratory facilities at the University of Geneva following standard procedures through cation-exchange columns. Measurements were performed at the University of Geneva on a 7-collector Finnigan MAT 262 thermal ionization mass spectrometer (TIMS) with extended geometry and stigmatic focusing using double Re filaments. The Sr isotopic ratios were corrected to an $^{88}\text{Sr}/^{86}\text{Sr}$ ratio of 8.375209 and normalized to the Eimer & Amend (E&A) SrCO_3 standard with $^{88}\text{Sr}/^{86}\text{Sr} = 0.708000$ using an average of $0.708056 \pm 5 \times 10^{-6}$ (2σ , $n=59$). Nd isotopic ratios were corrected for mass fractionation relative to a $^{146}\text{Nd}/^{144}\text{Nd}$ ratio of 0.7219 and normalized to the La Jolla standard value ($^{146}\text{Nd}/^{144}\text{Nd} = 0.511835 \pm 4 \times 10^{-6}$ (2σ , $n=91$)). Chemical and isotopic results are presented in Table 1.

Boron concentrations were determined at the Department of Earth Science in Rice University. Whole-rock powders were weighed and dissolved in HF and then dried at 70°C to prevent boron volatilization. $10\mu\text{l}$ of 1% mannitol solution ($\text{C}_6\text{H}_8(\text{OH})_6$) were added to help retain boron in solution. Solid precipitates were dissolved in HCl and then diluted in sub-boiled H_2O . The resulting solution was separated in three aliquots, two of which were spiked with known amounts of boron from a calibrated solution. The three aliquots were then analyzed in the ICP-AES; controlling for Fe interference using calibrated solutions of B and Fe. One international rock standard and a blank were also analyzed following every three unknowns. The typical uncertainty, on the basis of replicate analyses, is ± 2 ppm.

Major elements

Villalobos lavas are characterized by early Fe and Ti enrichments, and strong MgO, Al_2O_3 , and CaO decreases from mafic to intermediate lavas, whereas K_2O and Na_2O contents increase at a high rate with increasing silica (Figure 4). Nevado de Longaví as a whole is characterized

by low FeO^*/MgO ratios and variable, but low K_2O enrichments with increasing SiO_2 (Figure 5). NLV Units 1 to 4 are characterized by progressively lower K_2O -enrichment rates as a function of SiO_2 (Figure 5B). Whereas Unit 1 andesites have K_2O contents similar to those of other volcanoes of the region, Unit 4 is characterized by the lowest values in the SVZ. Main cone andesites have intermediate K_2O contents (Unit 3b < Unit 3a). Maximum Al_2O_3 contents in mafic NLV lavas are lower than in Villalobos lavas, but they decrease much less markedly towards andesites. Consequently, NLV dacites and andesites define the upper limit of Al_2O_3 contents for SVZ with comparable SiO_2 wt%. Unit 4 defines a trend of increasing Al_2O_3 in mafic compositions, followed by a decrease in more evolved magmas, with an inflection at about 57 wt% SiO_2 . This is also the point of inflection for the MgO trend of Unit 4, which decreases steeply in mafic magmas and less so towards more evolved compositions. Evolved samples from Unit 1 show decreasing Na_2O and increasing Mg# trends, which are difficult to reconcile with closed-system evolution.

Major element mass-balance models were fit to the trends defined by each unit. Each model was calculated using starting compositions similar to the most mafic samples within each unit, and average mineral composition were extracted to reproduce the chemical trends. The mineral proportions and the anorthite contents of plagioclase were adjusted by trial-and-error but in keeping with the observed mineralogy. No attempt was made to fit silica-rich samples from Unit 1 because open-system processes seem to predominate in their compositions. Table 2 and Figure 6 summarize the mineral assemblages that best reproduce the variations within each series. In particular, the models reproduce the different K_2O enrichment patterns for each unit and the increasing and then decreasing trend in Al_2O_3 for Unit 4.

Trace elements

Most incompatible trace elements follow the behavior of K_2O ; *i.e.*, there are systematic decreases in the rates of enrichment as a function of increasing SiO_2 from Villalobos to Holocene NLV magmas. This tendency is particularly marked for highly incompatible elements such as Rb, Zr, Th, LREE, Nb, Hf, and U (Figure 7). Differences in incompatible element concentrations are most significant in intermediate and evolved

compositions, but for many elements there are significant differences among mafic lavas as well. Exceptions to this general pattern are the high Th, U, and Pb values in Unit 2. Y and HREE contents increase with increasing SiO₂ in Villalobos lavas. These elements remain more or less constant in Units 1 to 3, and then decrease with increasing differentiation in Unit 4. Similar

Y and HREE depletions have not been observed at other SVZ centers. As a consequence, the La/Yb ratios of Holocene NLV lavas are higher than those at most other SVZ volcanoes. Only lavas from volcanoes in the northernmost SVZ (TMS) have higher La/Yb, but unlike NLV magmas, they are preferentially enriched in La (Figure 8). Silica- and glass-rich samples from Unit 1

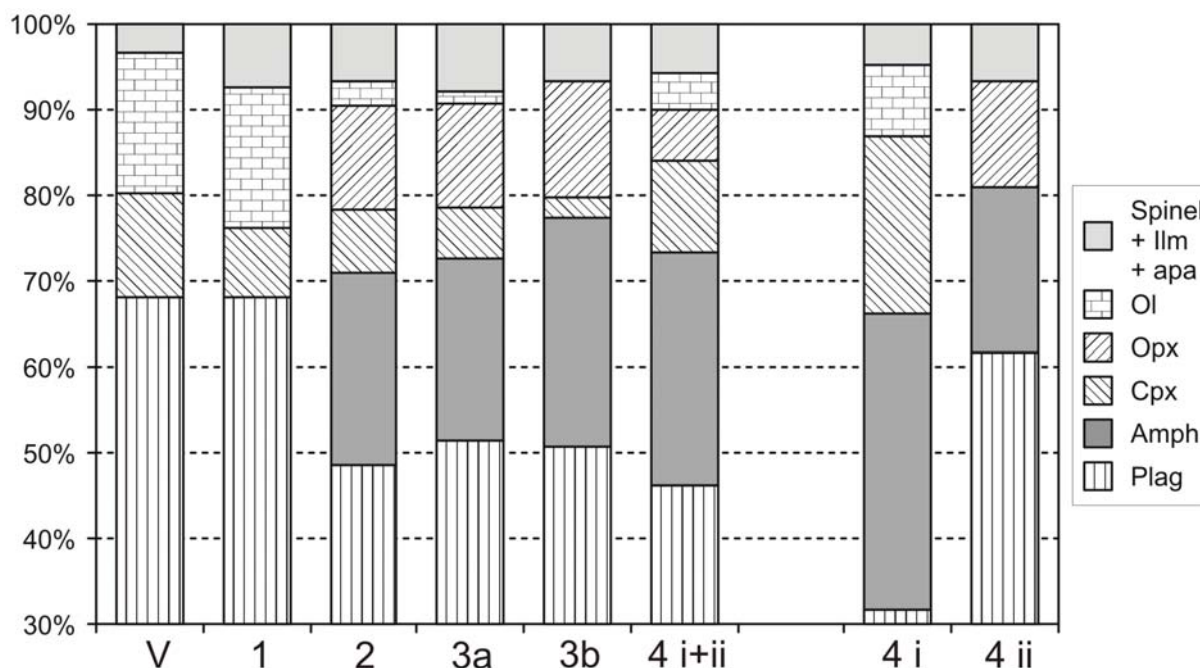


Figure 6. Summary of the mineral assemblages that best reproduce the major-element trends for each unit, which are labeled along the base of the diagram. Holocene trends were modeled in two stages, which are illustrated separately to the right (4 i and 4 ii) and combined in the column labeled 4 i+ii. For numerical values see Table 2.

	Villalobos	Unit 1	Unit 2	Unit 3a	Unit 3b	Unit 4 (total)	Unit 4 (part i)	Unit 4 (part ii)
Starting SiO ₂	50.73	51.91	52.12	53.24	55.73	53.98	53.98	58.35
End SiO ₂	56.13	55.63	58.56	60.94	66.69	64.98	58.35	64.98
Mass fraction extracted	0.6	0.3	0.5	0.5	0.5	0.58	0.3	0.4
Plagioclase An content	70	80	73	72	80	71	85	57
Mineral proportions extracted (wt%)								
Plagioclase	69.8	68.1	48.5	51.4	50.7	46.2	31.7	61.7
Amphibole	0	0	22.4	21.2	26.8	27.1	34.5	19.2
Clinopyroxene	12.1	8.2	7.5	6.0	2.4	10.7	20.7	0
Orthopyroxene	0	0	11.9	12.1	13.4	6.0	0	12.3
Olivine	14.8	16.3	3.0	1.5	0	4.3	8.3	0
Spinel	2.7	6.8	6.3	7.0	6.0	5.2	4.8	5.6
Ilmenite	0.7	0.5	0.3	0.3	0.6	0	0	0
Apatite	0	0	0	0.6	0.1	0.5	0	1.1
Bulk SiO ₂ extracted	46.42	42.66	44.86	44.64	43.99	45.33	43.01	47.81

Table 2. Mineral proportions (wt%) used to fit mass-balance models. See also Figures 6 and 16 for graphical representations of the models.

show elevated La/Yb ratios coupled with high La contents, which indicates again that open system processes are more important than in this one than in other units.

Other trace elements thought to be fluid-mobile, such as Ba and Pb (also Na₂O, Li, Be, and Cs) show less of a difference among units. The highly fluid-mobile element boron shows a behavior opposite to that of immobile elements; *i.e.* systematically higher concentrations in younger units (Figure 7F). Ratios of fluid-mobile to fluid-immobile incompatible elements

increase from Villalobos to the Holocene of NLV. Sr behaves much like Al₂O₃ in that it increases with increasing differentiation in the Unit 4 mafic enclave suite and then decreases past 57% SiO₂. Sr decreases are in general less steep for NLV units than for Villalobos lavas. Andesites and dacites from NLV commonly have Sr contents >500 ppm. Mafic lavas from Units 1 and 2 are particularly enriched in Sr (up to 800 ppm) in comparison to mafic magmas of either Villalobos or the younger NLV units.

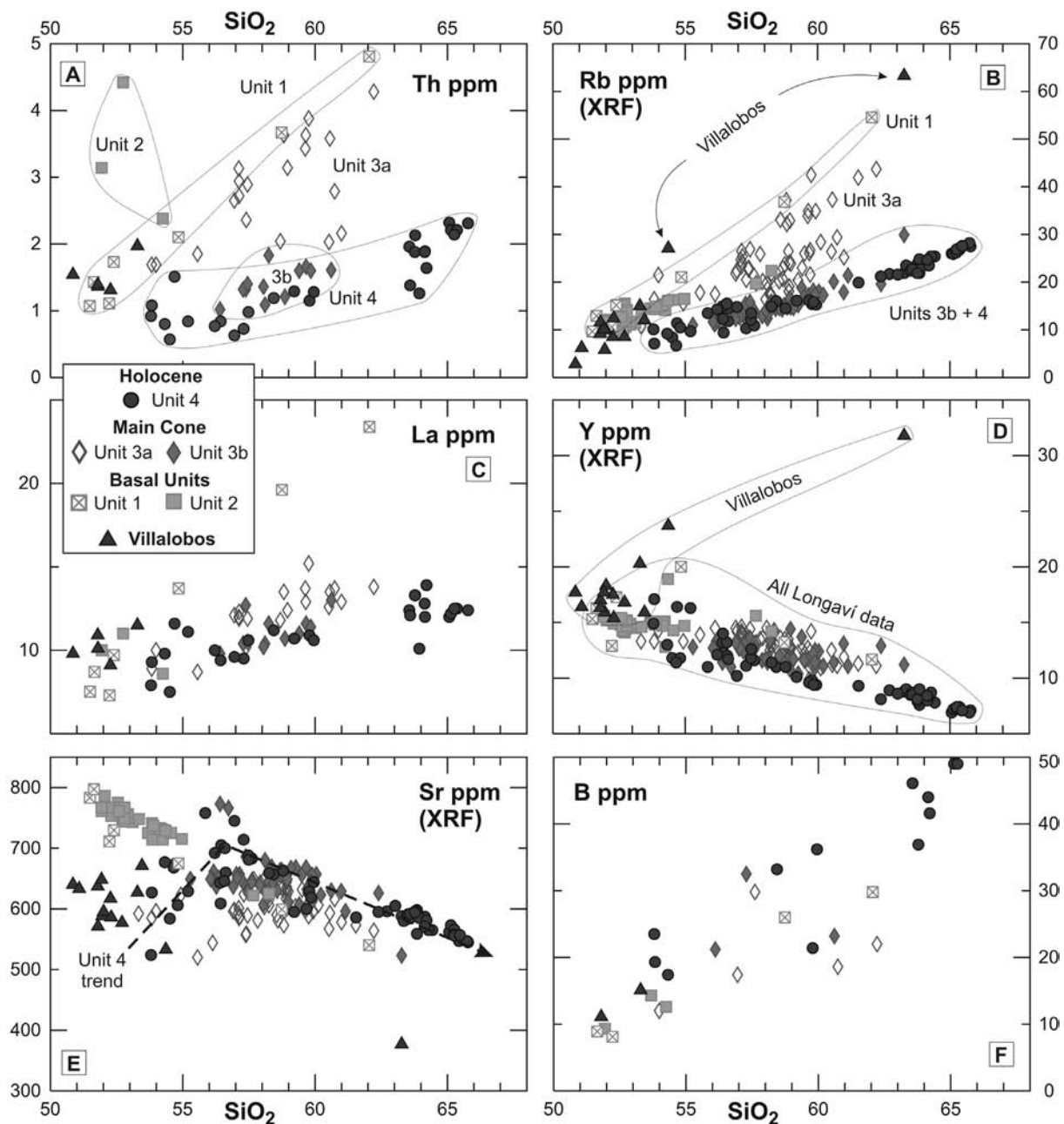


Figure 7. Selected trace elements for Longaví and Villalobos lavas. A sustained decrease in incompatible element content (for a given SiO₂ content) from old to young units is clearly seen for Th, Rb and La, similarly to K₂O, although unit 2 lavas contain high Th contents (as well as U and Pb). Boron shows an opposite tendency of higher contents in young units. Y decreases with increasing SiO₂ for in all Longaví units, but increases in Villalobos lavas. Note the inflection in Sr trend for Unit 4 at 57% SiO₂, analogous to Al₂O₃ abundances. Th and La as determined by ICP-MS, B by ICP-AES; Y and Rb by XRF as specified.

Isotopes

20 samples were analyzed for Sr and Nd isotopes (Table 1). Analyzed samples define a relatively narrow range of values. In terms of the geographical position of NLV in the Quaternary SVZ arc, these isotopic values are consistent with the regional SVZ along-arc trend. NLV isotopic data straddle the intersection of the fields defined by the volcanic centers north and south of this latitude (Figure 9), with most $^{87}\text{Sr}/^{86}\text{Sr}$ around 0.7040. The most “crustal” isotopic signature (high $^{87}\text{Sr}/^{86}\text{Sr}$ and low $^{143}\text{Nd}/^{144}\text{Nd}$) corresponds to samples from Unit 2, whereas samples from Unit 1 have low $^{143}\text{Nd}/^{144}\text{Nd}$ values and low $^{87}\text{Sr}/^{86}\text{Sr}$ ratios. Samples from Villalobos, Units 3b, and 4 are all confined to limited range of $^{87}\text{Sr}/^{86}\text{Sr}$ and $^{143}\text{Nd}/^{144}\text{Nd}$ values (0.70392–0.70408 and 0.512749–0.512812 respectively). All Unit 4 evolved lavas, and three out of four mafic enclaves, share an even more restricted range of isotopic values.

MINERAL CHEMISTRY

All major mineral phases in all units were analyzed with the CAMECA-SamX-50 electron microprobe of the Institut de Minéralogie et de Géochimie at Lausanne University. Accelerating voltage used was 15 kV, and beam current was set to 15 nA for plagioclase and amphibole, and to 30 nA for olivines, pyroxenes and opaque minerals. Peak counting times were between 15 and 40 seconds per element depending on its abundance, and background counting time was one-third to one-half of the peak counting times. Several thousand data points were collected in order to fully characterize the mineralogy of selected samples from all units. Here we focus on the mineral chemistry data that we consider to show systematic differences among units and reveal important aspects of the different magmatic processes acting in the area from Pleistocene to recent times.

Fe-Ti oxides

Temperature and $f\text{O}_2$ were calculated on the basis of coexisting Fe-Ti oxide compositions using the ILMAT spreadsheet of LePage (2003) considering the thermobarometer of Spencer and Lindsley (1981) with the corrections of Andersen and Lindsley (1985); ulvöspinel and ilmenite molecular fractions were calculated following Stormer (1983). Only pairs of oxides

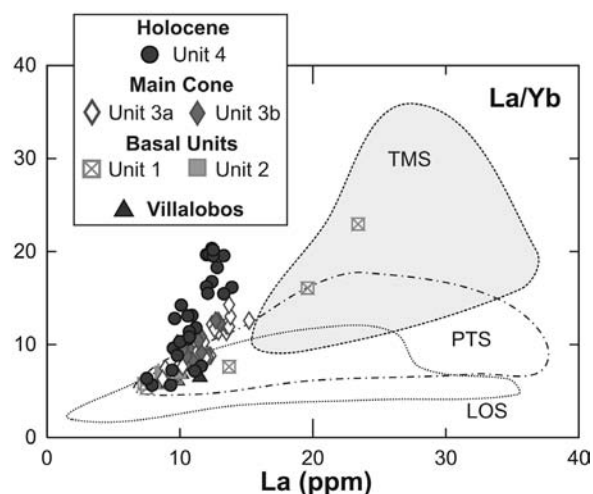


Figure 8. La/Yb ratios of NLV rocks as a function of La content and fields of compositions for other SVZ segments. Note that NLV (especially Holocene) magmas exhibit high La/Yb ratios at relatively low La contents, with the exception of Unit 1 samples, which are enriched in La, similarly to what is observed in the northernmost segment (TMS) of the SVZ.

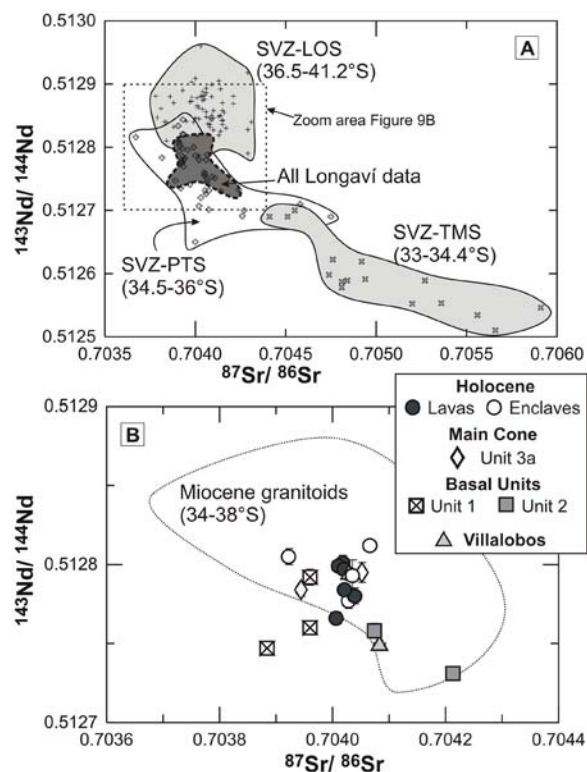


Figure 9. Sr and Nd isotopic composition of Longavi and Villalobos lavas. Fields for other SVZ segments are shown in **A**, and range of isotopic ratios of basement granitoids shown in **B** (Spikings *et al.*, unpublished data). Analytical error bars are about the size of symbols.

that satisfy the equilibrium condition of Bacon & Hirshmann (1988) were considered, and these results are shown in Figure 10A. Villalobos lavas are the least oxidized, with $f\text{O}_2$ values corresponding to 1 log unit below the NNO buffer; Villalobos lavas also record higher temperatures than all but a few pairs in NLV

units. Basal Units 1 and 2 fall on or between the NNO and NNO-1 buffer curves. Main-cone lavas from Units 3a and 3b cover a range of fO_2 values between NNO and NNO+1.6 with significant scatter (a large number of samples was analyzed from both units). Unit 4 magmas show a concentration of points at values around NNO+1.7. These are, to our knowledge, the highest fO_2 values reported for this part of the Andes. The Holocene Longaví magmas, ranging from mafic enclaves to the most evolved magmas from this volcano, record a tighter temperature grouping than any other unit. This probably reflects the fact that they are cogenetic, and suggests that thermal equilibration between host dacites and enclaves was largely attained.

According to these data, the oxidation state of magmas in the area has increased nearly three fO_2 log-units during the Quaternary. This change in redox state is accompanied by increases in fluid-mobile-to-immobile element ratios (proxies for slab fluids; Figures 10B and 10C), suggesting a relationship between the proportion of the fluid component in magmas and their oxidation state.

Plagioclase

A very large range of plagioclase compositions from An₉₀ to An₃ is recorded in lavas from Villalobos and Longaví volcanoes, with Villalobos and Unit 1 basalts exhibiting the widest An distributions (Figure 11). Glass-

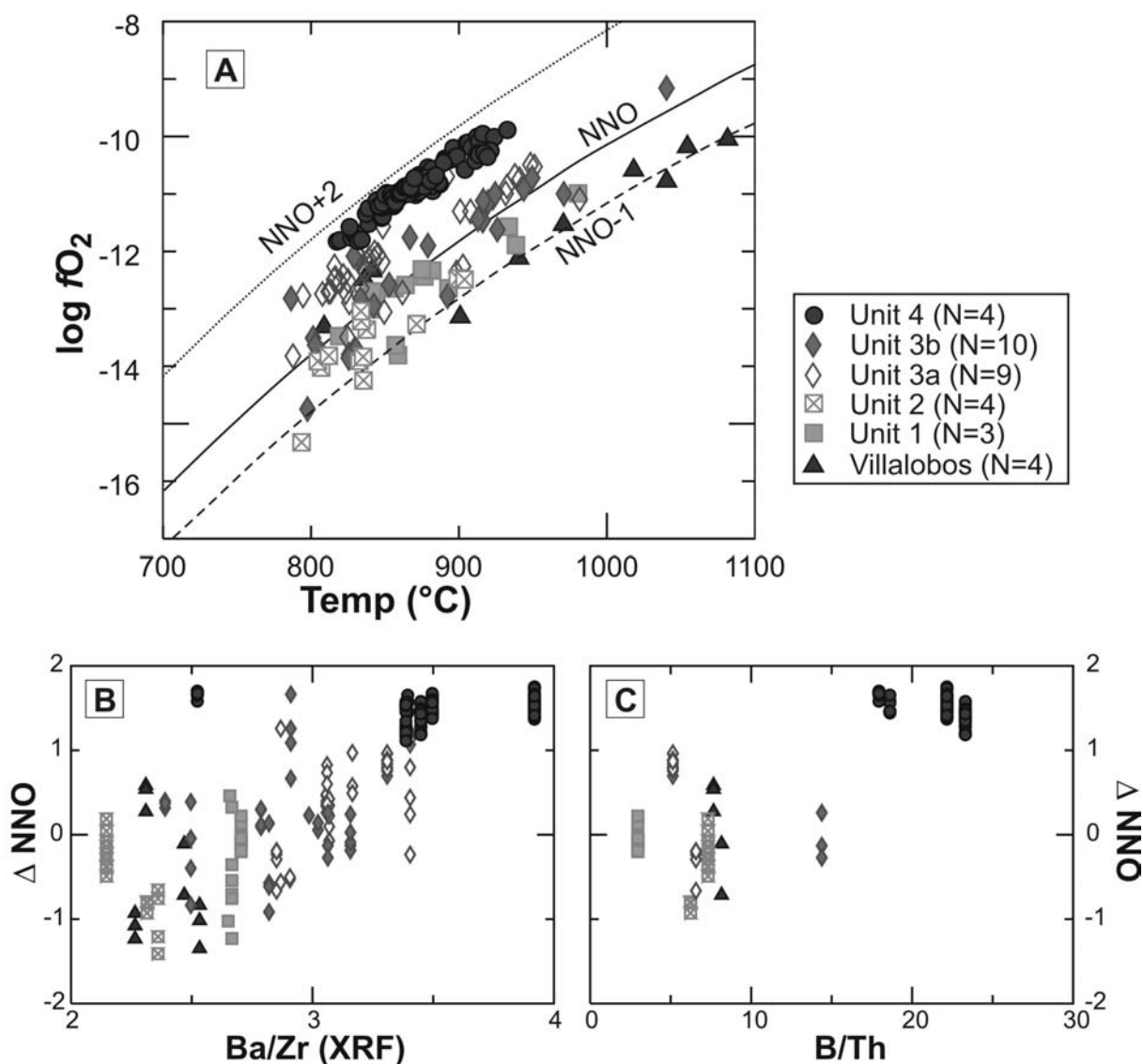


Figure 10. A: Temperature-oxygen fugacity plot from Fe-Ti oxide data. NNO buffer curve calculated following Huebner and Sato (1970) at 0.2 GPa pressure. Number of samples analyzed per unit is indicated in parenthesis. Data for Unit 4 from Rodríguez (in prep.) B and C: Whole-rock trace element ratios versus fO_2 value above the NNO buffer (ΔNNO).

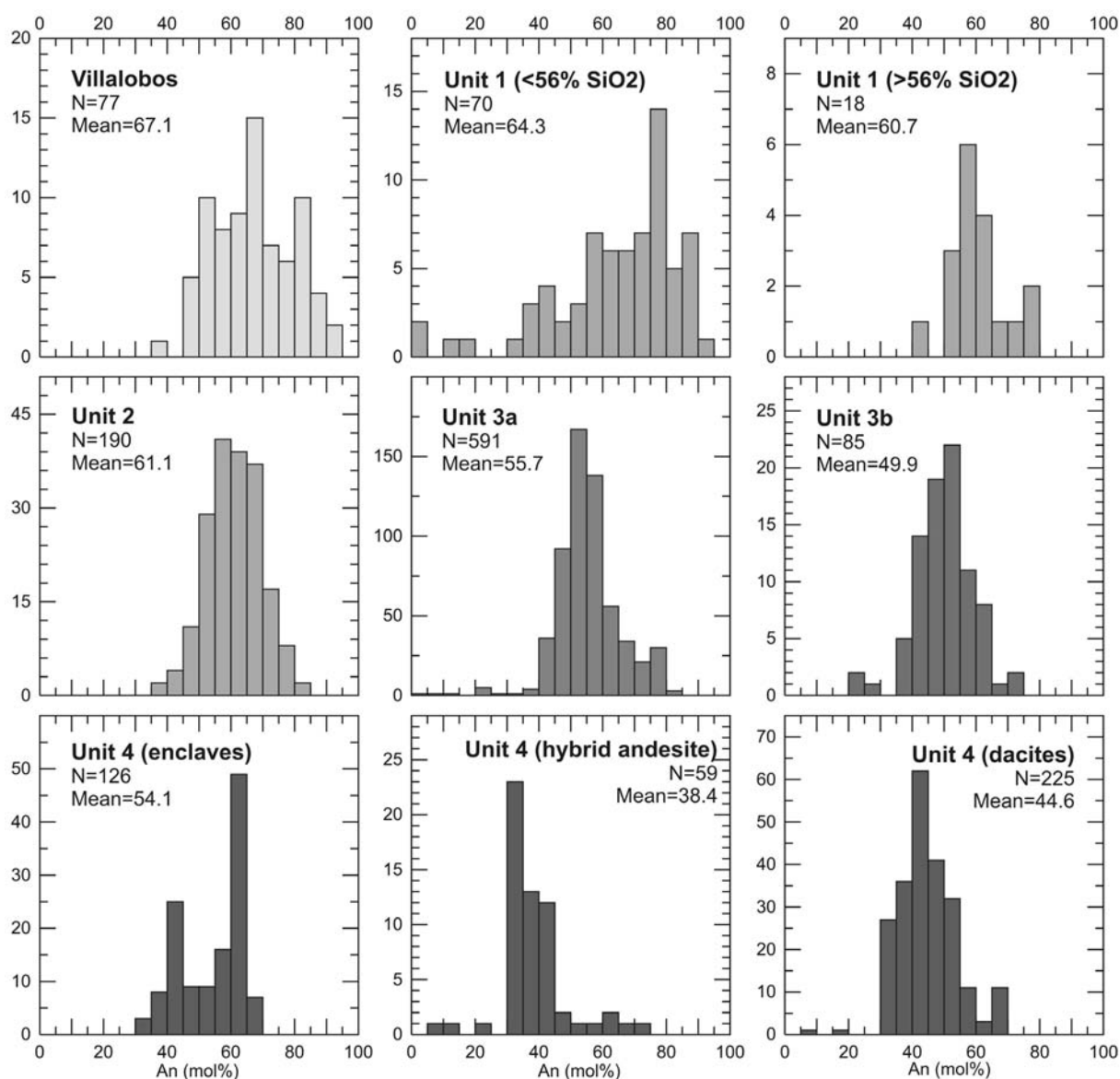


Figure 11. Histograms of plagioclase compositions (in terms of An mol%) for the units discussed in the text. Mafic and evolved samples from Unit 1 are shown separately, as well as Holocene dacites, andesite, and mafic enclaves.

rich andesitic samples from Unit 1 have a more restricted compositional range (An_{80-50}), despite the evolved glass in which they are immersed. Marked modes around An_{45} to An_{65} characterize basaltic andesites and andesites from Unit 2 and main-cone lavas, whereas the predominant plagioclase composition in Holocene dacites is slightly more sodic, between An_{35} and An_{55} . Unit 4 mafic enclaves have a pronounced mode at An_{60-65} , and in the hybrid Castillo andesite plagioclase compositions of An_{30-40} predominate.

The orthoclase content of plagioclases mimics the differences in whole-rock K_2O among the lava units (Figure 12). Plagioclase from Units 3b and 4 have systematically lower Or contents (for a given An value) than those from Villalobos and Units 1 and 2; crystals from Unit 3a span a whole

range of intermediate Or values. Both Fe and Mg contents in plagioclase crystals from Units 3b and 4 are also lower than those in the preceding units, but the Fe/Mg ratio continuously increases from Villalobos through Holocene NLV. Average plagioclase compositions from the different units are presented in Table 3

Amphibole

Amphibole is a common phenocrysts phase in K_2O -rich evolved lavas north of $36^\circ S$, (Hildreth and Moorbath, 1988 and references therein), but it is usually subordinate to anhydrous ferromagnesian phases (Ferguson *et al.*, 1992; Feeley *et al.*, 1998; Sruoga *et al.*, 2005). South of $36^\circ S$ it has only been found in small amounts in evolved lavas from the Mocho-Choshuenco

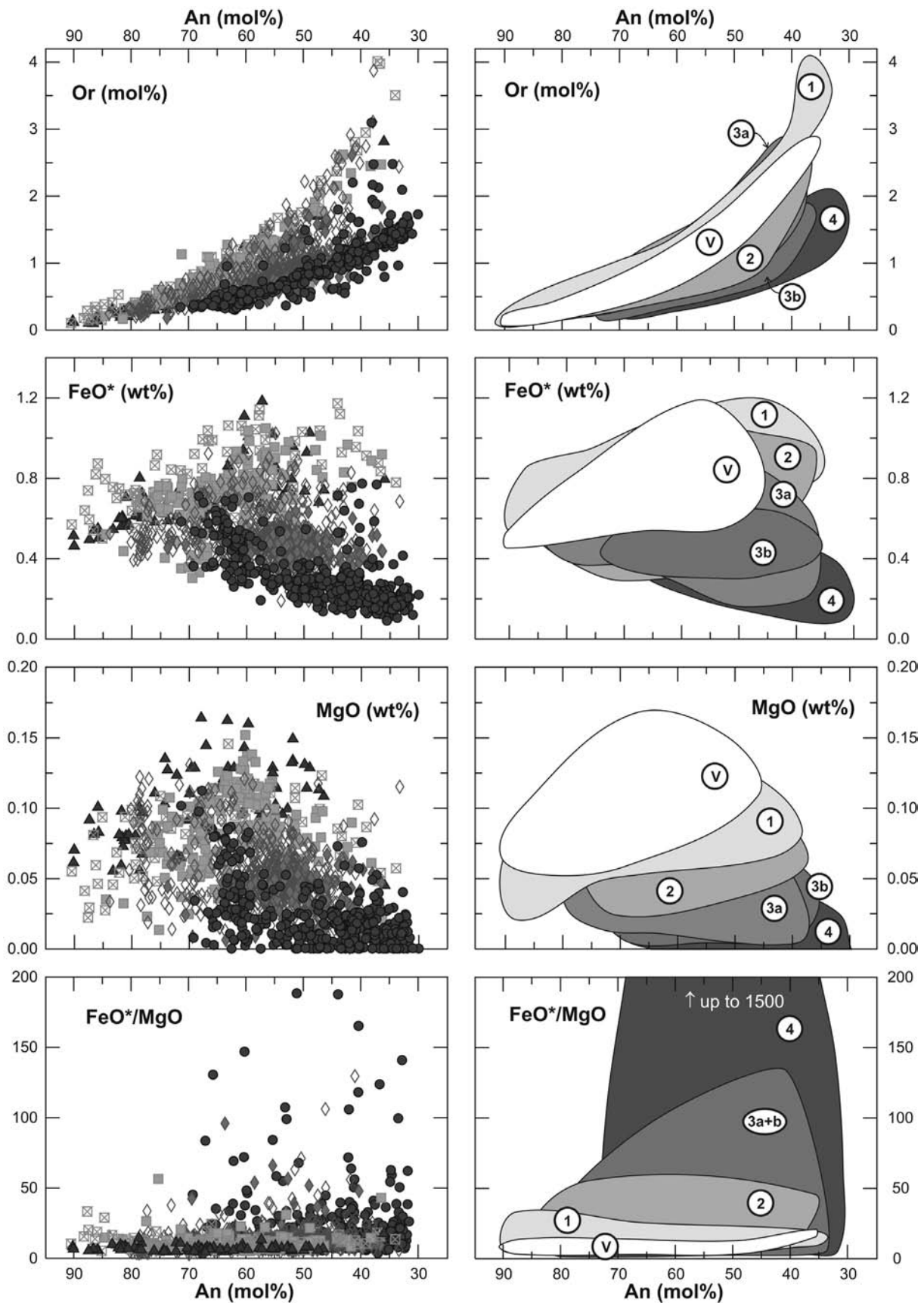


Figure 12. Plagioclase compositions from different units. Symbols in the left column diagrams are like those in previous figures. Diagrams in the right column are drawn fields including >95% of the points for each unit. Field labels are V: Villalobos volcano; 1, 2, 3a, 3b, and 4 refer to the basal, main-cone, and Holocene NLV Units as defined in the text.

complex, 39.9°S (McMillan *et al.*, 1989), and from the Pleistocene Tronador volcanic complex, 41.2°S (Mella *et al.*, 2005). It is, however, a more important phase in andesites from Calbuco volcano, 41.3°S (López-Escobar *et al.*, 1995b), and is possibly also present in some andesites and dacites south of this latitude (López-Escobar *et al.*, 1993). Amphibole is the predominant ferromagnesian phase in Holocene NLV dacites (and their included enclaves), and is an abundant phase in many main-cone andesitic lavas with SiO₂ as low as 57 wt%. Andesites from the north basal unit (Unit 2) also contain scarce amphibole phenocrysts.

Amphiboles in NLV lavas define three distinct compositional groups. High-Al amphiboles

(Al₂O₃ >11 wt%), which classify mostly as Mg-hastingsite according to Leake *et al.* (1997), are common to all amphibole-bearing units (Units 2 to 4; Table 4). Mg-hastingsite amphiboles contain appreciable amounts of Cr₂O₃ (up to 1 wt%) and show a wide variation in Mg# (78-58) with nearly constant tetrahedral Si/Al ratio (Figure 13). Amphiboles of this composition form up to 90 vol% of cumulate-textured xenoliths collected in young NLV lavas (Chapter 3). Low-Al amphiboles (Al₂O₃ <10 wt%), which classify mostly as Mg-hornblende, have been exclusively found in Unit 4, mostly in dacites but also as late phases in mafic enclaves. They are characterized by a wide variation in tetrahedral Si/Al ratios, which positively correlates with Mg# and

Average plagioclase compositions over the range An ₅₇₋₆₃						
Unit	pre-NLV	NLV				
	Villalobos	1	2	3a	3b	4
N	10	12	48	112	8	55
SiO ₂ (wt%)	52.66 (71)	52.18 (46)	52.51 (64)	52.40 (97)	51.80 (62)	52.60 (75)
Al ₂ O ₃ (wt%)	29.14 (40)	29.03 (30)	29.22 (39)	29.43 (40)	29.86 (39)	29.81 (34)
FeO* (wt%)	0.85 (19)	0.89 (19)	0.74 (13)	0.54 (12)	0.45 (6)	0.41 (12)
MgO (wt%)	0.11 (2)	0.10 (1)	0.10 (3)	0.05 (2)	0.03 (1)	0.03 (2)
CaO (wt%)	12.32 (39)	12.26 (26)	12.43 (28)	12.33 (37)	12.43 (39)	12.54 (37)
Na ₂ O (wt%)	4.52 (22)	4.53 (18)	4.48 (17)	4.59 (20)	4.39 (23)	4.45 (18)
K ₂ O (wt%)	0.18 (4)	0.21 (2)	0.14 (3)	0.13 (3)	0.10 (6)	0.08 (2)
Total	99.78 (41)	99.21 (28)	99.64 (55)	99.50 (81)	99.07 (28)	99.94 (48)
Ab (mol%)	39.46 (178)	39.55 (138)	39.12 (137)	39.93 (174)	38.76 (192)	38.91 (157)
An (mol%)	59.53 (191)	59.23 (147)	60.03 (141)	59.29 (173)	60.64 (195)	60.59 (161)
Or (mol%)	1.01 (22)	1.20 (12)	0.83 (18)	0.72 (16)	0.59 (34)	0.47 (10)

Average plagioclase compositions over the range An ₄₇₋₅₃						
Unit	pre-NLV	NLV				
	Villalobos	1	2	3a	3b	4
N	9	6	25	162	27	64
SiO ₂ (wt%)	55.19 (66)	54.28 (33)	54.73 (53)	54.57 (94)	53.80 (71)	55.36 (69)
Al ₂ O ₃ (wt%)	27.64 (52)	27.52 (30)	27.78 (47)	28.01 (46)	28.04 (35)	27.90 (36)
FeO* (wt%)	0.79 (15)	0.91 (14)	0.59 (21)	0.47 (12)	0.48 (8)	0.28 (7)
MgO (wt%)	0.12 (2)	0.10 (1)	0.07 (2)	0.04 (2)	0.04 (2)	0.01 (1)
CaO (wt%)	10.60 (36)	10.57 (41)	10.49 (42)	10.59 (36)	10.53 (34)	10.47 (38)
Na ₂ O (wt%)	5.50 (23)	5.46 (19)	5.58 (20)	5.60 (19)	5.60 (19)	5.73 (18)
K ₂ O (wt%)	0.25 (3)	0.30 (3)	0.19 (8)	0.18 (5)	0.17 (6)	0.14 (3)
Total	100.12 (26)	99.17 (48)	99.45 (65)	99.51 (85)	98.67 (49)	99.90 (47)
Ab (mol%)	47.68 (179)	47.47 (172)	48.49 (161)	48.34 (159)	48.57 (152)	49.36 (157)
An (mol%)	50.83 (192)	50.78 (182)	50.39 (176)	50.53 (167)	50.46 (157)	49.83 (163)
Or (mol%)	1.45 (15)	1.69 (15)	1.09 (44)	1.05 (29)	0.95 (34)	0.80 (17)

Table 3. Averaged plagioclase compositions for the different units. Notice systematic decrease in FeO* and MgO content of plagioclase towards young units within the two compositional ranges presented (An₅₇₋₆₃ and An₄₇₋₅₃). N=number of point analyses considered within the specified An range. Numbers in parentheses stand for the standard deviation expressed in terms of the last unit cited.

negatively with K. A third group of amphiboles with intermediate Al_2O_3 but higher TiO_2 and K_2O contents than the other groups is represented by variably reacted amphibole crystals that commonly contain euhedral plagioclase and/or opx inclusions. These amphiboles are Ti-edenites, and are found exclusively in Unit 3a lavas in combination with fresh Mg-hastingsite crystals. They are compositionally and texturally similar to post-cumulus amphiboles in some noritic xenoliths from NLV lavas (Chapter 3), and we interpret them as xenocrysts resulting from disaggregation of partially molten xenoliths.

Pyroxenes and Olivine

Pyroxene is an abundant phase in many lavas of the study area. Most andesites from units 1 to 3 contain both orthopyroxene and clinopyroxene, whereas basalts from Villalobos volcano contain mostly clinopyroxene; orthopyroxene is extremely rare even in Villalobos intermediate lavas (only one $\text{Mg}\#=72$ opx microphenocryst analyzed). On the other hand, Holocene dacites

and enclaves completely lack clinopyroxene and orthopyroxene is only present as a late phase.

The range of clinopyroxene compositions is similar in all units, although Unit 3b displays a more limited variability with $\text{Mg}\#$ 75-85. Unit 3a hosts the most Cr- and Al-rich clinopyroxene analyzed, with values up to 0.9 wt% Cr_2O_3 and 7.5 wt% Al_2O_3 (Figure 14). A few analyses from unit 2 also extend to high Cr and Al values, although the vast majority are restricted to $\text{Al}_2\text{O}_3 < 4$ wt% and $\text{Cr}_2\text{O}_3 < 0.1$ wt%, where most pyroxenes from units 1 and 3b are concentrated. Clinopyroxene in Villalobos lavas have relatively high Cr_2O_3 contents, but Al_2O_3 is low and comparable to most clinopyroxene in younger units.

Orthopyroxene in Unit 4 dacites and enclaves display distinctive low Wo (~1 mol%) and TiO_2 (0.1 wt%) contents, whereas orthopyroxene in andesites from Units 1, 2, and 3 that have 2-3 mol% Wo (and up to 7%). A few grains of orthopyroxene from Unit 4 have Wo contents over 2%, but these correspond to the hybrid Castillo Andesite (Rodríguez, in prep). Excluding these few points, orthopyroxene in Unit 4 is

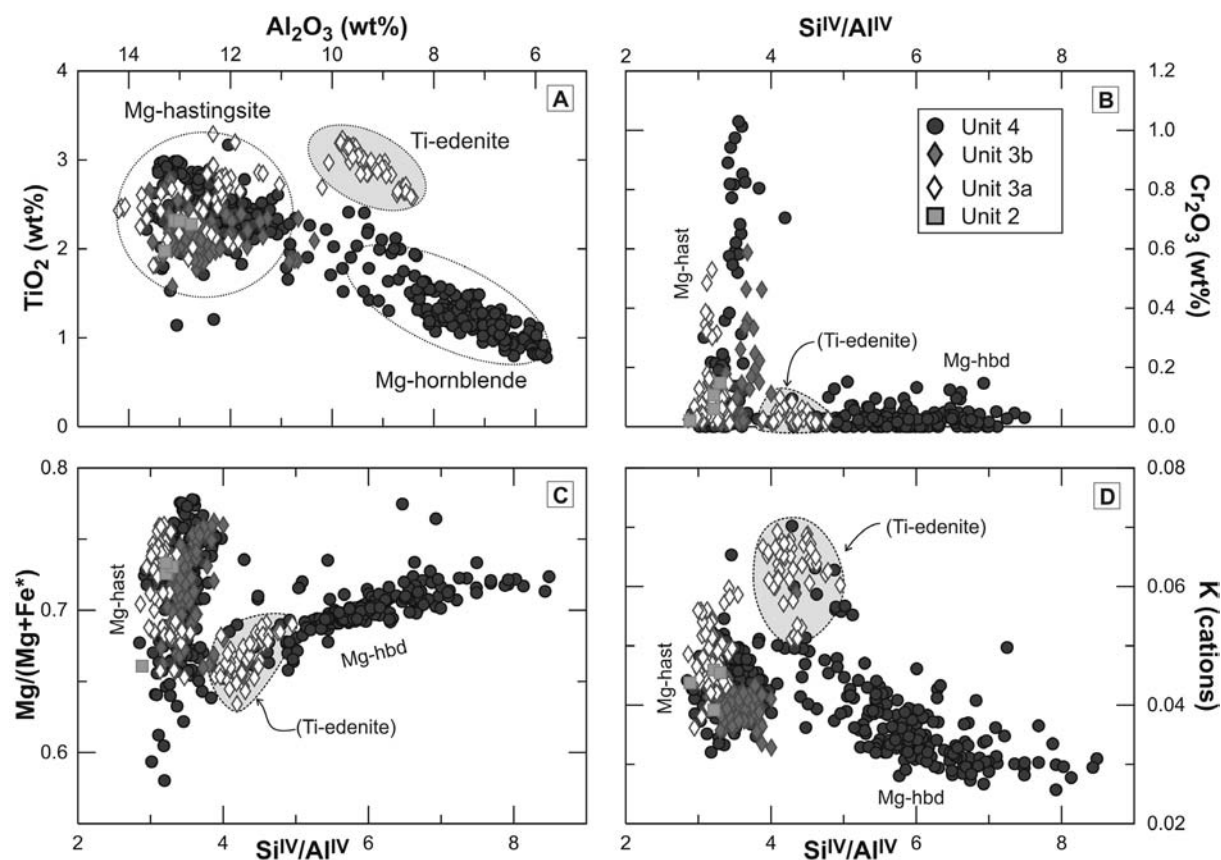


Figure 13. Compositions of amphibole phenocrysts (and xenocrysts) in NLV lavas. Cation proportions calculated assuming sum of cations=13 (excluding Ca, Na and K) and total cation charges balanced to 23 oxygens. Note that Mg-Hastingsites maintain a constant ratio of Si to Al in tetrahedral coordination ($\text{Si}^{\text{IV}}/\text{Al}^{\text{IV}}$) over a large range of $\text{Mg}\#$ and Cr contents. Mg-hornblendes have highly variable $\text{Si}^{\text{IV}}/\text{Al}^{\text{IV}}$ ratios coupled to increasing $\text{Mg}\#$ and decreasing alkali contents. Amphiboles of Ti-edenitic compositions are interpreted as xenocrysts (see text).

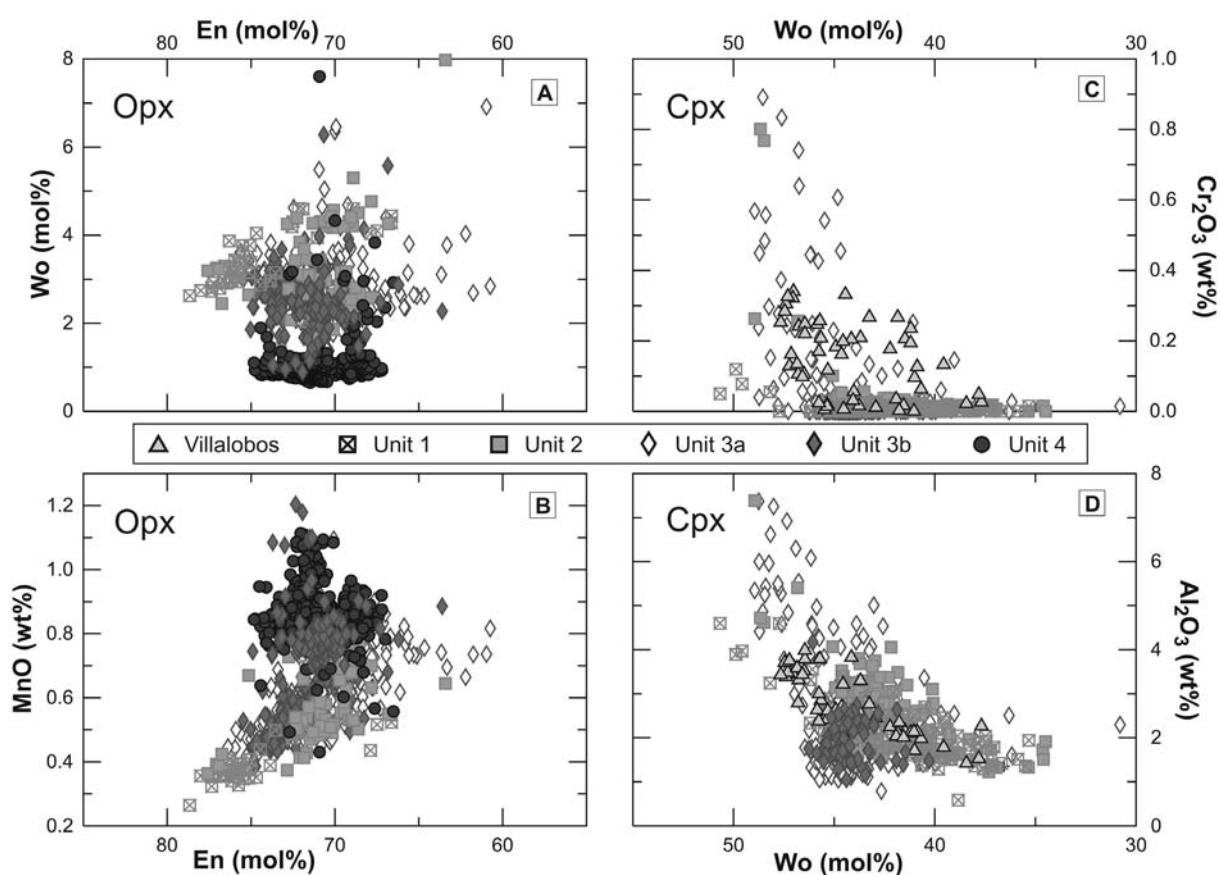


Figure 14. Chemical composition of ortho- and clinopyroxene from NLV lavas. Note that orthopyroxene from Unit 4 dacites and enclaves clustering at high MnO and low Wo contents.

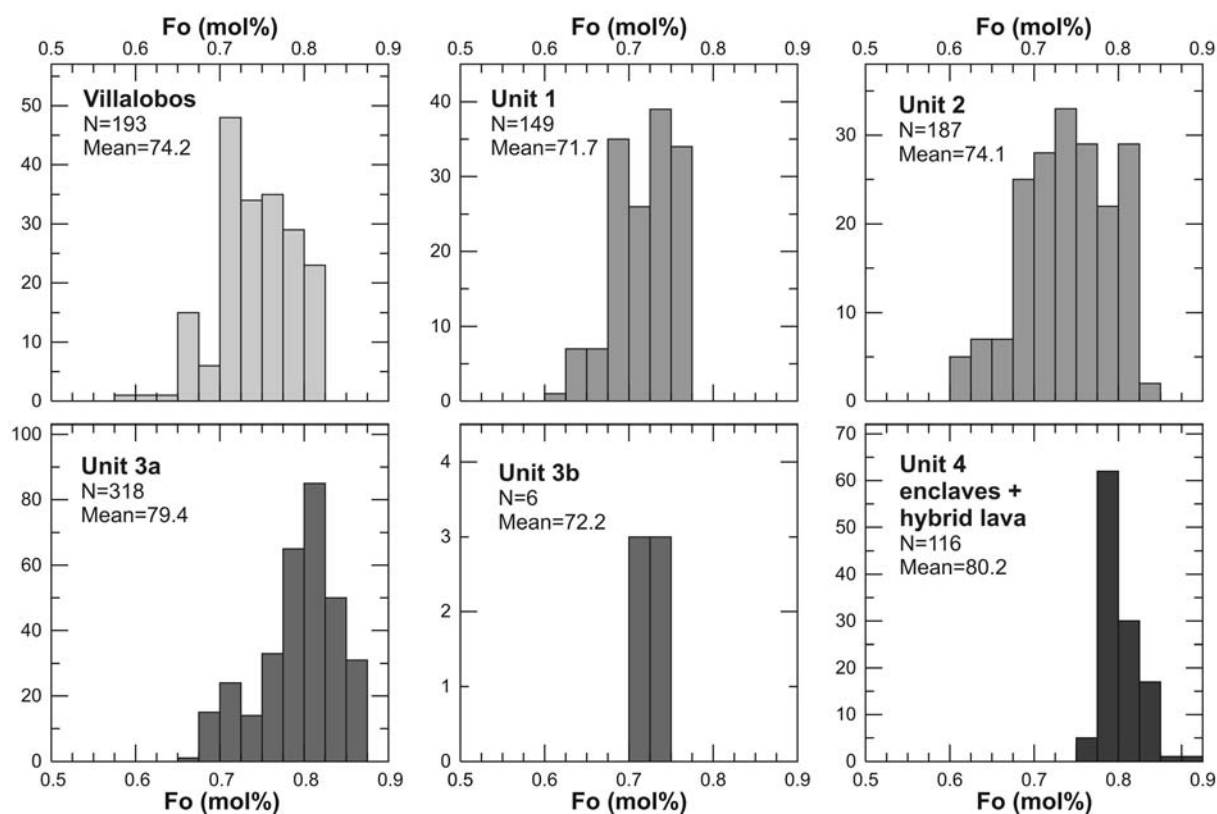


Figure 15. Forsterite (Fo) content of olivines in NLV and Villalobos lavas, separated by unit. Note the progressive narrowing of the range of compositions towards more Fo-rich olivines from old to young units. N stands for the total number of analyses per unit.

Unit	3a												3b			
	2		NL050B		NL043A		LMG01.8		LUG01.5		NL028A		LLG01.2			
Sample	NL113		Enclave		Lava											
Sample type	Lava	Lava	8677-	8677-	8640-	8640-	7182-	7182-	7147-	7147-	7147-	7147-	8400-	8400-	7164-	7164-
Label	11946-09-2	11946-09-3	16-6	16-3	02-3	02-5	14-1	14-2	04-1	04-4	05-1	06-4	01-7	01-10	03-11	01-L2_1
Amph. type	Mg-hast	Mg-hast	Ti-eden	Ti-eden	Ti-eden	Ti-eden	Mg-hast	Mg-hast	Ti-eden	Ti-eden	Mg-hast	Mg-hast	Mg-hast	Mg-hast	Mg-hast	Mg-hast
SiO ₂	42.78	43.04	45.73	46.58	44.55	45.03	42.75	42.89	45.78	45.51	43.21	42.51	41.57	41.99	43.54	45.06
TiO ₂	2.31	2.28	2.65	2.59	3.16	2.99	2.61	2.46	3.10	3.09	2.69	2.43	2.89	2.37	2.39	1.85
Al ₂ O ₃	13.00	12.77	8.71	8.45	9.67	9.43	12.85	12.61	9.48	9.72	12.04	14.20	13.02	13.63	12.87	12.52
FeO*	9.95	10.06	12.42	11.96	13.24	12.61	9.69	9.75	13.33	12.46	12.79	9.32	12.70	12.29	10.68	8.69
MnO	0.13	0.13	0.18	0.23	0.24	0.23	0.13	0.07	0.22	0.00	0.28	0.02	0.19	0.17	0.15	0.06
MgO	15.34	15.30	14.67	14.95	13.82	14.29	15.53	15.83	14.12	13.86	13.49	15.41	13.23	13.32	14.38	15.42
Cr ₂ O ₃	0.06	0.15	0.01	0.01	0.05	0.06	0.30	0.06	0.00	0.05	0.07	0.05	0.00	0.01	0.00	0.11
CaO	11.74	11.96	11.45	11.54	11.38	11.42	11.63	11.39	11.20	11.44	11.70	12.12	11.58	11.38	11.32	11.28
Na ₂ O	2.76	2.74	2.69	2.97	2.49	2.21	2.96	2.74	3.09	3.12	3.24	3.00	3.24	3.36	3.09	2.90
K ₂ O	0.22	0.25	0.35	0.33	0.36	0.36	0.28	0.28	0.32	0.38	0.27	0.31	0.27	0.21	0.22	0.23
F	0.03	0.01	0.14	0.14	0.05	0.01	0.06	0.05	0.02	0.03	0.04	0.01	0.17	0.04	0.00	0.01
Cl	0.00	0.00	0.01	0.02	0.01	0.01	0.00	0.00	0.01	0.02	0.00	0.01	0.01	0.00	0.00	0.00
Total	98.33	98.69	99.03	99.76	99.01	98.67	98.79	98.13	100.66	99.67	99.83	99.37	98.86	98.78	98.65	98.13
TiO ₂ /Al ₂ O ₃	0.18	0.18	0.30	0.31	0.33	0.32	0.20	0.19	0.33	0.32	0.22	0.17	0.22	0.17	0.19	0.15
Ions PFU																
Si ^{IV}	6.10	6.14	6.58	6.66	6.42	6.47	6.09	6.10	6.49	6.55	6.21	6.02	6.03	6.06	6.22	6.40
Al ^{IV}	1.90	1.86	1.42	1.34	1.58	1.53	1.91	1.90	1.51	1.45	1.79	1.98	1.97	1.94	1.78	1.60
Al ^{VI}	0.29	0.29	0.05	0.08	0.06	0.07	0.25	0.21	0.08	0.19	0.25	0.38	0.26	0.37	0.39	0.50
Ti	0.25	0.24	0.29	0.28	0.34	0.32	0.28	0.26	0.33	0.33	0.29	0.26	0.32	0.26	0.26	0.20
Fe ³⁺	0.74	0.63	0.52	0.36	0.58	0.62	0.71	0.90	0.47	0.15	0.42	0.53	0.59	0.58	0.52	0.44
Mg	3.26	3.25	3.15	3.18	2.97	3.06	3.30	3.36	2.99	2.97	2.89	3.25	2.86	2.86	3.06	3.27
Fe ²⁺	0.45	0.57	0.97	1.07	1.02	0.89	0.45	0.26	1.11	1.35	1.12	0.57	0.95	0.91	0.76	0.59
Mn	0.02	0.02	0.02	0.03	0.03	0.03	0.02	0.01	0.03	0.00	0.03	0.00	0.02	0.02	0.02	0.01
Ca	1.79	1.83	1.76	1.77	1.76	1.76	1.78	1.74	1.70	1.76	1.80	1.84	1.80	1.76	1.73	1.72
Na (M)	0.21	0.17	0.24	0.23	0.24	0.24	0.22	0.26	0.30	0.24	0.20	0.16	0.20	0.24	0.27	0.28
Na (A)	0.56	0.59	0.51	0.59	0.45	0.37	0.59	0.49	0.55	0.63	0.71	0.66	0.71	0.70	0.59	0.51
K	0.04	0.05	0.06	0.06	0.07	0.07	0.05	0.05	0.06	0.07	0.05	0.06	0.05	0.04	0.04	0.04
Total	15.60	15.63	15.58	15.65	15.52	15.44	15.64	15.54	15.61	15.70	15.75	15.72	15.76	15.74	15.63	15.56
Si ^{IV} /Al ^{IV}	3.21	3.30	4.62	4.95	4.07	4.23	3.19	3.21	4.31	4.51	3.47	3.03	3.06	3.12	3.49	4.00
A-site cations	0.60	0.63	0.58	0.65	0.52	0.44	0.64	0.54	0.61	0.70	0.75	0.72	0.76	0.74	0.63	0.56
#Mg	73.31	73.05	67.80	69.01	65.05	66.89	74.08	74.32	65.38	66.47	65.28	74.65	65.00	65.89	70.59	75.98

Table 4. Representative analyses of amphibole in NLV lavas. Ions per formula unit (PFU) calculated as in Figure 13.

Unit Sample Sample type	LLINC01.1 Enclave				MDCP01.1 Enclave				MADHST-2 Lava				LRBPomez01.1 Pumice					
	7150- 14-1 Mg-hast	7150- 14-2 Mg-hast	7150- 02-1 Mg-horn	7150- 09-1 Mg-horn	7331- A-L_1 Mg-hast	7331- C-L_5 Mg-hast	7331- D-L_2 Mg-hast	8404- 02-13 Mg-hast	8404- 10-L1_8 Mg-hast	8404- 10-L2_6 Mg-horn	8404- 10-L2_2 Mg-horn	8404- 09-3 Mg-horn	8404- 09-4 Mg-horn	7304- 30-2_1 Mg-hast	7304- 2-1_2 Mg-horn	7304- 25-1_8 Mg-horn	7304- 5-2 Mg-horn	7304- 10-1_9 Mg-horn
SiO ₂	43.56	42.69	47.79	49.24	42.54	42.68	43.08	43.30	43.18	43.74	45.99	48.08	50.08	42.92	44.29	47.35	50.51	50.76
TiO ₂	2.79	2.28	1.62	1.15	2.83	2.63	2.96	1.66	2.45	2.34	2.18	1.30	1.03	2.33	2.23	1.49	0.93	0.91
Al ₂ O ₃	12.25	12.51	8.22	6.69	12.59	13.51	12.97	10.87	12.49	11.78	9.30	6.88	5.98	12.02	12.74	9.73	6.50	6.11
FeO*	9.83	10.98	12.72	12.19	10.14	13.39	10.34	13.46	9.23	11.70	12.48	11.89	11.43	13.93	8.24	12.82	12.38	11.04
MnO	0.12	0.13	0.25	0.36	0.12	0.12	0.07	0.26	0.12	0.12	0.31	0.32	0.26	0.34	0.12	0.26	0.32	0.28
MgO	15.35	14.75	15.01	15.80	15.12	13.39	15.27	13.33	15.87	14.65	14.73	15.77	16.71	12.85	16.19	13.84	15.29	17.03
Cr ₂ O ₃	-	-	-	-	0.01	0.03	0.22	0.80	0.25	0.02	0.05	0.02	0.03	0.04	0.68	0.00	0.00	0.03
CaO	11.46	11.50	10.98	10.88	11.70	11.52	11.93	11.25	11.71	11.39	11.22	10.96	10.73	11.32	11.81	10.60	10.83	10.95
Na ₂ O	2.61	2.56	1.82	1.43	2.71	2.66	2.75	2.18	2.70	2.42	2.06	1.58	1.41	2.40	2.55	1.81	1.77	1.31
K ₂ O	0.21	0.24	0.23	0.20	0.25	0.25	0.25	0.27	0.27	0.27	0.27	0.19	0.28	0.35	0.22	0.30	0.24	0.17
F	0.04	0.02	0.02	0.02	0.03	0.01	0.00	0.04	0.05	0.04	0.04	0.03	0.05	0.03	0.06	0.03	0.05	0.05
Cl	0.00	0.00	0.01	0.01	0.00	0.00	0.00	0.00	0.01	0.01	0.01	0.01	0.01	0.01	0.00	0.03	0.01	0.01
Total	98.22	97.68	98.67	97.96	98.04	100.20	99.84	97.42	98.33	98.49	98.64	97.03	98.00	98.56	99.13	95.81	99.28	98.64
TiO ₂ /Al ₂ O ₃	0.23	0.18	0.20	0.17	0.22	0.19	0.23	0.15	0.20	0.20	0.23	0.19	0.17	0.19	0.17	0.15	0.14	0.15
Ions PFU	6.20	6.14	6.76	6.96	6.10	6.04	6.08	6.35	6.15	6.24	6.55	6.88	7.03	6.20	6.25	6.55	6.74	7.06
Si ^{IV}	1.80	1.86	1.24	1.04	1.90	1.96	1.92	1.65	1.85	1.76	1.45	1.12	0.97	1.80	1.75	1.45	1.26	0.94
Al ^{IV}	0.26	0.26	0.13	0.07	0.23	0.29	0.24	0.22	0.25	0.22	0.11	0.04	0.02	0.25	0.37	0.23	0.10	0.06
Ti	0.30	0.25	0.17	0.12	0.30	0.28	0.31	0.18	0.26	0.25	0.23	0.14	0.11	0.25	0.24	0.16	0.17	0.10
Fe ³⁺	0.71	0.82	0.91	1.02	0.68	0.84	0.64	0.88	0.72	0.85	0.84	0.99	1.10	0.81	0.62	1.03	1.01	1.07
Mg	3.26	3.16	3.16	3.33	3.23	2.83	3.21	2.91	3.37	3.12	3.13	3.36	3.50	2.77	3.41	3.01	3.24	3.53
Fe ²⁺	0.46	0.50	0.60	0.42	0.54	0.74	0.58	0.77	0.38	0.54	0.65	0.43	0.25	0.88	0.35	0.54	0.45	0.21
Mn	0.01	0.02	0.03	0.04	0.01	0.01	0.01	0.03	0.02	0.01	0.04	0.04	0.03	0.04	0.01	0.03	0.04	0.03
Ca	1.75	1.77	1.66	1.65	1.80	1.75	1.81	1.77	1.79	1.74	1.71	1.68	1.61	1.75	1.79	1.66	1.66	1.63
Na (M)	0.25	0.23	0.34	0.35	0.20	0.25	0.19	0.23	0.21	0.26	0.29	0.32	0.38	0.25	0.21	0.34	0.34	0.35
Na (A)	0.47	0.49	0.16	0.04	0.55	0.48	0.56	0.39	0.53	0.41	0.28	0.12	0.00	0.43	0.48	0.17	0.14	0.00
K	0.04	0.04	0.04	0.04	0.05	0.05	0.05	0.05	0.05	0.05	0.05	0.03	0.05	0.07	0.04	0.05	0.04	0.03
Total	15.51	15.53	15.21	15.08	15.60	15.52	15.60	15.44	15.58	15.46	15.33	15.15	15.05	15.49	15.52	15.23	15.19	14.98
Si ^{IV} /Al ^{IV}	3.45	3.29	5.44	6.66	3.21	3.08	3.17	3.84	3.33	3.55	4.52	6.13	7.25	3.45	3.57	4.53	5.33	7.49
A-site cations	0.51	0.53	0.21	0.08	0.60	0.52	0.60	0.44	0.58	0.46	0.33	0.15	0.05	0.49	0.52	0.23	0.19	0.03
#Mg	73.57	70.54	67.77	69.80	72.66	64.05	72.47	63.84	75.41	69.06	67.78	70.28	72.27	62.18	77.78	65.81	68.99	70.14

Table 4. (continued)

characterized by relatively low Mg# (67-75) and high Mn contents (typically >0.8, and up to 1.1 wt%). The most magnesian orthopyroxene analyzed (En>75) correspond to unzoned, Cr-rich phenocrysts from the most silica-rich sample (~62 wt% SiO₂) from Unit 2, in contact with a glass with 68% SiO₂ and 0.6% MgO, which strongly suggest a hybrid origin for the silica-rich samples of this unit.

Olivine is commonly present in mafic lavas from Villalobos and basal NLV units, and its compositions are widely distributed between Fo₆₀ and Fo₈₅ (Figure 15). It is also occasionally found in Unit 3a, it is extremely rare in Unit 3b andesites, and is only present in a few mafic enclaves and some mantled relics in the Holocene hybrid andesite. Olivine compositions in Units 3a and 4 have a narrower range of more Mg- and Ni-rich olivine compositions (although unit 3b is probably under-represented), suggesting that in these units olivine only crystallized from relatively mafic liquids, whereas in older magmas it continued to be stable in more evolved compositions.

DISCUSSION

There are systematic variations in the nature of the magmatism in the area of Nevado de Longaví volcano during the Quaternary, from mainly basaltic, tholeiitic, relatively dry and reduced during the early Pleistocene to very hydrous and oxidized during the Holocene. These variations are manifested by major-element differentiation trends, phenocryst assemblages, trace element concentrations, and oxidation state. Units of intermediate age (3a-3b) are intermediate in character, yet the internal trends follow the overall progression. Most of these variations are consistent with magmas becoming progressively more hydrous with time. Young volcanics from NLV are very different from their precursors and distinct from other magmas in the Quaternary arc. We infer that a local factor is controlling the generation of water-rich melts in the asthenosphere, and that this is first manifested during the Quaternary. We argue that the subducted segment of the oceanic Mocha Fracture Zone is a potentially efficient water supplier to the magmatic source region.

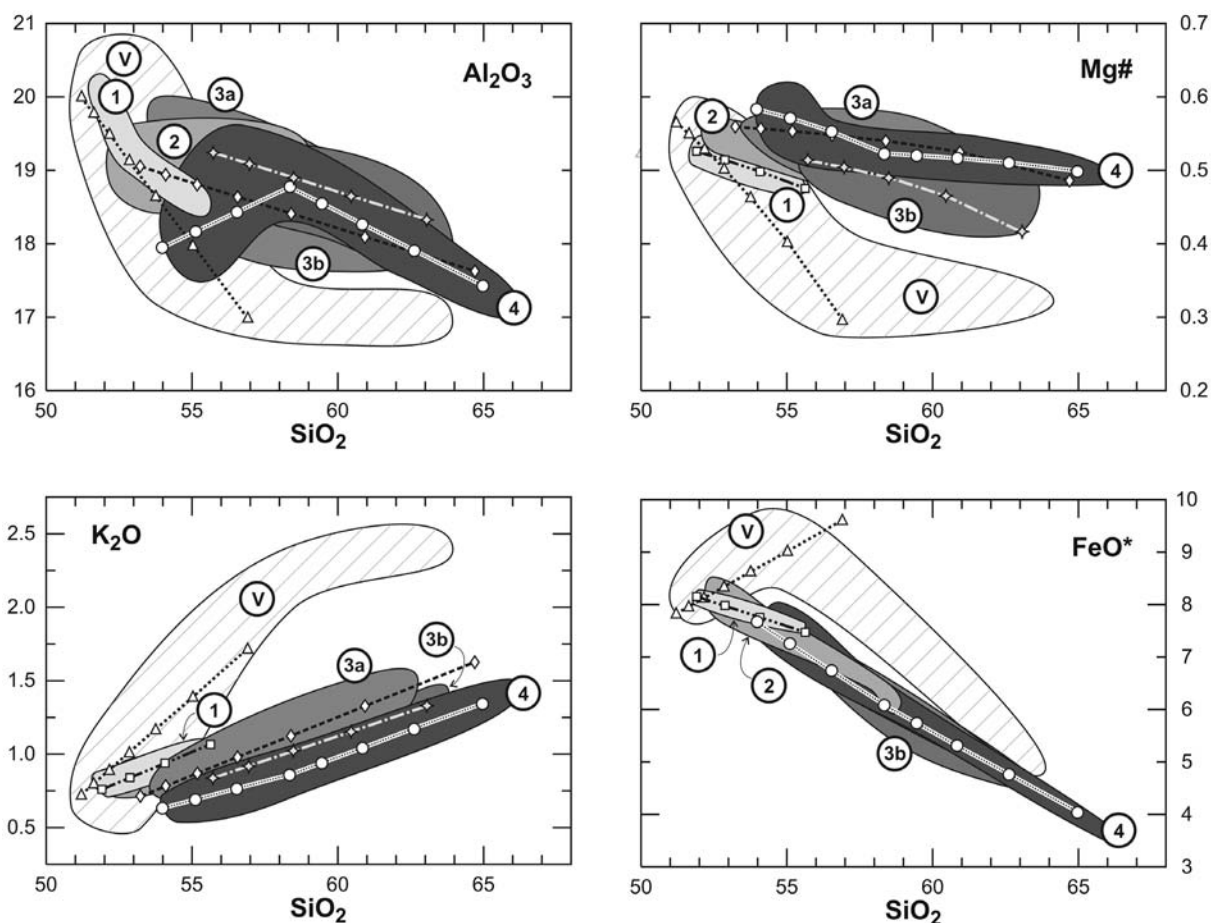


Figure 16. Mass-balance fractionation models for Villalobos and NLV units. Data normalized to 100%, all iron as FeO. Model parameters in Table 2 and Figure 6.

Closed-system evolution

Magmatic evolution seems to be primarily the consequence of crystal fractionation, although assimilation of crustal lithologies and magma mixing probably also occurred. The variety of intermediate to evolved magma compositions at NLV is the result of differences in fractionating mineral assemblages and a shift in the composition of the mafic magmas. Both of these effects are consistent with a temporal increase in the water contents of magmas.

Mass balance models (Table 2) are approximations of the mineral assemblages required to reproduce the major element trends within each unit. Models such as these are crude simplifications of much more complex systems where mineral proportions and compositions change continuously, but they still provide information on the main controls on magma differentiation. The change from anhydrous mineral assemblages for Villalobos lavas and NLV Unit 1 to amphibole-rich associations from Unit 2 onwards is consistent with the observed mineralogy. The increasing proportion of amphibole is accompanied by a substantial decrease in the amount of fractionated plagioclase, which reproduces the gently decreasing Al_2O_3 patterns typical of NLV magmas (Figure 16). Olivine is the only major phase that can drive residual liquids to higher silica contents in early units, since both plagioclase and clinopyroxene have SiO_2 contents comparable to those of basaltic liquids (~50 wt%). Olivine proportions in younger units are much lower, and orthopyroxene becomes correspondingly more important. Mg-hastingsitic amphibole (~43 wt% SiO_2) takes the predominant role in raising the SiO_2 of residual magmas in these younger units. The change from olivine- to amphibole-driven differentiation is consistent with young andesites having higher Mg#'s than older, less water-rich magmas.

Fractionation of plagioclase-rich, high- SiO_2 assemblages in Villalobos lavas resulted in limited silica increases in the derivative liquids but rapidly increasing alkalis and decreasing MgO and Al_2O_3 . This differentiation pattern probably explains the large range of olivine phenocryst compositions recorded in Villalobos and Unit 1 lavas. Olivine stability is favored by rapidly increasing K_2O because alkalis have the effect of expanding the olivine primary phase volume (Grove and Juster, 1989; Longhi, 1991). In NLV Units 2 through 4, amphibole-

driven differentiation rapidly increases the SiO_2 content of derivative liquids, thereby favoring crystallization of orthopyroxene rather than olivine, which is consistent with the narrow range of Fo-rich olivine compositions.

Limited spinel fractionation (<3 wt%) from Villalobos lavas is consistent with the observed early iron enrichment, and high-temperature ilmenite is required to limit TiO_2 . The low proportion of oxides relative to silicates crystallizing from Villalobos magmas probably relates to the reduced nature of these magmas, as inferred from natural Fe-Ti oxides and low magmatic water contents (Sisson and Grove, 1993). Spinel proportions are higher for all NLV units (>5 wt%), consistent with increasing water contents and increasing oxygen fugacity, which also has the effect of increasing the oxide saturation temperatures (Pichavant *et al.*, 2002).

Plagioclase compositions record the changing magmatic conditions that prevailed during the temporal evolution of NLV in two ways. The orthoclase contents of plagioclase at a given An-content decrease continuously from Villalobos to Unit 4, in accord with the shift in K_2O enrichments in intermediate and evolved magmas. The coherence between plagioclase and whole-rock chemistry indicates that most plagioclase crystals probably crystallized directly from their host magmas. In addition, crystallization experiments by Prouteau and Scaillet (2003) indicate that the orthoclase content of plagioclase decreases with increasing magmatic water content. There is also a regular decrease in the FeO^* and MgO contents in plagioclase with time, which we interpret as a delay in the appearance of plagioclase due to increasing water contents in magmas (*e.g.* Sisson and Grove, 1993); plagioclase in young magmas started crystallizing after liquids were depleted in iron and magnesium to a greater extent than magmas from the older units. Higher iron contents in plagioclase in more oxidized magmas is in principle favored by the ability of Fe^{3+} to substitute for Al^{3+} (Phinney, 1992), but as oxidized magmas are also wetter, the suppression of plagioclase crystallization dominates.

A better indication of the increasing oxygen fugacity of the magmas is given by the FeO^*/MgO ratio in plagioclase, which shows a spectacular increase from old to young units. Since the partition coefficients of Fe^{2+} , Fe^{3+} , and Mg^{2+} do not change dramatically with oxygen fugacity or plagioclase composition (Bindeman

et al., 1998; Lundgaard and Tegner, 2004), such an increase in the FeO^*/MgO ratio probably indicates a high $\text{Fe}^{3+}/\text{Fe}^{2+}$ ratio in the coexisting magma.

Fractionation of significant amounts of amphibole from NLV magmas contributes to the low incompatible element contents of evolved NLV magmas because it lowers the bulk silica content of the fractionated mineral assemblage, and also because amphibole more readily accommodates a number of elements that are highly incompatible with respect to anhydrous phases. Amphibole fractionation is consistent with the high modal abundances of this phase in late NLV lavas, and is corroborated by presumably cogenetic amphibole-rich, cumulate-textured blocks recovered from young lavas (Chapter 3). The high Cr and Mg#’s of some Mg-hastingsites indicate that amphibole is an early phase in the crystallization sequence. Amphibole in calc-alkaline mafic magmas has been produced experimentally at various pressures under water-rich and water-saturated conditions, either as a liquidus phase or following olivine and augite (Sisson and Grove, 1993; Moore and Carmichael, 1998; Müntener *et al.*, 2001; Pichavant *et al.*, 2002; Grove *et al.*, 2003; Grove *et al.*, 2005). According to the relationship among experimental amphiboles described by Grove *et al.* (2005), the most magnesian amphiboles in NLV (Mg# = 0.78) could have precipitated from mafic magmas with ~9 wt% H_2O .

Al-poor Mg-hornblende, found only in Unit 4, records a stage of late evolution that does not seem to have been attained by older units. The increasing $\text{Si}^{\text{IV}}/\text{Al}^{\text{IV}}$ ratios attest to increasingly SiO_2 -rich character of the residual liquids from which they crystallized. Al-poor amphiboles crystallize from rather evolved liquids as is suggested by comparison with experimental data (Figure 17A). A linear regression through the low-pressure experimental data ($r^2=0.8$) has been used to estimate the $\text{SiO}_2/\text{Al}_2\text{O}_3$ ratio of the liquid from which amphiboles could have crystallized. This calculated $\text{SiO}_2/\text{Al}_2\text{O}_3$ ratio can in turn be transformed into a SiO_2 content given the approximately linear relationship between $\text{SiO}_2/\text{Al}_2\text{O}_3$ and SiO_2 ($r^2=0.9$) in the range of natural whole-rock compositions. A linear relationship probably does not hold true for more evolved melts saturated in feldspars, which leads to overestimates in the calculated SiO_2 of melts. These approximate liquid compositions in equilibrium with amphiboles are compared to the actual whole-rock composition of their host lavas (Figure 17B). Calculated values for Mg-hastingsitic amphiboles lie at or above the 1:1-line for mafic samples but below that line for dacites. This indicates that Mg-hastingsite could be a liquidus phase in mafic enclaves whereas most amphiboles of this composition in andesites and dacites are inherited from earlier stages of evolution (*antecrysts*). Mg-hornblende, on the other hand, could be a near-liquidus

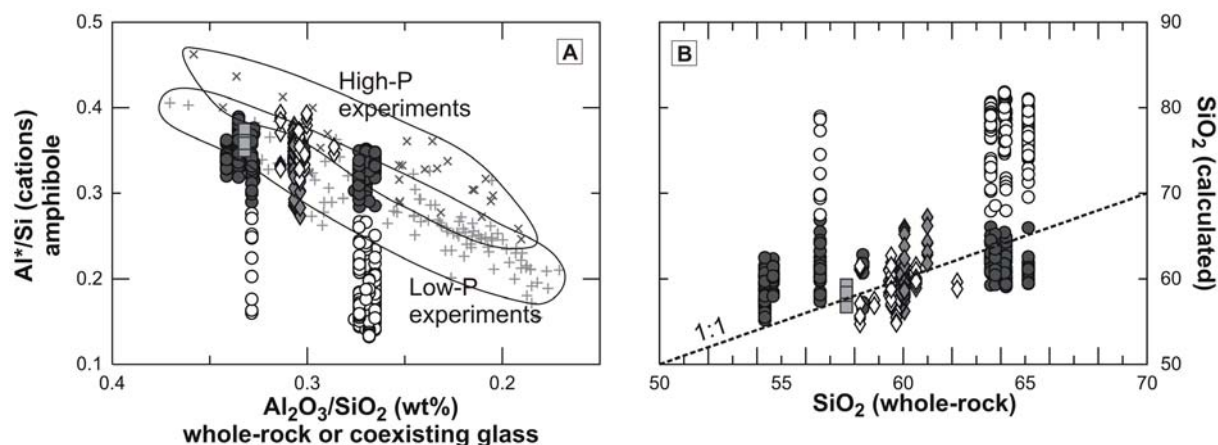


Figure 17. A: NLV amphiboles compared to experimental compositions. X-axis is the composition of coexisting glass for experimental data and whole-rock composition for natural samples. Fields of high- ($P > 0.5$ GPa) and low-pressure experiments are highlighted. Symbols for units as in preceding figures. Filled circles = Mg-hastingsite; hollow circles = Mg-hornblende. **B:** Calculated SiO_2 of liquid in equilibrium with amphiboles by linear regression of low-P experimental amphiboles. A linear relationship between whole-rock SiO_2 and $\text{SiO}_2/\text{Al}_2\text{O}_3$ has been assumed, which is a valid approximation for the range of whole-rock compositions, but might overestimate the calculated SiO_2 in more evolved liquids. Experimental data from Rutherford and Devine (1988), Sisson and Grove (1993), Grove *et al.* (1997), Moore and Carmichael (1998), Martel *et al.* (1999), Prouteau *et al.* (1999), Scaillet and Evans (1999), Hilyard *et al.* (2000), Müntener *et al.* (2001), Pichavant *et al.* (2002), Prouteau and Scaillet (2003), and Costa *et al.* (2004).

phase in dacites and more evolved residual melts such as those preserved as glass pockets in enclaves and in the groundmass of dacites. The associated increases in Mg# probably results from the scarcity of ferrous iron in the oxidized residual liquids. Incorporation of Fe³⁺ in the crystal structure has to be compensated in terms of electrical charges by decreases in Ti⁴⁺ contents and in A-site occupancy despite the high alkali contents in liquids (see Figures 13A and 13D). Mg-hornblende did not crystallize in pre-Holocene units, consistent with the lack of evolved pre-Holocene magmas. It could be speculated that advanced evolution leading to dacitic magmas took place in a shallow magma chamber which was only developed in Holocene times.

If the fractionation model advocated here, and by Rodríguez (in prep) is correct, the minerals that crystallized during the early evolution of Unit 4 magmas have largely disappeared from the nearly aphyric enclave suite. The only surviving phenocryst phase is scarce amphibole-rimmed, Fo-rich olivine. The modeled fractionating assemblage requires significant amounts of clinopyroxene and calcic plagioclase that are present in presumably cogenetic amphibole cumulates (Chapter 3), but not in the quenched mafic enclaves or dacites. Physical separation of phenocrysts may have been important, but another possible mechanism is that these water-rich magmas became superheated upon adiabatic ascent and crossed the water-undersaturated liquidus. Superheated water-rich magmas will dissolve the solid phases present, and crystallization resumes only after the water-saturated liquidus is attained (Annen *et al.*, 2006). At the point that crystallization resumes amphibole is probably the liquidus phase of Unit 4 enclaves, whereas plagioclase crystallization was suppressed due to the high water contents, and thus highly calcic plagioclase did not crystallize again. Andesitic magmas with 10-7 wt% H₂O are expected to crystallize amphibole at the water-saturated liquidus (Annen *et al.*, 2006).

Garnet is probably among the early phases that did not survive magma ascent. Amphibole fractionation accounts for part of the HREE depletions in NLV evolved magmas, but the steep Y and HREE depletion patterns of Unit 4 mafic magmas (Figure 18) suggests that trace amounts of garnet (<2 wt%) could be involved during the evolution of mafic magmas (Rodríguez, in prep). Amphibole fractionation cannot produce such

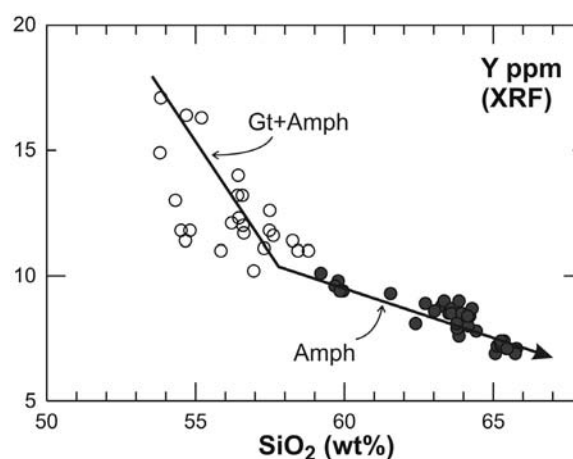


Figure 18. Yttrium variation diagram for Unit 4 magmas. The steep Y decrease defined by the mafic enclave suite (open circles) is thought to reflect garnet fractionation, whereas the gently decreasing trend of the evolved lavas (filled symbols) can be explained by amphibole fractionation. The lines drawn are only indicative. Modeled trends are presented by Rodríguez (in prep).

a pattern because it would require partition coefficients of the order of ~7-8 (assuming amphibole makes ~1/3 of the fractionated assemblage, table 2), whereas D_Y and D_{HREE} for amphibole in basalts are generally <2 (Dalpé and Baker, 2000 and references therein). Further Y and HREE depletion from 57 to 65 wt% SiO₂ might not require garnet because amphibole partition coefficients increase in silicic liquids. D_Y values of about 6-7 would suffice to explain the observed depletion, which are well within the published values for silicic liquids (Ewart and Griffin, 1994; Sisson, 1994). Garnet can be a stable phase in hydrous mafic and intermediate magmas at crustal pressures $P > \sim 0.8$ GPa as has been experimentally determined (Müntener *et al.*, 2001; Ulmer *et al.*, 2003; Ulmer and Müntener, 2005; Alonso-Pérez *et al.*, in prep). This suggests that much of the crystallization of mafic NLV magmas could be taking place in the deep crust (Annen *et al.*, 2006).

Open-system processes

Crystal fractionation is probably responsible for many of the distinctive characteristics of NLV lavas. It seems unlikely that the compositional trends at NLV could be explained by mixing of silicic crustal melts with mantle derived basalts, as this would require a silicic component with extremely low incompatible element contents. To produce a melt with incompatible element concentrations like those of the Holocene dacites by an acceptably moderate amount of

melting (20-5%) would require a source with incompatible element concentrations that were 0.5-0.1 of those in Rudnick and Gao's (2003) estimated lower crustal composition.

Even if a purely crustal origin for evolved NLV magmas seems unlikely, evidence for open-system processes is found in many lavas in the forms of disequilibrium textures, partially molten plutonic xenoliths, and from mineral chemistry. For example, glass-rich andesitic blocks from Unit 1 contain plagioclase and unzoned Cr-rich pyroxenes of more primitive character than Unit 1 basalts, that could not have crystallized from a liquid such as the evolved glass of the groundmass. Such andesitic compositions have never been found in lava outcrops, and probably represent mixing and quenching before equilibration could take place.

Radiogenic isotopes provide few constraints because of the lack of contrast with basement lithologies. Incompatible element concentrations provide an alternative approach to detect crustal contributions by comparing the incompatible element enrichments of evolved and intermediate lavas relative to the concentrations in mafic magmas. This is illustrated in Figure 19, where two evolved samples from

each unit are normalized to a mafic sample from the same unit. This comparison relies on the assumption that lavas within units are genetically linked. In closed-system evolution, the maximum enrichment factor is given by $1/F$ if the element is perfectly incompatible (*i.e.* $D=0$), where F is the mass fraction extracted by fractionation. Any enrichment above this theoretical maximum indicates open-system inputs such as mixing with crustal partial melts. Values below this factor indicate that the element is being incorporated to some extent into the solid fraction ($D>0$). Unit 4 dacites (Figure 19F) constitute a remarkable example of nearly closed-system evolution, wherein the most incompatible elements define a flat "plateau" at a value of 2, in agreement with the ~50% fractionation estimated with the major-element mass-balance models. Unit 3b andesites have larger enrichments for the highly incompatible elements Rb and Th than for other elements, and this is even more pronounced for Unit 3a samples. Glassy blocks from Unit 1 show a more disturbed pattern, with up to eight-fold Rb enrichment, up to four-fold Th, and significant LREE enrichments (see also Figure 8).

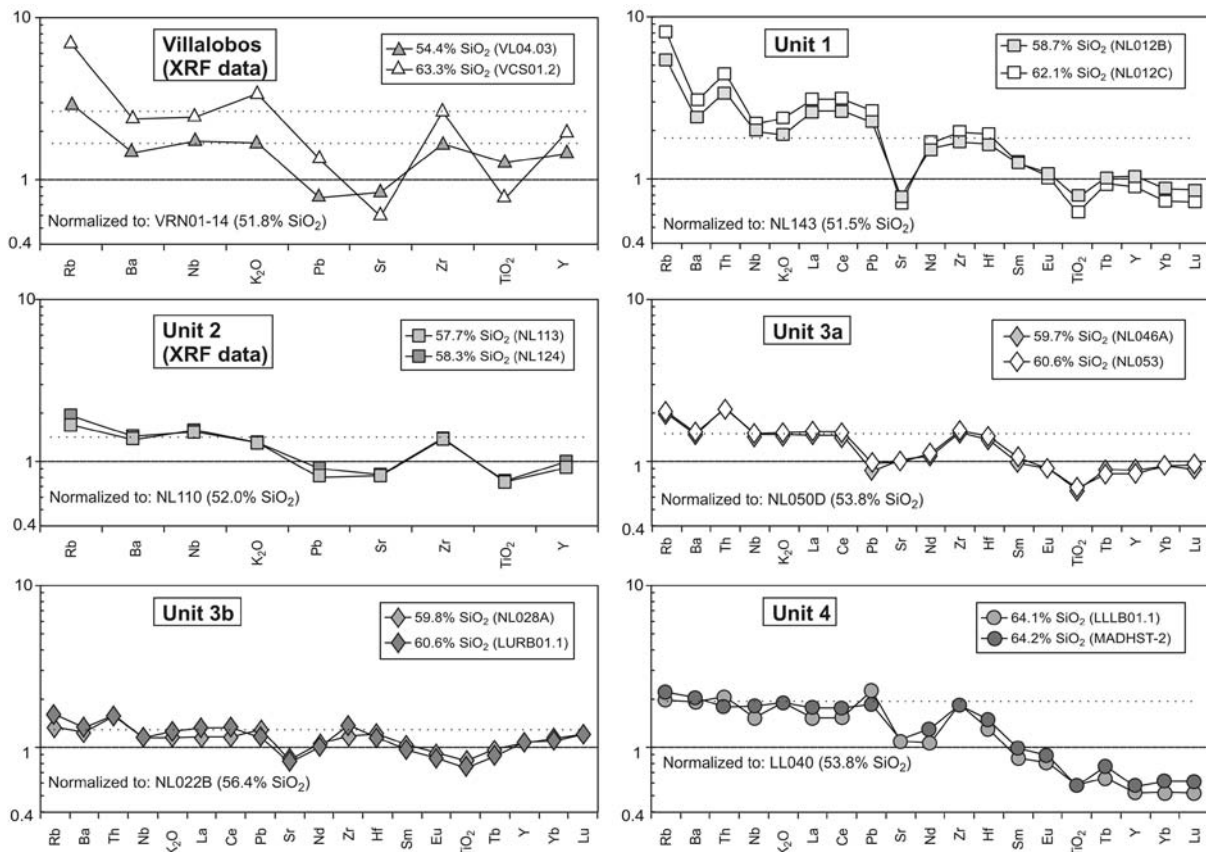


Figure 19. Multi-element spidergrams illustrating the compositions of the two most evolved samples of each unit, normalized to a mafic sample of the same unit. Dotted lines represent the estimated maximum level of enrichment due to closed-system differentiation.

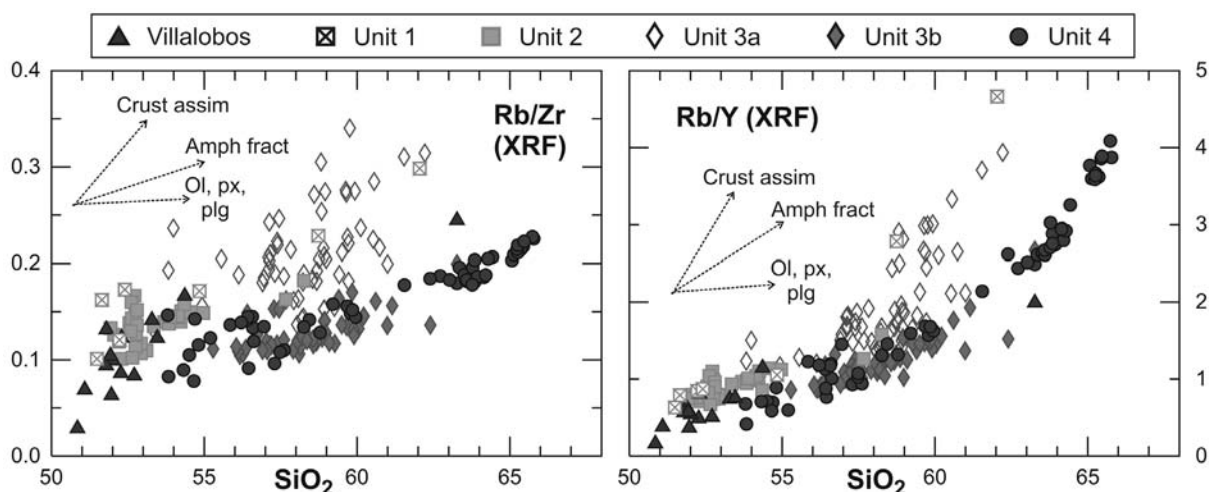


Figure 20. Rb/Zr and Rb/Y ratios of Villalobos and NLV lavas. Vectors of crustal assimilation, amphibole fractionation, and anhydrous assemblage fractionation are proposed.

These patterns of excess enrichments of the highly incompatible element Rb over other trace elements can be used as indicators of the participation of a shallow crustal component (Figure 19). Rb/Zr is particularly useful because Rb will be readily concentrated in low-degree silicic melts upon breakdown of biotite and eutectic melting of alkali-feldspar, whereas Zr will remain in refractory zircon, unless bulk crystals are incorporated into the host magma. Evolved andesites from Unit 1 and most andesites from Unit 3a exhibit elevated Rb/Zr ratios relative to the rest of the units, in agreement with the presence of amphibole xenocrysts in the latter and crystal-glass disequilibrium in the former (Figure 20). The gently increasing trend displayed by Units 2, 3b and 4 can be explained by amphibole-dominated fractionation because amphibole has a higher preference for Zr than for Rb (e.g. Green *et al.*, 1993; Ewart and Griffin, 1994; Brenan *et al.*, 1995). A similar behavior is observed for Rb/Y ratios, although the trend of amphibole fractionation is steeper due to the greater affinity of amphibole for HREE and Y (Ewart and Griffin, 1994; Sisson, 1994). Villalobos lavas also show increasing Rb/Zr and Rb/Y ratios with increasing silica. This strongly suggests important crustal assimilation because no amphibole fractionation can be invoked, and anhydrous mineral fractionation will exert only a minor influence on these ratios. However, even the highest Rb/Zr ratios of Unit 3a andesites are at the low end of the SVZ array. All these observations suggest that crustal assimilation plays a relatively minor role in NLV magma evolution. Holocene dacites have values comparable to dacites and rhyolites from Puyehue Volcano, which has been often cited as

an example of nearly closed-system evolution (Gerlach *et al.*, 1988).

Origin of mafic magmas

Crystal fractionation of dry or hydrous mineral assemblages together with minor crustal contributions can explain most of the compositional diversity of intermediate and evolved lavas in this study area. There are also significant differences among mafic compositions at the origin of each one of these fractionation trends. In this section we explore the origin of these differences at the mafic end at the spectrum (MgO 4.5-6.5%).

The most magnesian (~6% MgO) lavas from Villalobos and NLV Unit 2 are basalts with ~52 wt% SiO₂, whereas for the same MgO content, Unit 4 quenched mafic enclaves have 54-55 wt% SiO₂. Unit 4 enclaves have higher Mg#s than basalts, due largely to the early iron enrichments in Villalobos lavas (e.g. see Figures 4 and 16). Cr and Ni contents are similarly low in all units (<200 and <90 ppm respectively), indicating that they have undergone similar degrees of fractionation from their respective primitive magmas (Figure 21). The nearly 2 wt% higher SiO₂ in Unit 4 mafic magmas is not necessarily due to mixing with more evolved melts, as incompatible elements are actually lower in Unit 4 enclaves than in basalts from Villalobos and basal NLV units (Figure 22). This is especially marked for the highly incompatible elements Th and U, but also for K, Ti, LREE, Zr and Hf (Figure 23).

Although some of these differences among mafic magma compositions might reflect different early differentiation histories, trace

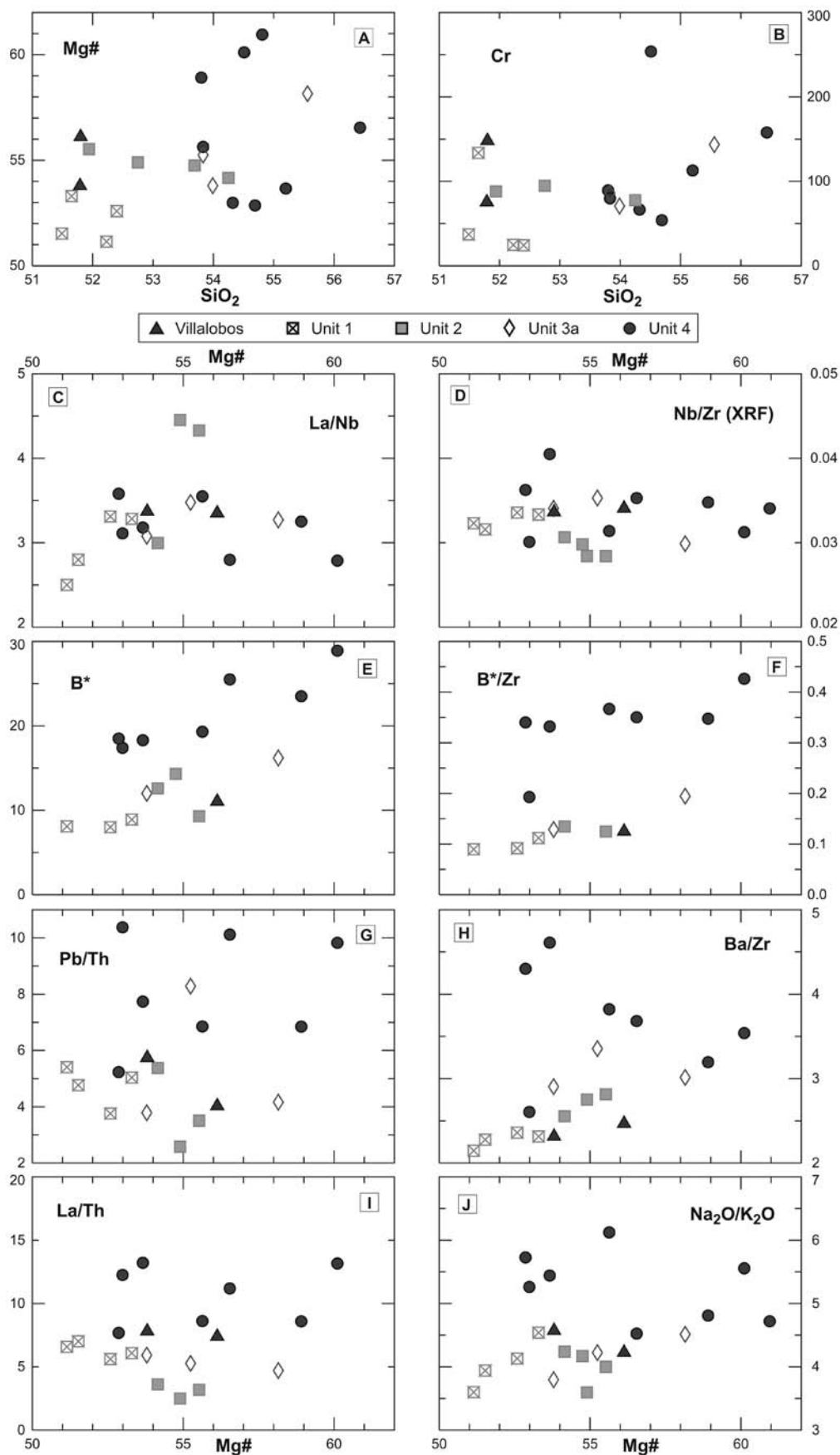


Figure 21. Variation chemical diagrams for samples with $\text{MgO} > 4.5$ wt%. **A and B:** Holocene mafic enclaves have Mg# and Cr contents comparable to those of older basalts despite their higher SiO_2 contents. **C and D:** Ratios of similarly immobile elements (La/Nb, Nb/Zr), thus probably characteristic of the mantle source, are constant for mafic magmas from all units. **E through J:** Concentration of the highly fluid-mobile element B and ratios of mobile to immobile element are high in Holocene enclaves compared to older basalts. B* is combined ICP-AES and ICP-MS data (see table 1).

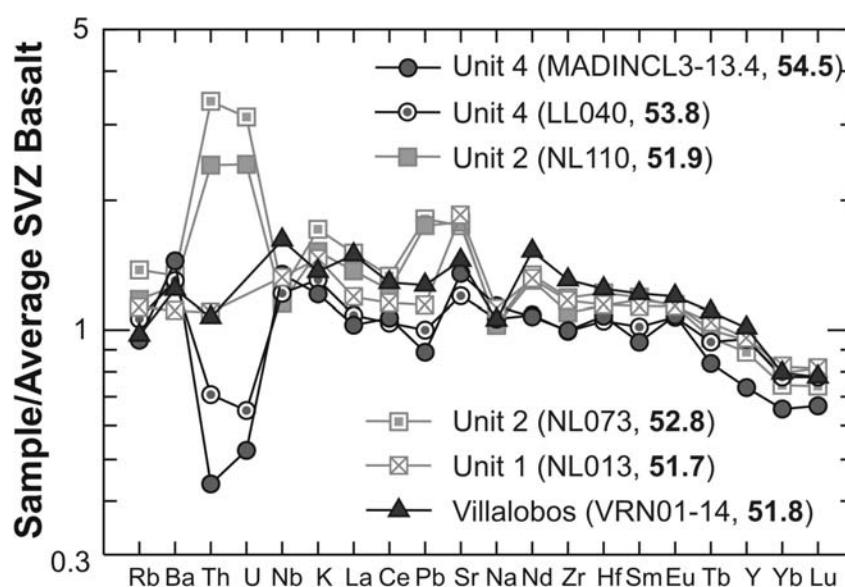
element ratios seem to indicate that the differentiation series were derived from different primitive magmas. Ratios of elements that are thought to behave similarly during mantle melting (e.g. La/Nb, Nb/Zr, Figure 21C and 21D) display similar ranges of variation for mafic magmas from all units in accord with derivation from similar mantle sources. Elements that are considered to be fluid-mobile (e.g. B, Ba, Pb) are systematically enriched relative to fluid-immobile elements in the Unit 4 mafic enclaves (Figure 21E to 21H). Samples from Villalobos and NLV Unit 1 tend to have low values for these ratios, whereas Units 2 and 3a have intermediate values (e.g. B and Ba/Zr). Similarly, La/Th and Na₂O/K₂O ratios are systematically higher in Unit 4 enclaves than in earlier mafic magmas, and these values, although scattered, do not systematically change with decreasing Mg#. These constraints indicate that early differentiation is probably not the primary cause of the observed differences. Instead, the compositions of mantle-derived primitive magmas changed over time. Increasing ratios of fluid-mobile to fluid-immobile elements suggest that primitive magmas were characterized by increasing proportions of slab-derived fluids that were added to mantle peridotites of closely similar initial compositions.

An increase in the amount of slab-derived fluids fluxed into the mantle wedge would lead to increasing degrees of melting if other parameters remained constant (notably temperature), because the extent of mantle melting is a strong function of the amount of water present as long as the source is fertile enough so that clinopyroxene is not completely

consumed (Stolper and Newman, 1994; Hirschmann *et al.*, 1999). Derivation of NLV mafic magmas from progressively higher degree mantle melts is consistent with the observed major and trace element characteristics. It has been determined experimentally that hydrous peridotite melts have higher SiO₂ contents (on a volatile-free basis) than anhydrous melts at the same P-T conditions (Hirose and Kawamoto, 1995; Gaetani and Grove, 1998), and that for a given temperature, increasing degrees of melting produce liquids with increasing SiO₂ and decreasing Al₂O₃ contents (Hirose and Kawamoto, 1995; Hirose, 1997). These differences in melt composition are mainly due to the expansion of the olivine stability field with increasing water (Ulmer, 2001), which leads to a high pyroxene/olivine contribution to silicate liquids during hydrous melting. It is therefore possible that the high SiO₂ of the most magnesian Unit 4 mafic enclaves reflects, at least in part, a primary feature of the primitive magma from which they are derived rather than early fractionation. High-degree partial melts would also be consistent with the low concentrations of incompatible elements observed in Unit 4 mafic magmas, despite their relatively high silica contents.

The increase in the amounts of fluids that flux the mantle is best explained by the arrival of the subducted segment of the Mocha Fracture Zone (MFZ). Oceanic fracture zones commonly host partly or fully serpentinized peridotites (e.g. Bach *et al.*, 2004). Fully serpentinized peridotites can contain up to 13 wt% H₂O, *i.e.* an order of magnitude more than altered oceanic crust, and may thus transport large quantities of water to

Figure 22. Multielement spidergram for selected mafic samples. In parenthesis are indicated sample code and SiO₂ content (in wt%, anhydrous basis). All analyses normalized to the average composition of ~30 SVZ basalts. Values used for normalization (in ppm) are Rb: 11.4, Ba: 166, Th: 1.3, U: 0.4, Nb: 2, K: 4317, La: 7.3, Ce: 18.1, Pb: 6.3, Sr: 432, Na: 22850, Nd: 10.9, Zr: 68, Hf: 1.8, Sm: 2.9, Eu: 0.97, Tb: 0.49, Y: 17, Yb: 1.8, Lu: 0.27.



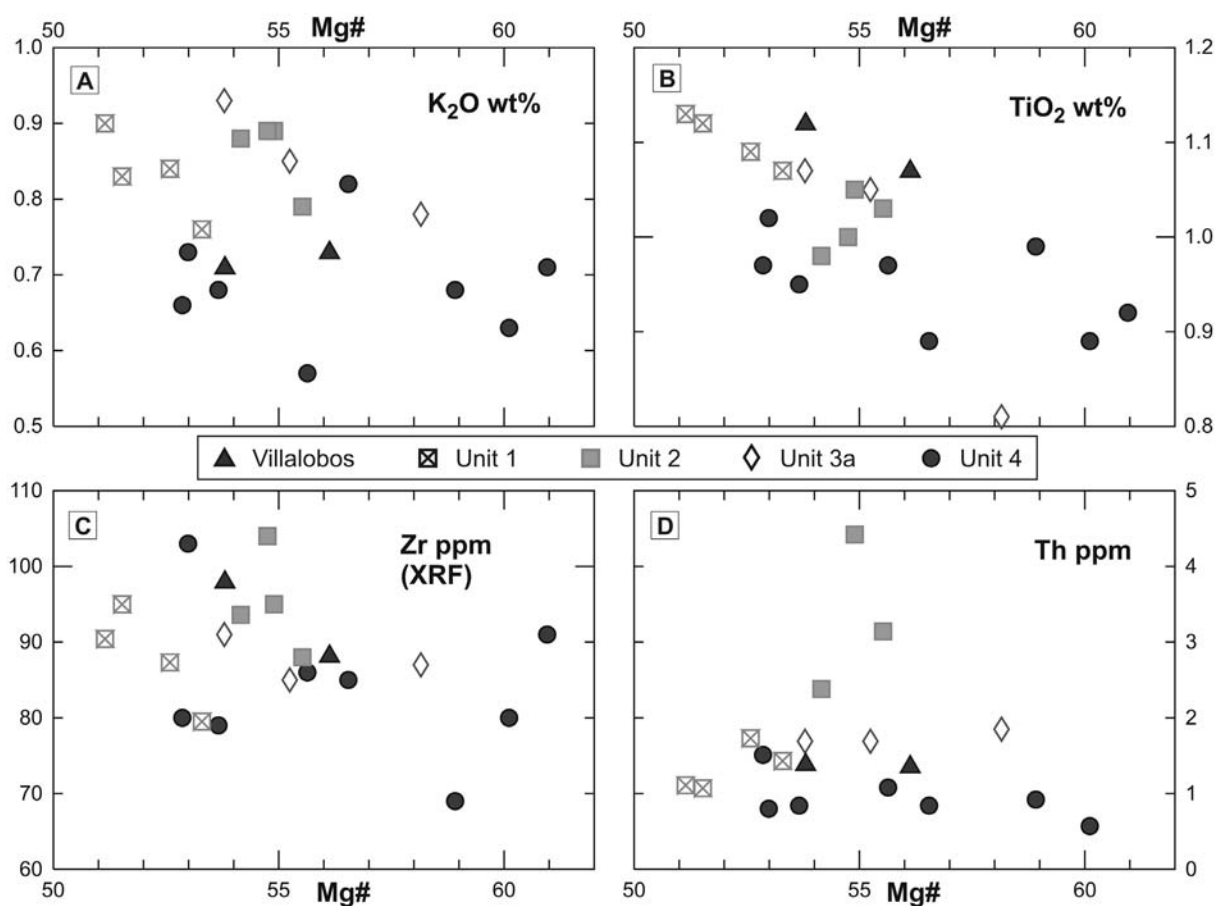


Figure 23. Incompatible element contents against Mg# for samples with MgO >4.5 wt%. Note the low concentrations in Unit 4 magmas.

the subarc mantle (Ulmer and Trommsdorff, 1995). Magmas from Seguam Island in the Aleutian arc, located above the projection of the Amlia oceanic fracture zone, show most of the chemical characteristics of NLV magmas, including low incompatible element contents and high fluid-mobile to fluid-immobile element ratios (Singer *et al.*, 1996; Jicha *et al.*, 2004).

High-degree partial melts are consistent with the overall low concentrations of incompatible elements observed in Unit 4 mafic magmas (Figure 23). However, Th and U are considerably more depleted in Unit 4 enclaves than other incompatible elements (Figure 22), which cannot be explained by higher degrees of melting. It is possible that low Th and U is a primary feature of the fluids flushing the melting region; *i.e.* that serpentinite-derived fluids have lower Th and U than those released by normal altered oceanic crust + sediments. The nature and composition of subduction zone fluids remain largely unconstrained, but there are some indications that this could be the case. Fluid inclusions formed during dehydration breakdown of antigorite serpentinite have negative Th anomalies but no U depletion,

although it is unclear if this is a primary feature of the serpentinite or the result of interaction with external crustal sources (Scambelluri *et al.*, 2001). Furthermore, the passage of large amounts of slab-derived fluids through the inverted mantle gradient might induce mantle metasomatism with phlogopite precipitation, thus retaining part of the Th and U inventory of the fluids prior to mantle melting.

The opposite case of elevated Th and U concentrations (as well as high Pb and Sr) is a notable feature of Unit 2 basalts. These high abundances correlate with relatively high ⁸⁷Sr/⁸⁶Sr and low ¹⁴³Nd/¹⁴⁴Nd ratios, suggesting a crustal contribution (Figure 24). Elevated Th/La ratios suggest that this source could be subducted sediments that enter the asthenospheric mantle in the form of hydrous partial melts. Whereas U, Pb and Sr are thought to be relatively mobile in fluids, Th is considered to be fluid-immobile but readily concentrated in partial melts (Plank, 2005). One evolved sample from Unit 3a shows a similar tendency as Unit 2 basalts, and might reflect the transitional character of the lower main cone lavas. This transitional sediment signature could mark the

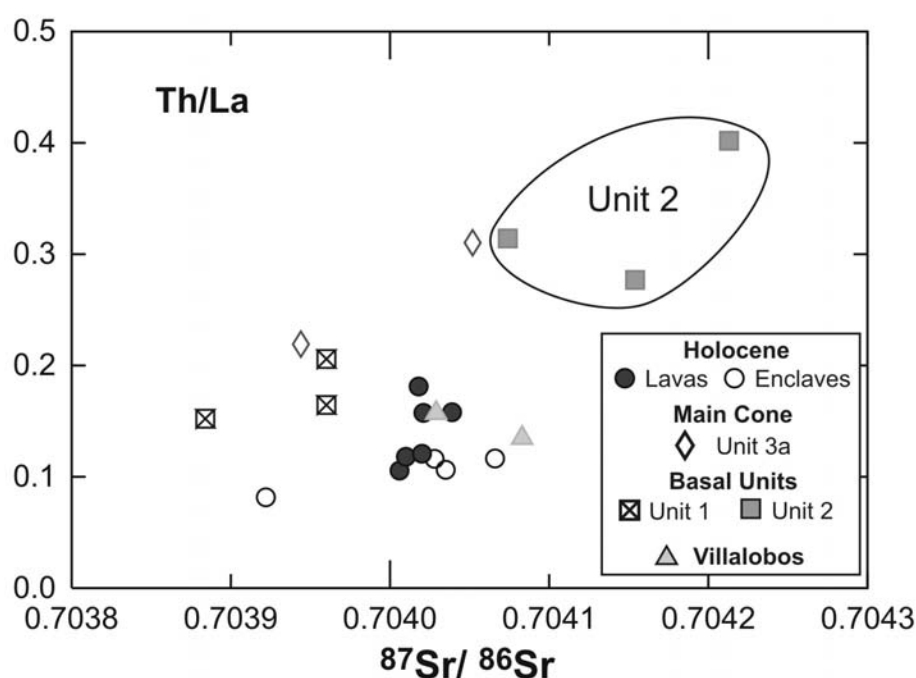


Figure 24. Thorium/lanthanum ratio versus $^{87}\text{Sr}/^{86}\text{Sr}$. The high values in both parameters in samples from Unit 2 might indicate participation of subducted sediments (Plank, 2005).

inception of the MFZ in the area. Sediments trapped in the trough of the fracture zone, thus, apparently contributed to mantle melts only during a short, transitional period. Subsequent magmatism was mainly influenced by low-Th and U fluids from serpentinite dehydration.

A causal link between the MFZ and the chemical peculiarities of NLV magmatism is consistent with the highly localized occurrence of these magmas both in space and time. As the intersection of the MFZ and the SVZ migrates southwards, it would be expected to find older, highly wet magmas north of Longaví. No other magmas with the characteristics of NLV dacites have been documented in the recent SVZ, but two Miocene incompatible-element-poor adakite-like occurrences are known round the latitude of Santiago ($33^{\circ}30'S$). Manquehue-type intrusives (Sellés, 1999) and the Teniente Porphyry intrusive (Kay *et al.*, 2005) show many of the characteristics of NLV magmas, including elevated Sr/Y and Ba/Th ratios, low incompatible element contents and high modal amphibole proportions. A detailed comparison is out of the scope of this contribution, and is only mentioned to highlight the fact that magmas similar to NLV lavas might have occurred in other times and locations.

CONCLUSIONS

The 1 Ma to present sequence of volcanic rocks studied records a long-term change in the nature of the magmas erupted in the area. This change is recorded in the whole-rock composition of mafic to evolved magmas as well as in the chemistry of the mineral phases present in them. The oldest rocks studied (Villalobos volcano), which are relatively dry and reduced, fall within the regional along-arc variation trends depicted by SVZ volcanic centers. Conversely, the youngest erupted rocks are highly hydrous and oxidized magmas that do not conform to regional trends. The passage from “normal” to “anomalous” magma compositions appears to have been transitional as is attested by units with intermediate ages.

The evolution towards intermediate and evolved magmas is dominated by crystal fractionation of solid assemblages that include increasing amounts of amphibole and lesser proportions of plagioclase with decreasing age, in agreement with the observed phase proportions. Trace element enrichments indicative of open-system processes such as crustal assimilation are more important in old than in young units. Subducted sediments are an important component of one of the early units of NLV.

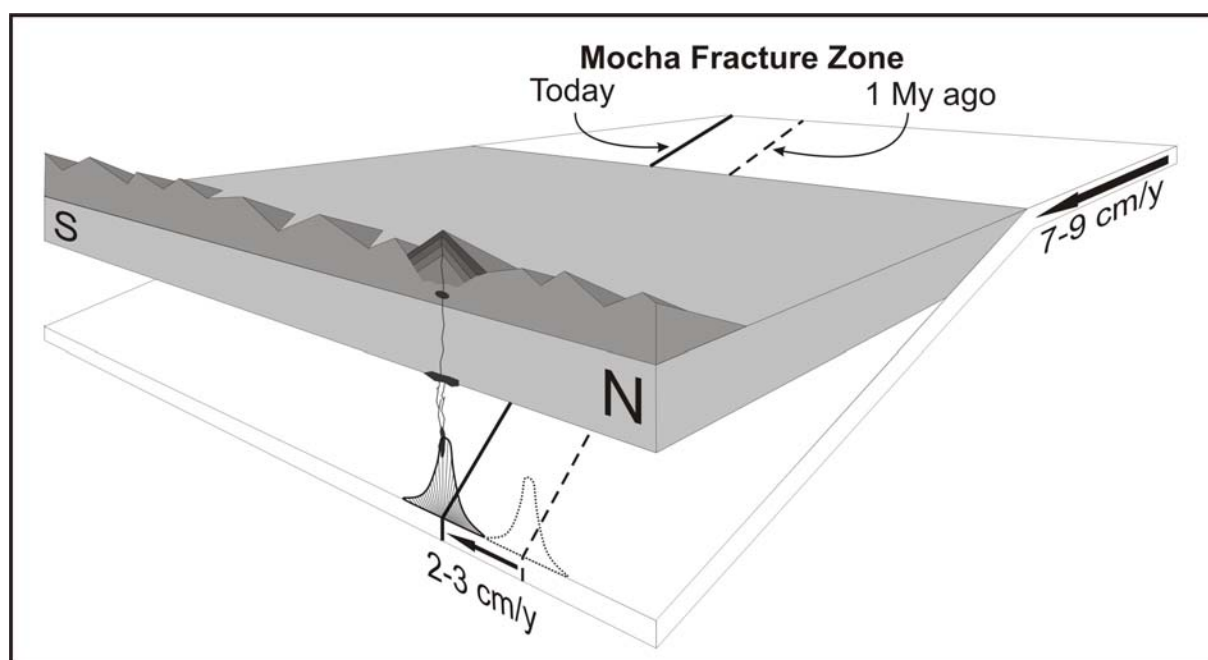


Figure 25. Schematic block-diagram of the southward-migrating Mocha fracture zone along the Southern Volcanic Zone.

The observed systematic changes along the stratigraphic section indicate a long-term increase in the proportion of fluid components that fluxed the mantle source. The potentially dominant source of such fluids is serpentinized oceanic mantle within the Mocha Fracture Zone. We conclude that the available data are consistent with an increasingly important role played by fluids from serpentinite dehydration as a consequence of the southward migration of the fracture zone (Figure 25).

REFERENCES

- Alonso-Pérez, R., Ulmer, P., Müntener, O., Thompson, A. and Harte, B. (in prep). *Trace element partitioning of fractionated garnet, low Mg-amphibole and plagioclase from a mantle-derived hydrous primary magma at the base of a growing island-arc.*
- Andersen, D.J. and Lindsley, D.H. (1985). *New (and final!) models for the Ti-magnetite/ilmenite geothermometer and oxygen barometer.* EOS Transactions, American Geophysical Union **66**(18): 416.
- Annen, C., Blundy, J. and Spark, R. (2006). *The genesis of intermediate and silicic magmas in deep crustal hot zones.* Journal of Petrology **47**(3): 505-539.
- Bach, W., Garrido, C.J., Paulick, H., Harvey, J. and Rosner, M. (2004). *Seawater-peridotite interactions: First insights from ODP Leg 209, MAR 15 degrees N.* Geochemistry Geophysics Geosystems (G-cubed) **5**: Q09F26, doi:10.1029/2004GC000744
- Bacon, C. (1986). *Magmatic inclusions in silicic and intermediate volcanic rocks.* Journal of Geophysical Research **91**(B6): 6091-6112.
- Bacon, C. and Hirschmann, M. (1988). *Mg/Mn partitioning as a test for equilibrium between coexisting Fe-Ti oxides.* American Mineralogist **73**: 57-61.
- Bindeman, I.N., Davis, A.M. and Drake, M.J. (1998). *Ion microprobe study of plagioclase-basalt partition experiments at natural concentration levels of trace elements.* Geochimica et Cosmochimica Acta **62**(7): 1175-1193.
- Bohm, M., Luth, S., Echtler, H., Asch, G., Bataille, K., Bruhn, C., Rietbrock, A. and Wigger, P. (2002). *The Southern Andes between 36° and 40°S latitude: seismicity and average seismic velocities.* Tectonophysics **356**(4): 275-289.
- Brenan, J.M., Shaw, H.F., Ryerson, F.J. and Phinney, D.L. (1995). *Experimental determination of trace-element partitioning between pargasite and a synthetic hydrous andesitic melt.* Earth and Planetary Science Letters **135**: 1-11.
- Costa, F., Scaillet, B. and Pichavant, M. (2004). *Petrological and Experimental Constraints on the Pre-eruption Conditions of Holocene Dacite from Volcan San Pedro (36°S, Chilean*

- Andes) and the Importance of Sulphur in Silicic Subduction-related Magmas. *Journal of Petrology* **45**(4): 855-881.
- Dalpé, C. and Baker, D.R.** (2000). *Experimental investigation of large-ion-lithophile-element, high-field-strength-element and rare-earth-element-partitioning between calcic amphibole and basaltic melt: the effects of pressure and oxygen fugacity.* *Contributions to Mineralogy and Petrology* **140**: 230-250.
- Dungan, M.A., Wulff, A. and Thomson, R.** (2001). *Eruptive Stratigraphy of the Tataro-San Pedro Complex, 36°S, Southern Volcanic Zone, Chilean Andes: Reconstruction Method and Implications for Magma Evolution at Long-lived Arc Volcanic Centers.* *Journal of Petrology* **42**(3): 555-626.
- Ewart, A. and Griffin, W.L.** (1994). *Application of proton-microprobe data to trace element partitioning in volcanic rocks.* *Chemical Geology* **117**(1-4): 251-284.
- Feeley, T.C., Dungan, M.A. and Frey, F.A.** (1998). *Geochemical constraints on the origin of mafic and silicic magmas at Cordón El Guadal, Tataro-San Pedro Complex, central Chile.* *Contributions to Mineralogy and Petrology* **131**(4): 393-411.
- Ferguson, K., Dungan, M., Davidson, J. and Colucci, M.** (1992). *The Tataro-San Pedro Volcano, 36°S, Chile: A chemical variable, dominantly mafic magmatic system.* *Journal of Petrology* **33**: 1-43.
- Folguera, A., Ramos, V.A., Hermanns, R.L. and Naranjo, J.** (2004). *Neotectonics in the foothills of the southernmost central Andes (37°–38°S): Evidence of strike-slip displacement along the Antihir-Copahue fault zone.* *Tectonics* **23**: TC5008.
- Gaetani, G.A. and Grove, T.L.** (1998). *The influence of water on melting of mantle peridotite.* *Contributions to Mineralogy and Petrology* **131**(4): 323-346.
- Gardeweg, M.** (1980). *Geología del área del Nevado de Longaví. Cordillera de Los Andes - VII Región del Maule.* Unpublished Thesis, 247 pp. Universidad de Chile, Santiago.
- Gerlach, D., Frey, F., Moreno, H. and López-Escobar, L.** (1988). *Recent volcanism in the Puyehue-Cordón Caulle Region, Southern Andes, Chile (40.5°S): Petrogenesis of evolved lavas.* *Journal of Petrology* **29**(2): 333-382.
- Green, T.H., Adam, J. and Site, S.H.** (1993). *Proton microprobe determined trace element partition coefficients between pargasite, augite and silicate or carbonatitic melts.* *EOS* **74**: 340.
- Grove, T.L., Baker, M.B., Price, R.C., Parman, S.W., Elkins-Tanton, L.T., Chatterjee, N. and Müntener, O.** (2005). *Magnesian andesite and dacite lavas from Mt. Shasta, northern California: products of fractional crystallization of H₂O-rich mantle melts.* *Contributions to Mineralogy and Petrology* **148**(5): 542-565.
- Grove, T.L., Donnelly-Nolan, J.M. and Housh, T.** (1997). *Magmatic processes that generated the rhyolite of Glass Mountain, Medicine Lake volcano, N. California.* *Contributions to Mineralogy and Petrology* **127**(3): 205-223.
- Grove, T.L., Elkins-Tanton, L.T., Parman, S.W., Chatterjee, N., Müntener, O. and Gaetani, G.A.** (2003). *Fractional crystallization and mantle-melting controls on calc-alkaline differentiation trends.* *Contributions to Mineralogy and Petrology* **145**(5): 515-533.
- Grove, T.L. and Juster, T.C.** (1989). *Experimental investigations of low-Ca pyroxene stability and pyroxene-olivine-liquid equilibria at 1-atm in natural basaltic and andesitic liquids.* *Contributions to Mineralogy and Petrology* **103**: 287-305.
- Herron, E.M.** (1981). *Chile margin near lat. 38°S: Evidence for a genetic relationship between continental and marine features or a cause of curious coincidences?* in L. D. Kulm, J. Dymond, E. J. Dasch and D. M. Hussong (eds.). *Nazca Plate: crustal formation and andean convergence.* *GSA Memoir*. **154**: 755-760.
- Hickey-Vargas, R., Moreno, H., López-Escobar, L. and Frey, F.A.** (1989). *Geochemical variations in Andean basaltic and silicic lavas from the Villarrica-Lanin volcanic chain (39.5° S): an evaluation of source heterogeneity, fractional crystallization and crustal assimilation.* *Contributions to Mineralogy and Petrology* **103**(3): 361-386.
- Hildreth, W. and Moorbath, S.** (1988). *Crustal contributions to arc magmatism in the Andes of Central Chile.* *Contributions to Mineralogy and Petrology* **98**(4): 455-489.
- Hilyard, M., Nielsen, R.L., Beard, J.S., Patiño-Douce, A. and Blencoe, J.** (2000). *Experimental determination of the partitioning behavior of rare earth and high field strength elements between pargasitic amphibole and natural silicate melts.* *Geochimica et Cosmochimica Acta* **64**(6): 1103-1120.

- Hirose, K. (1997). *Melting experiments on lherzolite KLB-1 under hydrous conditions and generation of high-magnesian andesitic melts*. *Geology* **25**(1): 42-44.
- Hirose, K. and Kawamoto, T. (1995). *Hydrous partial melting of lherzolite at 1 GPa: The effect of H₂O on the genesis of basaltic magmas*. *Earth and Planetary Science Letters* **133**(3-4): 463-473.
- Hirschmann, M.M., Asimow, P.D., Ghiorso, M.S. and Stolper, E.M. (1999). *Calculation of peridotite partial melting from thermodynamic models of minerals and melts. III. Controls on isobaric melt production and the effect of water on melt production*. *Journal of Petrology* **40**(5): 831-851.
- Huebner, J.S. and Sato, M. (1970). *The oxygen fugacity-temperature relationships of manganese oxide and nickel oxide buffers*. *American Mineralogist* **55**: 934-952.
- Jicha, B.R., Singer, B.S., Brophy, J.G., Fournelle, J.H., Johnson, C.M., Beard, B.L., Lapen, T.J. and Mahlen, N.J. (2004). *Variable impact of the subducted slab on Aleutian Island arc magma sources: evidence from Sr, Nd, Pb, and Hf isotopes and trace element abundances*. *Journal of Petrology* **45**(9): 1845-1875.
- Jordan, T.H., Burns, W.M., Veiga, R., Pángaro, F., Copeland, P., Kelley, S. and Mpodozis, C. (2001). *Extension and basin formation in the southern Andes caused by increased convergence rate: A mid-Cenozoic trigger for the Andes*. *Tectonics* **20**(3): 308-324.
- Kay, S., Godoy, E. and Kurtz, A. (2005). *Episodic arc migration, crustal thickening, subduction erosion, and magmatism in the south-central Andes*. *Geological Society of America Bulletin* **117**: 67-88.
- Kay, S.M., Burns, W.M., Copeland, P. and Mancilla, O. (in press). *Upper Cretaceous to Recent magmatism over the Neuquén basin: evidence for transient shallowing of the subduction zone under the Neuquén Andes (36°S to 38°S latitude)*. In S. M. Kay and V. A. Ramos (eds.). *Late Cretaceous to Recent magmatism and tectonism of the Southern Andean margin at the latitude of the Neuquén basin (36-39°S)*. GSA Special Paper.
- Leake, B., Woolley, A., Arps, C., Birch, W., Gilbert, M., Grice, J., Hawthorne, F., Kato, A., Kisch, H., Krivovichev, V., Linthout, K., Laird, J., Mandarino, J., Maresch, W., Nickel, E., Rock, N., Schumacher, J., Smith, D., Stephenson, N., Ungaretti, L., Whittaker, E. and Youzhi, G. (1997). *Nomenclature of amphiboles: Report of the Subcommittee on amphiboles of the International Mineralogical Association, Commission on New Minerals and Mineral Names*. *American Mineralogist* **82**: 1019-1037.
- LePage, L. (2003). *ILMAT: an excel worksheet for ilmenite--magnetite geothermometry and geobarometry*. *Computers and Geosciences* **29**(5): 673 - 678.
- Longhi, J. (1991). *Comparative liquidus equilibria of hyperstene-normative basalts at low pressure*. *American Mineralogist* **76**: 785-800.
- López-Escobar, L., Cembrano, J. and Moreno, H. (1995a). *Geochemistry and tectonics of the Chilean Southern Andes basaltic Quaternary volcanism (37-46°S)*. *Revista Geológica de Chile* **22**(2): 219-234.
- López-Escobar, L., Kilian, R., Kempton, P.D. and Tagiri, M. (1993). *Petrography and geochemistry of Quaternary rocks from the Southern Volcanic Zone of the Andes between 41°30' and 46°00'S, Chile*. *Revista Geológica de Chile* **20**(1): 35-55.
- López-Escobar, L., Parada, M.A., Hickey-Vargas, R., Frey, F.A., Kempton, P.D. and Moreno, H. (1995b). *Calbuco Volcano and minor eruptive centers distributed along the Liquiñe-Ofqui Fault Zone, Chile (41°-42° S): contrasting origin of andesitic and basaltic magma in the Southern Volcanic Zone of the Andes*. *Contributions to Mineralogy and Petrology* **119**(4): 345-361.
- Lundgaard, K.L. and Tegner, C. (2004). *Partitioning of ferric and ferrous iron between plagioclase and silicate melt*. *Contributions to Mineralogy and Petrology* **147**: 470-483.
- Martel, C., Pichavant, M., Holtz, F. and Scaillet, B. (1999). *Effects of fO₂ and H₂O on andesite phase relations between 2 and 4 kbar*. *Journal of Geophysical Research* **104**(B12): 29453-29470.
- McMillan, N., Harmon, R., Moobath, S., López-Escobar, L. and Strong, D. (1989). *Crustal sources involved in continental arc magmatism: A case study of Volcan Mocho-Choshuenco, southern Chile*. *Geology* **17**: 1152-1156.
- Mella, M., Muñoz, J., Vergara, M., Klohn, E., Farmer, L. and Stern, C. (2005). *Petrogenesis of the Pleistocene Tronador volcanic group, Andean Southern Volcanic Zone*. *Revista Geológica de Chile* **32**(1): 131-154.
- Miyashiro, A. (1974). *Volcanic rock series in island arcs and active continental margins*.

- American Journal of Sciences **274**: 321-355.
- Moore, G. and Carmichael, I.S.E.** (1998). *The hydrous phase equilibria (to 3 kbar) of an andesite and basaltic andesite from western Mexico: constraints on water content and conditions of phenocryst growth.* Contributions to Mineralogy and Petrology **130**(3 - 4): 304-319.
- Müntener, O., Kelemen, P. and Grove, T.** (2001). *The role of H₂O during crystallization of primitive arc magmas under uppermost mantle conditions and genesis of igneous pyroxenites: an experimental study.* Contributions to Mineralogy and Petrology **141**(6): 643-658.
- Muñoz, J. and Niemeyer, C.** (1984). *Hoja Laguna del Maule, Regiones del Maule y del Bío Bío.* Carta Geológica de Chile **64**, SERNAGEOMIN, Santiago. Map scale 1:250.000 and accompanying booklet, 97 p.
- Phinney, W.C.** (1992). *Partition coefficients for iron between plagioclase and basalt as a function of oxygen fugacity: Implications for Archean and lunar anorthosites.* Geochimica et Cosmochimica Acta **56**(5): 1885-1895.
- Pichavant, M., Martel, C., J., B. and Scaillet, B.** (2002). *Physical conditions, structure and dynamics of a zoned magma chamber: Mount Pelée (Martinique, Lesser Antilles Arc).* Journal of Geophysical Research **107**(B5): ECV 2-1 - ECV 2-30.
- Plank, T.** (2005). *Constraints from Thorium/Lanthanum on sediment recycling at subduction zones and the evolution of continents.* Journal of Petrology **46**(5): 921-944.
- Prouteau, G. and Scaillet, B.** (2003). *Experimental Constraints on the Origin of the 1991 Pinatubo Dacite.* Journal of Petrology **44**(12): 2203-2241.
- Prouteau, G., Scaillet, B., Pichavant, M. and Maury, R.** (1999). *Fluid-present melting of ocean crust in subduction zones.* Geology **27**(12): 1111-1114.
- Ramos, V.A. and Folguera, A.** (2005). *Tectonic evolution of the Andes of Neuquén: constraints derived from the magmatic arc and foreland deformation.* In G. D. Veiga, L. A. Spalletti, J. A. Howell and E. Schwarz (eds.). *The Neuquén Basin, Argentina: A case study in sequence stratigraphy and basin dynamics.* Geological Society, London, Special Publications **252**: 15-35.
- Rhodes, J.M.** (1988). *Geochemistry of the 1984 Mauna Loa eruption: implications for magma storage and supply.* Journal of Geophysical Research **93**: 4453-4466.
- Rodríguez, C.** (in prep). *Intra-crustal Origin of Holocene Adakitic Magmas at Nevado de Longaví Volcano (Southern Volcanic Zone: 36.2°S).* Ph.D. Thesis, University of Geneva, Geneva
- Rudnick, R.L. and Gao, S.** (2003). *Composition of the continental crust.* In R. L. Rudnick (eds.). *The Crust.* Treatise on Geochemistry **3**: 1-64.
- Rutherford, M. and Devine, J.** (1988). *The May 18, 1980, eruption of Mount St. Helens, 3. Stability and chemistry of amphibole in the magma chamber.* Journal of Geophysical Research **93**(B10): 11949-11959.
- Scaillet, B. and Evans, B.** (1999). *The June 15, 1991 eruption of Mount Pinatubo. I. Phase equilibria and pre-eruption of P-T-fO₂-H₂O conditions of the dacite magma.* Journal of Petrology **40**(3): 381-411.
- Scambelluri, M., Bottazzi, P., Trommsdorff, V., Vannucci, R., Hermann, J., Gómez-Punaire, M.T. and López-Sánchez-Vizcaíno, V.** (2001). *Incompatible element-rich fluids released by antigorite breakdown in deeply subducted mantle.* Earth and Planetary Science Letters **192**: 457-470.
- Sellés, D.** (1999). *La Formación Abanico en el cuadrángulo Santiago (33°15'-33°30'S; 70°30'-70°45'O), Chile central: estratigrafía y geoquímica.* M.S. Thesis, 154 pp. Universidad de Chile, Santiago.
- Sellés, D., Rodríguez, C., Dungan, M.A., Naranjo, J. and Gardeweg, M.** (2004). *Geochemistry of Nevado de Longaví volcano (36.2°S): A compositional atypical arc volcano in the Southern Volcanic Zone of the Andes.* Revista Geológica de Chile **31**(2): 293-315.
- Singer, B.S., Leeman, W.P., Thirlwall, M.F. and Rogers, N.W.** (1996). *Does fracture zone subduction increase sediment flux and mantle melting in subduction zones? Trace element evidence from Aleutian arc basalts.* In G. E. Bebout, D. W. Scholl, S. H. Kirby and J. P. Platt (eds.). *Subduction top to bottom.* American Geophysical Union, Geophysical Monograph Series. **96**: 285-291.
- Sisson, T.W.** (1994). *Hornblende-melt trace-element partitioning measured by ion microprobe.* Chemical Geology **117**(1-4): 331-344.

- Sisson, T.W. and Grove, T.L.** (1993). *Experimental investigations of the role of H₂O in calc-alkaline differentiation and subduction zone magmatism*. Contributions to Mineralogy and Petrology **113**(2): 143-166.
- Spencer, K.J. and Lindsley, D.H.** (1981). *A solution model for coexisting iron-titanium oxides*. American Mineralogist **66**: 1189-1201.
- Sruoga, P., Llambías, E.J., Fauqué, L., Schonwandt, D. and Repol, D.G.** (2005). *Volcanological and geochemical evolution of the Diamante Caldera-Maipo volcano complex in the Southern Andes of Argentina (34°10'S)*. Journal of South American Earth Sciences **19**: 399-414.
- Stern, C.R.** (1991). *Role of subduction erosion in the generation of Andean magmas*. Geology **19**(1): 78-81.
- Stolper, E.M. and Newman, S.** (1994). *The role of water in the petrogenesis of Mariana trough magmas*. Earth and Planetary Science Letters **121**: 293-325.
- Stormer, J.** (1983). *The effects of recalculation on estimates of temperature and oxygen fugacity from analyses of multicomponent iron-titanium oxides*. American Mineralogist **68**: 586-594.
- Tassara, A., Götze, H.J., Schmidh, S. and Hackney, R.I.** (2006). *Three-dimensional density model of the Nazca plate and the Andean continental margin*. Journal of Geophysical Research **111**, B09404.
- Tassara, A. and Yañez, G.** (2003). *Relación entre el espesor elástico de la litosfera y la segmentación tectónica del margen andino (15-47°S)*. Revista Geológica de Chile **30**(2): 159-186.
- Tebbens, S.F. and Cande, S.C.** (1997). *Southeast Pacific tectonic evolution from early Oligocene to Present*. Journal of Geophysical Research **102**(B6): 12061-12084.
- Tormey, D., Hickey-Vargas, R., Frey, F. and López-Escobar, L.** (1991). *Recent lavas from the Andean volcanic front (33 to 42°S); interpretations of along-arc compositional variations*. In R. S. Harmon and C. W. Rapela (eds.). *Andean magmatism and its tectonic setting*. GSA Special Paper. **265**: 57-77.
- Ulmer, P.** (2001). *Partial melting in the mantle wedge - the role of H₂O in the genesis of mantle-derived 'arc-related' magmas*. Physics of The Earth and Planetary Interiors **127**(1-4): 215-232.
- Ulmer, P. and Müntener, O.** (2005). *"Adakites" formed by garnet fractionation at the base of the crust - an alternative scenario supported by field and experimental data*. Geophysical Research Abstracts **7**(09837).
- Ulmer, P., Müntener, O. and Alonso-Pérez, R.** (2003). *Potencial role of garnet fractionation in H₂O-undersaturated andesite liquids at high pressure: an experimental study and a comparison with the Kohistan arc*. Geophysical Research Abstracts **5**(08308).
- Ulmer, P. and Trommsdorff, V.** (1995). *Serpentine stability to mantle depths and subduction-related magmatism*. Science **268**: 858-861.
- Vergara, M., Morata, D., Hickey -Vargas, R., López-Escobar, L. and Beccar, I.** (1999). *Cenozoic tholeiitic volcanism in the Colbún area, Linares Precordillera, central Chile (35°35'-36°S)*. Revista Geológica de Chile **26**(1): 23-41.

CHAPTER 3

PLUTONIC-TEXTURED XENOLITHS IN NLV: CHARACTERIZATION AND PETROGENETIC SIGNIFICANCE.

INTRODUCTION

Nevado de Longaví volcano (NLV) is a late Quaternary edifice in the volcanic front of the Southern Volcanic Zone (SVZ) of the Chilean Andes (Figure 1). In the Chapter 2 we showed that there is a long-term evolution in the magmatism of this center from relatively dry magmas in pre-NLV and early NLV units to water-rich magmas in younger units. Young NLV lavas in particular have high amphibole modal abundances together with chemical characteristics that are not observed elsewhere in the ~1500 km long SVZ. Lavas from older units, on the other hand, lack amphibole altogether, and are chemically similar to certain other pyroxene-dominated SVZ lavas. The change in the nature of magmas is thought to result from an increase in fluids supplied to the mantle source as a consequence of the subduction of an oceanic fracture zone. The solid assemblages associated with magmatic evolution are inferred to have changed with time from dominantly anhydrous and plagioclase-rich to amphibole-rich.

More than fifty plutonic-textured xenoliths, mostly gabbroic, ranging in size from a few centimeters up to ~40 cm were collected from lavas and pyroclastic deposits of the different units of Nevado de Longaví Volcano (Figure 2). The majority of the xenoliths are of mafic to ultramafic lithologies that do not crop out in the area; only a small fraction of the xenoliths correspond to granitoids that can be readily identified as crustal fragments similar to the exposed Tertiary basement. The term *xenolith* is used here to designate rock fragments incorporated into magma in a solid or largely solid state, as opposed to *magmatic enclaves* that were entrained as largely molten blobs that quenched upon entrainment into magma. Enclaves, which are also abundant in NLV lavas, are addressed elsewhere (Chapter

2; Rodríguez *in prep.*; Sellés *et al.*, 2004). In this section I characterize the xenoliths collected in terms of their whole-rock and mineral chemistry and explore their origin and possible roles played in the genesis of NLV magmas. The issue of whether rock fragments in NLV lavas are true *xenoliths* in the sense pre-existing crust, or *autoliths* related to NLV magmatism, is addressed in this contribution.

XENOLITH TYPES

Most NLV xenoliths are holocrystalline to hypocrySTALLINE plutonic-textured rock fragments. Lithic fragments similar to the Tertiary basement granitoids have been exclusively found in the basal breccia of the Holocene Río

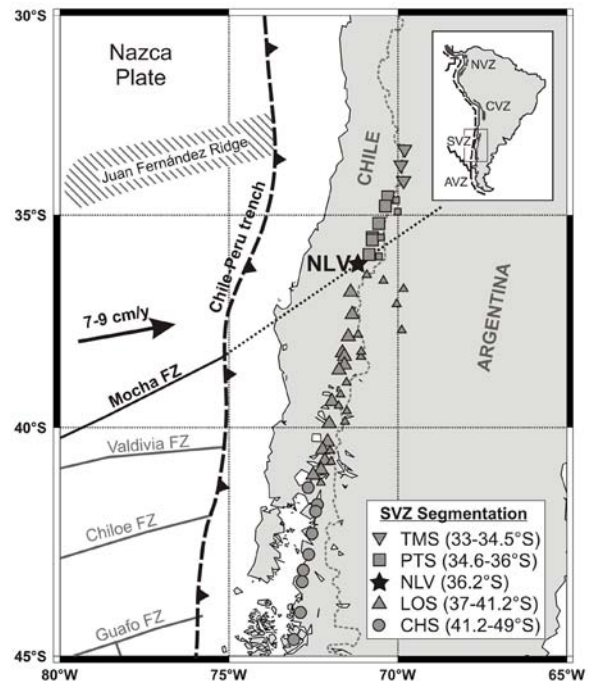


Figure 1. Location of the Nevado de Longaví volcano (star labeled NLV) in the Southern Volcanic Zone (SVZ). Location of SVZ volcanic centers shown with different symbols for different segments as defined in Chapter 2.

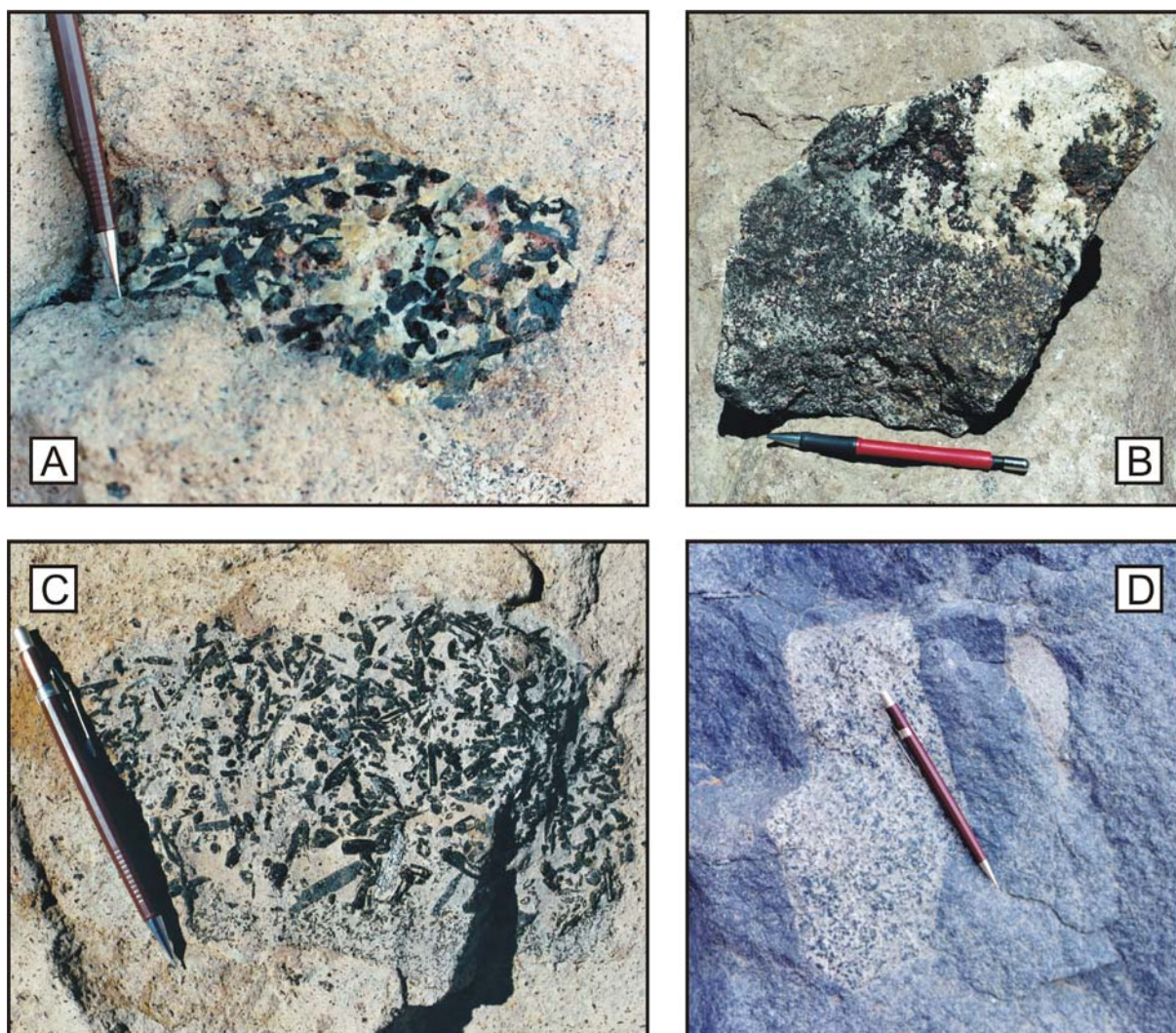


Figure 2. Field photographs of xenoliths. **A:** Small angular fragment of a coarse-grained amphibole gabbro composed of euhedral amphibole and large plagioclase crystals; reddish areas correspond to pockets of vesicular residual glass. **B:** Large block of cumulate-textured amphibole gabbro, displaying domains of amphibole and plagioclase concentration. **C:** Quenched crystal-mush (QCM) consisting of large skeletal amphibole crystals suspended in a gray, highly vesicular glassy mass; note hollow skeletal amphiboles filled with the same material. **D:** Angular fragment of a medium-grained norite. Black grains are orthopyroxene and small amounts of interstitial amphibole. Note rounded, finer-grained magmatic enclave to the right of scale pencil.

Blanco subplinian eruption. The remaining of the plutonic xenoliths, for which there is no evident basement outcrop equivalent, can be divided into two groups according to their mineralogy and textures. Group I includes the xenoliths in which the dominant ferromagnesian phases are hydrous minerals (amphibole or amphibole plus biotite). Xenoliths whose mineralogy is largely dominated by anhydrous phases (plagioclase + pyroxenes \pm olivine, with subordinate amphibole \pm biotite) belong to Group II. Group I xenoliths have been mainly recovered from young units of the volcano (Units 3b and 4 as defined in Chapter 2), whereas Group II xenoliths are largely from older units. Metamorphic xenoliths are rare at NLV, and correspond to granoblastic-textured rocks

composed of refractory minerals (plagioclase, Fe-Ti oxides, pyroxenes, corundum). A summary of the stratigraphic provenance of the different types of xenoliths is presented in (Figure 3).

Group I

Twenty-one samples of amphibole-rich xenoliths were collected from Holocene NLV units and main-cone lavas (mainly from Unit 3b, only one sample from Unit 3a; see Figure 3). Two types of amphibole-rich xenoliths are defined:

I-A. Amphibole gabbros. These are constituted almost exclusively of varying proportions of coarse (1-10 mm) amphibole and plagioclase crystals with interstitial glass-rich material. Minor pyroxene and olivine are present

only as small, rounded cores in amphiboles in two samples. Iron oxides and apatite are present in low abundance in some samples, and chalcopyrite and pyrrhotite are even less common. They are hornblende gabbros and plagioclase-bearing hornblendites according to their modal mineralogy (Le Maitre *et al.*, 1989), although we prefer the term amphibole gabbro because the amphibole present is not hornblende *sensu stricto*. Polygonal interstices between crystals are occupied by glass or microcrystalline material, which is highly variable in proportion. Glass-rich samples (30-45 vol% glass), which have broadly basaltic bulk compositions, are formed by a loosely packed network of euhedral plagioclase and skeletal amphibole crystals and large polygonal pockets of vesicular glass with minute plagioclase and oxide microlites (Figures 2C and 4C). Two glass separates were analyzed for major and trace elements and these have dacitic compositions (Table 1). We interpret these xenoliths as quenched crystal mushes (QCM); *i.e.* fragments of incompletely solidified mafic magma that quenched upon incorporation into andesitic host magmas. In this sense, QCM's can be regarded as intermediate between xenoliths and magmatic enclaves. Glass-poor amphibole gabbros (3-8 vol% glass) have amphibole and plagioclase proportions that vary even at the hand-specimen scale (Figure 2B). The most amphibole-rich samples contain up to 90 vol% of this mineral and are characterized by planar mineral orientations and highly subordinate interstitial plagioclase (Figures 2B and 4A).

Most amphiboles in these xenoliths are Al-rich magnesiohastingsites (14-10 wt% Al_2O_3). We refer to them collectively as Mg-hastingsite although some are pargasites and tchermakites

according to the classification scheme of Leake *et al.* (1997). They are fresh, unzoned crystals, often with dusty opaque rims up to $\sim 200 \mu\text{m}$ in width. Only in the sample collected from Unit 3a do amphibole crystals show breakdown textures with a characteristic halo of granular or fibrous pyroxenes, plagioclase and iron oxides (gabbroic-type of reaction products of Garcia and Jacobson, 1979). This kind of amphibole dehydration textures commonly occurs around the margins of amphiboles in Group II norite xenoliths. Plagioclase compositions are characterized by weakly zoned calcic cores (An_{80-90}) with sharply-defined albite-rich rims down to An_{35} . These sodic rims are a few microns wide in amphibole-rich gabbros and QCM, but are up to several hundreds microns thick in plagioclase-rich varieties. Mineral textures suggest that calcic plagioclase crystallized simultaneously or shortly after amphibole, whereas anorthite-rich rims are post-cumulus.

I-B. Amphibole-diorites. These are exclusively present in the Holocene units of the volcano (4 samples). Plagioclase (~ 60 vol%) and amphibole ($\sim 30\%$) are the most abundant phases. Minor amounts of Fe-Ti-oxides, orthopyroxene, quartz, biotite, and interstitial vesicular glass are also present in varying proportions (Figure 4D). Plagioclase $\text{An}_{65}\text{-An}_{30}$ is dominant, although calcic cores ($\text{An}_{80}\text{-An}_{90}$) are also present. Amphiboles have a wide range of compositions from 12 to 5 wt% Al_2O_3 . Al-rich amphiboles overlap the Mg-hastingsite compositions from the amphibole gabbros, but the most common composition corresponds to Mg-hornblende with $\text{Al}_2\text{O}_3 < 9$ wt%. Orthopyroxene grains have low Ca and high Mn contents similar to those found in Holocene dacites.

Xenoliths		NLV unit					
Group	Type	1	2	3a	3b	4	Unknown
I	Amphibole-bt-diorite					4	
	QCM				4		
	Amphibole-cumulates				3	1	
	Amphibole gabbros			1 (pm)	9	1	
II	Amph-norite			7	4	1?	2
	Gabbronorite + ol-gabbro		2	2	4	1?	
	Troctolite	1					
Metamorphic granoblastic rocks				1	2		
Basement biotite granitoids						4	

Figure 3. Stratigraphic provenance of xenoliths by type. The volcanic stratigraphy is described in Chapter 2. Loose fragments are shown under the columns "unknown unit" or with question marks if provenance from Holocene units is suspected. Sample marked with (pm) stands for the only amphibole gabbro sample with evidence of amphibole breakdown and partial melting.

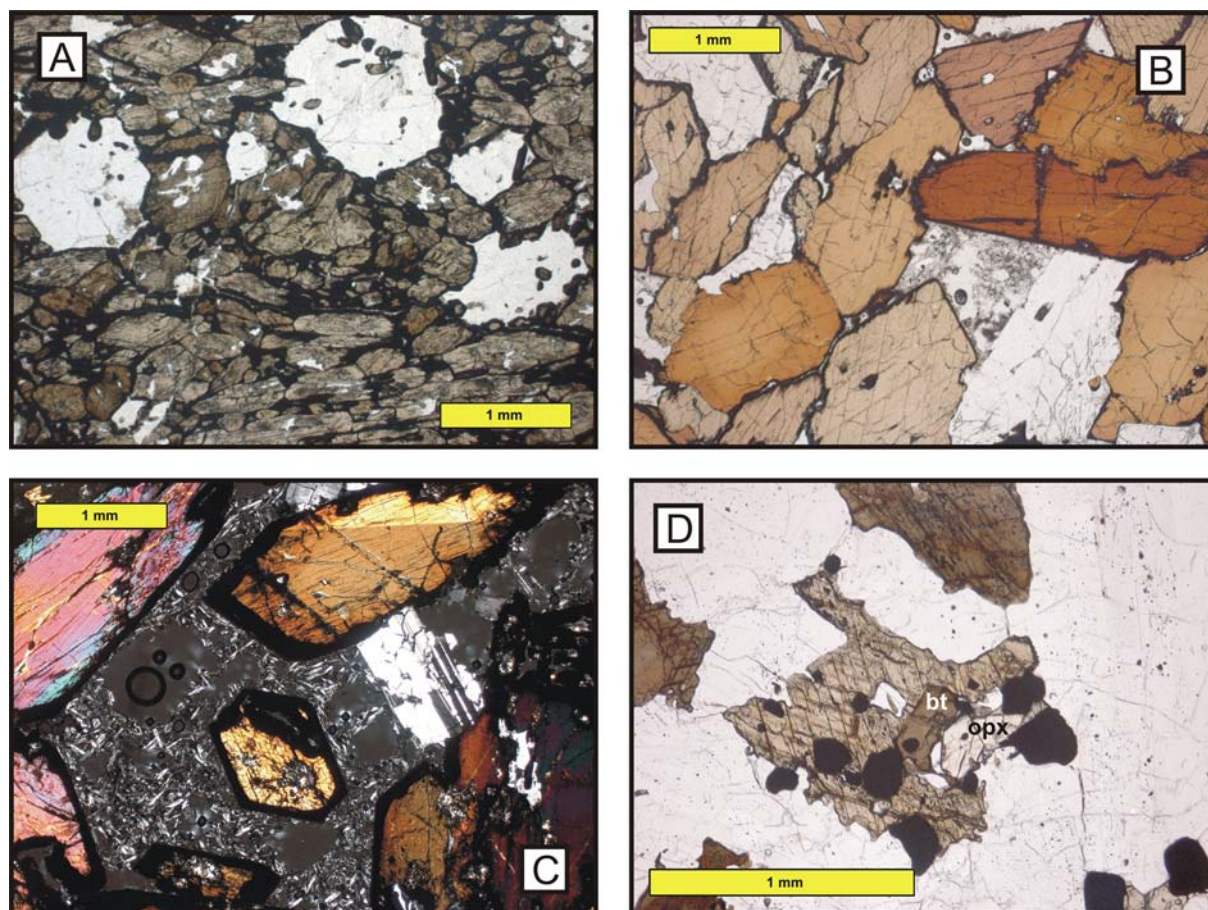


Figure 4. Photomicrographs of xenoliths of Group I. **A:** (sample NL120E) Cumulate texture in plagioclase-bearing hornblendite showing preferred orientation of amphiboles and interstitially-grown plagioclase. Amphibole inclusions in plagioclase have the same composition than surrounding crystals. **B:** (sample NL129G) Amphibole gabbro with mutually interfering amphibole and plagioclase. Note in the center of the picture a polygonal pocket of vesicular residual melt. **C:** (sample NL076) Quenched crystal mush, with large pockets of vesiculated residual melt and loosely connected euhedral amphibole and plagioclase crystals. **D:** (sample NL033B) Amphibole diorite dominated by plagioclase and subhedral to anhedral amphibole. In the center of the image, small biotite flake and orthopyroxene grain are labeled “bt” and “opx” respectively.

Group II

Group II xenoliths are mostly from the oldest units of the volcano, and are characterized by a dominantly anhydrous mineralogy in which orthopyroxene and plagioclase are usually >80 vol%. Amphibole and biotite do occasionally occur, but always in low modal proportions relative to pyroxene. Two sub-categories are defined on the basis of mineralogy and textures.

II-A. Amphibole-bearing norites. The most common xenolith type at this volcano (14 samples) is composed of abundant plagioclase $An_{60}-An_{30}$ (up to 70 vol%) and orthopyroxene (~20 vol%), with minor amounts of clinopyroxene and occasional orthopyroxene-rimmed olivine. Anhedral amphibole crystals, and occasionally also biotite, occur interstitial to plagioclase and pyroxene. Both minerals have undergone variable degrees of dehydration

breakdown to anhydrous granular aggregates (e.g. Figure 5B and C). There are often rounded pockets of grain-boundary melts associated with these breakdown textures (Figure 5C and D). Polygonal interstitial glass pockets, bounded by planar crystal faces, are also present in some samples. The amount of interstitial melt is usually low (<3%), but in two samples it represents ~20 vol%. Distinctive Ti-rich amphiboles in norites are titanian-edenite and titanian-magnesiohastingsite (Leake *et al.*, 1997), hereafter Ti-edenite. Orthopyroxene is typically subhedral and interstitial to plagioclase, and has compositions in the range $En_{76-60}Fs_{32-20}Wo_{1-3}$, although rim compositions can have En contents as low as 48.

II-B. Gabbro-norites and troctolite. These are xenoliths with high proportions of clinopyroxene and olivine relative to orthopyroxene and are the only lithologies that have been recovered from the oldest

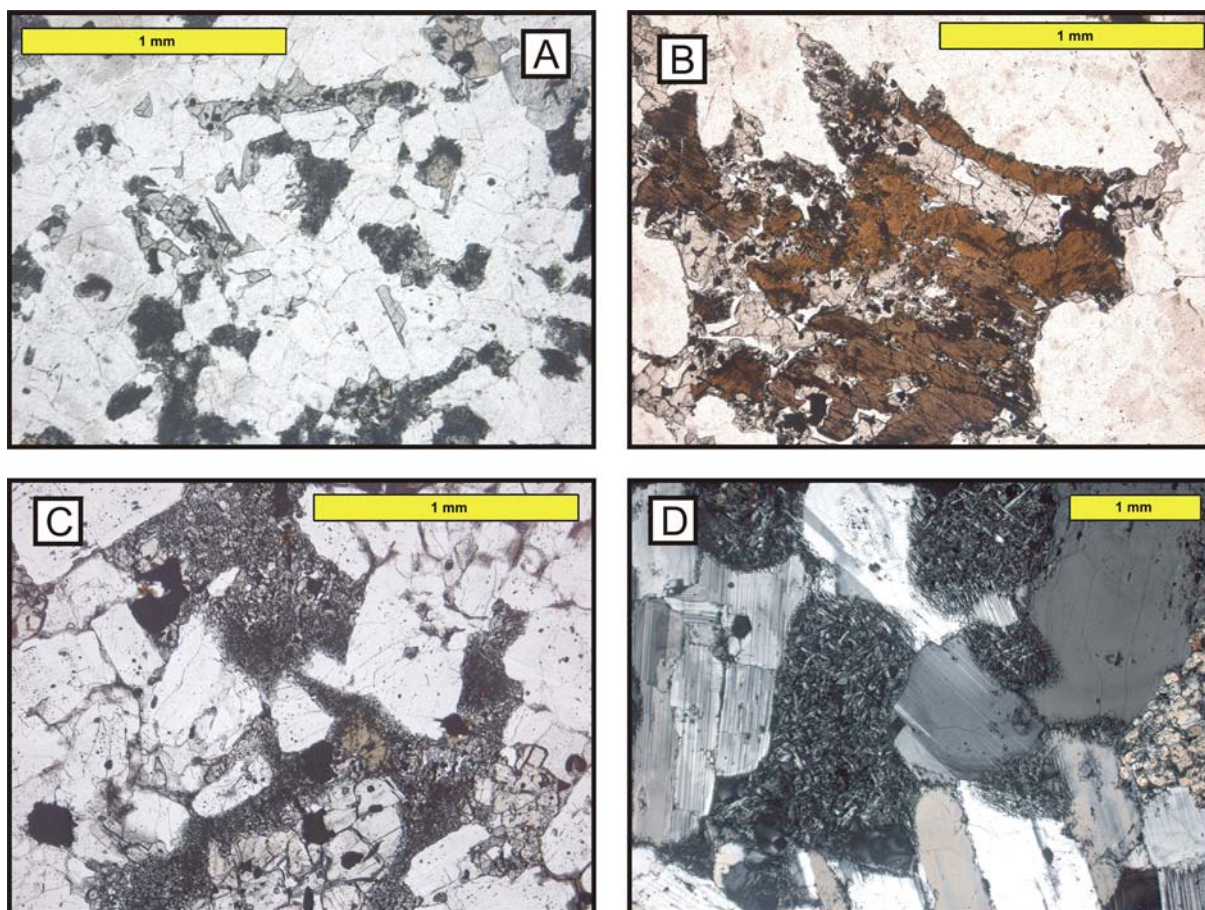


Figure 5. Photomicrographs of amphibole-bearing norite xenoliths (Group II). **A:** (sample NL030B) aspect of a medium-grained norite, formed mostly by plagioclase and orthopyroxene; dark, fine-grained areas around pyroxenes and interstitial to plagioclase probably represent former amphibole now transformed to a fine aggregate of anhydrous minerals. **B:** (sample NL034B) Interstitial anhedral amphibole surrounding a subhedral orthopyroxene crystal. Amphibole is little dehydrated to fine-grained pyroxenes and oxides towards the contacts with plagioclase. **C:** (sample LCBNINC01.3) Relic interstitial amphibole crystal. Fine-grained material around pyroxene and occupying most of the inter-plagioclase space is interpreted to represent former amphibole crystals, now completely dehydrated. Note dark melt films along plagioclase grain contacts. **D:** (sample LLG01.3B) Large, rounded pockets of microcrystalline material resulting from extensive partial melting, presumably triggered by amphibole dehydration (note granular pyroxene on the right-hand side of the picture).

units (Figure 3), but these are also found in younger lavas of the main cone. They range from gabbro-norites with subequal amounts of clinopyroxene and orthopyroxene to olivine gabbros (minor opx) and troctolite (plag + olivine). In comparison to norites, they have lower modal abundances of plagioclase with more calcic compositions, and orthopyroxene is richer in En and Wo. Mg# (molar $100 \cdot \text{Mg} / [\text{Mg} + \text{Fe}^{\text{total}}]$) in clinopyroxenes are high (>80), with Cr_2O_3 contents up to 0.4 wt%, and Fo-contents in olivine vary from 81 to 74 with relatively low Ni contents (<0.1 wt% NiO). Spinel inclusions in $\text{Fo}_{\sim 80}$ olivines in troctolite have low Cr_2O_3 ($\text{Cr}\# < 40$; $\text{Cr}\# = \text{molar } 100 \cdot \text{Cr} / [\text{Cr} + \text{Al}]$). Hydrous phases are absent. Although most xenoliths of this type are holocrystalline, a few samples contain polygonal-shaped residual-melt pockets.

Granoblastic metamorphic rocks

These are fine-grained, plagioclase-rich lithologies, characterized by prominent granoblastic textures with polygonal grain contacts and triple junctions (Figures 6C and 6D). We refer to them as *granulites* according to their textures and mineralogy, although the actual metamorphic grade is only broadly constrained. Only three samples of this kind have been recovered, and the mineral assemblage, textures, and mineral proportions are unique in each case. Sample **NL120C** contains subequal amounts of plagioclase $\text{An}_{65}\text{-An}_{80}$ and elongated opaque-rich domains, which define a subtle foliation. A small fraction of the opaque-rich domains (~ 30 vol%) are single magnetite or ilmenite grains and the rest are microcrystalline aggregates of dusty magnetite

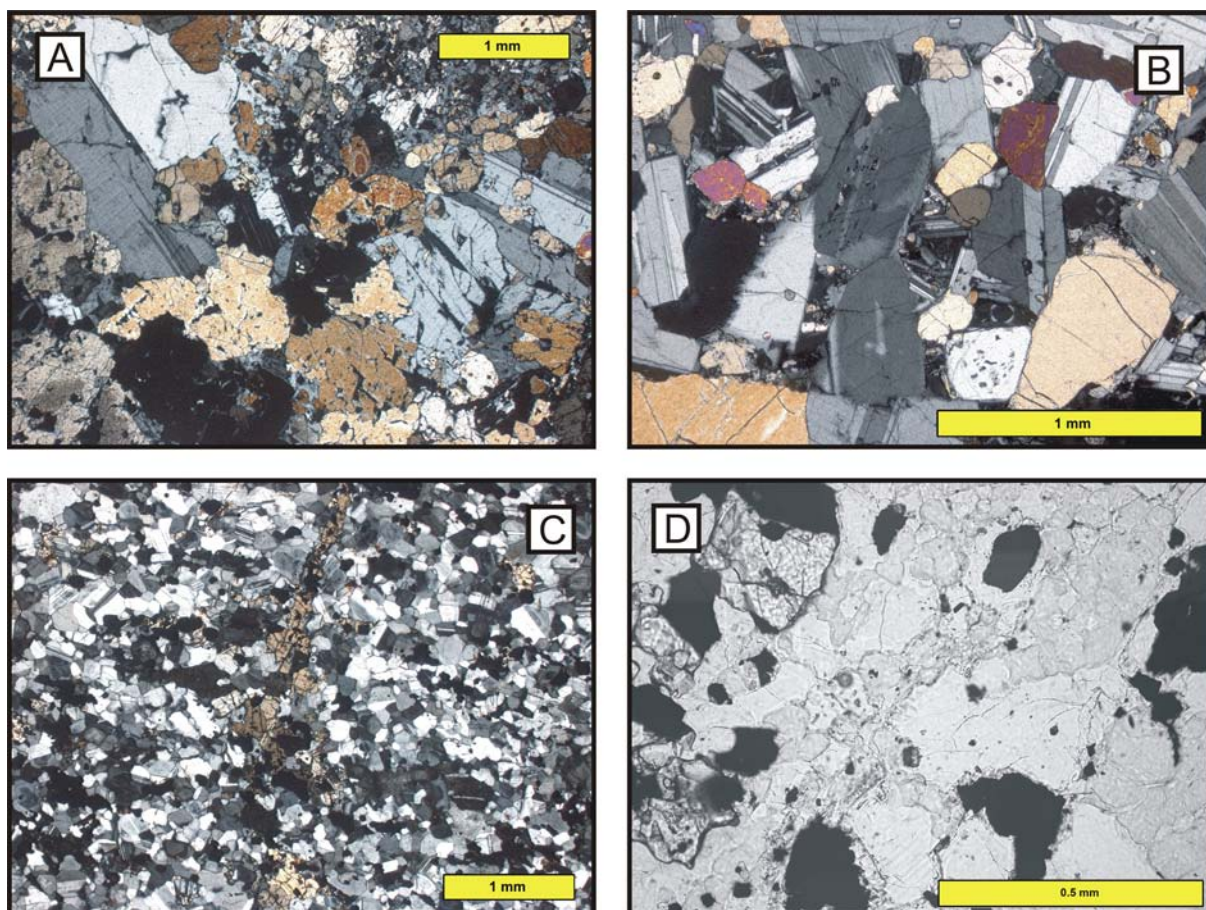


Figure 6. Photomicrographs of Group II and metamorphic xenoliths. **A:** (sample NL063) Inequigranular olivine gabbro with subhedral calcic plagioclase and anhedral olivine and clinopyroxene. **B:** (sample NL142) Coarse-grained troctolite composed of Fo_{80} olivine and An_{90} plagioclase phenocrysts. Interstitial space is mostly composed of plagioclase laths and pyroxene grains in vesicular residual glass. **C:** (sample NL129F) Mosaic granoblastic texture in fine-grained granulite. Note orthopyroxene vein crosscutting vertically at the center of the image. **D:** (sample LMGINC01.2) Granulite composed of corundum (high-relief mineral on the right of the image), cordierite (grey) and plagioclase (white). Some opaque aggregates might be pseudomorphs of former ferromagnesian phases.

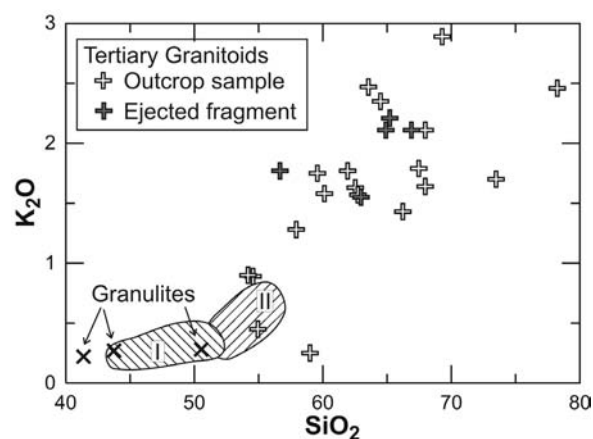
and silicates. In the core of these there are sometimes relics of orthopyroxene ($En_{\sim 70}$), low-Ca clinopyroxene ($Wo_{\sim 35}$), and halogen-rich Mg-hastingsite (up to 0.5 wt% F). Sample **NL129F** is an inequigranular, non-foliated granulite, with ~ 20 vol% orthopyroxene (En_{75} - En_{70}) in addition to plagioclase An_{45} - An_{60} and opaque minerals. Hydrous mineral relics also include halogen-rich Mg-hastingsite and biotite. Sample **LMGINC01.2** has a non-magmatic composition, with an Al_2O_3 content of 29 wt% and very low K and Rb concentrations. Aluminous phases form most of the sample, which is composed of plagioclase (An_{35} - An_{50}), cordierite, corundum, hercynite, magnetite, and ilmenite. Apatite and relics of orthopyroxene ($En_{\sim 77}$) are accessory

Figure 7. SiO_2 - K_2O composition of basement granitoids (hollow crosses) and samples of ballistically ejected fragments (filled crosses). Note the limited compositional overlap with NLV xenoliths (fields labeled I and II).

phases. Thin films of yellowish glass are present along some grain boundaries, but these are too narrow for microprobe analysis.

Tertiary biotite-bearing granitoids

The basement of the volcano consists of mildly folded Oligocene-Miocene



volcanosedimentary strata intruded by biotite-amphibole granitoids (Muñoz and Niemeyer, 1984). Subangular fragments of granitoid up to 1 m in diameter were ballistically ejected during the ~7 ka subplinian Río Blanco eruption (Rodríguez, *in prep.*). They lack evidence of partial melting or other reactions with the juvenile magma despite their fertile mineralogy, and were probably ripped from the basement at shallow levels during the explosive eruption. Tertiary granitoids in the area range from quartz-diorites to tonalites and granodiorites, with high SiO₂ and K₂O contents as compared to Group I and Group II xenoliths (Figure 7). They are composed of plagioclase, quartz, K-feldspar, biotite, and amphibole, and pyroxene is rare. Amphibole analyses in one sample yielded low Al₂O₃ (~5 wt%) actinolitic-hornblende compositions which are distinct

from the compositions of amphiboles in xenoliths of Groups I and II.

MINERAL CHEMISTRY

Plagioclase

The plagioclase compositions in amphibole gabbros (Group I-A) are marked by an abundance of highly calcic cores An₈₀-An₉₂ that are mantled by more sodic rims (down to An₃₅; Figure 8). Such rims are limited to the outermost edges of plagioclase crystals in hornblendites, whereas in amphibole gabbros they have widths of tens to hundreds of microns. Amphibole diorites (I-B) also contain some calcic cores, but the predominant plagioclase composition is in the range An₅₀-An₃₅. This is also the range of

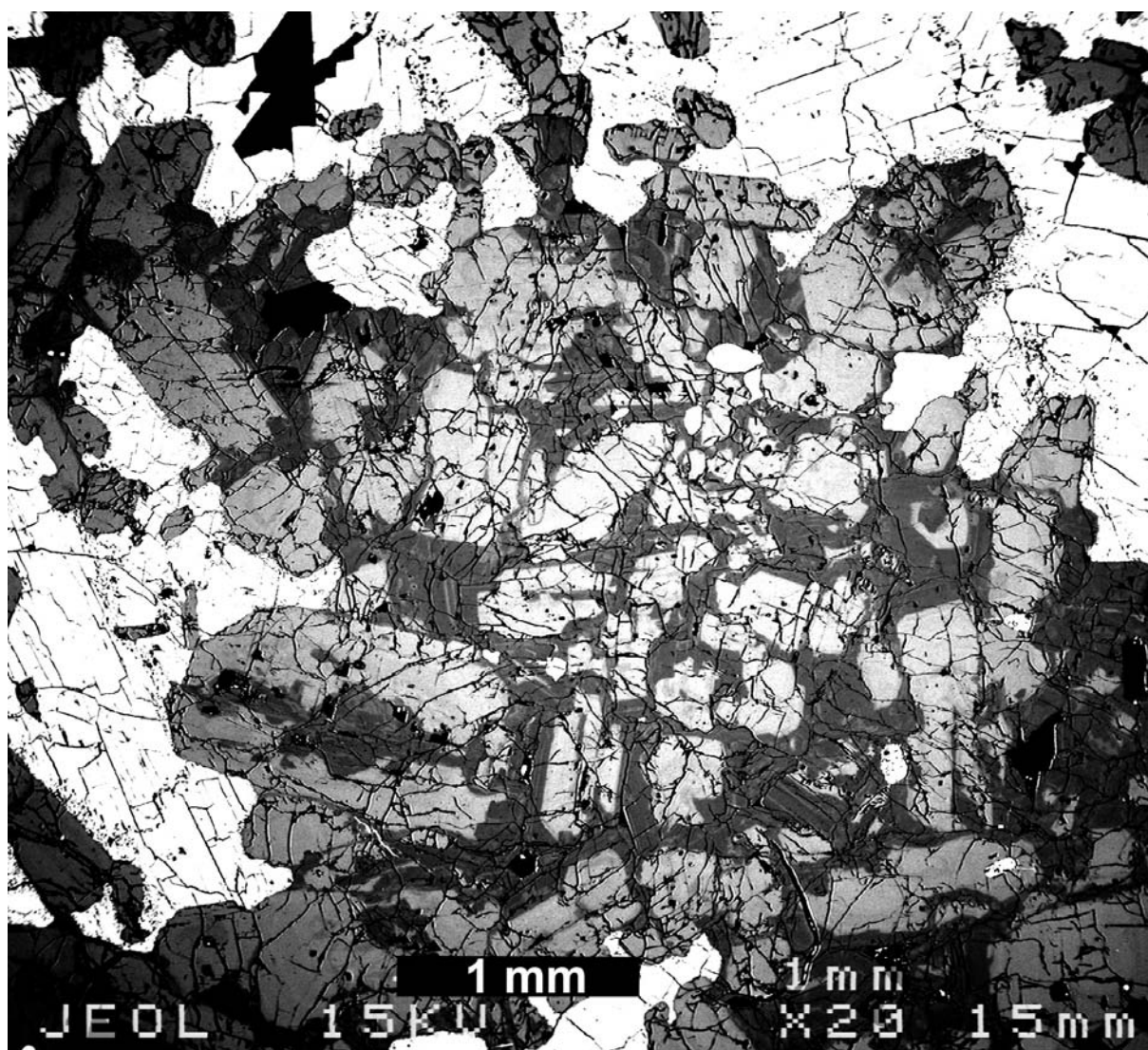


Figure 8. SEM image of an amphibole gabbro (sample NL129G). The center of the image corresponds to normally zoned plagioclase, with light gray calcic cores (An₉₀) and rims down to An₃₅. Note that plagioclase in contact with amphibole (bright areas) do not present albite-rich rims, indicating that calcic plagioclase crystallized simultaneously with amphibole, whereas sodic rims are a late phase.

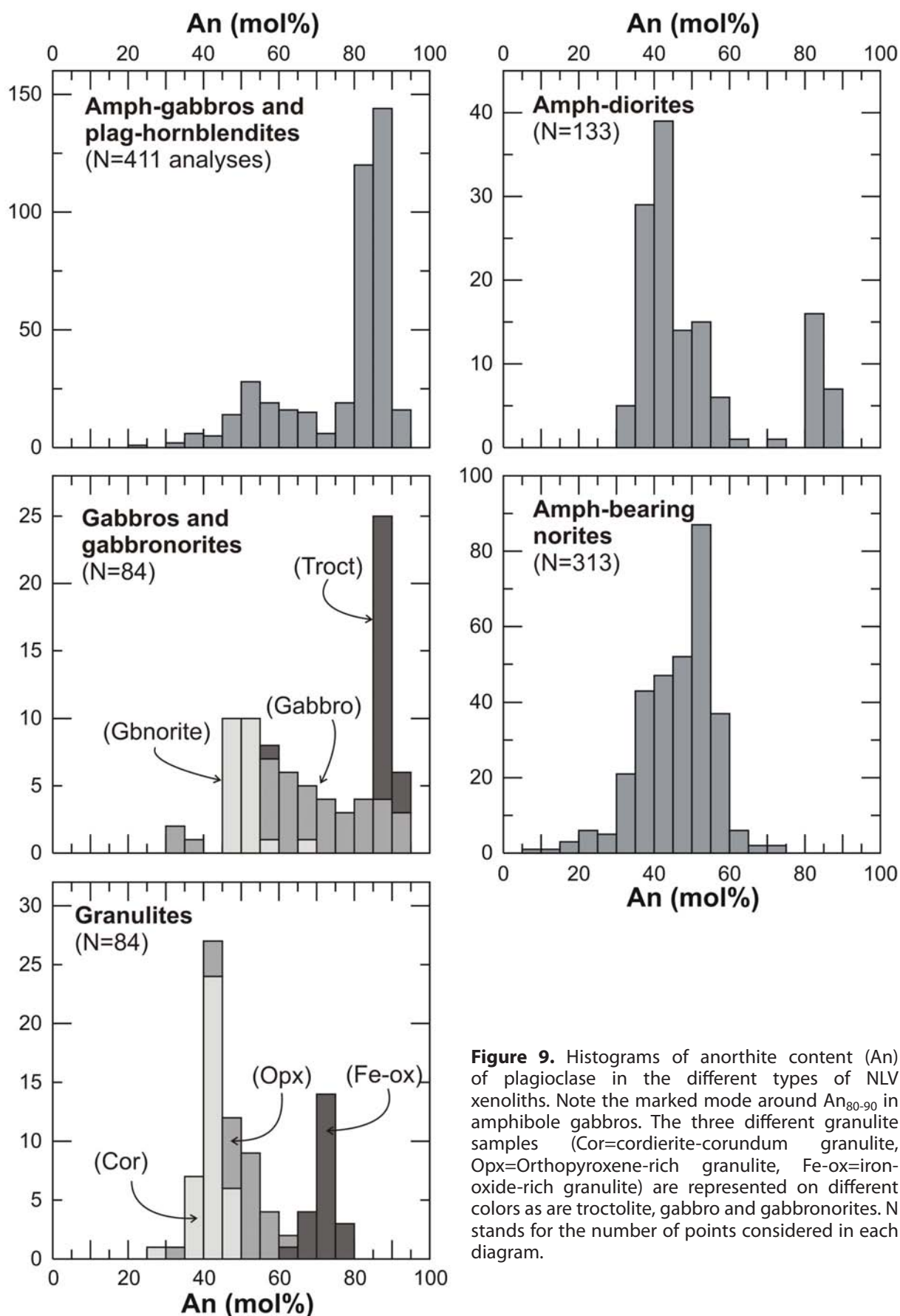


Figure 9. Histograms of anorthite content (An) of plagioclase in the different types of NLV xenoliths. Note the marked mode around An₈₀₋₉₀ in amphibole gabbros. The three different granulite samples (Cor=cordierite-corundum granulite, Opx=Orthopyroxene-rich granulite, Fe-ox=iron-oxide-rich granulite) are represented on different colors as are troctolite, gabbro and gabbronorites. N stands for the number of points considered in each diagram.

plagioclase compositions found in the Holocene dacites from which they were collected.

The Group II troctolite sample, and to a lesser extent the olivine-gabbros, contain significant

modal proportions of calcic plagioclase, whereas most norites and gabbronorites are dominated by less calcic plagioclase (An₆₀ to An₄₀; Figure 9). The three granulite samples

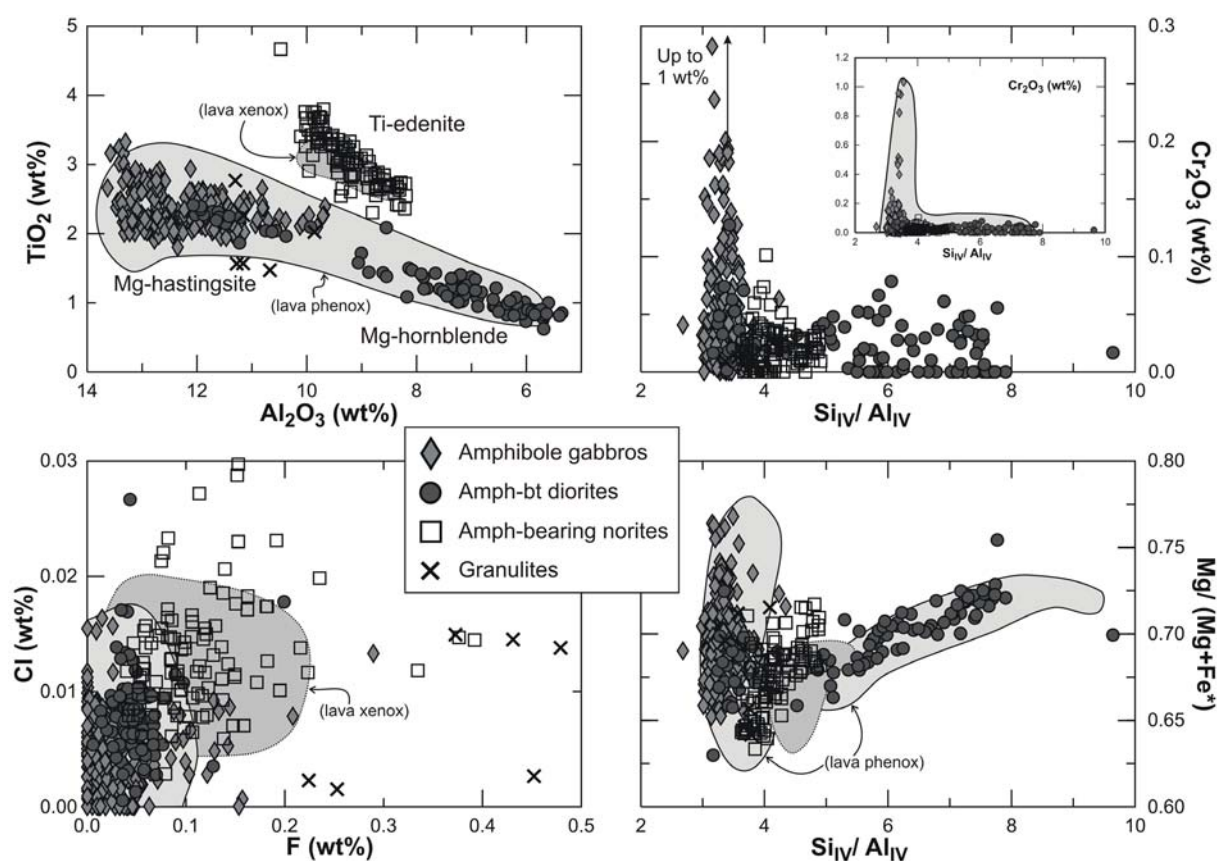


Figure 10. Composition of amphibole crystals in NLV xenoliths compared to the compositions of amphibole phenocrysts and xenocrysts in NLV lavas (grey fields). Structural formulae calculated assuming 13 cations (excluding Ca, Na, and K), and charges balances assuming 23 oxygens. $Fe^* = \text{total Fe}$.

each have different dominant compositions. These are An_{80-60} in the Fe-oxide-rich sample, An_{60-40} in the orthopyroxene-rich specimen, and An_{50-30} in the cordierite-corundum-bearing granulite.

Amphibole

Amphibole compositions define three distinct populations. **1**) Mg-hastingsites are characterized by elevated Al_2O_3 contents (14–10 wt% Al_2O_3), some of which have elevated Cr_2O_3 contents (up to 1 wt%). The Mg# of Mg-hastingsites ranges from 78 to 65 at a practically constant ratio of Si^{IV}/Al^{IV} between 3 and 4 (Si and Al cations in tetrahedral coordination; Figure 10). Alkalies in the A-site account for 0.8 to 0.4 cations per formula unit. **2**) Mg-hornblende has lower Al_2O_3 (9–5 wt%) and Cr_2O_3 (<0.1 wt%) contents, and the Si^{IV}/Al^{IV} ratios vary widely from 5 to 8. This ratio is positively correlated with Mg#'s that increase from 65 to 73 and decreasing A-site alkalis from 0.3 to practically 0. **3**) Ti-edenite is characterized by high TiO_2 and halogen contents. It has intermediate Al_2O_3 contents, with Si^{IV}/Al^{IV} ratios between 3.5 and

5. A-site occupancy is similar to Mg-hastingsite, whereas Cr_2O_3 is low, near the detection limit.

These same three amphibole populations have been identified among phenocrysts and xenocrysts in NLV lavas. Amphibole gabbros contain only Mg-hastingsite amphiboles that overlap the range of amphibole phenocryst compositions in NLV lavas from Unit 2 to Unit 4. Amphibole diorites contain a few Mg-hastingsites, but Mg-hornblende with similar compositions to those found in Holocene dacites and mafic enclaves are in the majority. Group II xenoliths contain exclusively anhedral, postcumulus Ti-edenite amphiboles that poikilitically enclose euhedral $An_{\sim 50}$ plagioclase and pyroxene inclusions. Variably reacted Ti-edenite with similar compositions and textures occur in some Unit 3a lavas. These have been interpreted as xenocrysts because they commonly coexist in the same sample with euhedral Mg-hastingsite. Unit 3a lavas also show chemical evidence of crustal assimilation (Chapter 2).

The scarce amphibole relics in the granulites have compositions close to Mg-hastingsite, but these share the elevated halogen and alkali

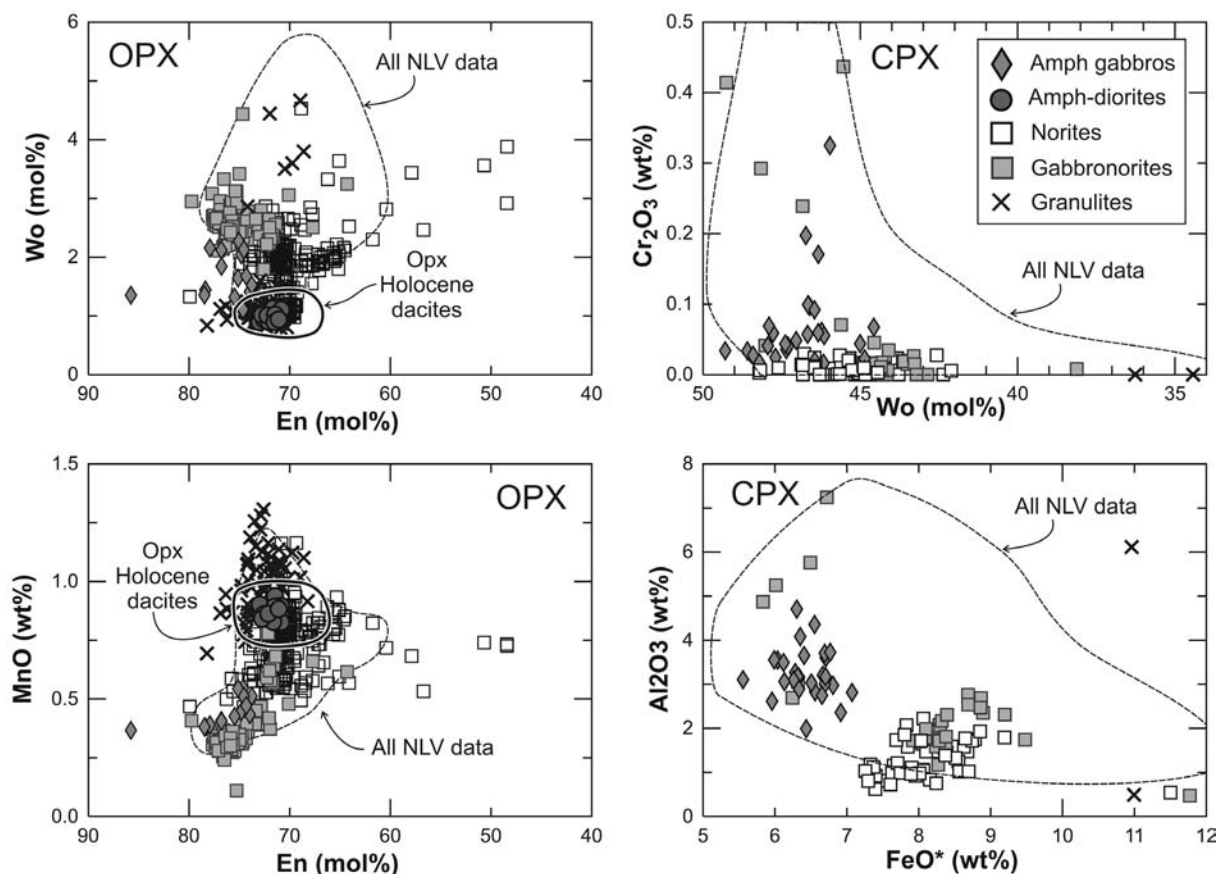


Figure 11. Composition of pyroxenes in xenoliths. Note the coincidence of orthopyroxene chemistry with the field of opx in NLV lavas. In particular, note that orthopyroxene in amphibole diorites fall strictly within the field of compositions of opx in Holocene dacites. FeO*=total iron as FeO.

contents of Ti-edenites. Amphiboles of this composition have not been found in NLV lavas.

Pyroxenes

Orthopyroxene is the main ferromagnesian phase in Group II xenoliths. Their compositions overlap and cover most of the range of compositions found in NLV lavas, although a few analyses extend the range to lower En contents (Figure 11). Orthopyroxenes in norites are generally less En- and Wo-rich than those from gabbros and gabbronorites of the same group. Among Group I-A amphibole gabbros, orthopyroxene has only been found as small rounded cores in a few amphibole crystals, and these have similar compositions to those in Group II gabbronorites. Orthopyroxene grains in Group I-B amphibole diorites are restricted to Wo-poor and MnO-rich compositions that are very close to the compositions of late-appearing orthopyroxene microphenocrysts in Holocene dacites. Granulites contain similar low-Wo orthopyroxene, and extend to even higher MnO contents than those in amphibole diorites.

Most clinopyroxenes from xenoliths fall within the range $En_{42-48}Fs_{6-12}Wo_{42-48}$. Only a few grains in gabbronorites and cores in amphibole gabbros contain significant Cr_2O_3 and Al_2O_3 (0.1-0.4 wt% and 2-7 wt% respectively). Clinopyroxene in norite xenoliths (II-A) has low Cr_2O_3 and Al_2O_3 . All of these compositions are also represented in NLV lavas, although these later have an even wider compositional variation. Two analyses from granulite sample have very low Wo contents (34-36).

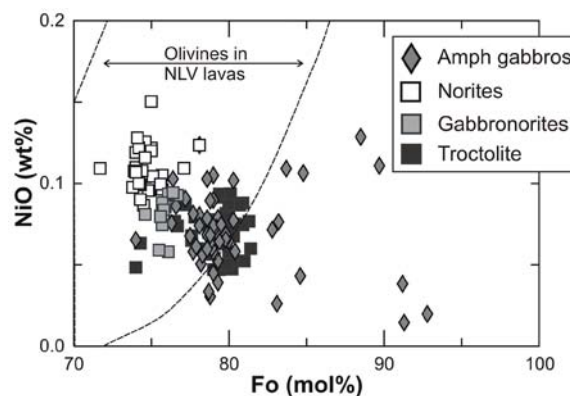


Figure 12. Fo-NiO composition of olivine crystals in xenoliths compared to the field of compositions in NLV lavas.

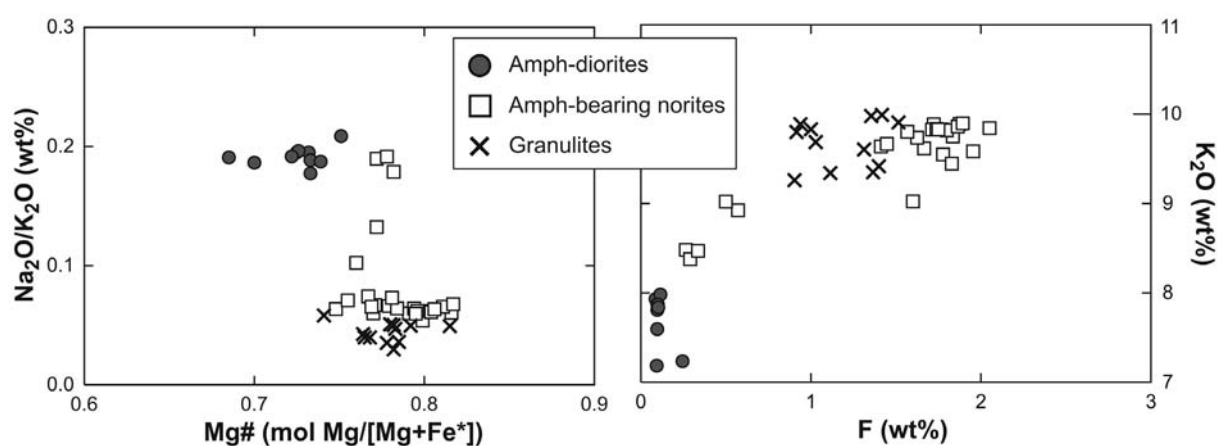


Figure 13. Biotite (phlogopite) compositions. Note the high F and K₂O contents of biotite crystals in norites and granulites (relative to those of diorites), which suggests crystallization from a highly evolved residual liquid or partial melt. Fe* = total Fe.

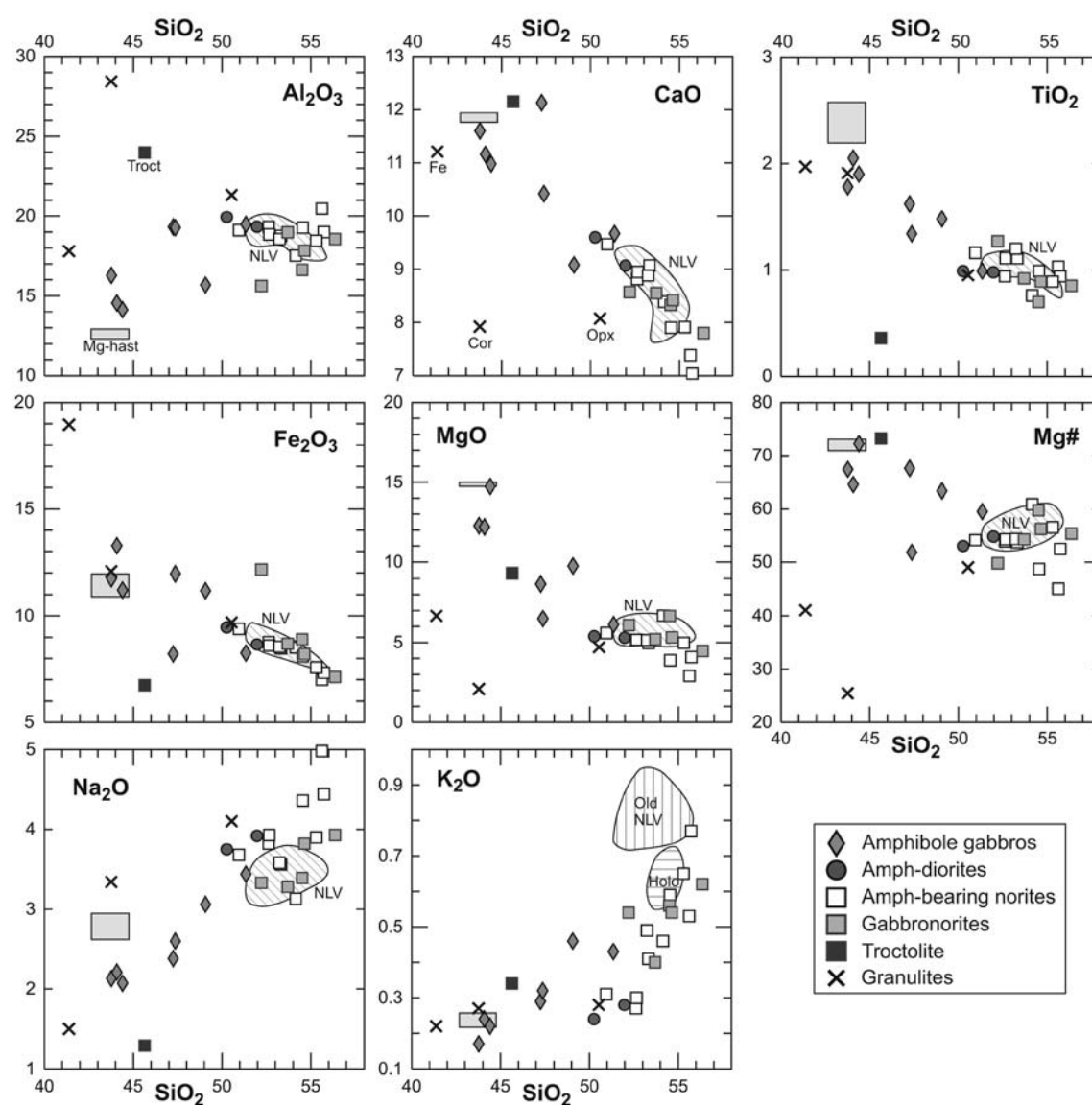


Figure 14. Major element composition of NLV xenoliths. The compositional fields of mafic NLV magmas ($\text{MgO} > 5$ wt%) are shown in fields labeled "NLV" (fields of Holocene and older units are distinguished for K₂O). Note that amphibole gabbros extend from basaltic compositions to the average compositions of Mg-hastingsite amphiboles (gray rectangles), whereas most Group II xenoliths have compositions similar to NLV mafic magmas. Troctolite composition is consistent with olivine and plagioclase accumulation. Granulites are more diverse, with non-magmatic compositions. Labels for granulites: Fe=iron-oxide-rich granulite; Cor=cordierite-corundum granulite; Opx=orthopyroxene-rich granulite.

Olivine

Olivine is a scarce phase in most NLV xenoliths, and is only a major constituent of troctolite and olivine gabbros of Group II-B. It is an accessory phase in II-A norites, and in I-A amphibole gabbros it is occasionally found as rounded cores in Mg-hastingsites. Olivines in the troctolite and amphibole gabbros are Fo_{~80} with low NiO contents (<0.1 wt%), whereas those in norites and gabbro-norites are slightly less magnesian (Fo₇₅) but richer in NiO. A few olivine cores in amphibole gabbros have higher Fo contents (up to Fo₉₃) with low NiO. These compositions are outside the range present in NLV lavas (Figure 12).

Biotite (phlogopite)

Biotite is a minor constituent of II-A amphibole-bearing norites and I-B amphibole diorites, and it has also been found as relics in the orthopyroxene granulite. Biotites in norites have a restricted composition with low Mg# (<0.75) and consistently high Na₂O/K₂O ratios of 0.2. Biotites in norites have both high and

low Na₂O/K₂O but with higher Mg#, and these are similar to biotite relics in granulites. Biotites in granulites and norites have elevated halogen contents (up to 2 wt%), as well as high K₂O contents relative to those in amphibole diorites (Figure 13).

WHOLE-ROCK CHEMISTRY

Twenty-eight xenolith samples were analyzed for whole-rock major elements by XRF and 22 of these were analyzed by XRF for trace elements. Thirteen samples were analyzed for trace elements by ICP-MS, and Sr and Nd isotopic ratios have been determined for three (Table 1). Analytical methods and precisions are like those described in Chapter 2.

All analyzed xenoliths have low SiO₂ contents (<57 wt%) that contrast with the evolved compositions of Tertiary basement plutons (Figure 7). Group I xenoliths cover the whole range of compositions extending from nearly basaltic (52 wt% SiO₂) to the average of Mg-hastingsitic amphiboles (43 wt% SiO₂), in agreement with the increasing modal abundances of this phase. The most amphibole-

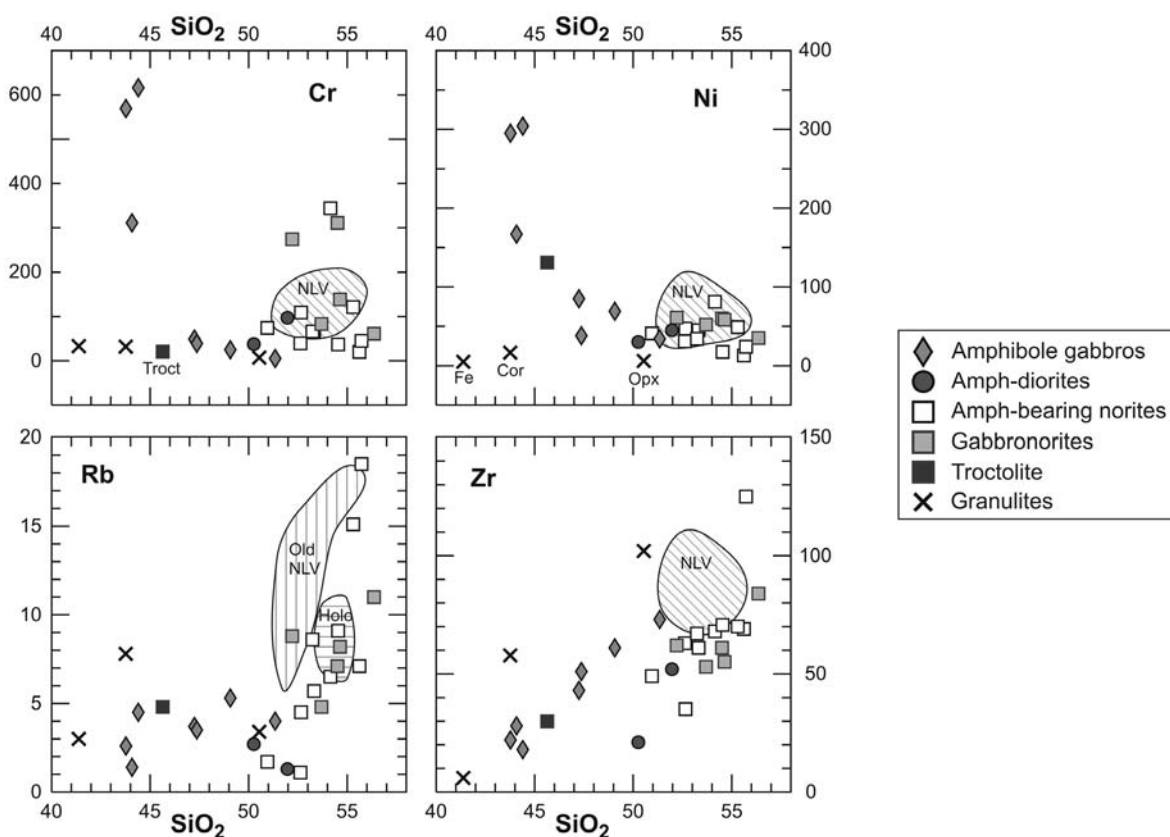


Figure 15. Selected trace element composition of NLV xenoliths and fields of NLV mafic magmas (MgO>5 wt%) shown for comparison (fields of Holocene and older units are distinguished for Rb). Note elevated Cr and Ni contents of amphibole gabbros and basalt-like composition of norites and gabbro-norites. Labels for granulites: Fe=iron-oxide-rich granulite; Cor=cordierite-corundum granulite; Opx=orthopyroxene-rich granulite. All elements as determined by XRF (see Table 1).

Table 1: Chemical composition of NLV xenoliths. Major elements by XRF, trace elements by ICP-MS and XRF (specified); b.d.l.=below detection limit. 2-sigma errors for isotopic ratios are in parenthesis in terms of the last digit cited. Samples marked with (*) have textural evidence of partial melting.

Group Type Sample	Group I								
	amph-gabbro				amph-diorite		QCM (whole-rock)		
	NL120E	NL120B	NL129C	LCBN01.3B(*)	NL033B	NL033A	NL062	NL076 (WR)	NL129E (WR)
SiO ₂	42.68	43.19	43.69	46.58	50.02	52.15	46.54	48.75	51.21
TiO ₂	1.74	1.85	2.03	1.60	0.99	0.98	1.32	1.47	0.99
Al ₂ O ₃	15.87	13.74	14.42	19.04	19.85	19.39	18.93	15.57	19.42
Fe ₂ O ₃	11.45	10.90	13.15	8.09	9.42	8.69	11.75	11.11	8.23
MnO	0.22	0.31	0.18	0.10	0.15	0.14	0.14	0.16	0.13
MgO	11.97	14.33	12.09	8.52	5.36	5.32	6.37	9.68	6.09
CaO	11.31	10.69	11.06	11.96	9.56	9.10	10.24	9.03	9.64
Na ₂ O	2.08	2.01	2.19	2.35	3.74	3.93	2.56	3.05	3.43
K ₂ O	0.17	0.22	0.24	0.29	0.24	0.28	0.32	0.46	0.43
P ₂ O ₅	0.04	0.04	0.07	0.05	0.20	0.35	0.09	0.08	0.16
LOI	1.39	1.41	0.07	-0.05	0.11	-0.02	0.87	0.48	0.30
Total	99.03	98.82	99.26	98.56	99.65	100.35	99.14	99.86	100.02
Nb (XRF)	2.3	2.2	3.3	2.3	-	2.8	2.7	3.3	2.5
Zr (XRF)	22	18	28	43	-	52	51	61	73
Y (XRF)	18.4	16.1	22.7	13.4	-	12.2	16.9	21.9	15.4
Sr (XRF)	420	289	338	561	-	791	671	374	658
Rb (XRF)	2.6	4.5	1.4	3.7	-	1.3	3.5	5.3	4
Th (XRF)	3	3	2	3	-	2	b.d.l.	3	b.d.l.
Pb (XRF)	b.d.l.	b.d.l.	b.d.l.	2	-	5	2	3	5
Ni (XRF)	295	304	167	85	-	45	38	69	34
Cr (XRF)	569	616	311	49	-	97	39	25	5
V (XRF)	346	419	415	326	-	179	254	260	146
Ba (XRF)	123	96	74	138	-	167	132	182	163
Sc	80	-	-	-	19	-	-	-	-
V	353	-	-	-	217	-	-	-	-
Cr	524	-	-	-	37	-	-	-	-
Co	50	-	-	-	29	-	-	-	-
Ni	243	-	-	-	30	-	-	-	-
Rb	3.4	-	-	-	2.7	-	-	-	-
Sr	432	-	-	-	745	-	-	-	-
Y	22.1	-	-	-	13.2	-	-	-	-
Zr	30	-	-	-	21	-	-	-	-
Nb	1.4	-	-	-	2.7	-	-	-	-
Cs	1.65	-	-	-	0.20	-	-	-	-
Ba	109	-	-	-	168	-	-	-	-
La	2.7	-	-	-	8.4	-	-	-	-
Ce	10.0	-	-	-	22.1	-	-	-	-
Pr	2.06	-	-	-	3.29	-	-	-	-
Nd	12.3	-	-	-	15.3	-	-	-	-
Sm	3.95	-	-	-	3.41	-	-	-	-
Eu	1.35	-	-	-	1.22	-	-	-	-
Gd	4.15	-	-	-	3.23	-	-	-	-
Tb	0.65	-	-	-	0.45	-	-	-	-
Dy	3.81	-	-	-	2.46	-	-	-	-
Ho	0.74	-	-	-	0.47	-	-	-	-
Er	1.98	-	-	-	1.25	-	-	-	-
Yb	1.61	-	-	-	1.23	-	-	-	-
Lu	0.23	-	-	-	0.17	-	-	-	-
Hf	1.26	-	-	-	0.87	-	-	-	-
Ta	0.07	-	-	-	0.14	-	-	-	-
Pb	1.0	-	-	-	5.9	-	-	-	-
Th	0.07	-	-	-	0.64	-	-	-	-
U	0.01	-	-	-	-	-	-	-	-
¹⁴³ Nd/ ¹⁴⁴ Nd	0.512770 (4)	-	-	-	-	-	-	-	-
⁸⁷ Sr/ ⁸⁶ Sr	0.70398 (1)	-	-	-	-	-	-	-	-

Table 1: (continued)

Group Type Sample	Group I		Group II						
	QCM-glass separates		amphibole-bearing norite						
	NL129E (liq)	NL076 (liq)	LCBNINC 01.3	NL030B	NL034B	NL027B	NL050C	GR036	NL030C
SiO ₂	61.95	65.80	47.65	51.06	52.49	52.71	53.42	53.95	54.46
TiO ₂	0.39	0.44	0.99	1.16	1.11	0.94	1.20	0.76	0.99
Al ₂ O ₃	19.22	17.12	16.77	19.15	18.79	19.35	18.62	17.46	19.24
Fe ₂ O ₃	4.07	3.59	7.57	9.41	8.59	8.78	8.57	8.48	8.09
MnO	0.09	0.07	0.14	0.13	0.13	0.14	0.13	0.16	0.12
MgO	1.46	1.67	4.43	5.61	5.15	5.17	5.16	6.65	3.87
CaO	5.15	3.52	8.11	9.49	8.92	8.82	8.92	8.36	7.89
Na ₂ O	5.92	5.30	3.18	3.68	3.92	3.82	3.60	3.12	4.35
K ₂ O	0.97	1.43	0.37	0.31	0.30	0.27	0.49	0.46	0.59
P ₂ O ₅	0.19	0.02	0.16	0.21	0.28	0.14	0.23	0.23	0.25
LOI	0.34	0.58	-0.21	-0.10	0.04	-0.09	-0.17	0.24	0.13
Total	99.74	99.55	89.18	100.13	99.74	100.07	100.19	99.94	100.00
Nb (XRF)	2.9	2.2	2.7	2.9	-	2.5	3.1	2.7	-
Zr (XRF)	141	125	61	49	-	63	67	68	-
Y (XRF)	10.4	4.6	9.9	16.2	-	8.4	16.2	14.1	-
Sr (XRF)	702	361	763	707	-	795	696	584	-
Rb (XRF)	12	20.3	5.7	1.7	-	1.1	8.6	6.5	-
Th (XRF)	b.d.l.	2	3	2	-	3	3	2	-
Pb (XRF)	10	8	44	9	-	6	7	8	-
Ni (XRF)	6	6	45	41	-	31	34	81	-
Cr (XRF)	10	2	64	74	-	39	66	344	-
V (XRF)	25	26	183	188	-	201	194	136	-
Ba (XRF)	331	342	230	162	-	175	217	249	-
Sc	-	-	-	-	20	20	26	-	21
V	-	-	-	-	261	230	219	-	144
Cr	-	-	-	-	109	42	68	-	37
Co	-	-	-	-	29	27	27	-	27
Ni	-	-	-	-	47	34	37	-	17
Rb	-	-	-	-	4.5	3.7	10.8	-	9.1
Sr	-	-	-	-	717	788	703	-	710
Y	-	-	-	-	15.4	8.7	17.4	-	16.8
Zr	-	-	-	-	35	46	61	-	71
Nb	-	-	-	-	2.9	2.5	3.1	-	3.6
Cs	-	-	-	-	0.77	0.29	0.41	-	0.34
Ba	-	-	-	-	217	162	209	-	275
La	-	-	-	-	9.8	6.8	8.7	-	10.0
Ce	-	-	-	-	23.5	16.7	20.9	-	23.9
Pr	-	-	-	-	3.66	2.48	3.07	-	3.61
Nd	-	-	-	-	17.2	11.3	14.5	-	17.5
Sm	-	-	-	-	3.99	2.23	3.69	-	4.15
Eu	-	-	-	-	1.23	0.93	1.17	-	1.42
Gd	-	-	-	-	3.84	2.14	3.79	-	4.06
Tb	-	-	-	-	0.54	0.32	0.58	-	0.57
Dy	-	-	-	-	2.95	1.59	3.19	-	3.17
Ho	-	-	-	-	0.58	0.31	0.62	-	0.60
Er	-	-	-	-	1.46	0.82	1.71	-	1.60
Yb	-	-	-	-	1.41	0.80	1.40	-	1.44
Lu	-	-	-	-	0.20	0.12	0.21	-	0.21
Hf	-	-	-	-	1.29	1.34	1.79	-	1.89
Ta	-	-	-	-	0.14	0.13	0.18	-	0.17
Pb	-	-	-	-	6.4	6.0	8.7	-	13.9
Th	-	-	-	-	1.14	0.64	1.43	-	0.94
U	-	-	-	-	-	-	-	-	-
¹⁴³ Nd/ ¹⁴⁴ Nd	-	-	-	-	-	-	-	-	-
⁸⁷ Sr/ ⁸⁶ Sr	-	-	-	-	-	-	-	-	-

Table 1: (continued)

Group Type	Group II								
	amph-bearing norite			gabbronorite					troctolite
Sample	NL054	LLG01.3B (*)	NL044	LMG01.9B	NL028B	NL030F	NL094	NL114B	NL142
SiO ₂	54.77	55.52	55.75	55.98	54.83	53.79	52.50	53.28	45.58
TiO ₂	0.88	1.03	0.94	0.84	0.70	0.88	1.27	0.91	0.36
Al ₂ O ₃	18.27	20.43	19.01	18.43	16.73	17.56	15.70	18.83	23.94
Fe ₂ O ₃	7.51	6.99	7.33	7.08	8.95	8.08	12.22	8.62	6.74
MnO	0.14	0.12	0.13	0.12	0.17	0.14	0.17	0.17	0.09
MgO	4.92	2.90	4.08	4.43	6.70	5.24	6.11	5.16	9.30
CaO	7.83	7.03	7.38	7.75	8.38	8.29	8.62	8.48	12.14
Na ₂ O	3.87	4.97	4.44	3.90	3.41	3.76	3.35	3.25	1.29
K ₂ O	0.64	0.53	0.77	0.62	0.56	0.53	0.54	0.40	0.34
P ₂ O ₅	0.20	0.31	0.20	0.17	0.15	0.18	0.09	0.11	0.09
LOI	-0.15	-0.23	-0.05	0.00	-0.28	-0.10	-0.18	0.19	-0.24
Total	98.91	99.59	100.00	99.34	100.37	98.38	100.44	99.43	99.65
Nb (XRF)	2.6	2.7	4.2	2.4	2	-	2.3	2.1	-
Zr (XRF)	70	69	125	84	61	-	62	53	-
Y (XRF)	10.2	5.3	17	8.3	9.1	-	11.3	9.1	-
Sr (XRF)	662	886	644	671	611	-	518	684	-
Rb (XRF)	15.1	7.1	18.5	11	7.1	-	8.8	4.8	-
Th (XRF)	3	3	4	3	3	-	3	3	-
Pb (XRF)	7	7	44	7	7	-	17	6	-
Ni (XRF)	49	13	24	35	60	-	61	52	-
Cr (XRF)	121	20	45	61	311	-	274	83	-
V (XRF)	130	131	136	139	137	-	336	161	-
Ba (XRF)	265	275	396	283	256	-	243	188	-
Sc	17	10	18	19	-	22	-	-	7
V	145	137	162	146	-	176	-	-	65
Cr	126	18	54	62	-	138	-	-	20
Co	25	34	22	58	-	30	-	-	48
Ni	56	16	30	36	-	58	-	-	131
Rb	16.3	9.1	20.4	12.7	-	8.2	-	-	4.8
Sr	660	852	637	-	-	637	-	-	853
Y	10.7	5.3	18.1	8.7	-	17.6	-	-	5.2
Zr	61	25	44	71	-	55	-	-	30
Nb	2.6	3.4	3.7	2.6	-	3.0	-	-	1.0
Cs	0.67	0.38	0.76	0.56	-	0.36	-	-	0.19
Ba	237	256	391	260	-	250	-	-	79
La	7.8	10.4	15.5	7.8	-	10.0	-	-	3.6
Ce	17.6	20.7	33.9	17.3	-	24.6	-	-	8.0
Pr	2.38	2.40	4.84	2.19	-	3.74	-	-	1.06
Nd	10.2	9.4	21.5	9.5	-	17.0	-	-	5.0
Sm	2.37	1.64	4.72	2.02	-	4.01	-	-	1.19
Eu	1.01	0.95	1.27	0.82	-	1.32	-	-	0.46
Gd	2.31	1.45	4.48	2.17	-	3.89	-	-	1.21
Tb	0.37	0.20	0.60	0.31	-	0.56	-	-	0.16
Dy	1.92	0.94	3.29	1.59	-	2.99	-	-	0.93
Ho	0.37	0.19	0.61	0.34	-	0.60	-	-	0.19
Er	1.03	0.49	1.59	0.85	-	1.56	-	-	0.50
Yb	0.96	0.50	1.52	0.78	-	1.60	-	-	0.46
Lu	0.15	0.08	0.22	0.13	-	0.23	-	-	0.07
Hf	1.59	0.75	1.36	1.82	-	1.65	-	-	0.73
Ta	0.16	0.51	0.23	0.83	-	0.15	-	-	0.06
Pb	7.5	9.0	54.8	7.7	-	16.2	-	-	10.7
Th	1.71	0.88	2.47	1.72	-	1.14	-	-	0.55
U	-	-	-	-	-	-	-	-	0.16
¹⁴³ Nd/ ¹⁴⁴ Nd	-	-	-	-	-	-	-	-	-
⁸⁷ Sr/ ⁸⁶ Sr	-	-	-	-	-	-	-	-	-

Table 1: (continued)

Group	Granulites		
	crd-crn	Fe-ox	opx
Sample	LMGINC01.2	NL120C	NL129F
SiO ₂	43.08	40.95	50.62
TiO ₂	1.88	1.95	0.95
Al ₂ O ₃	27.99	17.61	21.35
Fe ₂ O ₃	11.88	18.75	9.71
MnO	0.12	0.29	0.17
MgO	2.04	6.59	4.71
CaO	7.80	11.09	8.09
Na ₂ O	3.29	1.49	4.11
K ₂ O	0.27	0.22	0.28
P ₂ O ₅	0.10	0.02	0.17
LOI	-0.19	0.16	0.05
Total	98.28	99.13	100.20
Nb (XRF)	-	2.9	2.5
Zr (XRF)	-	6	102
Y (XRF)	-	23	10.5
Sr (XRF)	-	403	590
Rb (XRF)	-	3	3.4
Th (XRF)	-	2	3
Pb (XRF)	-	2	5
Ni (XRF)	-	5	6
Cr (XRF)	-	33	7
V (XRF)	-	601	188
Ba (XRF)	-	165	241
Sc	24	-	-
V	288	-	-
Cr	32	-	-
Co	30	-	-
Ni	17	-	-
Rb	7.8	-	-
Sr	731	-	-
Y	7.7	-	-
Zr	58	-	-
Nb	7.7	-	-
Cs	1.07	-	-
Ba	486	-	-
La	19.7	-	-
Ce	43.0	-	-
Pr	4.43	-	-
Nd	16.9	-	-
Sm	2.99	-	-
Eu	1.36	-	-
Gd	2.72	-	-
Tb	0.31	-	-
Dy	1.52	-	-
Ho	0.29	-	-
Er	0.78	-	-
Yb	0.72	-	-
Lu	0.11	-	-
Hf	1.62	-	-
Ta	0.48	-	-
Pb	13.7	-	-
Th	2.84	-	-
U	0.73	-	-
¹⁴³ Nd/ ¹⁴⁴ Nd	0.512796 (4)	0.512822 (6)	-
⁸⁷ Sr/ ⁸⁶ Sr	0.70413 (1)	0.70396 (1)	-

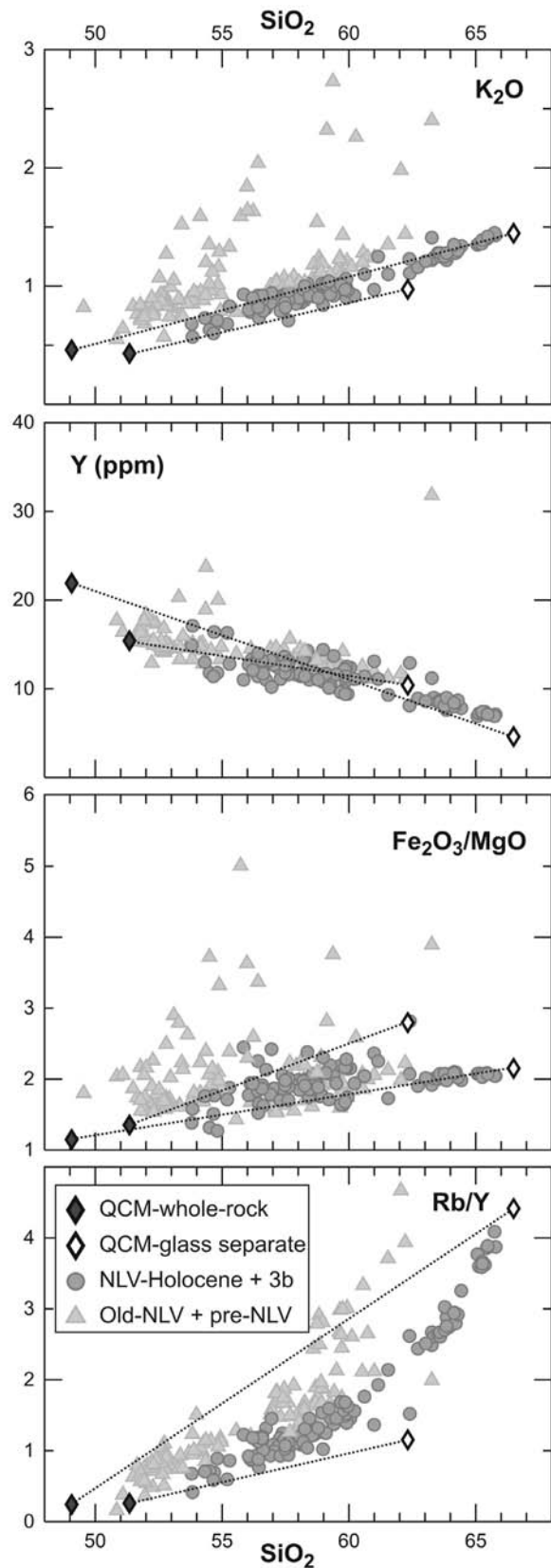


Figure 16. Chemistry of Group I quenched crystal-mushes (QCM). The compositions of whole-rock QCM and glass separates are compared to NLV lavas. Tie-lines drawn between corresponding samples. All values on anhydrous basis, all Fe as Fe₂O₃.

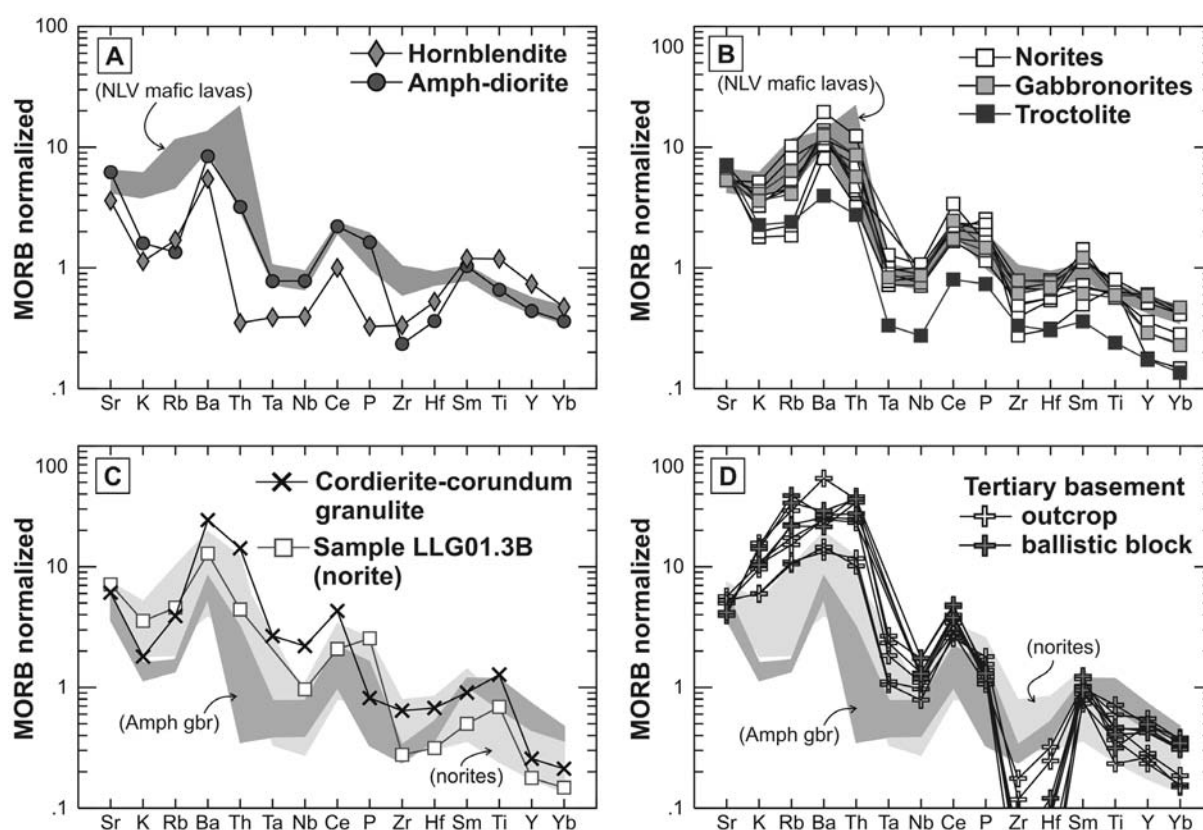


Figure 17. MORB-normalized (Pearce, 1983) spidergrams for the different types of xenoliths at NLV. **A:** Plagioclase-bearing hornblendite and amph-diorite compared to the range of NLV mafic magmas ($\text{MgO} > 5$ wt%). **B:** Group II xenoliths (except granulites). Note the overlap of most samples with the composition of NLV lavas. **C:** Cordierite-corundum granulite compared to Group I and II NLV xenoliths (shaded fields); also shown composition of a norite with advanced partial melting that shows similar K, Rb, Y and Yb depletions. **D:** Range of compositions from tertiary plutonic basement.

rich sample contains ~ 15 wt% MgO and ~ 12 wt% CaO, similar to the average composition of Mg-hastingsites (Figure 14), whereas Group I-B amphibole diorites and glass-rich QCM samples have nearly basaltic compositions. Group II norites and gabbronorites have compositions close to NLV mafic magmas, although they tend to have lower incompatible element contents (Figure 15). The troctolitic sample has elevated MgO, Al_2O_3 , and CaO, but low Fe_2O_3 , TiO_2 , and alkalis, reflecting olivine and calcic plagioclase accumulation. Granulites have also low silica contents (41-51 wt% SiO_2), with the orthopyroxene-rich sample being closest to a basaltic composition, whereas the cordierite- and iron-oxide-rich samples have very elevated Al_2O_3 and Fe_2O_3 respectively.

Interstitial glass in two of the gabbroic QCM samples was abundant enough to hand-pick for separates that were analyzed for major and trace elements by XRF (Table 1). Both QCM samples have nearly basaltic whole-rock compositions (Figure 16), except for high MgO and low Al_2O_3 in the most mafic sample (sample NL076) that probably reflects amphibole accumulation.

Residual glasses share some important characteristics of young NLV evolved lavas (Units 3b and 4), such as the low incompatible element contents (e.g. K_2O and Y), low $\text{Fe}_2\text{O}_3^*/\text{MgO}$ ratio, and low Rb/Y (< 4.5).

MORB-normalized trace element patterns of most Group II norites and gabbronorites are closely similar to those of NLV basalts (Figure

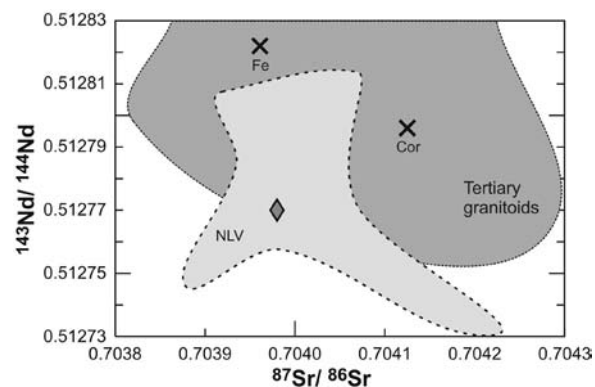


Figure 18. Sr and Nd isotopic ratios of analyzed xenoliths. Diamond=cumulate-textured amphibole gabbro; crosses=granulites. Isotopic compositions of NLV lavas and Tertiary granitoids shown in shaded fields.

17), with the exception of two samples that have relative K and Rb depletions. The troctolite sample also has a similar pattern, although at lower concentrations. Group I amphibole gabbros have lower incompatible element abundances than NLV basalts, but are relatively enriched in Ti, MREE, and HREE, for which amphibole has greater affinity (e.g. Dalpé and Baker, 2000). Cr and Ni, as well as MgO and TiO₂ contents are high in samples with high modal amphibole. Group I-B amphibole diorites overlap with the compositions of NLV basalts, except for lower K₂O, Rb, Zr, and Hf.

The trace element pattern for the cordierite-corundum granulite is characterized by negative Nb and Ta anomalies, suggesting that the protolith was an arc magmatic rock. The relatively high concentrations of most incompatible elements, as well as the sodic compositions of plagioclase (An_{~40}) suggest that the protolith rock type was more evolved than basalt. One of the noritic samples with ~20% partial-melt pockets (Figure 5D) has a trace element pattern that resembles that of the granulite.

Sr and Nd isotope ratios were determined for two granulite samples and one Group I amphibole cumulate. The amphibole cumulate sample falls within the range of isotopic values measured in NLV lavas (Figure 18), whereas granulites have higher ¹⁴³Nd/¹⁴⁴Nd than volcanic samples with comparable ⁸⁷Sr/⁸⁶Sr. The granulites are more closely comparable to the values obtained for Tertiary plutonic rocks (e.g. Muñoz *et al.*, 2000; Lucassen *et al.*, 2004; Kay *et al.*, 2005).

DISCUSSION

Group I-A. Despite their textural diversity, amphibole gabbros form a coherent group of rocks of similar mineralogy and mineral chemistry. They range in composition from broadly basaltic QCM to ultramafic amphibole cumulates. Amphibole accumulation and expulsion of residual liquid control most of the compositional diversity as seen from the major element trends being “pulled” towards the average composition of Mg-hastingsite. Amphibole gabbros contain significant amounts of vesicular glass bound by planar crystal phases, which can represent up to ~40 vol% in QCM’s. This indicates that amphibole gabbros were not completely solidified at the time of incorporation, and thus are potentially cogenetic to the host lavas. The glass-rich QCM, which seem to have been least affected by mineral accumulation, can be considered an approximation to the magma composition from which the gabbro’s amphibole and plagioclase crystallized. The residual liquids lost part of their volatiles when vapor-saturation was attained as is attested by the abundant vesicles, but there is no evidence of further modification of the bulk composition.

A suite of xenoliths from Volcán San Pedro (36°S, ~40 km northeast of Longaví) contain abundant anhedral, poikilitic amphibole crystals in a reaction relationship with refractory minerals. These xenoliths have exsolution and deformation textures, indicating that they are fragments of the pre-Quaternary basement. Amphibole is interpreted to have formed

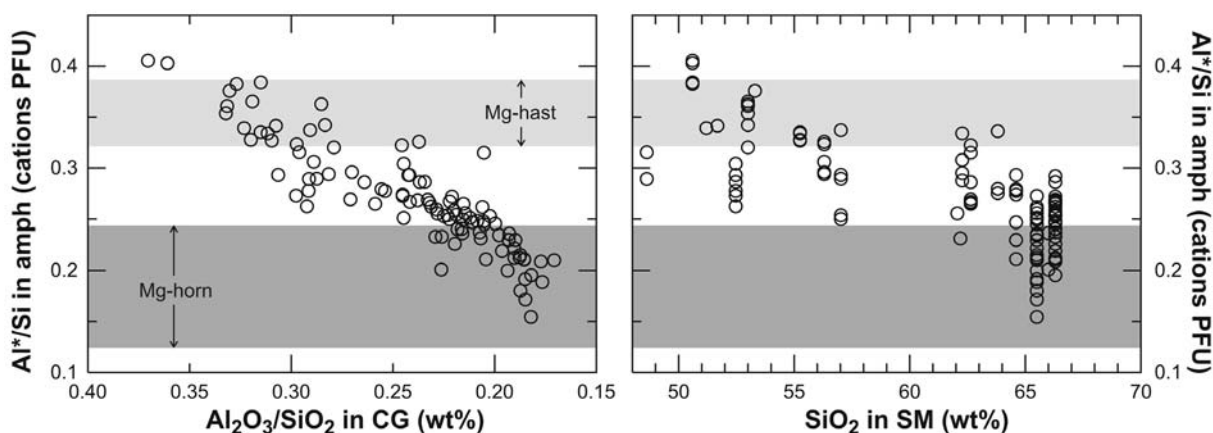


Figure 19. Compositions of low-pressure (<0.5 GPa) experimental amphiboles as a function of the chemistry of coexisting glass (CG) and bulk SiO₂ content of the starting materials (SM). Gray bands represents the composition of Mg-hastingsites and Mg-hornblende in Group I xenoliths. Al*=total Al in cation units. Data sources: Rutherford and Devine, 1988; Sisson and Grove, 1993; Grove *et al.*, 1997; Moore and Carmichael, 1998; Martel *et al.*, 1999; Prouteau *et al.*, 1999; Scaillet and Evans, 1999; Hilyard *et al.*, 2000; Pichavant *et al.*, 2002; Grove *et al.*, 2003; Prouteau and Scaillet, 2003; Costa *et al.*, 2004.

by reaction of olivine and pyroxene-bearing gabbroic cumulates with percolating evolved volatile-rich liquids or fluids (Costa *et al.*, 2002). NLV xenoliths, on the contrary, contain euhedral amphibole and residual melt pockets, which suggests a primary magmatic origin.

The compositions of the minerals in amphibole gabbros are consistent with crystallization from water-rich mafic magmas. A compilation of low-pressure (<0.5 GPa) hydrous crystallization experiments (Figure 19) shows that amphiboles with the Al^{total}/Si composition of Mg-hastingsites have been mostly obtained from mafic starting materials (Sisson and Grove, 1993; Grove *et al.*, 1997; Moore and Carmichael, 1998; Pichavant *et al.*, 2002; Grove *et al.*, 2003). Crystallization of Mg-hastingsite from mafic magmas is consistent with the high Mg numbers and Cr contents of some of them. Rounded Mg-rich olivine and pyroxene cores in some amphiboles could represent earlier, higher temperature phases that were present in the melt and partly reacted to produce amphibole. Peritectic reaction of the dominant $Fo_{\sim 80}$ olivine could account for the presence of Mg-rich but Ni-poor olivine compositions. Calcic plagioclase in amphibole gabbros also suggests that the magma from which they crystallized was mafic and water-rich. Water in magmas causes the stability field of plagioclase to retract relative to ferromagnesian minerals, and shifts plagioclase to more calcic compositions (*e.g.* Arculus and Wills, 1980; Sisson and Grove, 1993). Experiments at constant melt composition (near-liquidus crystallization) show that the An content of plagioclase increases almost linearly with increasing melt water content (Takagi *et al.*, 2005). For the starting material used in these experiments, An-rich plagioclase crystallized at pressures between 0.2 and 0.3 GPa. Experimental work by Panjasawatwong *et al.* (1995) has shown the strong control of melt CaO and Al_2O_3 on the An content of plagioclase, and concluded that An $_{\sim 90}$ plagioclase cannot crystallize from intermediate magmas under any P-T-H $_2O$ condition. Water-rich mafic melts such as the bulk QCM or the NLV Holocene mafic enclaves are suitable for crystallization of the mineral phases in amphibole gabbros.

Amphibole fractionation is the main mechanism involved in the genesis of evolved and intermediate NLV magmas (Chapter 2). The compositions of amphiboles in Group I-A xenoliths are indistinguishable from those in NLV lavas, which indicate that amphibole

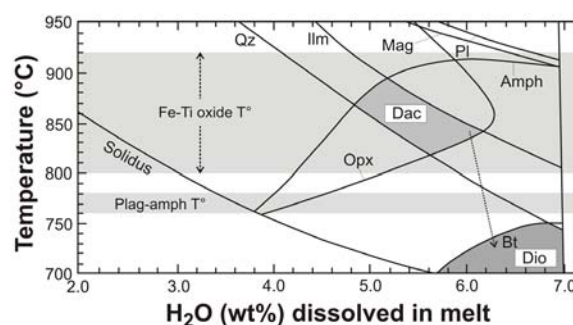


Figure 20. Experimental phase relations of the 1991 Pinatubo dacite at 0.22 GPa as a function of melt H $_2O$ content (from Scaillet & Evans, 1999). Shaded fields represent the mineral assemblage of NLV Holocene dacites (Dac) and of amphibole diorite xenoliths (Dio). Light gray bands represent the range of temperatures recorded by Fe-Ti oxides in dacites and amphibole-plagioclase temperatures in diorites.

gabbros could represent samples of the mineral assemblages fractionated from NLV magmas to produce dacitic liquids. This is consistent with the similar Sr and Nd isotopic compositions in lavas and amphibole cumulates. The residual liquids in the QCM are direct evidence that dacitic liquids broadly similar to NLV dacites can be produced by extraction of amphibole and calcic plagioclase from wet basaltic magmas. In particular, the low Y contents in QCM glasses suggest that amphibole alone can account for HREE depletions without garnet involvement.

Group I-B. Amphibole diorites, which also contain some Mg-hastingsite and calcic plagioclase cores, are dominated by a more evolved mineralogy that includes An $_{30-60}$ plagioclase, low-Al amphibole (Mg-hornblende), biotite, Wo-poor orthopyroxene, and quartz. A comparison of the compositions of experimental amphiboles to Mg-hornblendes indicates that these could have crystallized from evolved magmas ($SiO_2 > \sim 60$ wt%; Figure 19). Mg-hornblendes and orthopyroxene with identical composition are characteristic of Holocene NLV magmas, which suggest that amphibole diorites are crystal cumulates extracted from the Holocene dacites, in agreement with the exclusive occurrence of these xenoliths in this unit. NLV dacites, however, lack biotite and quartz, probably due to the high temperatures indicated by Fe-Ti-oxides thermometry. This can be visualized in a diagram with the 0.22 GPa phase relations of the 1991 Pinatubo dacite (Figure 20; Scaillet and Evans, 1999), which is very similar in composition to NLV dacites. Plagioclase-amphibole thermometry in diorites (Holland and Blundy, 1994) yielded

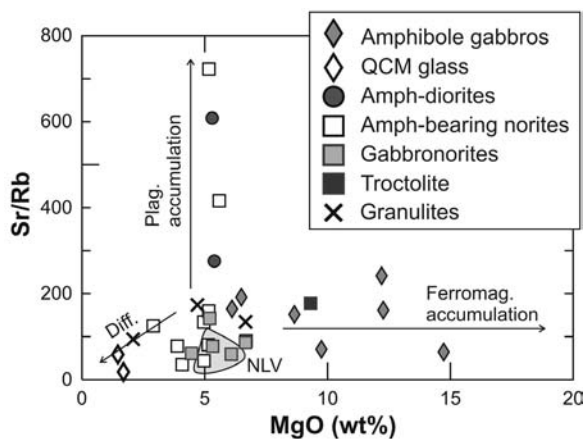


Figure 21. MgO vs. Sr/Rb plot indicating the trends of plagioclase and ferromagnesian phases accumulation. Also a trend of magmatic differentiation (Diff.) is proposed. Shaded field represents the compositions of NLV mafic magmas.

temperatures of ~760-780 °C for the least aluminous hornblendes that coexist with An₃₅-An₄₅ plagioclase. These temperatures are lower than those of NLV dacites, but are still 10-20°C higher than the biotite stability temperature. This small discrepancy might be attributed to the uncertainty in temperature determinations, or to high S in magmas which has the effect of stabilizing biotite at higher temperatures (Scaillet and Evans, 1999; Costa *et al.*, 2004).

The bulk compositions of amphibole diorites, however, are much less evolved than dacites, indicating that they do not simply represent solidified, marginal facies of the dacitic chamber; they are crystal cumulates extracted from a dacitic magma body. Plagioclase accumulation is suggested by their high Sr/Rb and Na₂O/K₂O ratios (Figures 21 and 23). Low concentrations

of incompatible elements in these diorites are consistent with residual melt expulsion.

Group II-A and II-B. Norites and gabbronorites have broadly basaltic compositions and trace element contents comparable to those of NLV basalts, which suggest that Group II xenoliths mostly represent solidified mafic magmas, although plagioclase accumulation could be important for some norites as is inferred from whole-rock chemistry. This is illustrated by the elevated Sr/Rb ratios of some norites (Figure 21), similar to those of Group I-B amphibole diorites. Accumulation of olivine ± plagioclase dominates the chemistry of the troctolite sample. Some Group II xenoliths are also chemically similar to the most mafic basement granitoid samples, but these latter are amphibole- and biotite-bearing quartz diorites that lack pyroxene, and are thus probably unrelated.

The mineralogy of Group II xenoliths is dominated by anhydrous phases, but postcumulus interstitial amphibole and biotite indicate that hydrous phases crystallized from volatile- and alkali-rich residual melts. Elevated halogen contents of Ti-edenitic amphiboles and phlogopite are consistent with their crystallization from residual, volatile-rich melts. Breakdown textures in the hydrous phases indicate that amphibole and biotite dehydrated and triggered grain-boundary melting upon incorporation in hot mafic magmas. Eventually norites disintegrated in the host magmas, and a small proportion of Ti-edenites ended up in the andesites as xenocrysts (Beard *et al.*, 2005). Although the preserved amount of glass from partial melting is generally low (1-3 vol%),

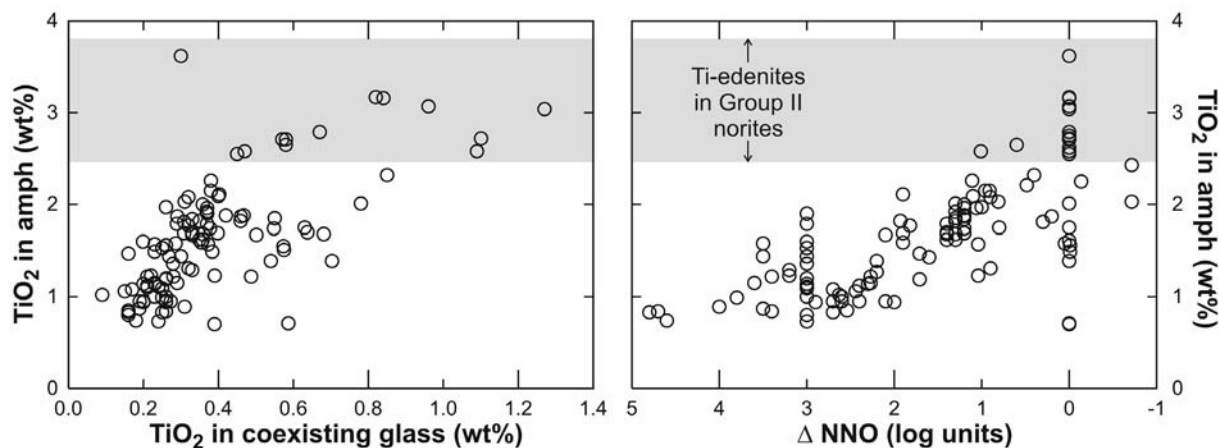


Figure 22. TiO₂ content of experimental amphiboles as a function of TiO₂ in the coexisting glass and of Δ-NNO conditions of the experiments. Range of TiO₂ content of amphiboles in Group II norites shown in gray bands. Data sources as in Figure 20.

there are examples where abundant glass in the xenoliths has locally mixed into the host magma. Group II norites could well represent the crustal component assimilated by some Unit 1 and Unit 3a NLV lavas as identified on the basis of trace element considerations (Chapter 2).

The high titanium contents of Ti-edenites in noritic xenoliths can potentially provide some constraints on the conditions of their formation. There is a positive correlation between the TiO_2 contents of experimentally produced amphiboles and coexisting glass (Figure 22). Increasing pressure has the effect of decreasing the TiO_2 content of amphibole, while temperature is poorly correlated with TiO_2 . A more robust control on amphibole TiO_2 contents seems to be exerted by the oxygen-fugacity of the system (Figure 22B). This indicates that Ti-edenites in norites probably crystallized from Ti-rich, low- $f\text{O}_2$ liquids. Residual liquids will be enriched in TiO_2 if silicate minerals start crystallizing before Fe-Ti oxides, which is only possible when the magmas are relatively low in H_2O and reduced (tholeiitic differentiation, Sisson and Grove, 1993). Water-poor and reduced magmas were erupted at NLV during the early stages of formation (Villalobos and basal NLV units), and they represent suitable magmas from which norites could have crystallized.

Metamorphic rocks. Granulite xenoliths are comparatively rare at NLV. They have major and trace element compositions that diverge to varying extents from bulk basaltic compositions and from compositions that could be controlled by mineral accumulation. Granulitic xenoliths in Calbuco volcano have been interpreted as relics of basalts with oceanic affinity that have undergone melt extraction by amphibole-dehydration melting (Hickey-Vargas *et al.*, 1995). Melt extraction from granulites at NLV is also consistent with their high-temperature refractory mineralogy. Whittington *et al.* (1998) showed that the assemblage of cordierite with biotite in quartz-free lithologies changes progressively with increasing temperature to biotite-spinel-cordierite and finally to spinel-cordierite, during which melt is continuously expelled from the system. The significance of cordierite-spinel assemblages as refractory relics after partial melting at relatively low pressures has been emphasized by Hensen (1986), Vielzeuf and Holloway (1988), and Nichols *et al.* (1992). Melt extraction from NLV

granulites is consistent with their relatively low incompatible element contents. P-T conditions of metamorphism of the cordierite-curundum granulite can be crudely estimated at <0.6 GPa and 700-1000°C considering that no garnet is present (Shimpo *et al.*, 2006). The broadly similar trace-element patterns of the corundum-bearing granulite and a norite that has undergone extensive partial melting suggests that melt extraction could be responsible for some of the chemical characteristics.

The negative Nb-Ta anomaly in the corundum granulite is most likely inherited from the protolith, which suggests magmatic arc provenance. However, cordierite-corundum bearing granulites are commonly interpreted as metapelites with originally high Al_2O_3 (Bindu, 1997; Kelly and Harley, 2004; Zou *et al.*, 2004; Markl, 2005; Salvioli-Mariani *et al.*, 2005). This would imply that the sedimentary protolith was derived by erosion of arc-volcanic material in order to keep the arc signature. A prolonged history of denudation, transport, deposition, and accretion of metapelites to the continental margin seems difficult to reconcile with the isotopic composition of granulites, which is comparable to that of Cenozoic rocks. The current low Rb contents of the granulites prevent significant build-up of ^{87}Sr , but Rb depletion probably occurred during metamorphism and melt extraction rather than being a primary feature of a metapelitic protolith. The chemical similarities of granulites to a norite sample that preserves textural evidence of partial melting (Figure 5D) strongly suggest that the granulites could be restites after extraction of melt from a mafic to intermediate plutonic precursor.

SUMMARY

A summary of the proposed interpretations for the origin of the different types of xenoliths is presented in Figure 23 in terms of the major element ratios $\text{CaO}/\text{Al}_2\text{O}_3$ and $\text{Na}_2\text{O}/\text{K}_2\text{O}$. Amphibole gabbros have compositions that extend from those of NLV mafic magmas (gray field in Figure 23A) towards the average composition of Mg-hastingsitic amphibole, which indicates that accumulation of this phase is the main mechanism that controls their chemistry. One amphibole gabbro sample that lies away from the trend towards Mg-hastingsite is best explained by accumulation of a mixture of amphibole and calcic plagioclase in a 87:13 proportion. Group I-B amphibole diorites

have $\text{Na}_2\text{O}/\text{K}_2\text{O}$ higher than mafic magmas, interpreted as plagioclase accumulation and residual melt expulsion. Most Group II xenoliths have compositions close to NLV mafic magmas, although some melt expulsion is indicated by their higher $\text{Na}_2\text{O}/\text{K}_2\text{O}$ values. Certain amphibole-bearing norites exhibit significant plagioclase accumulation (see also Figure 21). The norite sample labeled LLG01.3B, which has undergone significant grain-boundary melting, is displaced towards lower $\text{CaO}/\text{Al}_2\text{O}_3$ but higher $\text{Na}_2\text{O}/\text{K}_2\text{O}$ as do two of the granulite samples, which suggest that melt extraction could be

the processes involved in the formation of the granoblastic xenoliths.

The evolutionary trends complementary to extraction of these lithologies are shown schematically in Figure 23B. Amphibole-dominated fractionation in a mafic, water-rich system produces a trend of decreasing $\text{CaO}/\text{Al}_2\text{O}_3$ and $\text{Na}_2\text{O}/\text{K}_2\text{O}$ illustrated by the young Holocene magmas at NLV (Units 3b and 4), whose magmatic evolution is dominated by early amphibole + calcic plagioclase crystallization. This trend is parallel to the tie lines between basaltic QCM and their evolved

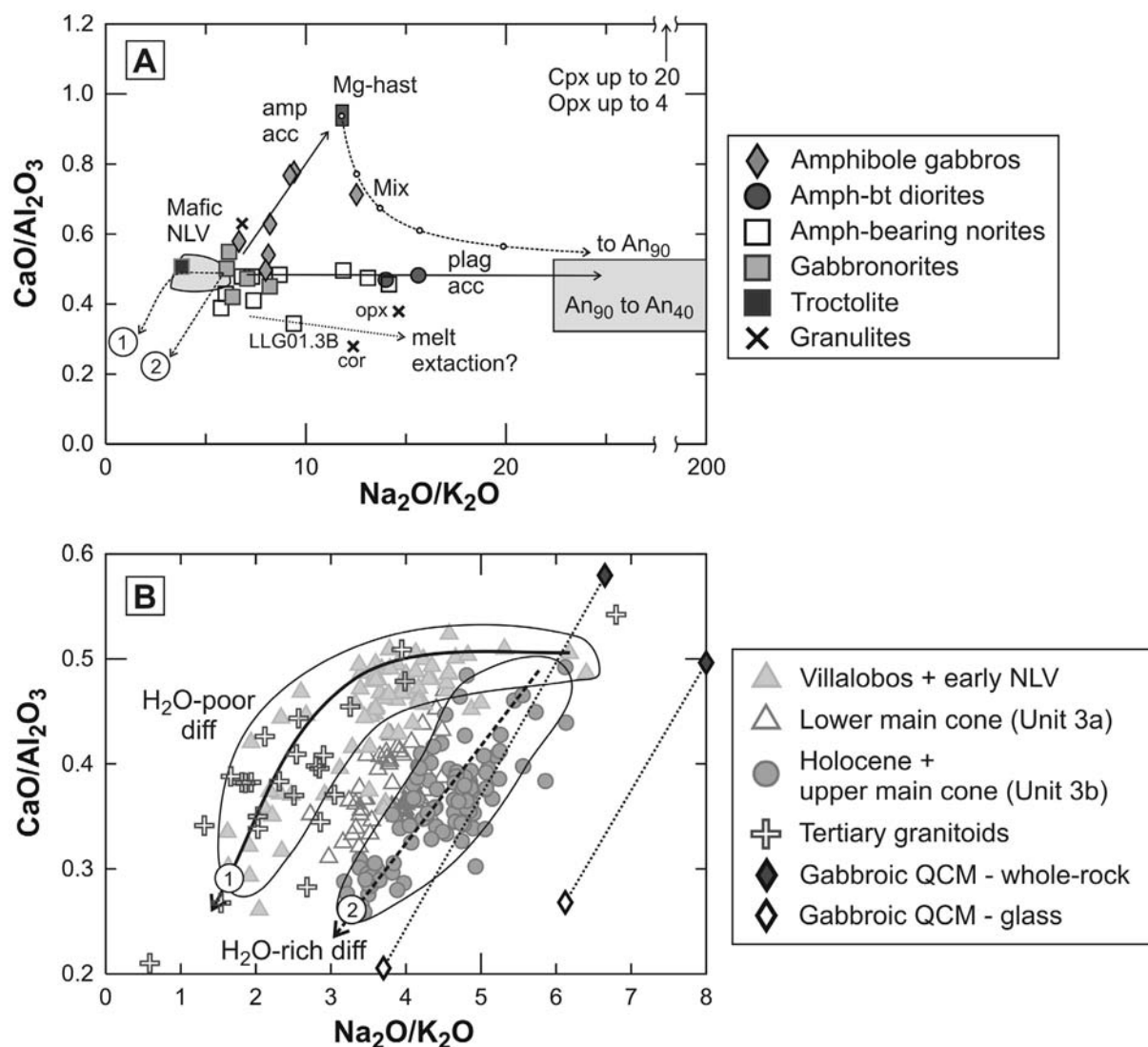


Figure 23. Summary diagram with the proposed processes recorded in NLV xenoliths. **A:** A reference starting composition close to NLV mafic lavas is presented in the shaded field. Amphibole accumulation towards average Mg-hastingsitic composition (box labeled Mg-hast) is recorded in amphibole gabbros. Sample away from the depicted trend lies in the mixing line between amphibole and An_{90} plagioclase. Increasing $\text{Na}_2\text{O}/\text{K}_2\text{O}$ ratio at constant $\text{CaO}/\text{Al}_2\text{O}_3$ for amph-diorites and norites is consistent with plagioclase accumulation (box includes An_{40} to An_{90} plagioclase compositions). Increasing $\text{Na}_2\text{O}/\text{K}_2\text{O}$ accompanied by decreasing $\text{CaO}/\text{Al}_2\text{O}_3$ could indicate melt extraction as is suggested by two of the granulites and a norite sample with advanced partial melting. **B:** Early extraction of plagioclase from basalts produces the water-poor differentiation path (1) observed in early Longaví units and pre-Longaví lavas (and the Tertiary plutons), whereas early amphibole crystallization produces the water-rich differentiation trend (2) depicted by young NLV lavas.

residual liquids. On a water poorer system, plagioclase-dominated fractionation produces a trend of decreasing $\text{Na}_2\text{O}/\text{K}_2\text{O}$ at constant $\text{CaO}/\text{Al}_2\text{O}_3$ value due to the small variation of this ratio in intermediate plagioclase. From andesite onwards, the trend bends down to lower $\text{CaO}/\text{Al}_2\text{O}_3$ probably due to pyroxene involvement. Such a trend is depicted by water-poor magmas from Villalobos volcano and the basal NLV units 1 and 2, but also by the Tertiary granitoids basement. Unit 3b lies in between the two previous trends, attesting for the transitory character of this unit in terms of magma evolution.

CONCLUSIONS

Except for fragments of Tertiary granitoids, most xenoliths at NLV seem to be closely related to the Quaternary magmatism in the area. The stratigraphic appearance of xenoliths seems to reproduce the trend of increasing magmatic water content during NLV evolution (Chapter 2). This strongly suggests that most xenoliths are broadly cogenetic with the host sequence. Group I xenoliths are most clearly autolithic. They commonly contain significant residual glass, and correspond in chemistry and mineralogy to the solid assemblages thought to have been extracted during magmatic evolution of the host sequence. Available isotopic analyses do not contradict this interpretation. The effects of the incorporation of cogenetic cumulates in to the host magma will in most cases be barely detectable by whole-rock geochemistry. Noritic xenoliths represent dryer mafic magmas such as those from the early volcanic units, although they cannot be discarded to correspond to older "dry" magmatism in the area (e.g. Miocene). The rare granulite xenoliths are potentially representative of pre-existing lithologies on the walls of the conduits, but a genetic relationship to broadly contemporaneous magmatism can not be precluded. We conclude that most xenoliths at NLV are probably autoliths, and can be considered the solid assemblages complementary to intermediate and evolved magmas.

REFERENCES

- Arculus, R.J. and Wills, K.J.A.** (1980). *The Petrology of Plutonic Blocks and Inclusions from the Lesser Antilles Island Arc*. *Journal of Petrology* **21**(4): 743-799.
- Beard, J.S., Ragland, P.C. and Crawford, M.L.** (2005). *Reactive bulk assimilation: A model for crust-mantle mixing in silicic magmas*. *Geology* **33**(8): 681-684.
- Bindu, R.S.** (1997). *Granulite facies spinel-cordierite assemblages from the Kerala Khondalite Belt, Southern India*. *Gondwana Research* **1**(1): 121-128.
- Costa, F., Dungan, M.A. and Singer, B.S.** (2002). *Hornblende- and Phlogopite-Bearing Gabbroic Xenoliths from Volcan San Pedro (36°S), Chilean Andes: Evidence for Melt and Fluid Migration and Reactions in Subduction-Related Plutons*. *Journal of Petrology* **43**(2): 219-241.
- Costa, F., Scaillet, B. and Pichavant, M.** (2004). *Petrological and Experimental Constraints on the Pre-eruption Conditions of Holocene Dacite from Volcan San Pedro (36°S, Chilean Andes) and the Importance of Sulphur in Silicic Subduction-related Magmas*. *Journal of Petrology* **45**(4): 855-881.
- Dalpé, C. and Baker, D.R.** (2000). *Experimental investigation of large-ion-lithophile-element-, high-field-strength-element and rare-earth-element-partitioning between calcic amphibole and basaltic melt: the effects of pressure and oxygen fugacity*. *Contributions to Mineralogy and Petrology* **140**: 230-250.
- Garcia, M.O. and Jacobson, S.S.** (1979). *Crystal clots, amphibole fractionation and the evolution of calc-alkaline magmas*. *Contributions to Mineralogy and Petrology* **69**(4): 319-327.
- Grove, T.L., Donnelly-Nolan, J.M. and Housh, T.** (1997). *Magmatic processes that generated the rhyolite of Glass Mountain, Medicine Lake volcano, N. California*. *Contributions to Mineralogy and Petrology* **127**(3): 205-223.
- Grove, T.L., Elkins-Tanton, L.T., Parman, S.W., Chatterjee, N., Müntener, O. and Gaetani, G.A.** (2003). *Fractional crystallization and mantle-melting controls on calc-alkaline differentiation trends*. *Contributions to Mineralogy and Petrology* **145**(5): 515-533.
- Hensen, B.J.** (1986). *Theoretical phase relations involving cordierite and garnet revisited: the influence of oxygen fugacity on the stability of sapphirine and spinel in the system Mg-Fe-Al-Si-O*. *Contributions to Mineralogy and Petrology* **92**(3): 362-367.
- Hickey-Vargas, R., Abdollahi, M.J., Parada, M.A., López-Escobar, L. and Frey, F.A.** (1995). *Crustal xenoliths from Calbuco Volcano, Andean Southern Volcanic Zone:*

- implications for crustal composition and magma-crust interaction. *Contributions to Mineralogy and Petrology* **119**(4): 331-344.
- Hilyard, M., Nielsen, R.L., Beard, J.S., Patiño-Douce, A. and Blencoe, J.** (2000). *Experimental determination of the partitioning behavior of rare earth and high field strength elements between pargasitic amphibole and natural silicate melts.* *Geochimica et Cosmochimica Acta* **64**(6): 1103-1120.
- Holland, T. and Blundy, J.** (1994). *Non-ideal interactions in calcic amphiboles and their bearing on amphibole-plagioclase thermometry.* *Contributions to Mineralogy and Petrology* **116**(4): 433-447.
- Kay, S., Godoy, E. and Kurtz, A.** (2005). *Episodic arc migration, crustal thickening, subduction erosion, and magmatism in the south-central Andes.* *Geological Society of America Bulletin* **117**: 67-88.
- Kelly, M.N. and Harley, S.L.** (2004). *Orthopyroxene-corundum in Mg-Al-rich granulites from the Oygarden Islands, East Antarctica.* *Journal of Petrology* **45**(7): 1481-1512.
- Le Maitre, R., Bateman, P., Dudek, A., Keller, J., Lameyre, J., Le Bas, M.J., Sabine, P.A., Schmidth, R., Sorensen, H., A., S., Woolley, A.R. and Zanettin, B.** (1989). *A Classification of igneous rocks and glossary of terms. Recommendations of the International Union of Geological Sciences Subcommittee on the Systematics of Igneous Rocks.* Oxford, Blackwell Scientific Publications. 193 p.
- Leake, B., Woolley, A., Arps, C., Birch, W., Gilbert, M., Grice, J., Hawthorne, F., Kato, A., Kisch, H., Krivovichev, V., Linthout, K., Laird, J., Mandarino, J., Maresch, W., Nickel, E., Rock, N., Schumacher, J., Smith, D., Stephenson, N., Ungaretti, L., Whittaker, E. and Youzhi, G.** (1997). *Nomenclature of amphiboles: Report of the Subcommittee on amphiboles of the International Mineralogical Association, Commission on New Minerals and Minerals Names.* *American Mineralogist* **82**: 1019-1037.
- Lucassen, F., Trumbull, R., Franz, G., Creixell, C., Vázquez, P., Romer, R. and Figueroa, O.** (2004). *Distinguishing crustal recycling and juvenile additions at active continental margins: the Paleozoic to recent compositional evolution of the Chilean Pacific margin (36-41°S).* *Journal of South American Earth Sciences* **17**: 103-119.
- Markl, G.** (2005). *Mullite-corundum-spinel-cordierite-plagioclase xenoliths in the Skaergard Marginal Border Group: multi-stage interaction between metasediments and basaltic magma.* *Contributions to Mineralogy and Petrology* **149**: 196-215.
- Martel, C., Pichavant, M., Holtz, F. and Scaillet, B.** (1999). *Effects of fO₂ and H₂O on andesite phase relations between 2 and 4 kbar.* *Journal of Geophysical Research* **104**(B12): 29453-29470.
- Moore, G. and Carmichael, I.S.E.** (1998). *The hydrous phase equilibria (to 3 kbar) of an andesite and basaltic andesite from western Mexico: constraints on water content and conditions of phenocryst growth.* *Contributions to Mineralogy and Petrology* **130**(3 - 4): 304-319.
- Müntener, O., Kelemen, P. and Grove, T.** (2001). *The role of H₂O during crystallization of primitive arc magmas under uppermost mantle conditions and genesis of igneous pyroxenites: an experimental study.* *Contributions to Mineralogy and Petrology* **141**(6): 643-658.
- Muñoz, J. and Niemeyer, C.** (1984). *Hoja Laguna del Maule, Regiones del Maule y del Bío Bío.* Carta Geológica de Chile, S. N. d. G. y. Minería, Santiago. map scale 1:250.000 and accompanying booklet, 97 p.
- Muñoz, J., Troncoso, R., Duhart, P., Crignola, P., Farmer, L. and Stern, C.** (2000). *The relation of the mid-Tertiary coastal magmatic belt in south-central Chile to the late Oligocene increase in plate convergence rate.* *Revista Geológica de Chile* **27**(2): 177-203.
- Nichols, G.T., Berry, R.F. and Green, D.H.** (1992). *Internally consistent gahnitic spinel-cordierite-garnet equilibria in the FMASHZn system: geothermobarometry and applications.* *Contributions to Mineralogy and Petrology* **111**(3): 362-377.
- Panjasawatwong, Y., Danyushevsky, L.V., Crawford, A.J. and Harris, K.L.** (1995). *An experimental study of the effects of melt composition on plagioclase - melt equilibria at 5 and 10 kbar: implications for the origin of magmatic high-An plagioclase.* *Contributions to Mineralogy and Petrology* **118**(4): 420-432.
- Pearce, J.A.** (1983). *Role of the sub-continental lithosphere in magma genesis at active continental margins.* in C. J. Hawkesworth

- and M. J. Norry (eds.). Continental basalts and mantle xenoliths. 230-249.
- Pichavant, M., Martel, C., J., B. and Scaillet, B.** (2002). *Physical conditions, structure and dynamics of a zoned magma chamber: Mount Pelée (Martinique, Lesser Antilles Arc)*. Journal of Geophysical Research **107**(B5): ECV 2-1 - ECV 2-30.
- Prouteau, G. and Scaillet, B.** (2003). *Experimental Constraints on the Origin of the 1991 Pinatubo Dacite*. Journal of Petrology **44**(12): 2203-2241.
- Prouteau, G., Scaillet, B., Pichavant, M. and Maury, R.** (1999). *Fluid-present melting of ocean crust in subduction zones*. Geology **27**(12): 1111-1114.
- Rodríguez, C.** (in prep). *Intra-crustal Origin of Holocene Adakitic Magmas at Nevado de Longaví Volcano (Southern Volcanic Zone: 36.2°S)*. Ph.D. Thesis, 120 pp. University of Geneva, Switzerland.
- Rutherford, M. and Devine, J.** (1988). *The May 18, 1980, eruption of Mount St. Helens, 3. Stability and chemistry of amphibole in the magma chamber*. Journal of Geophysical Research **93**(B10): 11949-11959.
- Salvioli-Mariani, E., Renzulli, A., Serri, G., Holm, P.M. and Toscani, L.** (2005). *Glass-bearing crustal xenoliths (buchites) erupted during the recent activity of Stromboli (Aeolian Islands)*. Lithos **81**: 255-277.
- Scaillet, B. and Evans, B.** (1999). *The June 15, 1991 eruption of Mount Pinatubo. I. Phase equilibria and pre-eruption of P-T-fO₂-H₂O conditions of the dacite magma*. Journal of Petrology **40**(3): 381-411.
- Sellés, D., Rodríguez, C., Dungan, M.A., Naranjo, J. and Gardeweg, M.** (2004). *Geochemistry of Nevado de Longaví volcano (36.2°S): A compositional atypical arc volcano in the Southern Volcanic Zone of the Andes*. Revista Geológica de Chile **31**(2): 293-315.
- Shimpo, M., Tsunogae, T. and Santosh, M.** (2006). *First report of garnet-corundum rocks from southern India: implications for prograde high-pressure (eclogite facies?) metamorphism*. Earth and Planetary Science Letters **242**: 111-129.
- Sisson, T.W. and Grove, T.L.** (1993). *Experimental investigations of the role of H₂O in calc-alkaline differentiation and subduction zone magmatism*. Contributions to Mineralogy and Petrology **113**(2): 143-166.
- Takagi, D., Sato, H. and Nakagawa, M.** (2005). *Experimental study of a low-alkali tholeiite at 1-5 kbar: optimal condition for the crystallization of high-An plagioclase in hydrous arc tholeiite*. Contributions to Mineralogy and Petrology **149**: 527-540.
- Vielzeuf, D. and Holloway, J.R.** (1988). *Experimental determination of the fluid-absent melting relations in the pelitic system*. Contributions to Mineralogy and Petrology **98**(3): 257-276.
- Whittington, A., Harris, N. and Baker, J.** (1998). *Low-pressure crustal anatexis: the significance of spinel and cordierite from metapelitic assemblages at Nanga Parbat, northern Pakistan*. in P. J. Treolar and P. J. O'Brien (eds.). What drives metamorphism and metamorphic reactions? Geological Society Special Publication. **138**: 183-198.
- Zou, H., McKeegan, K.D., Xu, X. and Zindler, A.** (2004). *Fe-Al-rich tridymite-hercynite xenoliths with positive cerium anomalies: preserved lateritic paleosols and implications for Miocene climate*. Chemical Geology **207**: 101-116.

REMERCIEMENTS

Je tiens avant tout à remercier le Professeur Michael Dungan pour m'avoir donné l'opportunité d'entreprendre ce travail de thèse. Avec lui, j'ai appris la complexité des systèmes magmatiques, les subtilités de la dégustation des vins, et l'actualité des buts marqués par les footballeurs sud-américains dans la ligue européenne. Merci Mike pour les innombrables heures de discussion sur ces sujets à combinaison explosive.

J'aimerais adresser mes remerciements aux membres du jury qui m'ont tant aidé. Bill Leeman, qui m'a chaleureusement accueilli dans son laboratoire ainsi que chez lui à deux reprises pour l'obtention des données de bore. Ses visions parfois peu orthodoxes du magmatisme en zones de subduction m'ont aidé à élargir ma propre vision. Peter Ulmer, qui a très généreusement partagé avec notre groupe des résultats non publiés ainsi que sa profonde compréhension des phases minérales dans les systèmes magmatiques. François Bussy, que j'ai souvent dérangé les week-ends à cause des caprices imprévus de la microsonde. Olivier Bachmann pour ses commentaires constructifs.

J'aimerais aussi remercier tous ceux qui m'ont consacré du temps pour discuter au sujet du Longaví, en particulier Othmar Müntener, Jon Blundy, Bruno Scaillet, Andrea Marzoli, George Morris, Richard Spikings et Fidel Costa.

Dans l'obtention de mes données isotopiques j'ai reçu énormément d'aide de la part de Massimo Chiaradia, Dave Chew et Denis Fontignie, merci à vous.

Au personnel de la Section des Sciences de la Terre, qui même surchargé de travail a toujours trouvé le temps de partager des mots aimables. Je pense en particulier à Jacqueline Berthoud, Jean-Marie Bocard, Gilbert Overnay, Ursula Eigenmann, Jacques Metzger et Fabio Capponi.

Felipe Espinoza, Pablo Salas, José Luis Palma, Charles Perring, Titín Ortega, Hermann Rojo et Juan Espinoza m'ont accompagné pour le travail de terrain, merci.

Il me manque de mots pour remercier ma famille qui à distance m'a toujours soutenu dans cette aventure scientifique en payant le prix fort (eux et moi) de l'absence prolongée.

Et je profite aussi de remercier Pizio, l'ami, professeur et collègue, avec qui j'ai une dette de longue date.

Mais cette thèse est beaucoup plus que ces feuilles tachetées d'encre que vous avez dans vos mains. Elle représente aussi plusieurs années de ma vie. Et cela restera dans mes souvenirs comme une expérience formidable grâce au gens que j'ai rencontré sur le chemin et qui m'ont généreusement offert leur amitié. Je pense notamment aux « mexicas » Sergio Galindo et Rocío Álvarez, à Cédric Rapaille et famille, à Régine Baumgartner et Ronner Bendezú, à Antoine de Haller et Carol Dolorier (et Astor, bien sûr), à Isabelle Chambeffort, à Alex Mišković et Anna, et aux membres du GLAG : Adiel Martínez, Antoine Fabre, Daniel Ariztegui, Georges Gorin, Fernando Guarín, Nicolás Waldmann.

Et surtout, je dois un énorme merci à celle que m'a soutenu, supporté et encouragé tout au long de ces années. Elle a été la compagne et la collègue sans qui je ne serai jamais arrivé jusqu'ici. Merci infiniment Carolina.

Cette étude a été possible grâce au soutien financier du Fonds National Suisse de la Recherche Scientifique, projet No. 2000-63950.00 et à la collaboration du Servicio Nacional de Geología y Minería (SERNAGEOMIN), Chili.

Pendant les années 2001-2003, l'auteur a bénéficié d'une bourse de la Commission Fédérale des Bourses pour Etudiants Etrangers de la Confédération Suisse. Le Fonds Mark Birkigt a accordé à l'auteur des bourses pour de frais de voyage aux congrès les années 2002, 2003 et 2005.

L'auteur remercie sincèrement ces institutions.